RUB

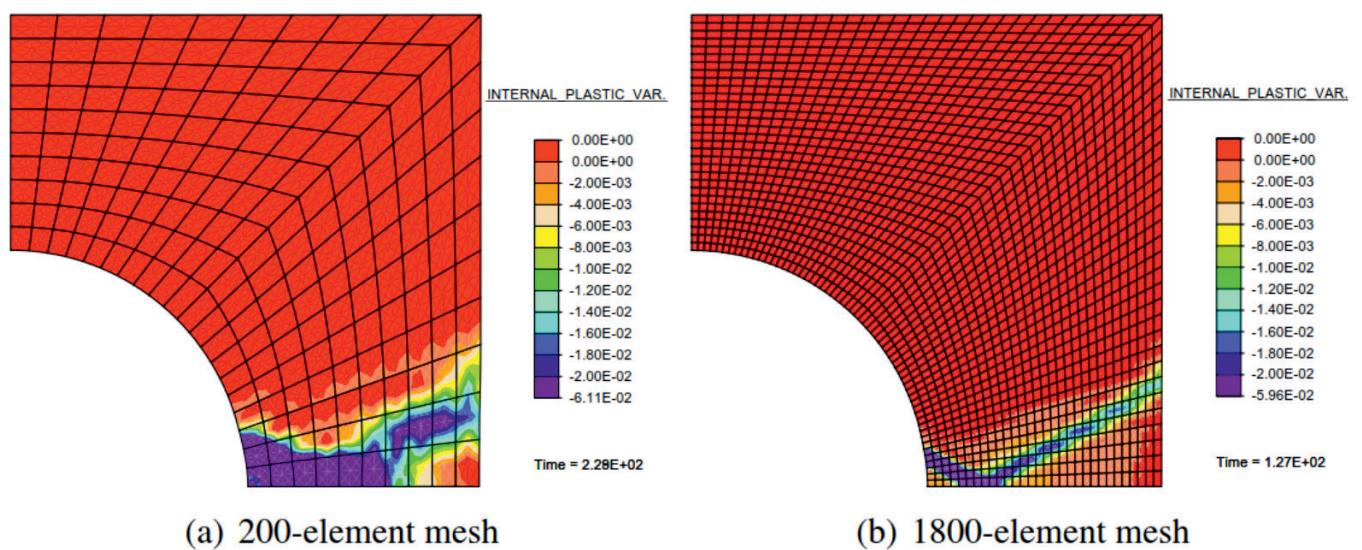# On a regularization framework for inelastic material models via gradient enhancement of the free energy function

Bojan Dimitrijevic

(a) 200-element mesh   (b) 1800-element mesh

Dissertation

On a regularization framework for inelastic material models via gradient enhancement of the free energy function

Zur Erlangung des akademischen Grades

Dr.-Ing.

vorgelegt der

Fakultät für Bauingenieurwesen

an der Ruhr-Universität Bochum

von

Bojan J. Dimitrijević,
geb. 27.07.1974 in Surdulica, Serbien

Dedicated to my mother

Abstract

Conventional inelastic material models with softening effects result in ill-posed boundary value problems due to the loss of ellipticity of the governing field equations. In the present work a regularization framework for inelastic material models via gradient enhancement of the Helmholtz free-energy function is investigated. The enhancement is defined by means of an interaction potential dependent on the difference between additionally introduced non-local variables and the suitably chosen potential function of the internal variables. The gradients of the newly introduced variables are used to regularize the model. The corresponding boundary value problem is formulated as a pure minimization of the potential functional with respect to the displacement fields and the additional (non-local) variable field. The formulation of the constitutive relations is performed in thermodynamically consistent way and it results in only small modifications compared to the models without regularization. The evolution of the internal variables is specified by a minimum principle for the dissipation potential, while the dissipation potential itself retains the form of the classical model.

The application of the proposed gradient enhancement strategy is demonstrated on several inelastic material models, including damage, plastic and coupled models. Representative numerical examples illustrate the behavior of the material models regularized by the proposed gradient enhancement strategy. It is shown that all material models treated in this thesis are successfully regularized. Furthermore, the influence of newly introduced model parameters on the global response of the system, distribution of inelastic variables and the calculation procedure is discussed.

Kurzfassung

Übliche inelastische Materialmodelle, die Materialentfestigung beschreiben, führen aufgrund des Verlustes der Elliptizität in den beschreibenden Feldgleichungen zu schlecht gestellten Randwertproblemen. In der hier vorgestellten Arbeit wird ein Ansatz zur Regularisierung inelastischer Materialmodelle mittels einer Gradientenerweiterung der Freien Helmholtz-Energie untersucht. Die Erweiterung des Models besteht darin, eine zusätzliche Feldvariable einzuführen, die durch einen Interaktionsterm mit den internen Variablen gekoppelt wird. Durch Bestrafen des Gradienten dieser Feldgröße wird eine Regularisierung des Models erreicht. Ausgehend von der Formulierung der reinen Minimierung des Gesamtpotentials bezüglich der Verschiebungen sowie der nicht-lokalen Feldvariablen wird das entsprechende Randwertproblem abgeleitet. Die konstitutiven Gleichungen werden in einer thermodynamisch konsistenten Art und Weise hergeleitet woraus sich nur kleine Abweichungen im Vergleich zu Modellen ohne diesen Regularisierungsansatz ergeben. Die Evolution der internen Variablen basiert auf dem Prinzip des Mimimums des Dissipationspotentials, wobei das Dissipationspotential unverändert bleibt bezogen auf das klassische Model.

Die Anwendung der vorgestellten Strategie der Gradientenerweiterung wird anhand verschiedener inelastischer Materialmodelle demonstriert, einschließlich Schädigungs- und Plastizitätsmodellen sowie deren Kopplung. Beispielhafte numerische Ergebnisse verdeutlichen das Verhalten der durch den vorgestellten Ansatz regularisierten Materialmodelle und den Einfluss der zusätzlich eingeführten numerischen Parameter auf die globale Systemantwort. Es wird gezeigt, dass alle in dieser Arbeit betrachteten Materialmodelle erfolgreich regularisiert werden können.

Acknowledgments

Mündliche Prüfung:

1. Gutachter: Prof. Dr. rer. nat. Klaus Hackl
2. Gutachter: Prof. Dr.-Ing. habil. Paul Steinmann

Contents

1. Introduction

In this thesis we focus on the investigation of a particular class of non-linear material behavior, namely softening behavior of materials accounting for inelastic effects. Two major inelastic effects are addressed here: damage defined as modification of the material physical properties due to the presence or the growth of microdefects (microcracks, voids, delamination etc.) and plasticity characterized by the development of permanent deformation caused by e.g. plastic slip along crystalline planes in metals, sliding over one another of grains and particles in soil or wooden chips in chipboard etc. in the microscale level.

It is a well known fact that the utilization of conventional inelastic material models with softening behavior leads to ill-posed boundary value problems due to loss of ellipticity of the governing field equations. In this case, the underlying continuum problem does not have regular solutions and the result obtained by numerical calculations merely reflects the specifics of the approximation of the problem. As a result, difficulties in the convergence of the discretized system of equations occur together with a strong dependence of the obtained results on the numerical approximation itself. A typical example of this problem is a pathological dependence of the results on the discretization mesh in the calculations utilizing the finite element method in conjunction with inelastic material models experiencing a softening regime. In this case one obtains localization of the inelastic process within a small zone, whose size is determined merely by the mesh resolution.

There are several strategies proposed to overcome this problem that take into consideration an internal material length scale in one form or another. One of them is the introduction of non-local interactions into the model. That task can be accomplished following two approaches: integral-type or gradient-type. The integral strategy introduces non-local variables as weighted averages of the local variables over a neighborhood of the point under consideration, whereas the gradient approach relies on the introduction of higher order gradient terms (mostly Laplacean) into governing evolution equations.

In the present contribution a regularization strategy based on gradient enhancement of the free energy function is presented. The enhancement is formulated by introducing a list of additional variables, which is coupled to the list of internal variables via an interaction term. By penalizing the gradients of the additional variables, one attains the regularization of the problem. The corresponding boundary value problem is formulated as a pure minimization of the potential functional with respect to displacements and additional variables.

The thesis is organized as follows: In chapter 2 a rough description of fundamental mechanical quantities (like the deformation, stress etc.) is given. Furthermore, the thermomechanical balance laws are presented, which constitute the basis for the discussion in the chapter 3. Chapter 3 contains the description of the constitutive laws, elastic as well as inelastic. The evolution of the inelastic internal variables is specified based on the minimum principle for the dissipation potential and the issue of localization is discussed in the same chapter. In the chapter 4 the regularization strategy based on the gradient enhancement of the free-energy

function is presented and some aspects related to the thermodynamics and the practical implementation are highlighted. The application of the proposed strategy onto several selected material models is demonstrated in chapter 5, whereas is its implementation in the context of finite element method depicted in chapter 6. Some representative numerical examples which illustrate specific aspects of the gradient enhancement framework as well as the behavior of the resulting material models are gathered in chapter 7. Finally, conclusions are drawn in chapter 8.

2. Fundamentals of thermomechanical material modeling

The aim of this chapter is a presentation of a rough description of

- motion and deformation (kinematics),

- stress in a continuum (kinetics) and

- fundamental laws governing the motion of a continuum (balance relations).

The provided results are material-independent and therefore form the basis for the subsequent formulation of the mathematical models describing the behavior of materials involving irreversible effects.

2.1. Kinematics

Continuum kinematics deals with the geometry of a body, its motion in space as well as its deformation during motion. It considers a body as an ensemble of material points whose initial and current position is characterized by means of the position and displacement vectors. By considering the immediate vicinity of material points one gets to the concept of strains, which describe the deformation of a material body. The strains and related quantities are first obtained without further assumptions in a non-linear form and afterwards they are reduced to a linear description according to the small deformation theory.

2.1.1. Motion and deformation

A continuum body $\mathcal{B}$ is a composition of material points or particles in the three- dimensional Euclidean space at some instant of time t. It moves in space from one instance in time to another, occupying a continuous sequence of geometrical regions $\Omega_0, \ldots, \Omega$, called *configurations* of $\mathcal{B}$ at that time t. The configuration Ω_0 at initial time, taken here without loss of generality as $t = 0$, is referred to as the *reference* (*initial*, *undeformed*) *configuration*. The position of a typical point P of the body $\mathcal{B}$ (Figure 2.1) in the initial configuration is uniquely identified by the reference position vector $\boldsymbol{X}$

$$\boldsymbol{X} = X_i \, \boldsymbol{e}_i. \tag{2.1}$$

The configuration Ω occupied by the body $\mathcal{B}$ at a subsequent time $t = t^* > 0$ is called *current* (or *deformed*) *configuration*. The typical point P that is related to the position vector $\boldsymbol{X}$ in the reference configuration, occupies a position uniquely identified by the current position vector $\boldsymbol{x}$ in the deformed configuration (Figure 2.1). It is assumed that the description
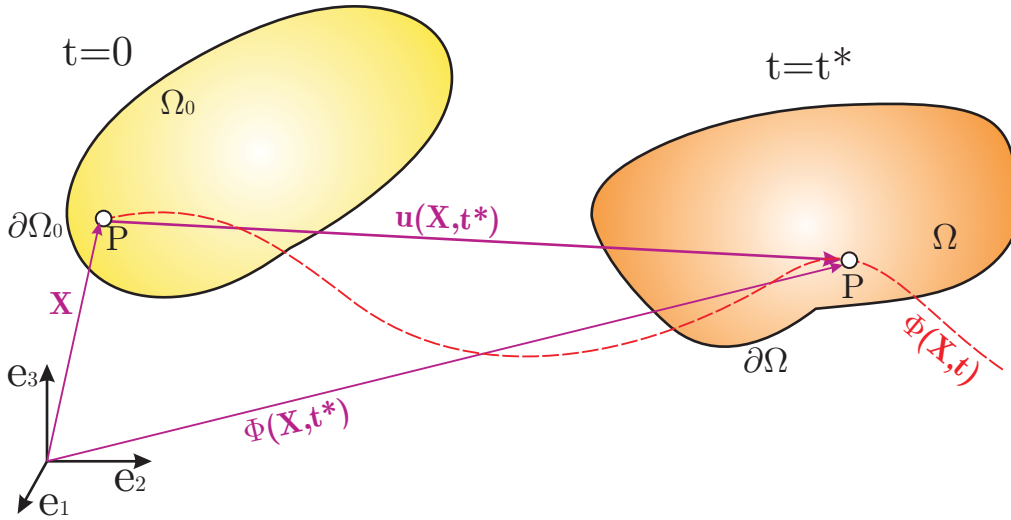
Figure 2.1.: Configurations and motion of a body $\mathcal{B}$

of the current position vector is done utilizing the same basis vectors and with respect to the same origin as in the case of the reference configuration

$$\boldsymbol{x} = x_i \, \boldsymbol{e}_i. \tag{2.2}$$

The motion of the body $\mathcal{B}$ is specified by a vector field $\boldsymbol{\Phi}$, that maps the reference position vectors $\boldsymbol{X}$ onto the current ones $\boldsymbol{x}$ for all points of the undeformed configuration Ω_0 and for all times t

$$\boldsymbol{x} = \boldsymbol{\Phi}(\boldsymbol{X}, t). \tag{2.3}$$

For every single time t the mapping $\boldsymbol{\Phi}$ is called a *deformation*. Hence, the parametric equation (2.3) determines successive positions $\boldsymbol{x}$ of a typical point P in space for arbitrary time t, thus forming a curve in the Euclidean space which is called the *trajectory* of the point P. The motion $\boldsymbol{\Phi}$ is assumed to posses the continuous derivatives with respect to time and space, cf. Holzapfel (2000). Furthermore, the mapping $\boldsymbol{\Phi}$ is assumed to be uniquely invertible. Hence, there exists the inverse mapping (called *inverse motion*) $\boldsymbol{\Phi}^{-1}$

$$\boldsymbol{X} = \boldsymbol{\Phi}^{-1}(\boldsymbol{x}, t), \tag{2.4}$$

which answer the question which reference position vector $\boldsymbol{X} \in \Omega_0$ is related to the point P determined by the position vector $\boldsymbol{x} \in \Omega$ at the current instant of time.

Physical phenomena associated with the deformation $\boldsymbol{\Phi}$ of a body $\mathcal{B}$ may be described using fields defined over the reference configuration $\psi(\boldsymbol{X}, t)$ (ψ stands here for an arbitrary field of interest), or using fields defined over the current configuration $\psi(\boldsymbol{x}, t)$. The former is the so-called *Lagrangean* or *material* description and the later is the *Eulerian* or *spatial* description. In the material description attention is paid to a material point, and it is observed what happens with that point as it moves. Predominant application of this description is in the field of solid mechanics. On the contrary, in the spatial description attention is paid to a fixed point in space, and it is investigated what happens at that point as time changes. This description is mainly applied in the field of fluid mechanics, though it is sometimes used in the solid mechanics as well.

2.1.2. Displacement, velocity and acceleration

The vector field obtained as a difference between the current and the reference position vectors of the body $\mathcal{B}$ at a certain time t is called a *displacement field* at the instant of time t

$$\boldsymbol{u}(\boldsymbol{X}, t) = \boldsymbol{x}(\boldsymbol{X}, t) - \boldsymbol{X}. \tag{2.5}$$

The velocity of a material point represents the rate of change of its position vector, i.e. the time derivative of the deformation mapping holding the reference position vector $\boldsymbol{X}$ fixed

$$\boldsymbol{v}(\boldsymbol{X}, t) = \dot{\boldsymbol{\Phi}}(\boldsymbol{X}, t) = \frac{D\boldsymbol{\Phi}}{Dt}(\boldsymbol{X}, t) = \left.\frac{\partial\boldsymbol{\Phi}(\boldsymbol{X}, t)}{\partial t}\right|_{\boldsymbol{X}} = \frac{\partial\boldsymbol{\Phi}}{\partial t}. \tag{2.6}$$

Taking into consideration the definition of the displacement field (2.5), the velocity of a material point can be alternatively expressed as

$$\boldsymbol{v}(\boldsymbol{X}, t) = \dot{\boldsymbol{\Phi}}(\boldsymbol{X}, t) = \frac{D(\boldsymbol{X} + \boldsymbol{u}(\boldsymbol{X}, t))}{Dt} = \left.\frac{\partial\boldsymbol{u}(\boldsymbol{X}, t)}{\partial t}\right|_{\boldsymbol{X}} = \dot{\boldsymbol{u}}(\boldsymbol{X}, t). \tag{2.7}$$

The acceleration of a material point represents the rate of change of velocity of a material point, defined as time derivative of the velocity field holding the reference position vector $\boldsymbol{X}$ fixed

$$\boldsymbol{a}(\boldsymbol{X}, t) = \dot{\boldsymbol{v}}(\boldsymbol{X}, t) = \frac{D^2\boldsymbol{\Phi}}{Dt^2}(\boldsymbol{X}, t) = \left.\frac{\partial^2\boldsymbol{\Phi}(\boldsymbol{X}, t)}{\partial t^2}\right|_{\boldsymbol{X}} = \frac{\partial^2\boldsymbol{\Phi}}{\partial t^2}. \tag{2.8}$$

Taking once again into consideration the definition of the displacement field (2.5) and the alternative representation of the velocity (2.7), the acceleration can be expressed as

$$\boldsymbol{a}(\boldsymbol{X}, t) = \dot{\boldsymbol{v}}(\boldsymbol{X}, t) = \frac{D^2(\boldsymbol{X} + \boldsymbol{u}(\boldsymbol{X}, t))}{Dt^2} = \left.\frac{\partial^2\boldsymbol{u}(\boldsymbol{X}, t)}{\partial t^2}\right|_{\boldsymbol{X}} = \ddot{\boldsymbol{u}}(\boldsymbol{X}, t). \tag{2.9}$$

The derivative $D(\cdot)/Dt$ at fixed $\boldsymbol{X}$ is called the *Lagrangian* (or *material*) *time derivative*. As far as the quantity under observation is defined in material description, it is equivalent to a simple partial time derivative of the underlying field. However, the requirement of keeping the reference vector $\boldsymbol{X}$ fixed makes the material time derivative of a quantity defined in spatial description more complicated. Considering a smooth spatial field $\psi(\boldsymbol{x}, t)$, its material time derivative (denoted as $D(\psi(\boldsymbol{x}, t))/Dt$ or $\dot{\psi}(\boldsymbol{x}, t)$) is obtained as

$$\frac{D(\psi(\boldsymbol{x}, t))}{Dt} = \dot{\psi}(\boldsymbol{x}, t) = \left.\frac{\partial\psi\left(\boldsymbol{\Phi}(\boldsymbol{X}, t), t\right)}{\partial t}\right|_{\boldsymbol{X} = \boldsymbol{\Phi}^{-1}(\boldsymbol{x}, t)}. \tag{2.10}$$

Utilizing the chain rule of differentiation, it can be found from (2.10) that:

$$\frac{D(\psi(\boldsymbol{x}, t))}{Dt} = \dot{\psi}(\boldsymbol{x}, t) = \left.\frac{\partial\psi(\boldsymbol{x}, t)}{\partial t}\right|_{\boldsymbol{x}} + \left.\frac{\partial\psi(\boldsymbol{x}, t)}{\partial \boldsymbol{x}}\right|_{t} \cdot \boldsymbol{v}(\boldsymbol{x}, t). \tag{2.11}$$

The first term on the right hand-side (partial time derivative at fixed $\boldsymbol{x}$) is called the *Eulerian* (or *spatial*) *time derivative*, while the second term is called the *convective* (or *transport*) *rate of change of* ψ , cf. Holzapfel (2000). The relation (2.11) is very useful since it allows to find the total (material) time derivative of some field on a basis of local information in the current configuration (the spatial time derivative and the spatial gradient of a field) and the velocity of a point, without knowing the motion $\boldsymbol{\Phi}(\boldsymbol{X}, t)$ explicitly. Hence, in the Eulerian description the acceleration is

$$\boldsymbol{a}(\boldsymbol{x}, t) = \dot{\boldsymbol{v}}(\boldsymbol{x}, t) = \frac{\partial\boldsymbol{v}(\boldsymbol{x}, t)}{\partial t} + \frac{\partial\boldsymbol{v}(\boldsymbol{x}, t)}{\partial \boldsymbol{x}} \cdot \boldsymbol{v}(\boldsymbol{x}, t). \tag{2.12}$$

2.1.3. Deformation of line, volume and surface elements
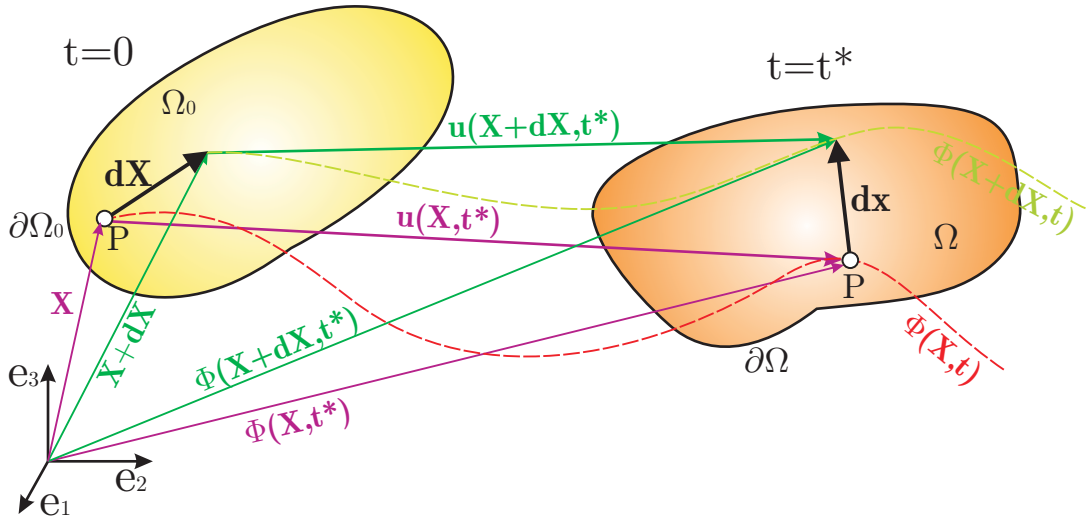
Figure 2.2.: Deformation of an infinitesimal line element $d\boldsymbol{X}$

Let us consider an infinitesimal oriented line element $d\boldsymbol{X}$, placed at a typical point P of the body $\mathcal{B}$ in the reference configuration Ω_0 (Figure 2.2). During a motion $\boldsymbol{\Phi}(\boldsymbol{X}, t)$ this line element is mapped onto an infinitesimal line element $d\boldsymbol{x}$ in the current configuration Ω. Focusing on a certain instant of time $t = t^*$, the spatial (or deformed) line element can be expressed utilizing the deformation mapping $\boldsymbol{\Phi}(\boldsymbol{X}, t^*)$

$$d\boldsymbol{x} = \boldsymbol{\Phi}(\boldsymbol{X} + d\boldsymbol{X}, t^*) - \boldsymbol{\Phi}(\boldsymbol{X}, t^*) \tag{2.13}$$

Since the deformation at any fixed time $t = t^*$ does not depend on intermediate stages in motion, but solely on the geometry of the reference Ω_0 and the current configuration Ω, the explicit dependence on time in (2.13) can be omitted. Expanding $\boldsymbol{\Phi}$ in a Taylor series around the point $\boldsymbol{X}$ one obtains

$$d\boldsymbol{x} = \frac{\partial \boldsymbol{\Phi}(\boldsymbol{X})}{\partial \boldsymbol{X}} \cdot d\boldsymbol{X} + h.o.t. \tag{2.14}$$

Neglecting the terms of higher order and introducing the *deformation gradient*

$$\boldsymbol{F} = \frac{\partial \boldsymbol{\Phi}(\boldsymbol{X})}{\partial \boldsymbol{X}} = \frac{\partial \boldsymbol{x}}{\partial \boldsymbol{X}}, \tag{2.15}$$

the mapping of the differential line element of the reference configuration $d\boldsymbol{X}$ to the current line element $d\boldsymbol{x}$ is expressed in the following form

$$d\boldsymbol{x} = \boldsymbol{F} \cdot d\boldsymbol{X}. \tag{2.16}$$

It is assumed that the description of both reference and current configuration is performed employing the same set of basis vectors $\boldsymbol{e}_i$. Hence, the *deformation gradient tensor* is a two-point tensor with one index describing spatial coordinates x_i, and the other reference coordinates X_J

$$\boldsymbol{F} = \frac{\partial x_i}{\partial X_J} \, \boldsymbol{e}_i \otimes \boldsymbol{e}_J. \tag{2.17}$$

In general, $\boldsymbol{F}$ is an unsymmetric second order tensor. The assumption that the deformation mapping is uniquely invertible has been already stated and recalling the definition of the

inverse motion (2.4), one can find that its derivative with respect to the current position $\boldsymbol{x}$ is the inverse of the deformation gradient

$$\boldsymbol{F}^{-1} = \frac{\partial \boldsymbol{\Phi}^{-1}(\boldsymbol{x}, t)}{\partial \boldsymbol{x}} = \frac{\partial \boldsymbol{X}}{\partial \boldsymbol{x}}, \qquad \boldsymbol{F}^{-1} = \frac{\partial X_I}{\partial x_j}\, \boldsymbol{e}_I \otimes \boldsymbol{e}_j. \tag{2.18}$$

Furthermore, the mapping of the differential line element of the current configuration $d\boldsymbol{x}$ to the reference line element $d\boldsymbol{X}$ is expressed in the form

$$d\boldsymbol{X} = \boldsymbol{F}^{-1} \cdot d\boldsymbol{x}. \tag{2.19}$$

The assumption of uniquely invertible deformation mapping implies the nonsingularity of the tensor $\boldsymbol{F}$. That can be assured if its determinant fulfills the condition $\det \boldsymbol{F} \neq 0$. Introducing the definition of the displacement field (2.5) into (2.15) and (2.18), one obtains the deformation gradient and its inverse in terms of the corresponding displacement derivatives

$$\boldsymbol{F} = \frac{\partial \boldsymbol{x}}{\partial \boldsymbol{X}} = \frac{\partial (\boldsymbol{X} + \boldsymbol{u})}{\partial \boldsymbol{X}} = \mathbf{I} + \frac{\partial \boldsymbol{u}}{\partial \boldsymbol{X}}, \quad \boldsymbol{F}^{-1} = \frac{\partial \boldsymbol{X}}{\partial \boldsymbol{x}} = \frac{\partial (\boldsymbol{x} - \boldsymbol{u})}{\partial \boldsymbol{x}} = \mathbf{I} - \frac{\partial \boldsymbol{u}}{\partial \boldsymbol{x}}, \tag{2.20}$$

where the notion $\mathbf{I}$ stands for the second order unity tensor

$$\mathbf{I} = \delta_{ij}\, \boldsymbol{e}_I \otimes \boldsymbol{e}_j, \qquad \delta_{ij} = \begin{cases} 0 \mid i \neq j \\ 1 \mid i = j \end{cases} \tag{2.21}$$
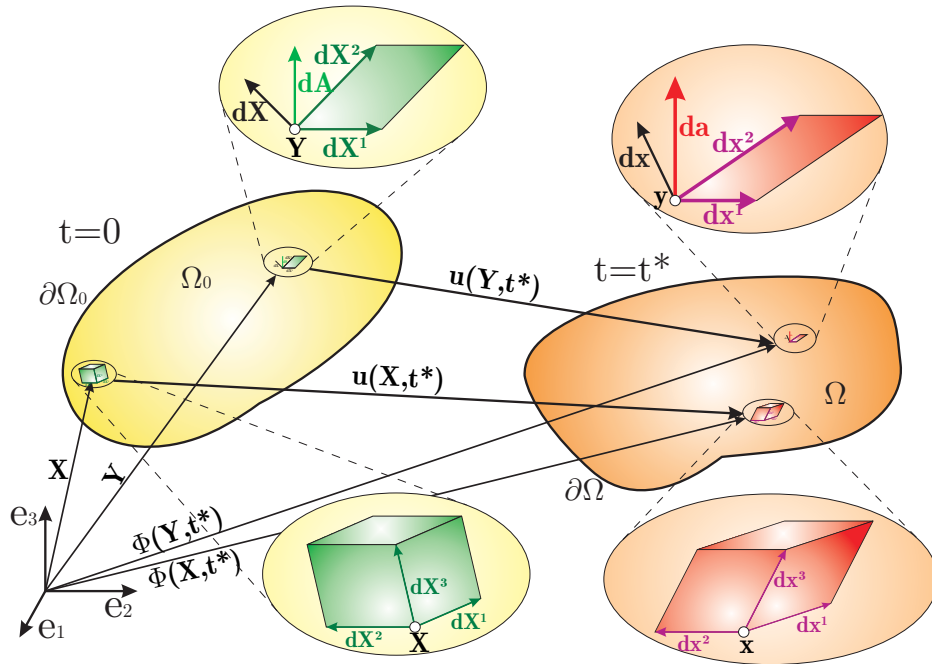
Figure 2.3.: Deformation of infinitesimal volume dV and surface dS elements

Let us consider three non-coplanar line elements $d\boldsymbol{X}^I$ in the reference configuration, Figure 2.3, and their mapped counterparts $d\boldsymbol{x}^I$ in the current configuration assuming in addition that both triads are positively oriented. They form the infinitesimal volume elements, whose volumes are

$$dV = d\boldsymbol{X}^1 \cdot (d\boldsymbol{X}^2 \times d\boldsymbol{X}^3) = \det \begin{bmatrix} d\boldsymbol{X}^1 & d\boldsymbol{X}^2 & d\boldsymbol{X}^3 \end{bmatrix}, \tag{2.22}$$

$$dv = d\boldsymbol{x}^1 \cdot (d\boldsymbol{x}^2 \times d\boldsymbol{x}^3) = \det \begin{bmatrix} d\boldsymbol{x}^1 & d\boldsymbol{x}^2 & d\boldsymbol{x}^3 \end{bmatrix}. \tag{2.23}$$

Taking the transformation relation (2.16) into consideration, the connection between the volume elements in the reference and in the current configuration is obtained

$$dv = \det \boldsymbol{F} dV = J \, dV. \tag{2.24}$$

The *Jacobi determinant* $J = \det \boldsymbol{F}$ is therefore the ratio of current to reference volume of a material volume element. This interpretation poses another strong requirement on deformation gradient $\boldsymbol{F}$. Namely, its determinant has to be strictly positive ($\det \boldsymbol{F} > 0$) in order to assure the impenetrability of matter (to prevent negative volumes).

In order to obtain the relation representing the mapping of the infinitesimal surface elements, two line elements $d\boldsymbol{X}^1$ and $d\boldsymbol{X}^2$ in the reference configuration are considered. They define a material surface element dA, with the associated surface vector

$$d\boldsymbol{A} = dA \, \boldsymbol{N}, \qquad \boldsymbol{N} = \frac{d\boldsymbol{X}^1 \times d\boldsymbol{X}^2}{\left\| d\boldsymbol{X}^1 \times d\boldsymbol{X}^2 \right\|}. \tag{2.25}$$

Material elements $d\boldsymbol{X}^1$ and $d\boldsymbol{X}^2$ map to the corresponding spatial elements $d\boldsymbol{x}^1$ and $d\boldsymbol{x}^2$ during a motion $\boldsymbol{\Phi}$, Figure 2.3. They form a spatial surface element da, with its associated surface vector

$$d\boldsymbol{a} = da \, \boldsymbol{n}, \qquad \boldsymbol{n} = \frac{d\boldsymbol{x}^1 \times d\boldsymbol{x}^2}{\left\| d\boldsymbol{x}^1 \times d\boldsymbol{x}^2 \right\|}. \tag{2.26}$$

Utilizing an additional reference vector $d\boldsymbol{X}$, non-coplanar with $d\boldsymbol{X}^1$ and $d\boldsymbol{X}^2$ but otherwise arbitrary, and its mapped counterpart $d\boldsymbol{x}$, one can connect the resulting infinitesimal volume elements via the relation (2.24)

$$dv = d\boldsymbol{a} \cdot d\boldsymbol{x} = J d\boldsymbol{A} \cdot d\boldsymbol{X}. \tag{2.27}$$

Substitution of (2.16) yields *Nanson's formula*

$$d\boldsymbol{a} = J \, \boldsymbol{F}^{-T} \cdot d\boldsymbol{A}, \tag{2.28}$$

which shows the relation between the elements of the infinitesimally small areas da and $d\boldsymbol{A}$ on the current and reference configuration.

2.1.4. Deformation measures

The deformation gradient is the fundamental kinematic tensor that characterizes changes of material elements. However, it is not the most suitable measure of the deformation, since it is not free from contribution of the rigid body motion. In general, a motion $\boldsymbol{\Phi}$ of a body will change its shape (form and size), position and orientation. Consider a pure change of the position (a so-called rigid-body translation), which can be represented by the mapping

$$\boldsymbol{x}(\boldsymbol{X}, t) = \boldsymbol{c}(t). \tag{2.29}$$

It is obvious that the deformation gradient $\boldsymbol{F}$ is not affected by it and is equal to the one of the undeformed state $\boldsymbol{F} = \mathbf{I}$. However, that is not the case with the change of orientation (a so-called rigid-body rotation) of a body. The mapping in this case reads

$$\boldsymbol{x}(\boldsymbol{X}, t) = \boldsymbol{Q}(t) \cdot \boldsymbol{X}, \tag{2.30}$$

with the tensor $\boldsymbol{Q}$ specified to be proper orthogonal. Clearly, the deformation gradient $\boldsymbol{F}$ is not equal to the one of the undeformed state. Hence, a rigid-body rotation does affect $\boldsymbol{F}$. In order to separate this influence from the part that comes from the pure deformation (change in lengths of linear elements and in angles between them), one can make use of the polar decomposition theorem, cf. Başar and Weichert (2000). It states that any second order tensor $\boldsymbol{F}$ can be split up multiplicatively into an arbitrary proper orthogonal tensor $\boldsymbol{R}$ and a positive definite second order tensor $\boldsymbol{U}$ or $\boldsymbol{V}$ of the form

$$\boldsymbol{F} = \boldsymbol{R} \cdot \boldsymbol{U} = \boldsymbol{V} \cdot \boldsymbol{R}. \tag{2.31}$$

The decomposition (2.31) is in general not unique. Its uniqueness is assured introducing the additional assumption that both $\boldsymbol{U}$ and $\boldsymbol{V}$ are symmetric

$$\boldsymbol{U} = \boldsymbol{U}^T, \qquad \boldsymbol{V} = \boldsymbol{V}^T. \tag{2.32}$$

These second order tensors are called the *right* and *left stretch tensor*, respectively. Due to the fact that the *rotation tensor* $\boldsymbol{R}$ is proper orthogonal

$$\boldsymbol{R} \cdot \boldsymbol{R}^T = \boldsymbol{R}^T \cdot \boldsymbol{R} = \mathbf{I}, \qquad \det \boldsymbol{R} = 1, \tag{2.33}$$

it follows that

$$\det \boldsymbol{F} = \det \boldsymbol{U} = \det \boldsymbol{V}. \tag{2.34}$$

The polar decomposition theorem may be illustrated graphically as shown in the Figure 2.4. It follows that the deformation of an infinitesimal volume element at $\boldsymbol{X}$ can be considered
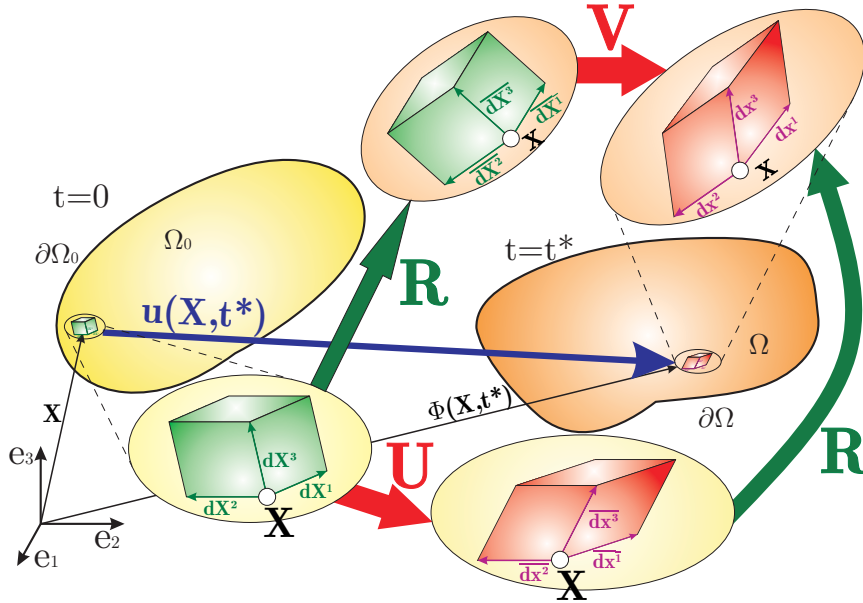
Figure 2.4.: Illustration of the polar decomposition $\boldsymbol{F} = \boldsymbol{R} \cdot \boldsymbol{U} = \boldsymbol{V} \cdot \boldsymbol{R}$

as the successive application of (cf. Başar and Weichert (2000)):

$\boldsymbol{F} = \boldsymbol{R} \cdot \boldsymbol{U}$		$\boldsymbol{F} = \boldsymbol{V} \cdot \boldsymbol{R}$	
a stretch by the tensor $\boldsymbol{U}$:	$\overline{d\boldsymbol{x}^i} = \boldsymbol{U} \cdot d\boldsymbol{X}^i$	*a translation by* $\boldsymbol{u}$:	$\boldsymbol{x} = \boldsymbol{X} + \boldsymbol{u}$
a rigid-body rotation by $\boldsymbol{R}$:	$d\boldsymbol{x}^i = \boldsymbol{R} \cdot \overline{d\boldsymbol{x}^i}$	*a rigid-body rotation by* $\boldsymbol{R}$:	$\overline{d\boldsymbol{X}^i} = \boldsymbol{R} \cdot d\boldsymbol{X}^i$
a translation by $\boldsymbol{u}$:	$\boldsymbol{x} = \boldsymbol{X} + \boldsymbol{u}$	*a stretch by the tensor* $\boldsymbol{V}$:	$d\boldsymbol{x}^i = \boldsymbol{V} \cdot \overline{d\boldsymbol{X}^i}$

Hence, the right stretch tensor U is a tensor of the reference configuration, while the left stretch tensor V belongs to the current configuration. They are related to each other through the relations

$$V = R \cdot U \cdot R^T, \qquad U = R^T \cdot V \cdot R. \tag{2.35}$$

Denoting the eigenvalues of U by λ_i and the corresponding orthonormal unit eigenvectors by N_i, tensor U can be represented through its spectral decomposition [1]

$$U = \sum_{i=1}^{3} \lambda_i \, N_i \otimes N_i. \tag{2.36}$$

From the relations (2.35) and (2.36) it follows that the left and the right stretch tensor U and V have the same eigenvalues λ_i (called *principal stretches*). The eigenvectors n_i of the tensor V in the current configuration (called *Eulerian principal axes*) are obtained by rotation of the corresponding eigenvectors N_i of the tensor U in the reference configuration (called *Lagrangian principal axes*)

$$V = \sum_{i=1}^{3} \lambda_i \, n_i \otimes n_i, \qquad n_i = R \cdot N_i. \tag{2.37}$$

Combining the spectral decomposition of the stretch tensors (2.36) and (2.37) with the definition of the polar decomposition of the deformation gradient (2.31), one obtains

$$F = \sum_{i=1}^{3} \lambda_i \, n_i \otimes N_i, \qquad R = \sum_{i=1}^{3} n_i \otimes N_i. \tag{2.38}$$

In general, one has to solve a system of 9 linear equations with 9 unknowns in order to find the components of the tensors R, U and V, which is a time consuming task. Therefore one introduces a so-called *deformation tensors* which describe deformations without being influenced by a pure rotation. In that purpose is the orthogonality condition of the rotation tensor $R^T = R^{-1}$ utilized

$$C := F^T \cdot F = (R \cdot U)^T \cdot R \cdot U = U^T \cdot R^T \cdot R \cdot U = U^2, \tag{2.39}$$

$$B := F \cdot F^T = V \cdot R \cdot (V \cdot R)^T = V \cdot R \cdot R^T \cdot V^T = V^2. \tag{2.40}$$

The tensors C and B are called the *right Cauchy-Green deformation tensor* and the *left Cauchy-Green deformation tensor*, respectively. The first one (C) is a tensor of the reference configuration, while the second one (B) belongs to the reference configuration. They are related by

$$C = F^{-1} \cdot B \cdot F, \qquad B = F \cdot C \cdot F^{-1}. \tag{2.41}$$

In view of (2.39) and (2.40) the spectral decomposition of the right and left Cauchy-Green deformation tensor reads

$$C = \sum_{i=1}^{3} \lambda_i^2 \, N_i \otimes N_i, \qquad B = \sum_{i=1}^{3} \lambda_i^2 \, n_i \otimes n_i. \tag{2.42}$$

Hence, the eigenvalues of the left and right Cauchy-Green tensor are equal to the squared eigenvalues of the left and right stretch tensor, respectively.

---

[1]For details on spectral decomposition of a second order tensor see the section A.3.2.
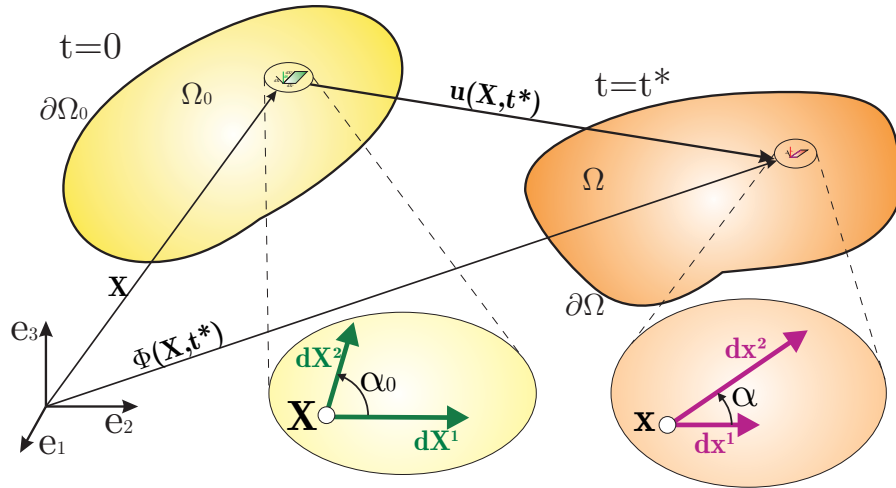
Figure 2.5.: Infinitesimal line elements in reference and current configuration

Let us consider two infinitesimal line elements $d\boldsymbol{X}^1$ and $d\boldsymbol{X}^2$ in the reference configuration, Figure 2.5. After the deformation they are mapped on the line elements $d\boldsymbol{x}^1$ and $d\boldsymbol{x}^2$ in the current configuration. The scalar products of those vectors are obtained as [2]

$$
\begin{aligned}
d\boldsymbol{x}^1 \cdot d\boldsymbol{x}^2 &= (\boldsymbol{F} \cdot d\boldsymbol{X}^1) \cdot (\boldsymbol{F} \cdot d\boldsymbol{X}^2) = d\boldsymbol{X}^1 \cdot (\boldsymbol{F}^T \cdot \boldsymbol{F}) \cdot d\boldsymbol{X}^2 \\
&= d\boldsymbol{X}^1 \cdot \boldsymbol{C} \cdot d\boldsymbol{X}^2, && (2.43) \\
d\boldsymbol{X}^1 \cdot d\boldsymbol{X}^2 &= (\boldsymbol{F}^{-1} \cdot d\boldsymbol{x}^1) \cdot (\boldsymbol{F}^{-1} \cdot d\boldsymbol{x}^2) = d\boldsymbol{x}^1 \cdot (\boldsymbol{F}^{-T} \cdot \boldsymbol{F}^{-1}) \cdot d\boldsymbol{x}^2 \\
&= d\boldsymbol{x}^1 \cdot \boldsymbol{B}^{-1} \cdot d\boldsymbol{x}^2. && (2.44)
\end{aligned}
$$

Therefore, one can utilize the right Cauchy-Green tensor $\boldsymbol{C}$ to express the scalar product of two line elements in the current configuration through the line elements of the reference configuration. In an analogous manner, the inverse of the left Cauchy-Green tensor ($\boldsymbol{B}^{-1}$) can be used to express the initial scalar product of two line elements identified in the current configuration.

2.1.5. Strain measures

With the introduction of the deformation tensors $\boldsymbol{C}$ and $\boldsymbol{B}$ is the influence of the rigid body rotation on the deformation efficiently removed. Let us consider a motion that maps an infinitesimal line element $d\boldsymbol{X}$ in the reference configuration on the line element $d\boldsymbol{x}$ in the current configuration. Squared norms of the corresponding vectors are evaluated utilizing the right and the left Cauchy-Green tensor and the relations (2.43) and (2.44) as

$$
ds^2 = d\boldsymbol{x} \cdot d\boldsymbol{x} = d\boldsymbol{X} \cdot \boldsymbol{C} \cdot d\boldsymbol{X}, \tag{2.45}
$$

$$
dS^2 = d\boldsymbol{X} \cdot d\boldsymbol{X} = d\boldsymbol{x} \cdot \boldsymbol{B}^{-1} \cdot d\boldsymbol{x}. \tag{2.46}
$$

---

[2] From the definition of the scalar product $\boldsymbol{a} \cdot \boldsymbol{b} = \|\boldsymbol{a}\| \, \|\boldsymbol{b}\| \, \cos(\sphericalangle(\boldsymbol{a}, \boldsymbol{b}))$ it follows that the difference in the scalar products of the reference vectors and that of the current vectors is affected by pure deformation (change of size and shape) only. Furthermore, by definition holds $\boldsymbol{a} \cdot \boldsymbol{b} = \boldsymbol{b} \cdot \boldsymbol{a}$

However, deformation tensors do not quantify the actual change in length of the line element under consideration. This change can be expressed in view of (2.45) and (2.46) in the following two forms

$$
\begin{aligned}
ds^2 - dS^2 &= d\boldsymbol{x} \cdot d\boldsymbol{x} - d\boldsymbol{X} \cdot d\boldsymbol{X} \\
&= d\boldsymbol{X} \cdot \boldsymbol{C} \cdot d\boldsymbol{X} - d\boldsymbol{X} \cdot \mathbf{I} \cdot d\boldsymbol{X} \\
&= d\boldsymbol{X} \cdot (\boldsymbol{C} - \mathbf{I}) \cdot d\boldsymbol{X},
\end{aligned}
\tag{2.47}
$$

$$
\begin{aligned}
ds^2 - dS^2 &= d\boldsymbol{x} \cdot d\boldsymbol{x} - d\boldsymbol{X} \cdot d\boldsymbol{X} \\
&= d\boldsymbol{x} \cdot \mathbf{I} \cdot d\boldsymbol{x} - d\boldsymbol{x} \cdot \boldsymbol{B}^{-1} \cdot d\boldsymbol{x} \\
&= d\boldsymbol{x} \cdot \left(\mathbf{I} - \boldsymbol{B}^{-1}\right) \cdot d\boldsymbol{x}.
\end{aligned}
\tag{2.48}
$$

From the above expressions one can define the so-called *Green-Lagrange strain tensor* $\boldsymbol{E}$ and the so-called *Almansi strain tensor* $\boldsymbol{e}$

$$
\boldsymbol{E} := \frac{1}{2}\left(\boldsymbol{C} - \mathbf{I}\right), \qquad \boldsymbol{e} := \frac{1}{2}\left(\mathbf{I} - \boldsymbol{B}^{-1}\right),
\tag{2.49}
$$

leading to

$$
ds^2 - dS^2 = d\boldsymbol{X} \cdot (2\,\boldsymbol{E}) \cdot d\boldsymbol{X} = d\boldsymbol{x} \cdot (2\,\boldsymbol{e}) \cdot d\boldsymbol{x}.
\tag{2.50}
$$

Thus, the *Green-Lagrange strain tensor* $\boldsymbol{E}$ gives the change in the squared length of the infinitesimal line element $d\boldsymbol{X}$ identified in the reference configuration Ω_0, while the *Almansi strain tensor* $\boldsymbol{e}$ permits to evaluate changes of length if an infinitesimal line element $d\boldsymbol{x}$ is identified in the current configuration Ω.[3] Both $\boldsymbol{E}$ and $\boldsymbol{e}$ are symmetric tensors, see (2.42) and (2.49), and both vanish in the undeformed state or for the rigid body motion, cf. Başar and Weichert (2000). They are related to each other by so-called *push-forward* ($\boldsymbol{E} \rightarrow \boldsymbol{e}$) and *pull-back* ($\boldsymbol{E} \leftarrow \boldsymbol{e}$) operations

$$
\boldsymbol{e} = \boldsymbol{F}^{-T} \cdot \boldsymbol{E} \cdot \boldsymbol{F}^{-1}, \qquad \boldsymbol{E} = \boldsymbol{F}^{T} \cdot \boldsymbol{e} \cdot \boldsymbol{F}.
\tag{2.51}
$$

Recalling the definition of the displacement vector (2.5) and the representation of the deformation gradient and its inverse in terms of displacement derivatives (2.20), Green-Lagrange and Almansi strain tensors can be expressed alternatively as

$$
\boldsymbol{E} = \frac{1}{2}\left(\frac{\partial \boldsymbol{u}}{\partial \boldsymbol{X}} + \left(\frac{\partial \boldsymbol{u}}{\partial \boldsymbol{X}}\right)^{T} + \left(\frac{\partial \boldsymbol{u}}{\partial \boldsymbol{X}}\right)^{T} \cdot \frac{\partial \boldsymbol{u}}{\partial \boldsymbol{X}}\right),
\tag{2.52}
$$

$$
\boldsymbol{e} = \frac{1}{2}\left(\frac{\partial \boldsymbol{u}}{\partial \boldsymbol{x}} + \left(\frac{\partial \boldsymbol{u}}{\partial \boldsymbol{x}}\right)^{T} - \left(\frac{\partial \boldsymbol{u}}{\partial \boldsymbol{x}}\right)^{T} \cdot \frac{\partial \boldsymbol{u}}{\partial \boldsymbol{x}}\right).
\tag{2.53}
$$

In index notation (2.52) and (2.53) read

$$
\boldsymbol{E} = \frac{1}{2}\left(\frac{\partial u_I}{\partial X_J} + \frac{\partial u_J}{\partial X_I} + \frac{\partial u_K}{\partial X_I}\frac{\partial u_K}{\partial X_J}\right)\boldsymbol{e}_I \otimes \boldsymbol{e}_J,
\tag{2.54}
$$

$$
\boldsymbol{e} = \frac{1}{2}\left(\frac{\partial u_i}{\partial x_j} + \frac{\partial u_j}{\partial x_i} - \frac{\partial u_k}{\partial x_i}\frac{\partial u_k}{\partial x_j}\right)\boldsymbol{e}_i \otimes \boldsymbol{e}_j.
\tag{2.55}
$$

---

[3]The scaling factor $\frac{1}{2}$ is introduced to maintain backward compatibility with the classical engineering definition of strain

2.1.6. Deformation and strain rates

Consider an infinitesimal oriented line element $d\boldsymbol{X}$, placed at a typical point P of the body $\mathcal{B}$ in the reference configuration Ω_0, Figure 2.6. During a motion $\boldsymbol{\Phi}(\boldsymbol{X},t)$ this line element is mapped onto a infinitesimal line element $d\boldsymbol{x}$ in the current configuration Ω by the deformation gradient $\boldsymbol{F}(\boldsymbol{X},t)$

$$d\boldsymbol{x} = \boldsymbol{F}(\boldsymbol{X},t) \cdot d\boldsymbol{X}. \tag{2.56}$$

Taking the material time derivative $(D(\cdot)/Dt$ at fixed $\boldsymbol{X})$ of this relation, one obtains the infinitesimal velocity change

$$d\boldsymbol{v} = \frac{D\boldsymbol{F}(\boldsymbol{X},t)}{Dt} \cdot d\boldsymbol{X} = \dot{\boldsymbol{F}}(\boldsymbol{X},t) \cdot d\boldsymbol{X}. \tag{2.57}$$

In view of (2.57), the material rate of the deformation gradient $\dot{\boldsymbol{F}}$ can be interpreted as a tensor that maps the line elements connecting two infinitesimally distant points P and Q in the reference configuration, Figure 2.6, on the relative velocity $d\boldsymbol{v}$ presenting the difference of the velocity vectors of these two points, cf. Başar and Weichert (2000). Therefore, the
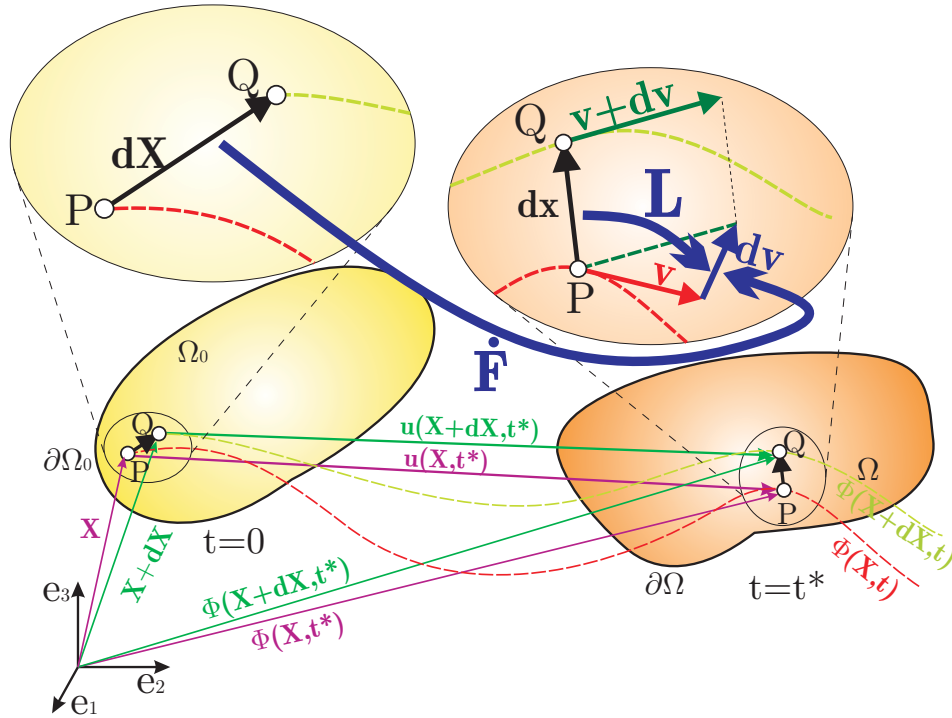
Figure 2.6.: Infinitesimal line elements in reference and current configuration

material rate of the deformation gradient $\dot{\boldsymbol{F}}$ at some instant of time is equal to the partial derivative of the velocity field with respect to the reference coordinates keeping the time fixed

$$\dot{\boldsymbol{F}} = \left.\frac{\partial \boldsymbol{v}(\boldsymbol{X},t)}{\partial \boldsymbol{X}}\right|_t = \frac{d\boldsymbol{v}}{d\boldsymbol{X}} \tag{2.58}$$

Using (2.57) and (2.56) one can relate the infinitesimal line element $d\boldsymbol{x}$ in the current configuration to the infinitesimal change in velocity vectors of its end points, Figure 2.6

$$d\boldsymbol{v} = \frac{D\boldsymbol{F}(\boldsymbol{X},t)}{Dt} \cdot d\boldsymbol{X} = \dot{\boldsymbol{F}}(\boldsymbol{X},t) \cdot \boldsymbol{F}^{-1}(\boldsymbol{x},t) \cdot d\boldsymbol{x} = \boldsymbol{L}(\boldsymbol{x},t) \cdot d\boldsymbol{x}, \tag{2.59}$$

through the so-called *spatial velocity gradient* $\boldsymbol{L}$. It is obtained by taking the partial derivative of the velocity field with respect to the current coordinates keeping the time fixed

$$\boldsymbol{L} := \dot{\boldsymbol{F}} \cdot \boldsymbol{F}^{-1} = \left.\frac{\partial \boldsymbol{v}(\boldsymbol{x}, t)}{\partial \boldsymbol{x}}\right|_t = \frac{d\boldsymbol{v}}{d\boldsymbol{x}}. \tag{2.60}$$

As a second order tensor the spatial velocity gradient $\boldsymbol{L}$ can be presented in the form

$$\boldsymbol{L} = \boldsymbol{D} + \boldsymbol{W} \tag{2.61}$$

as a sum of a symmetric tensor $\boldsymbol{D}$, called the *rate of deformation tensor* and a skew-symmetric $\boldsymbol{W}$, called the *spin tensor*

$$\boldsymbol{D} := \frac{1}{2}(\boldsymbol{L} + \boldsymbol{L}^T) = \frac{1}{2}\left(\frac{\partial \boldsymbol{v}}{\partial \boldsymbol{x}} + \left(\frac{\partial \boldsymbol{v}}{\partial \boldsymbol{x}}\right)^T\right), \tag{2.62}$$

$$\boldsymbol{W} := \frac{1}{2}(\boldsymbol{L} - \boldsymbol{L}^T) = \frac{1}{2}\left(\frac{\partial \boldsymbol{v}}{\partial \boldsymbol{x}} - \left(\frac{\partial \boldsymbol{v}}{\partial \boldsymbol{x}}\right)^T\right). \tag{2.63}$$

The material time derivative of the change in length of the infinitesimal line element undergoing a motion $\boldsymbol{\Phi}(\boldsymbol{X}, t)$ can be expressed in view of (2.50) as

$$\frac{D}{Dt}\left(ds^2 - dS^2\right) = 2\, d\boldsymbol{X} \cdot \dot{\boldsymbol{E}} \cdot d\boldsymbol{X}. \tag{2.64}$$

Alternatively, using the relations (2.50) and (2.59) it follows

$$\begin{aligned}
\frac{D}{Dt}\left(ds^2 - dS^2\right) &= 2\left(d\boldsymbol{v} \cdot \boldsymbol{e} \cdot d\boldsymbol{x} + d\boldsymbol{x} \cdot \dot{\boldsymbol{e}} \cdot d\boldsymbol{x} + d\boldsymbol{x} \cdot \boldsymbol{e} \cdot d\boldsymbol{v}\right) \\
&= 2\, d\boldsymbol{x} \cdot \left(\boldsymbol{L}^T \cdot \boldsymbol{e} + \dot{\boldsymbol{e}} + \boldsymbol{e} \cdot \boldsymbol{L}\right) \cdot d\boldsymbol{x}.
\end{aligned} \tag{2.65}$$

The connection between the material time derivative of the Green-Lagrange strain tensor $\dot{\boldsymbol{E}}$ and the rate of deformation tensor $\boldsymbol{D}$ can be deduced from the definitions (2.49), (2.39), (2.60) and (2.62) as

$$\dot{\boldsymbol{E}} = \boldsymbol{F}^T \cdot \boldsymbol{D} \cdot \boldsymbol{F}, \qquad \boldsymbol{D} = \boldsymbol{F}^{-T} \cdot \dot{\boldsymbol{E}} \cdot \boldsymbol{F}^{-1}. \tag{2.66}$$

In order to establish the connection between the material time derivative of the Almansi strain tensor $\dot{\boldsymbol{e}}$ and the rate of deformation tensor $\boldsymbol{D}$, one forms the material time derivative of the squared length of the infinitesimal line element in the current configuration

$$\frac{D}{Dt}\left(ds^2\right) = 2\, d\boldsymbol{x} \cdot d\boldsymbol{v} = 2\, d\boldsymbol{x} \cdot \boldsymbol{L} \cdot d\boldsymbol{x} = 2\, d\boldsymbol{x} \cdot \boldsymbol{D} \cdot d\boldsymbol{x}. \tag{2.67}$$

In view of this result and using the fact that the length of the line element in the reference configuration remains constant during deformation, consideration of (2.65) leads to

$$\boldsymbol{D} = \boldsymbol{L}^T \cdot \boldsymbol{e} + \dot{\boldsymbol{e}} + \boldsymbol{e} \cdot \boldsymbol{L}, \qquad \dot{\boldsymbol{e}} = \boldsymbol{D} - \boldsymbol{L}^T \cdot \boldsymbol{e} - \boldsymbol{e} \cdot \boldsymbol{L}. \tag{2.68}$$

The term on the right-hand side of the first equation is defined as the so-called *Lie-derivative* of the Almansi strain tensor and is usually denoted as $\mathrm{L_v}$

$$\mathrm{L_v}\, \boldsymbol{e} := \boldsymbol{L}^T \cdot \boldsymbol{e} + \dot{\boldsymbol{e}} + \boldsymbol{e} \cdot \boldsymbol{L} = \boldsymbol{D}. \tag{2.69}$$

Recalling the definition of the displacement (2.5) the velocity vector (2.6) and the representation of the Green-Lagrange and Almansi strain tensor in terms of displacement derivatives (2.20), the rate of the Green-Lagrange strain tensor can be expressed alternatively as

$$\dot{\boldsymbol{E}} = \frac{1}{2} \left(\frac{\partial \boldsymbol{v}}{\partial \boldsymbol{X}} + \left(\frac{\partial \boldsymbol{v}}{\partial \boldsymbol{X}} \right)^T + \left(\frac{\partial \boldsymbol{v}}{\partial \boldsymbol{X}} \right)^T \cdot \frac{\partial \boldsymbol{u}}{\partial \boldsymbol{X}} + \left(\frac{\partial \boldsymbol{u}}{\partial \boldsymbol{X}} \right)^T \cdot \frac{\partial \boldsymbol{v}}{\partial \boldsymbol{X}} \right). \tag{2.70}$$

In index notation (2.70) reads

$$\dot{\boldsymbol{E}} = \frac{1}{2} \left(\frac{\partial v_I}{\partial X_J} + \frac{\partial v_J}{\partial X_I} + 2 \frac{\partial v_K}{\partial X_I} \frac{\partial u_K}{\partial X_J} \right) \boldsymbol{e}_I \otimes \boldsymbol{e}_J, \tag{2.71}$$

Before proceeding, the relations for the material time derivatives of the surface and volume elements have to be specified, in which purpose one considers the derivative of the volume ratio $J = \det \boldsymbol{F}$

$$\frac{D}{Dt}(J) = \dot{J} = \frac{\partial J}{\partial \boldsymbol{F}} : \dot{\boldsymbol{F}} = J \, \boldsymbol{F}^{-T} : (\boldsymbol{L} \cdot \boldsymbol{F}) = J \operatorname{tr} \boldsymbol{L}. \tag{2.72}$$

Using the definition of tensor $\boldsymbol{L}$ (2.60) and its additive split (2.61), we deduce from (2.72)

$$\dot{J} = J \operatorname{tr} \boldsymbol{D} = J \operatorname{div} \boldsymbol{v} = J \frac{\partial v_i}{\partial x_i} \tag{2.73}$$

Since from (2.27)

$$d\dot{v} = \dot{J} \, dV = \dot{J} \, J^{-1} \, dv, \tag{2.74}$$

the material time derivative of the volume element is in view of (2.73)

$$d\dot{v} = \operatorname{div} \boldsymbol{v} \, dv = \operatorname{tr} \boldsymbol{D} \, dv, \tag{2.75}$$

Finally, recalling the Nanson's formula (2.28), the definitions of surface vectors (2.25) and (2.26), and utilizing the time derivative of the Jacobian (2.73), after some manipulation one obtains the material time derivative of the infinitesimal area element, cf. Başar and Weichert (2000)

$$d\dot{a} = \left(\dot{J} \, \boldsymbol{n} \cdot \boldsymbol{F}^{-T} \cdot \boldsymbol{N} + J \, \boldsymbol{n} \cdot \overline{(\boldsymbol{F}^{-T})} \cdot \boldsymbol{N} \right) dA = (\operatorname{tr} \boldsymbol{D} - \boldsymbol{n} \cdot \boldsymbol{D} \cdot \boldsymbol{n}) \, da. \tag{2.76}$$

2.1.7. Linearization of strain measures and strain rates

Throughout this section it is shown how to express the strain and deformation measures, as well as rates of strain and some important deformation quantities (e.g. Jacobi determinant) in terms of the displacement field and its space and time derivatives. In this thesis it is assumed that displacements remain small, which allows for simplification of the relations obtained so far. In that purpose, let us consider the displacement state $\boldsymbol{u}(\boldsymbol{X}, t) = \boldsymbol{u}(\boldsymbol{x}, t) = \boldsymbol{u}_0$ at certain time $t = t^*$. Denoting the displacement increment $\Delta \boldsymbol{u}$, one can perform linearization of all deformation-dependent quantities about the displacement state $\boldsymbol{u}_0$ using the so-called

Gâteaux-derivative [4]. We start from the relation (2.20) connecting the deformation gradient $\boldsymbol{F}$ to the material gradient of the displacement field, which leads to

$$\mathcal{L}\boldsymbol{F} = \boldsymbol{F}_0 + D\boldsymbol{F}(\boldsymbol{u})(\Delta\boldsymbol{u}) = \boldsymbol{F}_0 + \frac{\partial\Delta\boldsymbol{u}}{\partial\boldsymbol{X}} \ . \tag{2.77}$$

In view of the definitions of the Green-Lagrange strain tensor $\boldsymbol{E}$ (2.52) and the Almansi strain tensor $\boldsymbol{e}$ (2.53), one obtains

$$
\begin{aligned}
\mathcal{L}\boldsymbol{E} &= \boldsymbol{E}_0 + D\boldsymbol{E}(\boldsymbol{u})(\Delta\boldsymbol{u}) \\
&= \boldsymbol{E}_0 + \frac{1}{2}\left(\frac{\partial\Delta\boldsymbol{u}}{\partial\boldsymbol{X}} + \left(\frac{\partial\Delta\boldsymbol{u}}{\partial\boldsymbol{X}}\right)^T + \frac{\partial\Delta\boldsymbol{u}}{\partial\boldsymbol{X}}\cdot\left(\frac{\partial\boldsymbol{u}_0}{\partial\boldsymbol{X}}\right)^T + \left(\frac{\partial\Delta\boldsymbol{u}}{\partial\boldsymbol{X}}\right)^T\cdot\frac{\partial\boldsymbol{u}_0}{\partial\boldsymbol{X}}\right), \tag{2.78} \\
\mathcal{L}\boldsymbol{e} &= \boldsymbol{e}_0 + D\boldsymbol{e}(\boldsymbol{u})(\Delta\boldsymbol{u}) \\
&= \boldsymbol{e}_0 + \frac{1}{2}\left(\frac{\partial\Delta\boldsymbol{u}}{\partial\boldsymbol{x}} + \left(\frac{\partial\Delta\boldsymbol{u}}{\partial\boldsymbol{x}}\right)^T - \frac{\partial\Delta\boldsymbol{u}}{\partial\boldsymbol{x}}\cdot\left(\frac{\partial\boldsymbol{u}_0}{\partial\boldsymbol{x}}\right)^T - \left(\frac{\partial\Delta\boldsymbol{u}}{\partial\boldsymbol{x}}\right)^T\cdot\frac{\partial\boldsymbol{u}_0}{\partial\boldsymbol{x}}\right). \tag{2.79}
\end{aligned}
$$

Furthermore, the Jacobi determinant, which is an important quantity relating a deformed volume element to the undeformed one, see (2.24), is linearized as well. From its definition $J := \det \boldsymbol{F}$ it follows

$$
\begin{aligned}
\mathcal{L}J &= J_0 + DJ(\boldsymbol{u})(\Delta\boldsymbol{u}) = J_0 + J\,\boldsymbol{F}^{-T} : D\boldsymbol{F}(\boldsymbol{u})(\Delta\boldsymbol{u}) \\
&= J_0 + J_0\,\boldsymbol{F}^{-T} : \frac{\partial\Delta\boldsymbol{u}}{\partial\boldsymbol{X}} = J_0 + J_0\,\boldsymbol{F}^{-T} : \left(\frac{\partial\Delta\boldsymbol{u}}{\partial\boldsymbol{x}}\cdot\boldsymbol{F}\right) \\
&= J_0 + J_0\,\mathrm{div}\,\boldsymbol{u} = J_0\left(1 + \frac{\partial\Delta u_i}{\partial x_i}\right). \tag{2.80}
\end{aligned}
$$

Assuming that the linearization is performed around the reference (undeformed) state ($\boldsymbol{u}_0 = \boldsymbol{0}$), the displacement increment becomes equal to the displacement itself $\boldsymbol{u} = \Delta\boldsymbol{u}$. The initial values of the quantities under consideration are therefore

$$\boldsymbol{F}_0 = \mathbf{I}, \quad \boldsymbol{E}_0 = \boldsymbol{0}, \quad \boldsymbol{e}_0 = \boldsymbol{0}, \quad J_0 = 1. \tag{2.81}$$

An additional assumption that the displacement remains small has to be introduced in order to ensure satisfactory approximation of the original quantities by the linearized ones. In view of (2.5), this assumption leads further to the conclusion that $\boldsymbol{x} \approx \boldsymbol{X}$. Hence, the initial configuration Ω_0 of the body $\mathcal{B}$ can be considered coincident with the current configuration Ω. In this case we speak of the *geometrically linear theory*, or the *theory of small strains*. The linearized deformation gradient reads

$$\mathcal{L}\boldsymbol{F} = \mathbf{I} + \frac{\partial\boldsymbol{u}}{\partial\boldsymbol{X}}, \tag{2.82}$$

which is identical to the definition of the deformation gradient in terms of the displacement field (2.20) due to the fact that $\boldsymbol{F}$ is already linear in the displacement gradient. This result is given just for the sake of completeness, since the deformation gradient is in the theory of small strains not explicitly used. The main role in the small-strain theory plays the linearized

---

[4]For details on linearization and the *Gâteaux-derivative* see the section A.1.

strain tensor ε, obtained by linearization of either Green-Lagrange or Almansi strain tensor under adopted assumptions

$$\varepsilon := \mathcal{L}E = \mathcal{L}e = \frac{1}{2}\left(\frac{\partial \boldsymbol{u}}{\partial \boldsymbol{X}} + \left(\frac{\partial \boldsymbol{u}}{\partial \boldsymbol{X}}\right)^T\right) = \frac{1}{2}\left(\frac{\partial u_i}{\partial X_j} + \frac{\partial u_j}{\partial X_i}\right)\boldsymbol{e}_i \otimes \boldsymbol{e}_j. \tag{2.83}$$

Denoting for notational convenience

$$\nabla \boldsymbol{u} = \frac{\partial \boldsymbol{u}}{\partial \boldsymbol{X}} = \frac{\partial u_i}{\partial X_j}\boldsymbol{e}_i \otimes \boldsymbol{e}_j, \tag{2.84}$$

the definition of the linearized strain tensor (in further discussion just called the *strain tensor*) can be written as

$$\varepsilon = \mathcal{L}E = \mathcal{L}e = \frac{1}{2}\left(\nabla \boldsymbol{u} + (\nabla \boldsymbol{u})^T\right) \tag{2.85}$$

The linearized Jacobi determinant (2.80) attains, in view of the introduced assumptions, the following form

$$\mathcal{L}J = 1 + \operatorname{div}\boldsymbol{u} = \left(1 + \frac{\partial u_i}{\partial X_i}\right) = 1 + \operatorname{tr}\varepsilon. \tag{2.86}$$

The adopted assumption of small displacements allows for linerization of the rate quantities around the undeformed state, and in that purpose one starts by considering the material rate of the deformation gradient $\dot{\boldsymbol{F}}$ (2.58) and the spatial velocity gradient $\boldsymbol{L}$ (2.60). Since the initial configuration Ω_0 of the body $\mathcal{B}$ can be considered coincident with the current configuration Ω, it follows

$$\mathcal{L}\dot{\boldsymbol{F}} = \mathcal{L}\boldsymbol{L} = \frac{\partial \boldsymbol{v}}{\partial \boldsymbol{X}}. \tag{2.87}$$

Denoting for notational convenience

$$\nabla \boldsymbol{v} = \frac{\partial \boldsymbol{v}}{\partial \boldsymbol{X}} = \frac{\partial v_i}{\partial X_j}\boldsymbol{e}_i \otimes \boldsymbol{e}_j = \frac{\partial \dot{u}_i}{\partial X_j}\boldsymbol{e}_i \otimes \boldsymbol{e}_j, \tag{2.88}$$

the rate of deformation tensor $\boldsymbol{D}$ and the spin tensor $\boldsymbol{W}$ can be expressed as

$$\mathcal{L}\boldsymbol{D} = \boldsymbol{D} = \frac{1}{2}\left(\frac{\partial \boldsymbol{v}}{\partial \boldsymbol{X}} + \left(\frac{\partial \boldsymbol{v}}{\partial \boldsymbol{X}}\right)^T\right) = \frac{1}{2}\left(\frac{\partial \dot{u}_i}{\partial X_j} + \frac{\partial \dot{u}_j}{\partial X_i}\right)\boldsymbol{e}_i \otimes \boldsymbol{e}_j \tag{2.89}$$

$$\mathcal{L}\boldsymbol{W} = \boldsymbol{W} = \frac{1}{2}\left(\frac{\partial \boldsymbol{v}}{\partial \boldsymbol{X}} - \left(\frac{\partial \boldsymbol{v}}{\partial \boldsymbol{X}}\right)^T\right) = \frac{1}{2}\left(\frac{\partial \dot{u}_i}{\partial X_j} - \frac{\partial \dot{u}_j}{\partial X_i}\right)\boldsymbol{e}_i \otimes \boldsymbol{e}_j \tag{2.90}$$

Linearization of the rate of the Green-Lagrange strain tensor (2.70) about the reference state results in

$$\mathcal{L}\dot{\boldsymbol{E}} = \frac{1}{2}\left(\frac{\partial \boldsymbol{v}}{\partial \boldsymbol{X}} + \left(\frac{\partial \boldsymbol{v}}{\partial \boldsymbol{X}}\right)^T\right) = \frac{1}{2}\left(\nabla \dot{\boldsymbol{u}} + (\nabla \dot{\boldsymbol{u}})^T\right) = \dot{\varepsilon}. \tag{2.91}$$

In index notation (2.91) reads

$$\dot{\varepsilon} = \frac{1}{2}\left(\frac{\partial \dot{u}_i}{\partial X_j} + \frac{\partial \dot{u}_j}{\partial X_i}\right)\boldsymbol{e}_i \otimes \boldsymbol{e}_j, \tag{2.92}$$

which in view of (2.89) leads to the conclusion that in the small-strain theory the rate of the Green-Lagrange strain $\dot{\boldsymbol{E}}$ coincide with the Lie-derivative of the Almansi tensor $\mathrm{L_v}\,\boldsymbol{e}$. The rate of the deformation tensor becomes therefore simply the strain rate

$$\dot{\boldsymbol{\varepsilon}} = \boldsymbol{D}. \tag{2.93}$$

Finally, the time derivatives of the surface and volume elements should be specified. In that purpose one considers first the linearization of the material time derivative of Jacobi determinant (2.72) and (2.73), which in view of (2.81) results in

$$\mathcal{L}\dot{J} = \operatorname{tr}\boldsymbol{D} = \operatorname{tr}\dot{\boldsymbol{\varepsilon}}. \tag{2.94}$$

With this result at hands, one obtains from (2.74), (2.75) and (2.76) the linearized rates of change of volume $\dot{v}$ and surface $\dot{a}$ elements

$$\mathcal{L}d\dot{v} = \operatorname{tr}\dot{\boldsymbol{\varepsilon}}, \qquad \mathcal{L}d\dot{a} = (\operatorname{tr}\dot{\boldsymbol{\varepsilon}} - \boldsymbol{n}\cdot\dot{\boldsymbol{\varepsilon}}\cdot\boldsymbol{n}) = \dot{\boldsymbol{\varepsilon}} \,:\, (\mathbf{I} - \boldsymbol{n}\otimes\boldsymbol{n})\,. \tag{2.95}$$

2.2. Kinetics

In this section the relation between external and internal forces acting on a material body is described. Motion and deformation give rise to internal interactions between adjacent material particles in the interior part of the body. These interactions are reflected by the notion of stress, which is a measure of local internal forces. Together with the static and dynamic loads acting throughout the volume, these stresses form the local equilibrium of forces. This equilibrium must be satisfied throughout the current configuration Ω of the material body $\mathcal{B}$. However, in the context of the geometrically linear theory, which is used in this thesis, the current configuration coincides with the reference one Ω_0.

2.2.1. Cauchy stress tensor and Cauchy theorem
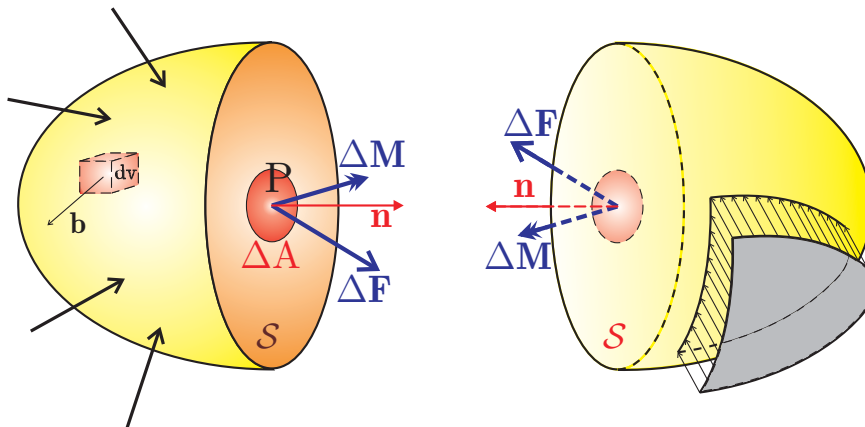
Figure 2.7.: Infinitesimal line elements in reference and current configuration

Let us consider an arbitrary typical point P inside the body in its deformed state. The body $\mathcal{B}$ is separated into two parts by a surface passing through P with the unit normal vector $\boldsymbol{n}$. The interaction between the two portions leads to the forces that are transmitted across the

surface. Taking a surface element ΔA in the vicinity of P, the resulting internal force and moment acting on the element are denoted as $\Delta\boldsymbol{F}$ and $\Delta\boldsymbol{M}$. Through the limit $\Delta A \to 0$ are the so-called *stress vector* $\mathbf{t}_n$ and the so-called *stress couple* $\mathbf{c}_n$

$$\lim_{\Delta A \to 0} \frac{\Delta\boldsymbol{F}}{\Delta A} = \frac{d\boldsymbol{F}}{dA} = \boldsymbol{t}_n, \qquad \lim_{\Delta A \to 0} \frac{\Delta\boldsymbol{M}}{\Delta A} = \frac{d\boldsymbol{M}}{dA} = \boldsymbol{c}_n \qquad (2.96)$$

defined. In the classical continuum mechanics theory, which is followed here, it is assumed that the stress-couple vanishes $\boldsymbol{c}_n = \boldsymbol{0}$ [5] . Hence, the action of one body on another across an infinitesimal surface area dA is adequately represented by a stress vector $\boldsymbol{t}_n$. The stress vector can be split in two parts: one in the direction of the surface normal $\boldsymbol{n}$ (called *normal stress*) and one being a projection of the stress vector onto the surface plane (called *shear* or *tangential stress*). Denoting as $\boldsymbol{t}_i$ the stress vector acting on the surface whose normal $\boldsymbol{n}$ is aligned with one of the basis vectors $\boldsymbol{e}_i$, its components are

$$\boldsymbol{t}_i = \sigma_{i1}\,\boldsymbol{e}_1 + \sigma_{i2}\,\boldsymbol{e}_2 + \sigma_{i3}\,\boldsymbol{e}_3 \qquad (2.97)$$

Let us separate at some point an infinitesimal tetrahedron (Figure 2.8) bounded by the
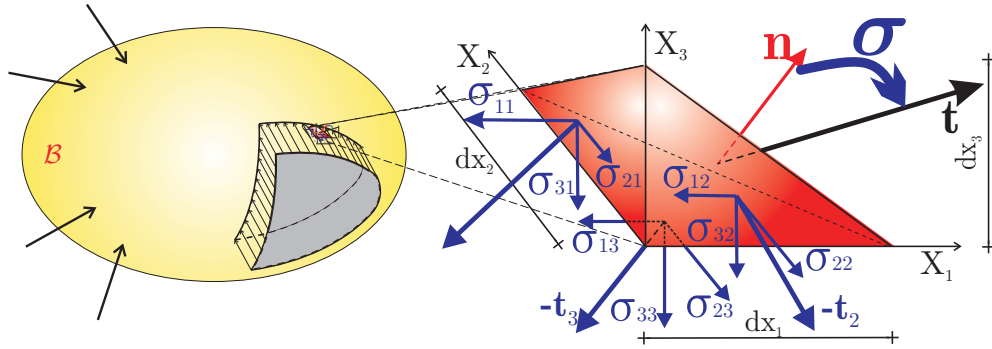
Figure 2.8.: Equilibrium of infinitesimal tetrahedron

surfaces $X_i = const$, $i = 1, 2, 3$ and a given surface whose unit normal vector is

$$\boldsymbol{n} = n_i\,\boldsymbol{e}_i. \qquad (2.98)$$

The faces $X_i = const$ of the tetrahedron have the areas $1/2\,dA_i$, and the surface with the unit normal $\boldsymbol{n}$ the area $1/2\,dA$, which are related in component form by $n_i\,dA = dA_i$, cf. Başar and Weichert (2000). The equilibrium of the infinitesimal tetrahedron is described by

$$\boldsymbol{t}\,dA = \sum_{i=1}^{3} \boldsymbol{t}_i\,dA_i = \boldsymbol{t}_i\,n_i\,dA, \qquad (2.99)$$

which leads with (2.97) to

$$\boldsymbol{t} = \boldsymbol{t}_j\,n_j = \sigma_{ij}\,n_j\,\boldsymbol{e}_i. \qquad (2.100)$$

Defining the so-called *Cauchy stress tensor* $\boldsymbol{\sigma}$ as

$$\boldsymbol{\sigma} = \boldsymbol{t}_i \otimes \boldsymbol{e}_i = \sigma_{ij}\,\boldsymbol{e}_i \otimes \boldsymbol{e}_j, \qquad (2.101)$$

---

[5]This assumption is not followed in th co-called *Coserat* theory, which includes rotations as additional variables, see e.g. Cosserat and Cosserat (1909); Eringen (1999)

the equilibrium of the infinitesimal tetrahedron (2.100) results in

$$t = \boldsymbol{\sigma} \cdot \boldsymbol{n}. \tag{2.102}$$

This result is known as *Cauchy theorem* and it states that the Cauchy stress $\boldsymbol{\sigma}$ is a tensor that maps the unit normal vector field $\boldsymbol{n}$ of an arbitrary surface onto the stress vector field $\boldsymbol{t}$ acting on that surface, Figure 2.8.

Consider again the split of the stress vector $\boldsymbol{t}$ acting on the an infinitesimal surface area dA into a component in the direction of the surface normal $\boldsymbol{n}$ (called *normal stress* and denoted σ) and a component being a projection of the stress vector onto the surface plane (called *shear stress* and denoted τ). These components can be obtained from the stress tensor by means of the projection tensors, cf. Holzapfel (2000), Brannon (2003)

$$\boldsymbol{P}_{\perp} = \boldsymbol{n} \otimes \boldsymbol{n}, \qquad \boldsymbol{P}_{\|} = \mathbf{I} - \boldsymbol{n} \otimes \boldsymbol{n}, \tag{2.103}$$

in the form

$$\sigma = \boldsymbol{\sigma} : \boldsymbol{P}_{\perp}, \qquad \tau = \boldsymbol{\sigma} : \boldsymbol{P}_{\|}. \tag{2.104}$$

If $\sigma > 0$ normal stresses are said to be *tensile*, while negative normal stresses $\sigma < 0$ are known as *compressive*. Those two types of loading are fundamentally different and in a lot of materials they cause different behavior. In contrary to that, the sign of a shear stress has no intrinsic physical meaning, the type of loading is the same.

2.2.2. Equilibrium conditions of an infinitesimal volume element

Consider an infinitesimal hexahedron whose faces are defined by normal vectors aligned with the basis vectors $\boldsymbol{e}_i$ and their negative counterparts $-\boldsymbol{e}_i$, Figure 2.9. The forces acting on a body can be deformation independent volume specific loads $\rho \, \boldsymbol{b}$, inertial forces $-\rho \, \ddot{\boldsymbol{u}}$ and the forces resulting from stress. The first two are both volume-specific loads, so that one can put them together into the volume load $\boldsymbol{f}$

$$\boldsymbol{f} = \rho \, \boldsymbol{b} - \rho \, \ddot{\boldsymbol{u}}, \tag{2.105}$$

acting in the center of the volume element. At the boundaries of the volume element the stress tensor maps the surface normals onto the stress vectors. Hence, stress components with the corresponding area elements contribute to the force equilibrium. The differential changes in the stress components and stress vectors, denoted as $d\sigma_{ij}$ and $d\boldsymbol{t}_i$ in Figure 2.9, are obtained as

$$d\sigma_{(ij)} = \frac{\partial \sigma_{(ij)}}{\partial X_{(j)}} \, dX_{(j)}, \qquad d\boldsymbol{t}_{(i)} = \frac{\partial \boldsymbol{t}_{(i)}}{\partial X_{(i)}} \, dX_{(i)} \qquad \text{(no summation)}. \tag{2.106}$$

The force equilibrium in the directions of base vectors results in

$$\operatorname{div} \boldsymbol{\sigma} + \boldsymbol{f} = \boldsymbol{0} \qquad \Rightarrow \qquad \frac{\partial \sigma_{ij}}{\partial X_j} + f_i = 0. \tag{2.107}$$

The moment equilibrium about the center of the infinitesimal hexahedron leads to the conclusion that the Cauchy stress tensor $\boldsymbol{\sigma}$ has to be symmetric

$$\boldsymbol{\sigma} = \sigma_{ij} \, \boldsymbol{e}_i \otimes \boldsymbol{e}_j \qquad \text{with} \ \ \sigma_{ij} = \sigma_{ji}. \tag{2.108}$$
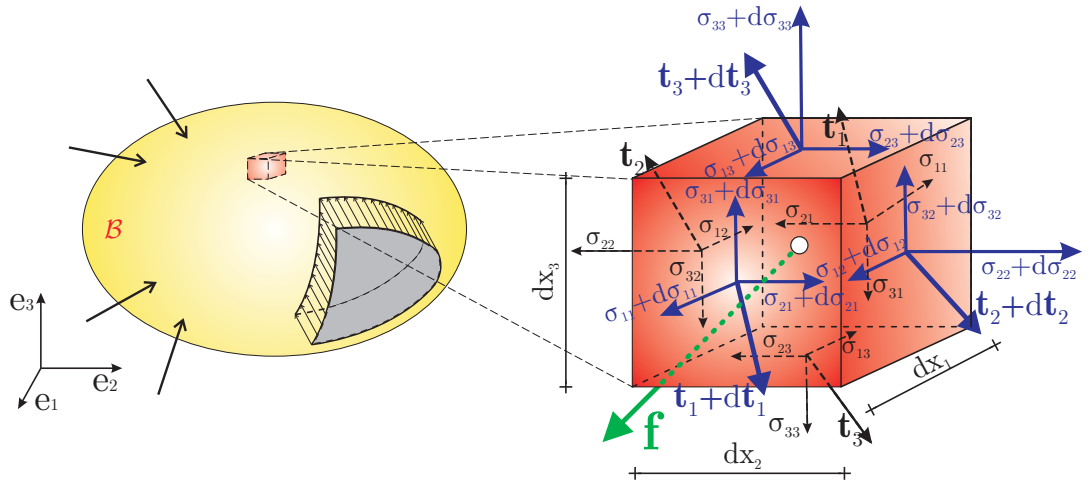
Figure 2.9.: Representation of infinitesimal equilibrium conditions

2.3. Balance laws

In this section is an overview on the balance relations of continuum thermodynamics provided. Physical quantities such as mass, momentum, energy and entropy can be exchanged between a thermodynamic system and its environment, which is mathematically described by thermodynamical balance relations. Balance relations for quantities that do not change within the thermodynamic system (denoted as *conservative quantities*), such are mass and energy, are named conservation laws. A detailed review on this subject can be found in Holzapfel (2000); Šilhavý (1996); Truesdell and Noll (2004).

2.3.1. Conservation of mass

Consider a continuum body $\mathcal{B}$, with the amount of material contained in it measured by a physical quantity called mass and denoted m. The mass m is a positive scalar measure which is invariant during a motion. Assuming that there are neither mass sources nor mass sinks within the system and that there is no mass exchange with the environment (closed system), the law of conservation of mass states that the mass of a body remains constant during the motion

$$\dot{m} = 0. \tag{2.109}$$

If ρ is a mass density of the body in the current configuration Ω, then its total mass in the current state is

$$m(t) = \int_\Omega \rho(\boldsymbol{x}, t) dv. \tag{2.110}$$

Recalling the connection between the volume elements in the reference and in the current configuration (2.24)

$$\dot{m} = \frac{D}{Dt} \int_{\Omega_0} \rho(\boldsymbol{x}, t) \, J \, dV = \int_{\Omega_0} (\dot{\rho} + \rho \, \operatorname{div} \boldsymbol{v}) \, J \, dV = 0, \tag{2.111}$$

in view of the relation (2.73) for the time derivative of the Jacobi determinant, it follows

$$\dot{m} = \int_{\Omega} \left(\dot{\rho} + \rho \, \frac{\partial v_i}{\partial x_i} \right) \, dv = \int_{\Omega} (\dot{\rho} + \rho \, \operatorname{tr} \boldsymbol{D}) \, dv = 0 \qquad (2.112)$$

This statement has to hold for every subdomain $\bar{\Omega} \in \Omega$ as well. Hence, the conservation of mass (2.112) can be expressed in the local form as

$$\dot{\rho} + \rho \, \operatorname{div} \boldsymbol{v} = \dot{\rho} + \rho \, \operatorname{tr} \boldsymbol{D} = 0 \qquad (2.113)$$

From the relations (2.109) and (2.110) an alternative form of the conservation condition can be deduced, cf. Başar and Weichert (2000)

$$\rho_0 \, dV = \rho \, dv, \qquad (2.114)$$

where $\rho_0(\boldsymbol{X})$ stands for the mass density of the reference configuration Ω_0.

Within the framework of the small deformation theory, which is assumed to sufficiently accurately describe problems dealt with throughout this thesis, one uses linearized relations presented in the section 2.1.7. In view of (2.94) and (2.95) the conservation condition (2.114) attains the form

$$\dot{\rho} + \rho \, \operatorname{tr} \dot{\boldsymbol{\varepsilon}} = 0 \qquad (2.115)$$

2.3.2. Balance of linear momentum

Consider a body $\mathcal{B}$ occupying a region Ω with boundary surface $\partial\Omega$ at time t. The body is subjected to volume forces $\boldsymbol{b}$ measured per unit mass and the surface forces $\boldsymbol{t}$ acting upon the boundary surface a with the outward normal vector $\boldsymbol{n}$ in its current state, Figure 2.10. It
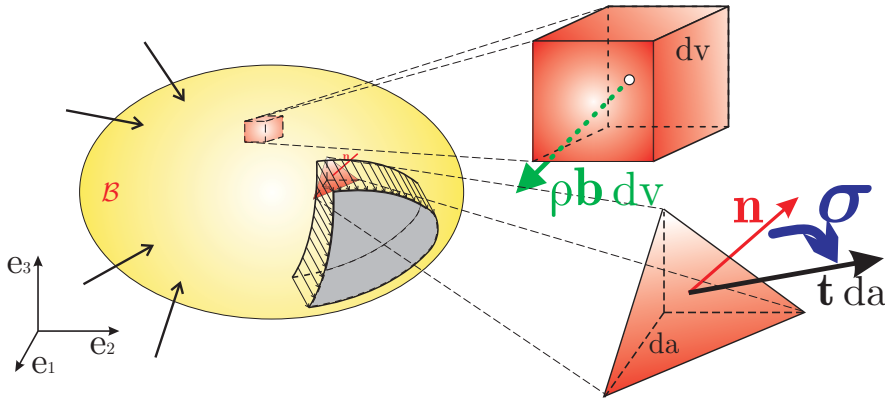
Figure 2.10.: Forces acting on a body $\mathcal{B}$

is assumed that the body is a closed system (no exchange of mass with the surroundings). The total *linear* (*translational*) *momentum* is defined by

$$\mathfrak{L} := \int_{\Omega} \rho \, \boldsymbol{v} \, dv, \qquad (2.116)$$

and the resultant external force applied on the body is described by

$$\boldsymbol{F} := \boldsymbol{F}_b + \boldsymbol{F}_t = \int_{\Omega} \rho \, \boldsymbol{b} \, dv + \int_{\partial\Omega} \boldsymbol{t} \, da. \qquad (2.117)$$

The *balance of linear momentum* states that the change of the total momentum $\mathfrak{L}$ is balanced by the external forces $\boldsymbol{F}$ acting on the body (consisting of volume forces $\boldsymbol{F}_b$ and surface forces $\boldsymbol{F}_t$)

$$\dot{\mathfrak{L}} = \boldsymbol{F}. \tag{2.118}$$

This postulate can be expressed in view of (2.116) and (2.117) as

$$\frac{D}{Dt} \int_{\Omega} \rho \, \boldsymbol{v} \, dv = \int_{\Omega} \rho \, \boldsymbol{b} \, dv + \int_{\partial\Omega} \boldsymbol{t} \, da. \tag{2.119}$$

Utilizing the conservation of mass (2.111) one ends up with

$$\int_{\Omega} \rho \, \dot{\boldsymbol{v}} \, dv = \int_{\Omega} \rho \, \boldsymbol{b} \, dv + \int_{\partial\Omega} \boldsymbol{t} \, da. \tag{2.120}$$

In order to obtain the local form of the balance of linear momentum one first has to use Cauchy-theorem (2.102) [6]

$$\int_{\partial\Omega} \boldsymbol{t} \, da = \int_{\partial\Omega} \boldsymbol{\sigma} \cdot \boldsymbol{n} \, da. \tag{2.121}$$

After applying the theorem of Gauß-Ostrogradski and using the definition of the acceleration field (2.9) the relation (2.120) becomes [7]

$$\int_{\Omega} (\operatorname{div} \boldsymbol{\sigma} + \rho \, \boldsymbol{b} - \rho \, \ddot{\boldsymbol{u}}) \, dv = \boldsymbol{0}. \tag{2.122}$$

This statement has to hold for every subdomain $\bar{\Omega} \in \Omega$ as well. Hence, the balance of linear momentum (2.122) can be expressed in the local form as

$$\operatorname{div} \boldsymbol{\sigma} + \boldsymbol{f} = \boldsymbol{0} \qquad \Rightarrow \qquad \frac{\partial \sigma_{ij}}{\partial x_j} + f_i = 0, \tag{2.123}$$

where $\boldsymbol{f}$ represents the total volume load, see (2.105).

Within the framework of the geometrically linear theory, which is used later in this thesis, the reference configuration Ω_0 of the body $\mathcal{B}$ can be considered coincident with the current configuration Ω. Therefore, one can replace the spatial coordinates with the reference ones in (2.123), leading to

$$\operatorname{div} \boldsymbol{\sigma} + \boldsymbol{f} = \boldsymbol{0} \qquad \Rightarrow \qquad \frac{\partial \sigma_{ij}}{\partial X_j} + f_i = 0, \tag{2.124}$$

The resulting equation is identical to the local equilibrium of forces on the infinitesimal volume element (2.106).

2.3.3. Balance of angular momentum

Consider again a body $\mathcal{B}$ occupying a region Ω with boundary surface $\partial\Omega$ at time t subjected to volume and surface forces $\boldsymbol{b}$ and $\boldsymbol{t}$, respectively (Figure 2.10). It is assumed that the

---

[6]For details on Cauchy theorem see the section 2.2.1

[7]For details on theorem of Gauß-Ostrogradski see the section A.2

body is a closed system (no exchange of mass with the surroundings) and that there are no distributed couples (the so-called *Boltzman-* (or *non-polar-*) continua). The total *angular* (*rotational*) *momentum* about an arbitrary point $\boldsymbol{x}_0$ is defined by

$$\mathfrak{J} := \int_\Omega (\boldsymbol{x} - \boldsymbol{x}_0) \times (\rho\,\boldsymbol{v})\,dv, \tag{2.125}$$

and the resultant moment of the external forces applied on the body is described by

$$\boldsymbol{M} := \boldsymbol{M}_b + \boldsymbol{M}_t = \int_\Omega (\boldsymbol{x} - \boldsymbol{x}_0) \times (\rho\,\boldsymbol{b})\,dv + \int_{\partial\Omega} (\boldsymbol{x} - \boldsymbol{x}_0) \times \boldsymbol{t}\,da. \tag{2.126}$$

The *balance of angular momentum* states that the change of the total rotational momentum $\mathfrak{J}$ is balanced by the moments of external forces $\boldsymbol{M}$ acting on the body (consisting of the moment of volume forces $\boldsymbol{M}_b$ and the moment of surface forces $\boldsymbol{M}_t$)

$$\dot{\mathfrak{J}} = \boldsymbol{M}. \tag{2.127}$$

This postulate can be expressed in view of (2.125) and (2.126) as

$$\frac{D}{Dt}\int_\Omega (\boldsymbol{x} - \boldsymbol{x}_0) \times (\rho\,\boldsymbol{v})\,dv = \int_\Omega (\boldsymbol{x} - \boldsymbol{x}_0) \times (\rho\,\boldsymbol{b})\,dv + \int_{\partial\Omega} (\boldsymbol{x} - \boldsymbol{x}_0) \times \boldsymbol{t}\,da. \tag{2.128}$$

Utilizing the conservation of mass (2.111), the balance of linear momentum (2.123) and the Cauchy theorem (2.102) one obtains

$$\int_\Omega (\boldsymbol{x} - \boldsymbol{x}_0) \times (\operatorname{div}\boldsymbol{\sigma} + \rho\,\boldsymbol{b})\,dv =$$
$$\int_\Omega (\boldsymbol{x} - \boldsymbol{x}_0) \times (\rho\,\boldsymbol{b})\,dv + \int_{\partial\Omega} (\boldsymbol{x} - \boldsymbol{x}_0) \times (\boldsymbol{\sigma}\cdot\boldsymbol{n})\,da. \tag{2.129}$$

After applying the theorem of Gauß-Ostrogradski and some manipulation, cf. Holzapfel (2000), the relation (2.129) becomes

$$\int_\Omega \mathbf{I} \times \boldsymbol{\sigma}\,dv = \mathbf{0}. \tag{2.130}$$

This statement has to hold for every subdomain $\bar{\Omega} \in \Omega$ as well, implying the symmetry of the Cauchy stress tensor

$$\boldsymbol{\sigma} = \boldsymbol{\sigma}^T \qquad \Leftrightarrow \qquad \sigma_{ij} = \sigma_{ji} \tag{2.131}$$

The result is identical to the one originating from the local moment equilibrium on the infinitesimal volume element (2.108).

2.3.4. Conservation of energy

In this section the postulate of energy balance in local and global form is presented. First, we introduce some common terminology.

All quantities describing a system at a certain state are called *thermodynamic state variables* and they generally depend on position and time. Equations that interrelate state variables are

called *constitutive equations* or *equations of state*. If there is no change in the values of state variables at any point in the system with time, the system is said to be in *thermodynamic equilibrium*. A process in a system that remains close to this state at each time is called a *quasi-static* process. A quasi-static process is a sufficiently slow process with enough time remaining for the system to adjust itself internally. Hence, the contribution due to dynamical quantities are negligible.

Let us consider again a body $\mathcal{B}$ occupying a region Ω with boundary surface $\partial\Omega$ at time t subjected to volume and surface forces $\boldsymbol{b}$ and $\boldsymbol{t}$, respectively. Additionally, thermal loading is considered in the form of *internal heat sources* of value r per unit mass and a *heat transfer* across the boundary surface of the body reflected by the *heat flux* $\boldsymbol{q}$ per unit area, Figure 2.11. It is assumed that the body is a closed system (no exchange of mass with the surroundings). The *total energy $E(t)$* of a body $\mathcal{B}$ is obtained as a sum of *internal energy $\mathcal{E}(t)$* and a *kinetic*

Figure 2.11.: Forces and thermal loads acting on a body $\mathcal{B}$

energy $\mathcal{K}(t)$

$$E = \mathcal{E} + \mathcal{K}. \tag{2.132}$$

The internal and kinetic energy are defined by

$$\mathcal{E} := \int_\Omega \rho \, e \, dv, \qquad \mathcal{K} := \int_\Omega \frac{1}{2}\rho \, \boldsymbol{v} \cdot \boldsymbol{v} \, dv, \tag{2.133}$$

where e represents the internal energy density (internal energy per unit mass). The *power of external forces* applied on the body is described by

$$\mathcal{P}_{ext} := \mathcal{P}_b + \mathcal{P}_t = \int_\Omega \rho \, \boldsymbol{b} \cdot \boldsymbol{v} \, dv + \int_{\partial\Omega} \boldsymbol{t} \cdot \boldsymbol{v} \, da, \tag{2.134}$$

while the *heat input* (*heat power*) due to the heat flux and the heat source is obtained as

$$\mathcal{Q} := \int_\Omega \rho \, r \, dv + \int_{\partial\Omega} q_n \, da. \tag{2.135}$$

The heat flux q_n represents the rate at which heat enters the body (inward normal flux) across the boundary surface $\partial\Omega$. It can be transformed using the Stoke's heat flux theorem to the so-called Cauchy heat flux vector $\boldsymbol{q}$

$$q_n = -\boldsymbol{q} \cdot \boldsymbol{n}, \tag{2.136}$$

where $\boldsymbol{n}$ stands for the outward unit normal to an infinitesimal surface element da of the boundary $\partial\Omega$.

The *balance of energy* states that the change of the total energy E of a body is balanced by the power of external forces $\mathcal{P}_{ext}$ and the heat introduced into the system $\mathcal{Q}$

$$\dot{E} = \mathcal{P}_{ext} + \mathcal{Q}. \tag{2.137}$$

This postulate can be expressed in view of (2.132), (2.133), (2.134) and (2.135) as

$$\frac{D}{Dt} \int_\Omega \rho \left(e + \frac{1}{2} \boldsymbol{v} \cdot \boldsymbol{v} \right) \, dv = \int_\Omega \rho \left(\boldsymbol{b} \cdot \boldsymbol{v} + r \right) \, dv + \int_{\partial\Omega} \left(\boldsymbol{t} \cdot \boldsymbol{v} - \boldsymbol{q} \cdot \boldsymbol{n} \right) \, da. \tag{2.138}$$

Utilizing the theorems of Cauchy (2.102) and Gauß-Ostrogradski, the last integral in (2.138) is transformed to

$$\int_{\partial\Omega} \left(\boldsymbol{t} \cdot \boldsymbol{v} - \boldsymbol{q} \cdot \boldsymbol{n} \right) \, da = \int_\Omega \mathrm{div} \left(\boldsymbol{v} \cdot \boldsymbol{\sigma} - \boldsymbol{q} \right) \, dv. \tag{2.139}$$

With this result at hands, one can use the conservation of mass (2.111) to obtain

$$\int_\Omega \rho \left(\dot{e} + \dot{\boldsymbol{v}} \cdot \boldsymbol{v} \right) \, dv = \int_\Omega \left[\mathrm{div} \left(\boldsymbol{v} \cdot \boldsymbol{\sigma} - \boldsymbol{q} \right) + \rho \left(\boldsymbol{b} \cdot \boldsymbol{v} + r \right) \right] \, dv. \tag{2.140}$$

This equation represents the global form of the balance of energy, called also *the first law of thermodynamics*. Stating that it has to hold for every subdomain $\bar{\Omega} \in \Omega$ as well, we end up with

$$\rho \left(\dot{e} + \dot{\boldsymbol{v}} \cdot \boldsymbol{v} \right) = \mathrm{div} \left(\boldsymbol{v} \cdot \boldsymbol{\sigma} - \boldsymbol{q} \right) + \rho \left(\boldsymbol{b} \cdot \boldsymbol{v} + r \right). \tag{2.141}$$

Relation (2.141) contains both changes of the internal and kinetic energy. With help of the balance of linear momentum (2.123) and the definition of the rate of deformation tensor $\boldsymbol{D}$ (2.62), one can separate these contributions into two balance laws. The one of interest for us is the *balance of internal energy*, expressed as

$$\int_\Omega \rho \, \dot{e} \, dv = \int_\Omega \left(\boldsymbol{\sigma} : \boldsymbol{D} - \mathrm{div} \, \boldsymbol{q} + \rho \, r \right) \, dv, \tag{2.142}$$

in global, or as

$$\rho \, \dot{e} = \boldsymbol{\sigma} : \boldsymbol{D} - \mathrm{div} \, \boldsymbol{q} + \rho \, r. \tag{2.143}$$

in its local form. The remaining part, or the *balance of kinetic energy* is nothing else then scaled (with the velocity $\boldsymbol{v}$) version of the balance of linear momentum. Hence, it brings no additional physical information.

Within the framework of the geometrically linear theory, which is used in this thesis, the reference configuration Ω_0 of the body $\mathcal{B}$ can be considered coincident with the current configuration Ω. Therefore, one can replace in (2.143) the spatial coordinates with the reference ones and the rate of the deformation tensor $\boldsymbol{D}$ with the rate of linearized strain tensor $\dot{\boldsymbol{\varepsilon}}$ (see (2.93)), leading to

$$\rho \, \dot{e} = \boldsymbol{\sigma} : \dot{\boldsymbol{\varepsilon}} - \mathrm{div} \, \boldsymbol{q} + \rho \, r \qquad \Rightarrow \qquad \rho \, \dot{e} = \sigma_{ij} \, \dot{\varepsilon}_{ij} - \frac{\partial q_i}{\partial X_i} + \rho \, r. \tag{2.144}$$

2.3.5. Balance of entropy

The balance of energy (2.140) governs the energy transfer within the thermodynamic process, but it is insensitive to its direction. However, natural processes show certain asymmetry, so that the transfer always goes in one direction. For example, heat always flows from the warmer to the colder part of the body. In order to capture this natural behavior, a state variable called *entropy* is introduced, which could be viewed as the measure of microscopic randomness and disorder, cf. Holzapfel (2000). The entropy of a body is denoted by $\mathcal{S}$ while its spatial density (entropy per unit mass) is denoted as $s(\boldsymbol{x}, t)$.

$$\mathcal{S} = \int_{\Omega} \rho \, s \, dv. \tag{2.145}$$

The *rate of entropy input* due to the entropy transported across the body surface and the entropy generated within the body is described by

$$\mathcal{H}_{ext} := \mathcal{H}_b + \mathcal{H}_t = \int_{\Omega} \rho \, r_h \, dv + \int_{\partial\Omega} h_n \, da. \tag{2.146}$$

The entropy flux h_n represents the rate at which entropy enters the body (inward normal flux) across the boundary surface $\partial\Omega$. It can be transformed using the Stoke's heat flux theorem to the so-called Cauchy entropy flux vector $\boldsymbol{h}$

$$h_n = -\boldsymbol{h} \cdot \boldsymbol{n}, \tag{2.147}$$

where $\boldsymbol{n}$ stands for the outward unit normal to an infinitesimal surface element da of the boundary $\partial\Omega$.

The *balance of entropy* states that the change of the total entropy $\mathcal{S}$ of a body is governed by the rate of entropy input $\mathcal{H}$ and by the production of entropy inside the system due to irreversible processes $\mathcal{S}_{irr}$, the later being *non-negative* quantity

$$\dot{\mathcal{S}} = \mathcal{H} + \dot{\mathcal{S}}_{irr}, \qquad \dot{\mathcal{S}}_{irr} \geq 0. \tag{2.148}$$

This postulate can be expressed in view of (2.145), (2.146) and (2.148) as

$$\dot{\mathcal{S}}_{irr} = \frac{D}{Dt} \int_{\Omega} \rho \, s \, dv - \int_{\Omega} \rho \, r_h \, dv + \int_{\partial\Omega} \boldsymbol{h} \cdot \boldsymbol{n} \, da \geq 0. \tag{2.149}$$

Utilizing the theorems of Cauchy (2.102) and Gauß-Ostrogradski together with the conservation of mass (2.111), the relation (2.149) is transformed to

$$\dot{\mathcal{S}}_{irr} = \int_{\Omega} (\rho \, \dot{s} - \rho \, r_h + \operatorname{div} \boldsymbol{h}) \, dv \geq 0. \tag{2.150}$$

This equation represents the global form of the balance of entropy, called also *the second law of thermodynamics*. At this point one can introduce a spatial density of the production of entropy inside the system due to irreversible processes $\dot{s}_{irr}$

$$\dot{\mathcal{S}} = \int_{\Omega} \rho \, \dot{s}_{irr} \, dv. \tag{2.151}$$

Stating that it has to hold for every subdomain $\bar{\Omega} \in \Omega$ as well, we end up with the local form of the second law of thermodynamics

$$\rho \, \dot{s}_{irr} = \rho \, \dot{s} - \rho \, r_h + \operatorname{div} \boldsymbol{h} \geq 0. \tag{2.152}$$

Very often is postulated that the rate of the entropy input is related to the thermal work (cf. Holzapfel (2000)) by

$$
\boldsymbol{h} = \frac{1}{\Theta}\,\boldsymbol{q}, \qquad r_h = \frac{r}{\Theta} \tag{2.153}
$$

With this assumption at hands, one can use the balance of internal energy (2.142) to obtain

$$
\dot{\mathcal{S}}_{irr} = \int_{\Omega} \rho\,\Theta\,\dot{s}_{irr}\,dv = \int_{\Omega} \rho\,\Theta\,\dot{s} - \rho\,\dot{e} + \boldsymbol{\sigma}:\boldsymbol{D} - \frac{1}{\Theta}\,\boldsymbol{q}\cdot\nabla\Theta\,dv \ \geq 0. \tag{2.154}
$$

This equation is called a *Clausius-Duhem inequality* in its global, or

$$
\rho\,\Theta\,\dot{s}_{irr} = \rho\,\Theta\,\dot{s} - \rho\,\dot{e} + \boldsymbol{\sigma}:\boldsymbol{D} - \frac{1}{\Theta}\,\boldsymbol{q}\cdot\nabla\Theta \ \geq 0 \tag{2.155}
$$

in its local form. In order to fulfill the requirement that the heat always flows from the warmer to the colder part of the body, it has to hold

$$
\frac{1}{\Theta}\,\boldsymbol{q}\cdot\nabla\Theta \ \leq 0. \tag{2.156}
$$

The requirement (2.156) is a so-called *heat conduction inequality*, which additionally implies that there is no heat flow without temperature gradient. In view of (2.156) one can state the Clausius-Duhem inequality in a stronger form, called *Clausius-Planck inequality*

$$
\dot{\mathcal{S}}_{irr} = \int_{\Omega} \rho\,\Theta\,\dot{s} - \rho\,\dot{e} + \boldsymbol{\sigma}:\boldsymbol{D}\,dv \ \geq 0, \tag{2.157}
$$

whose local form reads

$$
\mathcal{D}_{int} = \rho\,\Theta\,\dot{s} - \rho\,\dot{e} + \boldsymbol{\sigma}:\boldsymbol{D} \ \geq 0. \tag{2.158}
$$

The quantity $\mathcal{D}_{int}$ is called *internal dissipation* or *local production of entropy*. It is equal to zero for reversible processes, while inequality holds for irreversible ones.

In further discussion it is advantageous to work with the *Helmholtz free-energy function* ψ instead of the internal energy e. The Helmholtz free-energy function (shortly *free-energy function*) is defined by the Legendre transformation of e

$$
\psi = e - \Theta\,s. \tag{2.159}
$$

Utilizing (2.159) the global (2.154) and the local (2.155) form of the Clausius-Duhem inequality become

$$
\dot{\mathcal{S}}_{irr} = \int_{\Omega} \rho\,\Theta\,\dot{s}_{irr}\,dv = \int_{\Omega} \boldsymbol{\sigma}:\boldsymbol{D} - \rho\,\dot{\Theta}\,s - \rho\dot{\psi} - \frac{1}{\Theta}\,\boldsymbol{q}\cdot\nabla\Theta\,dv \ \geq 0, \tag{2.160}
$$

$$
\rho\,\Theta\,\dot{s}_{irr} = \boldsymbol{\sigma}:\boldsymbol{D} - \rho\,\dot{\Theta}\,s - \rho\dot{\psi} - \frac{1}{\Theta}\,\boldsymbol{q}\cdot\nabla\Theta \ \geq 0. \tag{2.161}
$$

The Clausius-Plank inequality is expressed in its global and local form in terms of free-energy function as

$$
\dot{\mathcal{S}}_{irr} = \int_{\Omega} \boldsymbol{\sigma}:\boldsymbol{D} - \rho\,\dot{\Theta}\,s - \rho\dot{\psi}\,dv \ \geq 0, \tag{2.162}
$$

$$\mathcal{D}_{int} = \boldsymbol{\sigma} : \boldsymbol{D} - \rho \, \dot{\Theta} \, s - \rho\dot{\psi} \; \geq 0. \tag{2.163}$$

Within the framework of the geometrically linear theory, which is used later in this thesis, the reference configuration Ω_0 of the body $\mathcal{B}$ can be considered coincident with the current configuration Ω. Therefore, one can replace in (2.160), (2.161), (2.162) and (2.163) the spatial coordinates with the reference ones and the rate of the deformation tensor $\boldsymbol{D}$ with the rate of linearized strain tensor $\dot{\varepsilon}$ (see (2.93)), leading to the Clausius-Duhem inequality of the linearized problem

$$\dot{\mathcal{S}}_{irr} = \int_{\Omega} \rho \, \Theta \, \dot{s}_{irr} \, dV = \int_{\Omega} \boldsymbol{\sigma} : \dot{\varepsilon} - \rho \, \dot{\Theta} \, s - \rho\dot{\psi} - \frac{1}{\Theta} \, \boldsymbol{q} \cdot \nabla\Theta \, dV \; \geq 0, \tag{2.164}$$

$$\rho \, \Theta \, \dot{s}_{irr} = \boldsymbol{\sigma} : \dot{\varepsilon} - \rho \, \dot{\Theta} \, s - \rho\dot{\psi} - \frac{1}{\Theta} \, \boldsymbol{q} \cdot \nabla\Theta \; \geq 0. \tag{2.165}$$

Within the same setting the Clausius-Plank inequality reads

$$\dot{\mathcal{S}}_{irr} = \int_{\Omega} \boldsymbol{\sigma} : \dot{\varepsilon} - \rho \, \dot{\Theta} \, s - \rho\dot{\psi} \, dV \; \geq 0, \tag{2.166}$$

$$\mathcal{D}_{int} = \boldsymbol{\sigma} : \dot{\varepsilon} - \rho \, \dot{\Theta} \, s - \rho\dot{\psi} \; \geq 0. \tag{2.167}$$

2.4. Consequences of the thermodynamic balance laws

In this section an overview on the restrictions put by the balance relations of continuum thermodynamics is provided together with some comments on the description of the thermomechanical coupling.

2.4.1. Thermodynamic consistency

The kinematic relations, derived in the section 2.1, and the balance laws, presented in the section 2.3, are material-independent in its formulation. Therefore, thermomechanical problems cannot be solved using this equations alone. In order to close the system, one needs additional relations called *constitutive equations*.

Constitutive equations describe the dependence of the so-called *response functions* (stress tensor $\boldsymbol{\sigma}$, temperature flux $\boldsymbol{q}$, entropy s and the free-energy ψ) on a set of *process variables* (linearized strain tensor ε, absolute temperature Θ and its gradient $\nabla\Theta$ etc.) The response functions of the body consisting of thermoelastic material (material that does not dissipate energy) can be described solely by the appropriate measure of the deformation (in the case of the geometrically linear theory that is the linearized strain tensor ε) and the temperature Θ. However, such description turned out to be inadequate for materials which do dissipate energy. In that case new state variables have to be introduced that are supposed to describe aspects of the internal structure of a material associated with the irreversible (dissipative) effects. They are called *internal variables* and are collected in the list

$$\boldsymbol{P} = \{\boldsymbol{P}_1, \boldsymbol{P}_2, \ldots, \boldsymbol{P}_{ni}\} \,. \tag{2.168}$$

The index ni stands for the total number of the elements P_i of the list P. These elements can be scalar or tensorial quantities.[8] The actual number of the elements depends on the material itself as well as the underlying theory. Similar to the quantities σ, q, s and ψ, a response function governing the evolution of P has to be defined. The evolution of internal variables is connected to the history of deformation, therefore they are often called *history variables*.

Adopting the principle of equipresence, cf. Truesdell and Noll (2004), which states that the response functions depend on the complete set of the process variables, unless that leads to the contradiction with the general physical laws or the assumed symmetries of the material, it follows

$$
\begin{aligned}
\psi &= \psi(\varepsilon, \Theta, \nabla\Theta, P) \\
\sigma &= \sigma(\varepsilon, \Theta, \nabla\Theta, P) \\
s &= s(\varepsilon, \Theta, \nabla\Theta, P) \\
q &= q(\varepsilon, \Theta, \nabla\Theta, P) \,.
\end{aligned}
\tag{2.169}
$$

Application of the material time rate to the Helmholtz free-energy (2.169_1) gives

$$
\dot{\psi} = \frac{\partial\psi}{\partial\varepsilon} : \dot{\varepsilon} \; + \; \frac{\partial\psi}{\partial\Theta}\,\dot{\Theta} \; + \; \frac{\partial\psi}{\partial(\nabla\Theta)} \cdot (\dot{\overline{\nabla\Theta}}) \; + \; \frac{\partial\psi}{\partial P} : \dot{P}.
\tag{2.170}
$$

Since P can be a collection of scalars and tensors of arbitrary order, the double dot product it is involved at in (2.170) has to be understood as the scalar product of $\dot{P}$ with a similarly structured object. Once the structure of P is known, the operator (:) may be interpreted accordingly (as a simple contraction of vectors, double contraction of second order tensors etc.). Substituting the relation (2.170) into (2.165), the local form of the Clausius-Duhem inequality becomes

$$
\left(\sigma - \rho\,\frac{\partial\psi}{\partial\varepsilon}\right) : \dot{\varepsilon} - \left(\rho\,s + \rho\,\frac{\partial\psi}{\partial\Theta}\right)\,\dot{\Theta}
$$
$$
- \left(\rho\,\frac{\partial\psi}{\partial(\nabla\Theta)}\right) \cdot (\dot{\overline{\nabla\Theta}}) - \rho\,\frac{\partial\psi}{\partial P} : \dot{P} - \frac{1}{\Theta}\,q \cdot \nabla\Theta \; \geq 0.
\tag{2.171}
$$

Let us now consider two extreme cases. The first one is a process of pure heating or cooling during which the strain and the internal variables remain constant and only the temperature varies in time but remains constant in space. Requirement of non-negative dissipation for arbitrary rates of temperature delivers the constitutive relation for the entropy

$$
s := -\frac{\partial\psi}{\partial\Theta}.
\tag{2.172}
$$

The second one is a process of pure elastic deformation, during which the temperature remains constant in time and space and the internal variables do not evolve. The dissipation must be non-negative for the arbitrary rates of the strain tensor, therefore one can deduce the constitutive relation for the stress tensor

$$
\sigma := \rho\,\frac{\partial\psi}{\partial\varepsilon}.
\tag{2.173}
$$

---

[8]This description includes naturally *vector* variables, since vectors are first order tensors.

Similar consideration leads to the statement that the free-energy function in the classical theory has to be independent of the temperature gradient[9]

$$\frac{\partial \psi}{\partial (\nabla \Theta)} = \mathbf{0} \qquad \Rightarrow \qquad \psi = \psi(\boldsymbol{\varepsilon}, \Theta, \boldsymbol{P}). \tag{2.174}$$

In this context the Helmholtz free-energy function is referred to as *thermodynamic potential*, since it has potential character for $\boldsymbol{\sigma}$ and s.

In view of (2.172), (2.173) and (2.174) the Clausius-Duhem inequality (2.171) takes the form

$$\boldsymbol{Q} : \dot{\boldsymbol{P}} - \frac{1}{\Theta}\, \boldsymbol{q} \cdot \nabla \Theta \ \geq 0, \tag{2.175}$$

where an additional quantity $\boldsymbol{Q}$ is being introduced for the sake of notational clarity. It represents the derivative of the free-energy function with respect to the list of the internal variables, rendering ψ as a thermodynamic potential for $\boldsymbol{Q}$

$$\boldsymbol{Q} := -\rho\, \frac{\partial \psi}{\partial \boldsymbol{P}}, \tag{2.176}$$

and therefore it is a list itself, structured in the same way as $\boldsymbol{P}$

$$\boldsymbol{Q} = \{\boldsymbol{Q}_1, \boldsymbol{Q}_2, \dots, \boldsymbol{Q}_{ni}\}\,, \qquad \boldsymbol{Q}_i = -\rho\, \frac{\partial \psi}{\partial \boldsymbol{P}_i}. \tag{2.177}$$

The first term in the remaining inequality (2.175) represents the mechanical dissipation, while the second comes from thermal dissipation. As it is already stated, the thermal dissipation has to fulfill the heat conduction inequality (2.156). A suitable constitutive law which relates the heat flux $\boldsymbol{q}$ to the temperature gradient $\nabla \Theta$ is furnished by the *Duhamel´s law of heat conduction*, cf. Holzapfel (2000)

$$\boldsymbol{q} = -\boldsymbol{K} \cdot \nabla \Theta, \qquad \Rightarrow \qquad q_i = -K_{ij}\, \frac{\partial \Theta}{\partial X_j} \tag{2.178}$$

In view of (2.156), the symmetric second order *thermal conductivity tensor* $\boldsymbol{K}$ is restricted to be positive-semidifinite. If the material under consideration is thermally isotropic (no preferred direction for the heat conduction), $\boldsymbol{K}$ becomes

$$\boldsymbol{K} = k\, \mathbf{I}, \tag{2.179}$$

and the constitutive relation for the heat flux reduces to

$$\boldsymbol{q} = -k\, \nabla \Theta, \qquad \Rightarrow \qquad q_i = -k\, \frac{\partial \Theta}{\partial X_i}, \tag{2.180}$$

which is known as *Fouirer´s law of heat conduction*.

Recalling the Clausius-Planck inequality (2.167) as a stronger requirement on the dissipation, one can see that it reduces to the mechanical dissipation from (2.175)

$$\mathcal{D}_{int} = \boldsymbol{Q} : \dot{\boldsymbol{P}} \ \geq 0. \tag{2.181}$$

What remains to be specified is the response function governing the evolution of the internal variables $\boldsymbol{P}$. This task is the subject of the forthcoming chapters.

---

[9]There exist non-classical theories of thermoelasticity that do take into consideration the dependence of the Helmholtz free-energy function on the gradient of the temperature field, see e.g. Bargmann and Steinmann (2006).

3. Inelastic constitutive modeling

In this chapter constitutive models describing the response behavior of a certain material under external loading are considered. The attention is restricted to the isothermal case, i.e. no temperature dependence is going to be considered. Based on the discussion in the previous chapter, a material is called *elastic* if it does not dissipate energy, i.e. its internal dissipation (2.167) is equal to zero. If this condition is not met, a material is referred to as *inelastic*, in which case one has to consider some micro-structural features in order to properly explain its macroscopic behavior. The first part of this chapter (section 3.1) recalls some basics of the elastic material modeling, while the rest is devoted to inelastic materials. The principle governing the evolution of internal variables within the concept of generalized standard material is presented in section 3.2, together with the inelastic constitutive models used later in the thesis. The issue of localization, which is a characteristics of the material models involving softening effects is discussed in section 3.3. Finally, an overview of the techniques for the regularization of the problem is given in section 3.4.

3.1. Elastic material response

In this section we consider constitutive relations which describe the behavior of a body consisting of a non-disipative (elastic) material. Following the discussion in the previous chapter, the response function of a stress tensor is obtained from the free energy function (see (2.173)), which is a thermodynamic potential for $\boldsymbol{\sigma}$. Such material is referred to as *hyperelastic*.

3.1.1. Elastic constitutive law

Motivated by the case of isothermal elastic deformations it is advantageous to employ simplified notation introducing the Helmholtz free-energy function per unit reference volume Ψ rather then per unit mass ψ. They are related to each other by

$$\Psi := \rho_0 \, \psi, \tag{3.1}$$

resulting in the following expression for the stress tensor

$$\boldsymbol{\sigma} := \frac{\partial \Psi}{\partial \boldsymbol{\varepsilon}}. \tag{3.2}$$

Let us consider the strain state $\boldsymbol{\varepsilon}(\boldsymbol{X}, t) = \boldsymbol{\varepsilon}_0$ at certain time $t = t^*$. Denoting the strain increment $\Delta\boldsymbol{\varepsilon}$, one can perform linearization of the stress tensor about the strain state $\boldsymbol{\varepsilon}_0$

using the Gâteaux-derivative [1]

$$\mathcal{L}\boldsymbol{\sigma} = \boldsymbol{\sigma}_0 + D\boldsymbol{\sigma}(\boldsymbol{\varepsilon})(\Delta\boldsymbol{\varepsilon}) = \boldsymbol{\sigma}_0 + \left.\frac{\partial^2\Psi}{\partial\boldsymbol{\varepsilon}\,\partial\boldsymbol{\varepsilon}}\right|_{\varepsilon_0} : \Delta\boldsymbol{\varepsilon}. \tag{3.3}$$

Furthermore, one refers to the second derivative term as a hyperelastic material tensor, which can be seen as a measure of the curvature of the free energy with respect to strains

$$\mathbb{C}(\boldsymbol{\varepsilon}) := \frac{\partial^2\Psi}{\partial\boldsymbol{\varepsilon}\,\partial\boldsymbol{\varepsilon}}, \qquad \mathbb{C} = \frac{\partial^2\Psi}{\partial\varepsilon_{ij}\,\partial\varepsilon_{kl}}\,\boldsymbol{e}_i \otimes \boldsymbol{e}_j \otimes \boldsymbol{e}_k \otimes \boldsymbol{e}_l. \tag{3.4}$$

In view of (3.4) relation (3.3) can be written as

$$\mathcal{L}\boldsymbol{\sigma} = \boldsymbol{\sigma}_0 + \mathbb{C}(\varepsilon_0) : \Delta\boldsymbol{\varepsilon}. \tag{3.5}$$

Although the free-energy function in the general case presented above results in the elastic material tensor dependent on strains, such forms are rarely used in small deformation theory (models of that kind are presented for example in Lade and Nelson (1987); Duncan and Chang (1970)). The vast majority of work is done employing free-energy function that leads to linear relation between the stress and strain tensor, so that (3.5) becomes

$$\boldsymbol{\sigma} = \boldsymbol{\sigma}_0 + \mathbb{C} : \Delta\boldsymbol{\varepsilon}. \tag{3.6}$$

Assuming that the linearization is performed around the the reference (undeformed) state ($\varepsilon_0 = 0$), the strain increment becomes equal to the linearized strain tensor itself, $\boldsymbol{\varepsilon} = \Delta\boldsymbol{\varepsilon}$. Additional assumption of an unstressed reference state ($\boldsymbol{\sigma}_0 = 0$) leads finally to

$$\boldsymbol{\sigma} = \mathbb{C} : \boldsymbol{\varepsilon}. \tag{3.7}$$

The corresponding form of free-energy reads

$$\Psi = \frac{1}{2}\,\boldsymbol{\varepsilon} : \mathbb{C} : \boldsymbol{\varepsilon} \qquad \Rightarrow \qquad \Psi = \frac{1}{2}\,C_{ijkl}\,\varepsilon_{ij}\,\varepsilon_{kl}. \tag{3.8}$$

Under the assumption of sufficiently smooth free energy, the order of partial derivation can be exchanged by Clairaut's theorem, which results in the so-called *major symmetry* of the elastic tensor

$$C_{ijkl} = C_{klij}. \tag{3.9}$$

In addition, the symmetry of the strain tensor imposes the so-called *minor symmetry* property of the elastic tensor

$$C_{ijkl} = C_{jikl} = C_{jilk} = C_{ijlk}. \tag{3.10}$$

Hence, the number of independent components of the elastic material tensor has reduced from original 81 to 21 in general case of anisotropic elasticity.

Let us now consider a linear isotropic material. A requirement of an invariant response $\boldsymbol{\sigma}$ under arbitrary rotations of material particle reduces further the number of independent components to two, cf. Başar and Weichert (2000). As a result one obtains the constitutive law for a *Hookean* material

$$\boldsymbol{\sigma} = \lambda\,\operatorname{tr}\boldsymbol{\varepsilon}\,\mathbf{I} + 2\mu\,\boldsymbol{\varepsilon}, \tag{3.11}$$

---

[1]For details on linearization and the *Gâteaux-derivative* see the section A.1.

involving the *Lamé material constants* λ and μ . The free-energy attains in the present case the form

$$\Psi = \frac{\lambda}{2} \left(\operatorname{tr} \boldsymbol{\varepsilon} \right)^2 + \mu \, \boldsymbol{\varepsilon} : \boldsymbol{\varepsilon} \qquad \Rightarrow \qquad \Psi = \frac{\lambda}{2} \, \varepsilon_{ii} + \mu \, \varepsilon_{ij} \, \varepsilon_{ij} \tag{3.12}$$

Apart from Lamé constants, there are several material parameters associated with the linear elastic material behavior. But among them only two can be specified independently. The relation between the material parameters used within this thesis, i.e. the *Young modulus E*, the *shear modulus G*, the *Poisson (transverse contraction) ratio ν* and the *bulk modulus K* is given by[2]

$$
\begin{aligned}
E &= \frac{\mu \, (3\lambda + 2\mu)}{\lambda + \mu} \qquad \nu = \frac{\lambda}{2\,(\lambda + \mu)} \qquad\qquad K = \lambda + \frac{2}{3}\,\mu \\
\mu &= \frac{E}{2\,(1 + \nu)} = G \qquad \lambda = \frac{E\,\nu}{(1 + \nu)\,(1 - 2\,\nu)} \qquad K = \frac{E}{3\,(1 - 2\,\nu)} \; .
\end{aligned}
\tag{3.13}
$$

In view of (3.12) and (3.8), the fourth-order elastic material tensor $\mathbb{C}$ is expressed as

$$
\begin{aligned}
\mathbb{C} = \lambda \, \mathbf{I} \otimes \mathbf{I} + 2\mu \, \mathbb{I} \\
\Rightarrow \quad \mathbb{C} = \left[\mu \, (\delta_{il}\delta_{jk} + \delta_{ik}\delta_{jl}) + \lambda \, \delta_{ij}\delta_{kl} \right] \, \boldsymbol{e}_i \otimes \boldsymbol{e}_j \otimes \boldsymbol{e}_k \otimes \boldsymbol{e}_l.
\end{aligned}
\tag{3.14}
$$

The fourth-order identity tensor $\mathbb{I}$ in (3.14) is defined as

$$\mathbb{I} = \frac{1}{2} \left(\delta_{il}\delta_{jk} + \delta_{ik}\delta_{jl} \right) \, \boldsymbol{e}_i \otimes \boldsymbol{e}_j \otimes \boldsymbol{e}_k \otimes \boldsymbol{e}_l. \tag{3.15}$$

Motivated by the decomposition of the stress tensor (relation (3.11)) into its spherical ($\operatorname{sph} \boldsymbol{\sigma}$) and deviatoric ($\operatorname{dev} \boldsymbol{\sigma}$) parts

$$\boldsymbol{\sigma} = \operatorname{sph} \boldsymbol{\sigma} + \operatorname{dev} \boldsymbol{\sigma}, \tag{3.16}$$

$$\operatorname{sph} \boldsymbol{\sigma} = \frac{1}{3} \left(\boldsymbol{\sigma} : \mathbf{I} \right) \, \mathbf{I} = K \, \operatorname{tr} \boldsymbol{\varepsilon} \, \mathbf{I}, \tag{3.17}$$

$$\operatorname{dev} \boldsymbol{\sigma} = \boldsymbol{\sigma} - \operatorname{sph} \boldsymbol{\sigma} = 2G \, \operatorname{dev} \boldsymbol{\varepsilon}, \tag{3.18}$$

and the formulation of $\mathbb{C}$ involving the bulk modulus K and the shear modulus G

$$
\begin{aligned}
\mathbb{C} = K \, \mathbf{I} \otimes \mathbf{I} + 2G \left(\mathbb{I} - \frac{1}{3}\mathbf{I} \otimes \mathbf{I} \right) \\
\Rightarrow \quad \mathbb{C} = \left[G \left(\delta_{il}\delta_{jk} + \delta_{ik}\delta_{jl} - \frac{2}{3} \, \delta_{ij}\delta_{kl} \right) + K \, \delta_{ij}\delta_{kl} \right] \, \boldsymbol{e}_i \otimes \boldsymbol{e}_j \otimes \boldsymbol{e}_k \otimes \boldsymbol{e}_l,
\end{aligned}
\tag{3.19}
$$

the fourth-order elastic material tensor can be alternatively decomposed into two parts, cf. Başar and Weichert (2000)

$$\mathbb{C} = \operatorname{sph} \mathbb{C} + \operatorname{dev} \mathbb{C}, \tag{3.20}$$

which are obtained as

$$
\begin{aligned}
\operatorname{sph} \mathbb{C} &= K \, \mathbf{I} \otimes \mathbf{I}, \\
\operatorname{dev} \mathbb{C} &= 2G \left(\mathbb{I} - \frac{1}{3}\mathbf{I} \otimes \mathbf{I} \right).
\end{aligned}
\tag{3.21}
$$

---

[2]Further relations between usually used elasticity constants can be found in Başar and Weichert (2000); Stein and Barthold (1996); Kuhl and Meschke (2003)

This form has advantages in the formulation of the deviatoric plasticity since it results in the direct decomposition of the stress tensor into a spherical part and a deviatoric part

$$
\begin{aligned}
\mathrm{sph}\,\boldsymbol{\sigma} &= \mathrm{sph}\,\mathbb{C} : \mathrm{sph}\,\boldsymbol{\varepsilon} \\
\mathrm{dev}\,\boldsymbol{\sigma} &= \mathrm{dev}\,\mathbb{C} : \mathrm{dev}\,\boldsymbol{\varepsilon}.
\end{aligned}
\tag{3.22}
$$

3.2. Inelastic material response

In this section we consider constitutive relations which describe the behavior of a body consisting of a dissipative (inelastic) material. The proper explanation of the underlying processes and the macroscopic material behaviour requires a consideration of some micro-structural features, which is still very demanding task. Hence, in common praxis one utilizes so-called *phenomenological models* which are focused on the description of the macroscopic behavior of a material. This task is accomplished by introduction of new state variables that are supposed to describe aspects of the internal material structure associated with the ir-reversible (dissipative) effects. Their precise physical interpretation is often less relevant and they are not observable or controllable. As a consequence, internal variables can be identified in the course of phenomenological experiments, but this identification merely re-flects macroscopic description assumptions used in their definition. That poses an additional problem: the evolution of internal variables, which is strongly connected to the history of deformation, has to be specified in a way consistent with the physical laws derived in chapter 2. In particular the internal dissipation $\mathcal{D}_{int}$ has to satisfy Clausius-Planck inequality (2.181). This condition can be automatically fulfilled introducing a dissipation potential dependent on the rates of internal variables, which is a subject of the following section.

3.2.1. Dissipation potential and generalized standard material

The discussion in this section is based on the concept of the so-called *generalized standard material*, introduced in Halphen and Nguyen (1975), which covers a number of inelastic material behaviors. The evolution of internal (inelastic) variables is governed by two po-tentials: the Helmholtz free-energy $\Psi(\boldsymbol{\varepsilon}, \boldsymbol{P})$ and the *dissipation potential* $J(\dot{\boldsymbol{P}})$ (see e.g. Hackl and Fischer (2008); Lorentz and Benallal (2005); Carstensen et al. (2002)). Restrict-ing our attention to the case of rate-independent material behavior, the dissipation potential is specified in the form

$$
J(\dot{\boldsymbol{P}}) = \sup_{\boldsymbol{Q}} \left[\boldsymbol{Q} : \dot{\boldsymbol{P}} - I_K(\boldsymbol{P}, \boldsymbol{Q}) \right].
\tag{3.23}
$$

The quantity I_K represents the characteristic function of a certain domain

$$
I_K(x) = \begin{cases} 0 & \text{if } \mathrm{x} \in \mathrm{K} \\ +\infty & \text{if } \mathrm{x} \notin \mathrm{K} \,, \end{cases}
\tag{3.24}
$$

with the domain K being defined through the set of m convex functions called inelastic constraints

$$
\mathrm{K} = \left\{ \boldsymbol{Q} \mid \phi_i(\boldsymbol{P}, \boldsymbol{Q}) \leq 0, \ i = 1, ..., m \right\}.
\tag{3.25}
$$

As it was discussed in section 2.4.1, the double contraction in (3.23) is to be understood as the scalar product of $\dot{\boldsymbol{P}}$ with a similarly structured object and interpreted accordingly. The relations (3.23 - 3.25) are one of the possible formulations of the *minimum principle for the dissipation potential*, cf. Hackl and Fischer (2008).

Restricting ourselves to the isothermal case and employing the Helmholtz free-energy function per unit reference volume Ψ (3.1), the response function for $\boldsymbol{Q}$ becomes

$$\boldsymbol{Q} := -\frac{\partial \Psi}{\partial \boldsymbol{P}}. \tag{3.26}$$

From the definition of the dissipation potential (3.23) it is obvious that within the classical concept of generalized standard medium the inelastic constraints (3.25) depend solely on the lists of internal variables $\boldsymbol{P}$ and their thermodynamic conjugates $\boldsymbol{Q}$. This requirement poses a severe restriction, since it excludes dependence on strain or stress tensors, which is a necessary requirement in the description of materials experiencing unsymmetric response with respect to tension and compression (e.g. tension sensitive materials like concrete, rocks etc.). However, following the discussion in Hackl and Fischer (2008), it is possible to include the dependence of the characteristic function I_K on the strain tensor as a parameter $I_K = I_K(\boldsymbol{P}, \boldsymbol{Q}, \boldsymbol{\varepsilon})$ using the definition of some (possibly all) inelastic constraints $\phi_i = \phi_i(\boldsymbol{P}, \boldsymbol{Q}, \boldsymbol{\varepsilon})$. A resulting extended dissipation potential reads

$$J(\dot{\boldsymbol{P}}) = \sup_{\boldsymbol{Q}} \left[\boldsymbol{Q} : \dot{\boldsymbol{P}} - I_K(\boldsymbol{P}, \boldsymbol{Q}, \boldsymbol{\varepsilon}) \right], \tag{3.27}$$

leading to a (possibly multiple) constrained optimization problem, cf. Simo and Hughes (1998), whose solution are the evolution equations for the internal variables

$$\dot{\boldsymbol{P}} = \sum_{i=1}^{m} \dot{\lambda}_i \frac{\partial \phi_i}{\partial \boldsymbol{Q}}, \tag{3.28}$$

subjected to corresponding Kuhn-Karush-Tucker optimality conditions

$$\dot{\lambda}_i \geq 0, \quad \phi_i \leq 0, \quad \dot{\lambda}_i \phi_i = 0, \quad \forall\, i = 1, ..., m. \tag{3.29}$$

From the conditions (3.29) one can define the set of indices of *active inelastic constraints*

$$\mathbb{S}_{act} = \left\{ j \in 1, ..., m \mid \phi_j = 0, \dot{\lambda}_j > 0 \right\}, \tag{3.30}$$

which can be used to modify the relation (3.28) into

$$\dot{\boldsymbol{P}} = \sum_{j \in \mathbb{S}_{act}} \dot{\lambda}_j \frac{\partial \phi_j}{\partial \boldsymbol{Q}}. \tag{3.31}$$

Relations (3.29)-(3.31) constitute the differential-algebraic system of equations driving the evolution of internal variables and therefore closing the formulation of the problem.

Let us consider the state $\boldsymbol{\varepsilon}(\boldsymbol{X}, t) = \boldsymbol{\varepsilon}_0$ and $\boldsymbol{P}(\boldsymbol{X}, t) = \boldsymbol{P}_0$ at certain time $t = t^*$. Denoting the increments of strain and internal variable list $\Delta\boldsymbol{\varepsilon}$ and $\Delta\boldsymbol{P}$ respectively, one can perform linearization of the stress tensor about the state $\boldsymbol{\varepsilon}_0$, $\boldsymbol{P}_0$ using the Gâteaux-derivative [3]

$$\mathcal{L}\boldsymbol{\sigma} = \boldsymbol{\sigma}_0 + D\boldsymbol{\sigma}(\boldsymbol{\varepsilon}, \boldsymbol{P})(\Delta\boldsymbol{\varepsilon}) + D\boldsymbol{\sigma}(\boldsymbol{\varepsilon}, \boldsymbol{P})(\Delta\boldsymbol{P}) =$$

$$\boldsymbol{\sigma}_0 + \left.\frac{\partial^2 \Psi}{\partial\boldsymbol{\varepsilon}\,\partial\boldsymbol{\varepsilon}}\right|_{\boldsymbol{\varepsilon}_0, \boldsymbol{P}_0} : \Delta\boldsymbol{\varepsilon} + \left.\frac{\partial^2 \Psi}{\partial\boldsymbol{\varepsilon}\,\partial\boldsymbol{P}}\right|_{\boldsymbol{\varepsilon}_0, \boldsymbol{P}_0} : \Delta\boldsymbol{P}. \tag{3.32}$$

---

[3]For details on linearization and the *Gâteaux-derivative* see the section A.1.

In the case that the evolution of inelastic variables take place we have from (3.29) $\phi_j = 0 \; \forall \; j \in \mathbb{S}_{act}$ and therefore the consistency condition

$$\Delta\phi_j = \frac{\partial\phi_j}{\partial\boldsymbol{P}} : \Delta\boldsymbol{P} + \frac{\partial\phi_j}{\partial\boldsymbol{Q}} : \Delta\boldsymbol{Q} + \frac{\partial\phi_j}{\partial\boldsymbol{\varepsilon}} : \Delta\boldsymbol{\varepsilon} = 0 \quad \forall \; j \in \mathbb{S}_{act} \tag{3.33}$$

has to be fulfilled. In view of (2.176) and (3.1), the incrementation of the list $\boldsymbol{Q}$ attains the form

$$\Delta\boldsymbol{Q} = -\frac{\partial^2\Psi}{\partial\boldsymbol{P}\,\partial\boldsymbol{P}} : \Delta\boldsymbol{P} - \frac{\partial^2\Psi}{\partial\boldsymbol{P}\,\partial\boldsymbol{\varepsilon}} : \Delta\boldsymbol{\varepsilon}, \tag{3.34}$$

which, taking into consideration relation (3.31), allows to express the consistency condition as

$$\Delta\phi_j = \sum_{k\in\mathbb{S}_{act}} \Delta\lambda_k \left(\frac{\partial\phi_j}{\partial\boldsymbol{P}} : \frac{\partial\phi_k}{\partial\boldsymbol{Q}} - \frac{\partial\phi_j}{\partial\boldsymbol{Q}} : \frac{\partial^2\Psi}{\partial\boldsymbol{P}\,\partial\boldsymbol{P}} : \frac{\partial\phi_k}{\partial\boldsymbol{Q}} \right)$$
$$+ \left(\frac{\partial\phi_j}{\partial\boldsymbol{\varepsilon}} - \frac{\partial\phi_j}{\partial\boldsymbol{Q}} : \frac{\partial^2\Psi}{\partial\boldsymbol{P}\,\partial\boldsymbol{\varepsilon}} \right) : \Delta\boldsymbol{\varepsilon} = 0 \quad \forall \; j \in \mathbb{S}_{act}. \tag{3.35}$$

Collecting the coefficients multiplying incrementation of inelastic consistency parameters $\Delta\lambda_k$ into a matrix

$$G_{jk} = \frac{\partial\phi_j}{\partial\boldsymbol{P}} : \frac{\partial\phi_k}{\partial\boldsymbol{Q}} - \frac{\partial\phi_j}{\partial\boldsymbol{Q}} : \frac{\partial^2\Psi}{\partial\boldsymbol{P}\,\partial\boldsymbol{P}} : \frac{\partial\phi_k}{\partial\boldsymbol{Q}} \tag{3.36}$$

and inverting it

$$G^{jk} = (G_{jk})^{-1}, \tag{3.37}$$

one can solve (3.35) for the increments of the inelastic consistency parameters

$$\Delta\lambda_j = \sum_{k\in\mathbb{S}_{act}} G^{jk} \cdot \left[\left(\frac{\partial\phi_k}{\partial\boldsymbol{Q}} : \frac{\partial^2\Psi}{\partial\boldsymbol{P}\,\partial\boldsymbol{\varepsilon}} - \frac{\partial\phi_k}{\partial\boldsymbol{\varepsilon}} \right) : \Delta\boldsymbol{\varepsilon} \right]. \tag{3.38}$$

In view of (3.38) and (3.31) the linearization of the stress tensor (3.32) becomes

$$\mathcal{L}\boldsymbol{\sigma} = \boldsymbol{\sigma}_0 + \frac{\partial^2\Psi}{\partial\boldsymbol{\varepsilon}\,\partial\boldsymbol{\varepsilon}} : \Delta\boldsymbol{\varepsilon}$$
$$+ \sum_{j\in\mathbb{S}_{act}} \sum_{k\in\mathbb{S}_{act}} G^{jk} \left[\left(\frac{\partial^2\Psi}{\partial\boldsymbol{\varepsilon}\,\partial\boldsymbol{P}} : \frac{\partial\phi_j}{\partial\boldsymbol{Q}} \right) \otimes \left(\frac{\partial\phi_k}{\partial\boldsymbol{Q}} : \frac{\partial^2\Psi}{\partial\boldsymbol{P}\,\partial\boldsymbol{\varepsilon}} \right) \right.$$
$$\left. - \left(\frac{\partial^2\Psi}{\partial\boldsymbol{\varepsilon}\,\partial\boldsymbol{P}} : \frac{\partial\phi_j}{\partial\boldsymbol{Q}} \right) \otimes \frac{\partial\phi_k}{\partial\boldsymbol{\varepsilon}} \right] : \Delta\boldsymbol{\varepsilon}. \tag{3.39}$$

Obviously, one can relate increments of the stress tensor to increments of the strain tensor in a manner analogous to the linear theory (3.6)

$$\mathcal{L}\boldsymbol{\sigma} = \boldsymbol{\sigma}_0 + \mathbb{C}^{IN}(\boldsymbol{\varepsilon}_0, \boldsymbol{P}_0) : \Delta\boldsymbol{\varepsilon}, \tag{3.40}$$

utilizing the so-called *inelastic (algorithmic) tangent* operator in the form

$$\mathbb{C}^{IN} = \frac{\partial^2\Psi}{\partial\boldsymbol{\varepsilon}\,\partial\boldsymbol{\varepsilon}} + \sum_{j\in\mathbb{S}_{act}} \sum_{k\in\mathbb{S}_{act}} G^{jk} \left[\left(\frac{\partial^2\Psi}{\partial\boldsymbol{\varepsilon}\,\partial\boldsymbol{P}} : \frac{\partial\phi_j}{\partial\boldsymbol{Q}} \right) \otimes \left(\frac{\partial\phi_k}{\partial\boldsymbol{Q}} : \frac{\partial^2\Psi}{\partial\boldsymbol{P}\,\partial\boldsymbol{\varepsilon}} \right) \right.$$
$$\left. - \left(\frac{\partial^2\Psi}{\partial\boldsymbol{\varepsilon}\,\partial\boldsymbol{P}} : \frac{\partial\phi_j}{\partial\boldsymbol{Q}} \right) \otimes \frac{\partial\phi_k}{\partial\boldsymbol{\varepsilon}} \right] \tag{3.41}$$

In general, the tangent operator $\mathbb{C}^{IN}$ is not going to be symmetric. Hence, very appealing symmetry property of generalized standard material, cf. Hackl (1997); Lorentz and Benallal (2005), is lost with the introduction of the explicit dependence of the elastic range on the strain tensor. That is clearly a drawback in numerical implementation of material models adopting this assumption. However, the realistic description of the macroscopic behavior of a wide range of materials is only possible if the dependence of yield functions on the strain is taken into account.

3.2.2. Damage material model

One defines damage as a modification of any material physical property due to the presence or the growth of defects (microcracks, voids, delamination etc.). Continuum damage models characterize, represent and model at the macroscopic scale the effects of distributed defects and their growth on the material behavior by a set of continuous damage variables. According to the pretty wide and abstract definition of the phenomena they describe, there is a variety of damage variables used in literature, ranging from scalars over first-, second-, forth- up to eighth-order tensors. A survey on this subject can be found in Skrzypek and Ganczarski (1999).

The evolution of damage, that means nucleation of new microcracks resulting in distributed
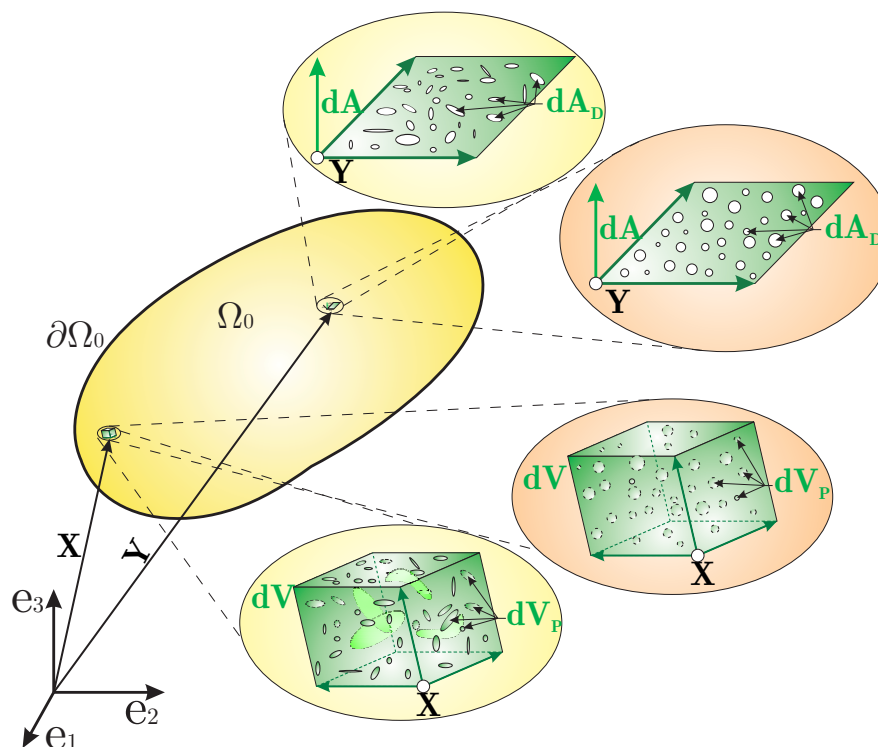
Figure 3.1.: Illustration of the isotropic damage assumption

microcracking, on the one hand, and propagation (growth) of already existing microcracks, on the other hand, induces anisotropy even in the initially isotropic materials. In order to take the anisotropic effects of the damage evolution into account, one has to introduce tensorial variables, e.g. Cordebois and Sidoroff (1982); Carol et al. (2001a,b); Govindjee et al. (1995); Chaboche (2003). However, in a lot of problems it is sufficient, at least from the phenomenological point of view, to assume that the development of damage does not affect

material isotropy. The Figure 3.1 illustrates such idealized situation: either the microcracks are randomly oriented so that no preferable direction exists or the microvoids have spherical shape. In these cases scalar damage variables adequately describe the local state of a damaged material. Based on the Figure 3.1, two classical interpretations of the scalar damage variable can be given. The first one (cf. Rabotnov (1968)) represents the ratio between the area dA_D of the intersection of all microcracks and microvoids with the total area dA of the plane section $D = dA_D/dA$. The second one (cf. Gurson (1977)) represents the current volume fraction of the voids in the representative volume element $D = dV_P/dV$. From both definitions follows $D \in [0, 1]$, where $D = 0$ stands for the undamaged material and $D = 1$ represents complete loss of integrity. For further details on the subject of continuum damage mechanics, one is referred to e.g. Lemaitre and Chaboche (1988); Krajcinovic (2002); Skrzypek and Ganczarski (1999).

In order to take isotropic damaging process into account the Helmholtz free-energy function of an elastic material (3.8) is modified in the form

$$\Psi \;=\; \frac{1}{2}\, f(d)\; (\boldsymbol{\varepsilon} : \mathbb{C} : \boldsymbol{\varepsilon}) \;+\; g(d). \tag{3.42}$$

The scalar variable d measures the degree of the material stiffness loss (reduction of the Young's modulus, see Ju (1990))

$$f(d) \;=\; \frac{E_c}{E_0}, \tag{3.43}$$

where E_c stands for the current effective Young's modulus (or better named secant stiffness modulus, cf. Willam (2002)) and E_0 represents its initial value. Strictly speaking, the initial material always contains some defects, but it is assumed that these are accounted for in the virgin material properties. The formulation (3.42) unifies the so-called *postulate of strain equivalence* (Chaboche (1984)) with the *postulate of energy equivalence* (Cordebois and Sidoroff (1982)), which could be restored for the specific forms of $f(d)$. Moreover, it allows for generalization of the damage variable d in the sense that it does not have to be restricted to the interval $[0, 1]$ any more. From the relation (3.43) one obtains the condition that has to be met by the *damage softening function* $f(d)$: it should be at least twice differentiable and has to satisfy the conditions

$$f(d) : (0, d_\infty) \to [0, 1) \mid \{f(0) = 1,\; f(d_\infty) = 0\}. \tag{3.44}$$

These conditions assure pure elastic behaviour of the undamaged material $d = 0$ and the complete material stiffness loss in the case limiting case $d = d_\infty$. Depending on the definition of the damage variable, its domain interval can be bounded from above by some constant value $d \in \Re^+$ (e.g. $d_\infty = 1$) or can be unbounded as well ($d_\infty \to \infty$). The lists of internal variables and their thermodynamic conjugates (3.26) involved in the formulation becomes trivial in this case

$$\boldsymbol{P} \;=\; \{d\}, \qquad \boldsymbol{Q} \;=\; \{\eta_d\}. \tag{3.45}$$

In view of (3.45) and (3.42) the constitutive relations for the stress tensor $\boldsymbol{\sigma}$ and the thermodynamic driving force η_d become

$$\boldsymbol{\sigma} \;=\; f(d)\, \mathbb{C} : \boldsymbol{\varepsilon}, \qquad \eta_d \;=\; -\frac{1}{2}\, f'(d)\; (\boldsymbol{\varepsilon} : \mathbb{C} : \boldsymbol{\varepsilon}) - g'(d). \tag{3.46}$$

The dissipation potential (3.27) specified for the present case reads

$$J(\dot{\boldsymbol{P}}) \;=\; \sup_{\eta_d} \left[\eta_d \, \dot{d} \;-\; I_K(d, \eta_d, \boldsymbol{\varepsilon}) \right].$$ (3.47)

In order to complete the conjugate potential $J(\dot{\boldsymbol{P}})$, the set of inelastic constraints defining an elastic domain I_K (relations (3.23) and (3.25)) has to be specified. Furthermore, a softening function $f(d)$ and the damage potential $g(d)$ have to be given. That task is accomplished in the following part of this section.

Damage models

The first damage model used in this thesis is denoted as *damage model I* and employs an energetic threshold condition, whose variances are used by e.g. Lorentz and Benallal (2005); Simo and Ju (1987); Lorentz and Andrieux (2003); Liebe et al. (2001); Dimitrijević and Hackl (2008).

The model quantities according to the consideration in sections 3.2.1 and 3.2.2 are summarized in Table 3.1. In addition, the material parameter r_1 represents the threshold value that triggers damage evolution. Apart from the specification of the model quantities, Table 3.1 contains the plots of the initial threshold surfaces in both principal strain and principal stress space as well as a stress vs. strain diagrams obtained for the monotonic uniaxial tension and compression put together for comparison. This model belongs to the category of generalized standard materials, cf. Halphen and Nguyen (1975); Hackl (1997), and therefore is particularly suitable for subsequent analysis as well as numerical implementation. However, due to its energetic formulation (see the plots in Table 3.1), it does not distinguish between the loading in tensile and compressive regime. That is a significant drawback in the modeling of concrete and rock material, which exhibit great sensitivity of their mechanical behavior to pressure, resulting in a dramatically lower strength in tension than in compression.

To resolve the problem, a formulation of the threshold condition dependent on the norm of the positive part of the strain tensor

$$\boldsymbol{\varepsilon}^+ \;=\; \sum_{i=1}^{3} \frac{1}{2} \left(\varepsilon_i + |\varepsilon_i| \right) \, \boldsymbol{n}_i \otimes \boldsymbol{n}_i \;=\; \sum_{i=1}^{3} \frac{1}{2} \left(\varepsilon_i + |\varepsilon_i| \right) \boldsymbol{N}_i$$ (3.54)

is introduced in Mazars and Pijaudier-Cabot (1989) and afterwards employed by e.g. Peerlings et al. (1998); Peerlings (1999); Peerlings et al. (2004). In the relation (3.54) ε_i stands for the eigenvalues of the strain tensor, while $\boldsymbol{n}_i$ and $\boldsymbol{N}_i$ stand for the corresponding eigenvectors and eigenbases.[4] Thermodynamically consistent variance of the Mazar's model is developed by Nedjar (2001) and subsequently used by e.g. Makowski et al. (2006); Dimitrijević and Hackl (2008). Its variance is summarized in Table 3.2 and it is denoted in sequel as *damage model II*. Model parameter r_1 represents the damage threshold, while the parameter a_1 controls the rate of softening. The inelastic tangent modulus of the model is presented in the relation (3.53) and attains symmetric form only in the case where all principal strains are positive. The Heaviside function

$$H(\varepsilon_i) \;=\; \begin{cases} 0 \,| \; \varepsilon_i \,<\, 0 \\ 1 \,| \; \varepsilon_i \,\leq\, 0 \end{cases}$$ (3.55)

---

[4]For details on spectral decomposition of a second order tensor see the section A.3.2.

Damage model I

(1) **Threshold function ϕ_d softening function $f(d)$ and damage potential $g(d)$:**

$$\phi_d := \eta_d - r_1 \leq 0, \qquad f(d) = e^{-d}, \qquad g(d) = 0 \tag{3.48}$$

(2) **Initial damage threshold surface in principal strain (left) and principal stress space (right):**
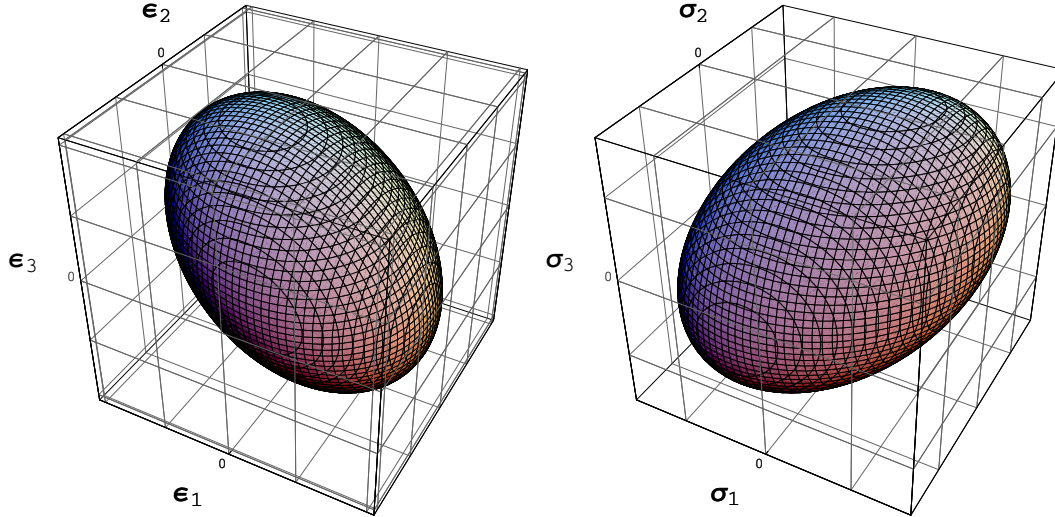
(3) **Stress tensor σ and the thermodynamic driving force η_d:**

$$\boldsymbol{\sigma} = e^{-d} \, \mathbb{C} : \boldsymbol{\varepsilon}, \qquad \eta_d = \frac{1}{2} \, e^{-d} \, (\boldsymbol{\varepsilon} : \mathbb{C} : \boldsymbol{\varepsilon}) \tag{3.49}$$

(4) **Combined stress-strain curves in uniaxial tension and compression:**
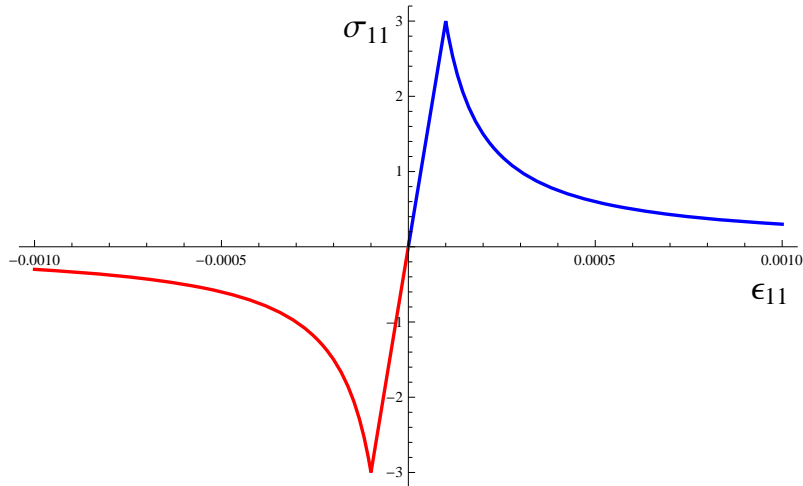
(5) **Inelastic tangent operator:**

$$\mathbb{C}^{IN} = e^{-d} \left(\mathbb{C} - \frac{1}{\frac{1}{2} (\boldsymbol{\varepsilon} : \mathbb{C} : \boldsymbol{\varepsilon})} \, (\mathbb{C} : \boldsymbol{\varepsilon}) \otimes (\mathbb{C} : \boldsymbol{\varepsilon}) \right) \tag{3.50}$$

Table 3.1.: Summary of the damage model I

Damage model II

(1) **Threshold function** ϕ_d **softening function** $f(d)$ **and damage potential** $g(d)$:

$$\phi_d := \eta_d - \frac{1}{2}\left(\boldsymbol{\varepsilon}^- : \mathbb{C} : \boldsymbol{\varepsilon}^- \; + \; \boldsymbol{\varepsilon}^+ : \mathbb{C} : \boldsymbol{\varepsilon}^- \; + \; \boldsymbol{\varepsilon}^- : \mathbb{C} : \boldsymbol{\varepsilon}^+\right) \; \leq \; 0,$$

$$f(d) = (1-d)^2, \qquad g(d) = \frac{1}{a_1} \, r_1 \, \frac{1}{(1-d)^{a_1}} \quad (3.51)$$

(2) **Initial damage threshold surface in principal strain (left) and principal stress space (right)**:
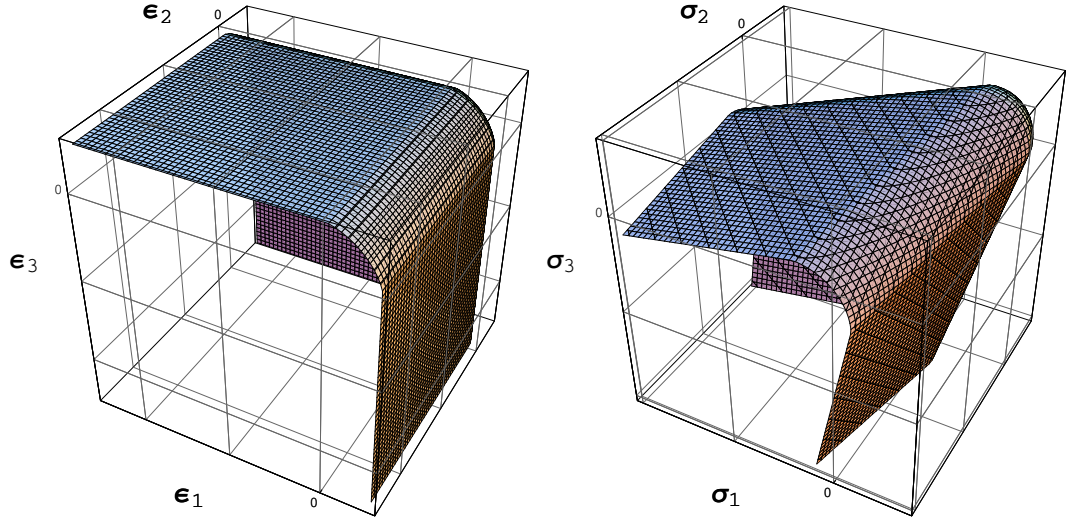
(3) **Stress tensor** $\boldsymbol{\sigma}$ **and the thermodynamic driving force** η_d:

$$\boldsymbol{\sigma} = (1-d)^2 \, \mathbb{C} : \boldsymbol{\varepsilon}, \qquad \eta_d = (1-d) \, \boldsymbol{\varepsilon} : \mathbb{C} : \boldsymbol{\varepsilon} - \frac{r_1}{(1-d)^{a_1+1}} \quad (3.52)$$

(4) **Combined stress-strain curves in uniaxial tension and compression**:
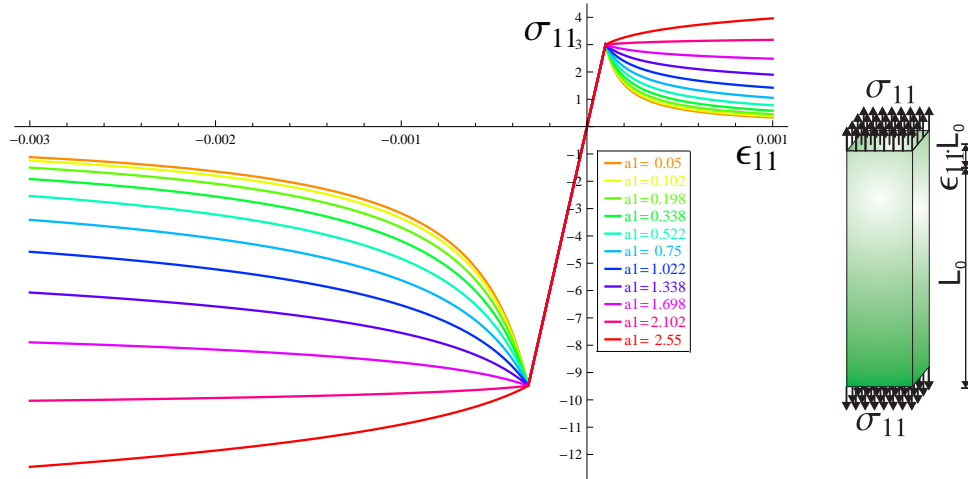
(5) **Inelastic tangent operator**:

$$\mathbb{C}^{IN} = (1-d)^2 \, \mathbb{C} \; - \; \frac{4(1-d)^2}{\boldsymbol{\varepsilon}^+ : \mathbb{C} : \boldsymbol{\varepsilon}^+ + \frac{r_1 \, (a_1+1)}{(1-d)^{a_1+2}}}$$

$$\left[(\mathbb{C} : \boldsymbol{\varepsilon}) \otimes \left(\sum_{i=1}^{3} H(\varepsilon_i) \left(\boldsymbol{N}_i : \mathbb{C} : \boldsymbol{\varepsilon}^+ \right) \boldsymbol{N}_i \right) \right] \quad (3.53)$$

Table 3.2.: Summary of the damage model II

assures that only eigenbases characterized by positive eigenvalues take part in the construction of the inelastic tangent. The Table 3.2 comprises, in addition, plots of the initial threshold surface in both principal strain and principal stress space as well as stress-strain diagrams obtained by monotonic uniaxial tension and compression tests. These results confirm the ability of the *damage model II* to describe the strength dependence on pressure. However, that capability is limited by the fact that the threshold is defined solely by one parameter. In order to demonstrate the weakness, the threshold value r_1 in (3.52) is calibrated to yield the correct strength in the uniaxial tensile test, i.e.

$$r_1 = \frac{f_t^2 (1 - \nu)}{E (1 - 2\nu)(1 + \nu)}. \tag{3.56}$$

The degree of difference between the uniaxial tensile f_t and compressive f_c strengths is then merely dependent on the value of Poisson's ratio ν, cf. Nedjar (2001)

$$f_c = \frac{f_t}{\nu} \sqrt{\frac{1 - \nu}{2}}. \tag{3.57}$$

The typical values of Poisson's ratio for e.g. concrete (0.15-0.21) and rocks like marble and granite (0.2-0.3) result in lower than experimentally obtained compressive strength values. To resolve this limitation, a dependence on at least two parameters has to be introduced, cf. Comi (2001); Comi and Perego (2001); Peerlings (1999).

3.2.3. Plastic material model

A lot of materials loaded to a sufficiently high stress exhibit permanent deformation. Such processes are described by the plasticity theory, whose phenomenological description relies on the introduction of the irreversible strains in the modeling of the macroscopic behavior of a material. The root of the permanent strains lays on the microscale level, e.g. dislocation sliding and nucleation thus generating plastic slip along crystalline planes in metals, cf. Lubliner (1997), sliding over one another of grains and particles in soil or wooden chips in chipboard Müller (2006). In concrete and rocks the permanent deformation is due to several mechanisms, the foremost of which are the opening and closing of cracks, reorientation of the aggregate grains and pore collapse at high confinement, cf. Jirásek and Bazant (2002); Vrech and Etse (2009).

Plastic deformation is irreversible and after unloading remains accumulated within the material, thus leading to residual geometric distortion. A small illustration of the microscale processes for metals, where the plastic deformation is the result slip on specific crystallographic planes in response to shear stress along these planes, and soil, where permanent shearing deformation occurs due to sliding of the particles over one another is given in the Figure 3.2. Due to different mechanisms on the microscale level, macroscopic behavior of materials undergoing plastic deformation varies significantly. While the crystallographic slip process in metals runs almost without volume change, sliding of particles and grains in soil-like materials is connected to the volume changes due to loosening and reorientation of the grain structure. The development of plastic strains in metals results in hardening (increase of the strength) of the material due to interaction of the propagating dislocations, cf. Kochman (2009). On the contrary, plastic deformation of soils, rock-like materials, wood has softening (decrease of the strength) as a consequence, owing to disintegration of grain structure (soil, wood) or opening of cracks (concrete, rocks). A detailed review on the theoretical and computational aspect of plasticity can be found in Hill (1950); Lubliner (1997);
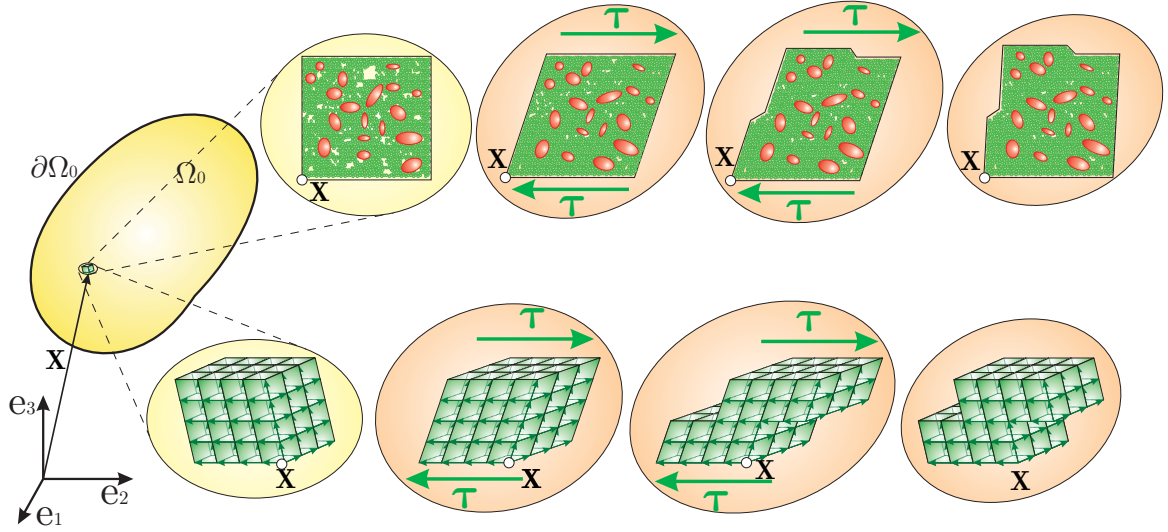
Figure 3.2.: Illustration of the microscale processes behind plastic strains

Simo and Hughes (1998); Han and Reddy (1999).

Assuming small strains, the total strain is decomposed into elastic ε_E and plastic ε_P parts

$$\varepsilon = \varepsilon_E + \varepsilon_P, \tag{3.58}$$

so that the elastic strain is recovered after unloading. In order to account for plastic strains, the Helmholtz free-energy function of an elastic material (3.8) is modified in the form

$$\Psi = \frac{1}{2}\,(\varepsilon - \varepsilon_P) : \mathbb{C} : (\varepsilon - \varepsilon_P) + W(\boldsymbol{\alpha}_P). \tag{3.59}$$

The plastic potential $W(\boldsymbol{\alpha}_P)$ defines hardening or softening behavior of a material under consideration as a function of a list of history-dependent variables $\boldsymbol{\alpha}_P$. Based on relations (3.58) and (3.59) a number of plasticity theories, like the classical ones of Rankine (1858); Tresca (1864); Mohr (1900); von Mises (1913); Drucker and Prager (1952), can be utilized in the description of a material response.

The consideration in the present thesis is restricted to the model based on the theory of von Mises (1913), which is defined under assumption that no plastic volumetric strain occurs. In view of the relations (3.19) and (3.20) which define volumetric-deviatoric split of the strain and the elastic material tensors, respectively, free energy function commonly used in the modeling of plasticity with isotropic hardening is obtained as

$$\Psi = \frac{1}{2}\,((\mathrm{tr}\,\boldsymbol{\varepsilon}\,\mathbf{I}) : \mathrm{sph}\,\mathbb{C} : (\mathrm{tr}\,\boldsymbol{\varepsilon}\,\mathbf{I}))$$
$$+ \frac{1}{2}\,(\mathrm{dev}\,\boldsymbol{\varepsilon} - \varepsilon_P) : \mathrm{dev}\,\mathbb{C} : (\mathrm{dev}\,\boldsymbol{\varepsilon} - \varepsilon_P) + W(\alpha_P). \tag{3.66}$$

The inherent assumption of all plasticity theories that the elastic material tensor $\mathbb{C}$ remains unaffected by plastic deformation is obvious from (3.66).

The lists of internal variables and their thermodynamic conjugates (3.26) involved in the formulation becomes in this case

$$\boldsymbol{P} = \{\varepsilon_P, \alpha_P\}, \qquad \boldsymbol{Q} = \{\boldsymbol{\sigma}_P, \eta_P\}. \tag{3.67}$$

Plastic model I

(1) Yield function ϕ_P and plastic potentials $W(\alpha_P)$:

$$\phi_P := \sqrt{\boldsymbol{\sigma}_P : \boldsymbol{\sigma}_P} - \eta_P \leq 0, \quad W_1(\alpha_P) = -r_2\,\alpha_P + \frac{1}{2}\,K_H\,\alpha_P^2 \quad (3.60)$$

(2) Initial plastic yield surface in principal stress space:
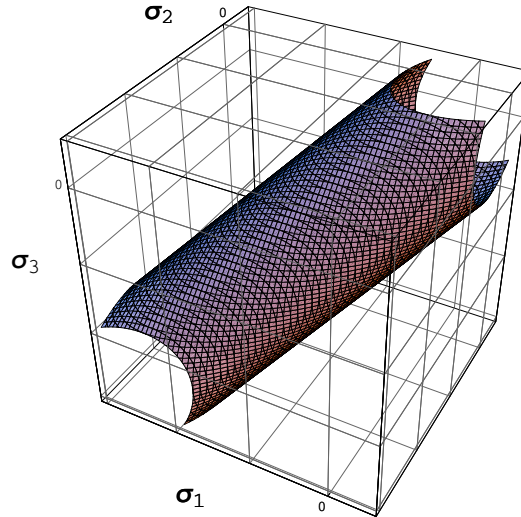
(3) Stress tensor $\boldsymbol{\sigma}$ and the thermodynamic driving forces $\boldsymbol{\sigma}_P$ and η_P:

$$\boldsymbol{\sigma} = \mathbb{C} : (\boldsymbol{\varepsilon} - \boldsymbol{\varepsilon}_P),$$

$$\boldsymbol{\sigma}_P = \operatorname{dev}\mathbb{C} : (\operatorname{dev}\boldsymbol{\varepsilon} - \boldsymbol{\varepsilon}_P), \qquad \eta_{P,1} = r_2 - K_H\,\alpha_P \quad (3.61)$$

(4) Stress-strain curves in uniaxial tension:
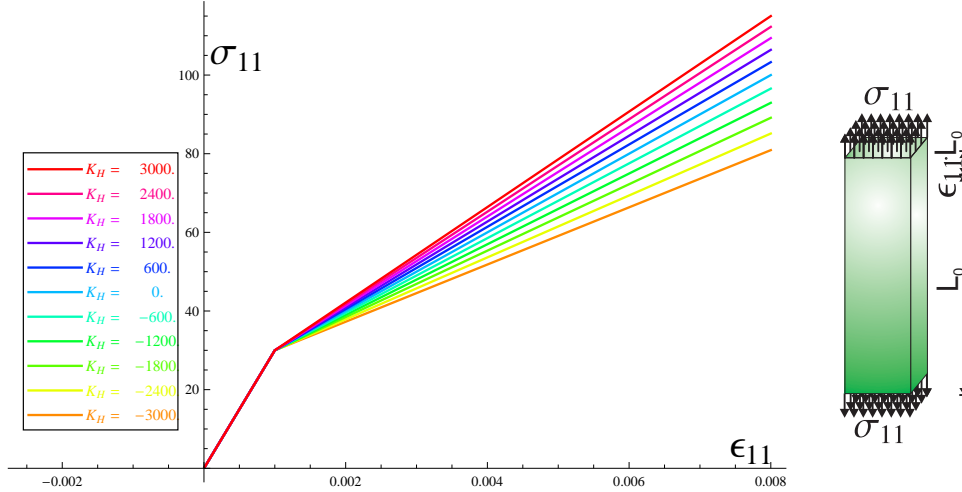
(5) Inelastic tangent operator:

$$\mathbb{C}^{IN} = \mathbb{C} - \frac{1}{\boldsymbol{\sigma}_P : \operatorname{dev}\mathbb{C} : \boldsymbol{\sigma}_P - K_H\,\boldsymbol{\sigma}_P : \boldsymbol{\sigma}_P}$$
$$[(\operatorname{dev}\mathbb{C} : \boldsymbol{\sigma}_P) \otimes (\operatorname{dev}\mathbb{C} : \boldsymbol{\sigma}_P)] \quad (3.62)$$

Table 3.3.: Summary of the plastic model I

Plastic model II

---

(1) **Yield function ϕ_P and plastic potential $W(\alpha_P)$:**

$$\phi_P := \sqrt{\boldsymbol{\sigma}_P : \boldsymbol{\sigma}_P} - \eta_P \leq 0,$$

$$W_2(\alpha_P) = -r_{2,\infty}\, \alpha_P + \frac{r_{2,0} - r_{2,\infty}}{K_H}\left(\frac{1}{K_H\,\alpha_P - 1} - 1\right) \quad (3.63)$$

(2) **Initial plastic yield surface in principal stress space:**

(3) **Stress tensor $\boldsymbol{\sigma}$ and the thermodynamic driving forces $\boldsymbol{\sigma}_P$ and η_P:**

$$\boldsymbol{\sigma} = \mathbb{C} : (\boldsymbol{\varepsilon} - \boldsymbol{\varepsilon}_P), \qquad \boldsymbol{\sigma}_P = \operatorname{dev}\mathbb{C} : (\operatorname{dev}\boldsymbol{\varepsilon} - \boldsymbol{\varepsilon}_P),$$

$$\eta_{P,2} = r_{2,\infty} + \frac{r_{2,0} - r_{2,\infty}}{(K_H\,\alpha_P - 1)^2} \quad (3.64)$$

(4) **Stress-strain curves in uniaxial tension:**

(5) **Inelastic tangent operator:**

$$\mathbb{C}^{IN} = \mathbb{C} - \frac{1}{\boldsymbol{\sigma}_P : \operatorname{dev}\mathbb{C} : \boldsymbol{\sigma}_P - 2K_H\,\dfrac{r_{2,0} - r_{2,\infty}}{(K_H\,\alpha_P - 1)^3}\,\boldsymbol{\sigma}_P : \boldsymbol{\sigma}_P}$$

$$[(\operatorname{dev}\mathbb{C} : \boldsymbol{\sigma}_P) \otimes (\operatorname{dev}\mathbb{C} : \boldsymbol{\sigma}_P)] \quad (3.65)$$

Table 3.4.: Summary of the plastic model II

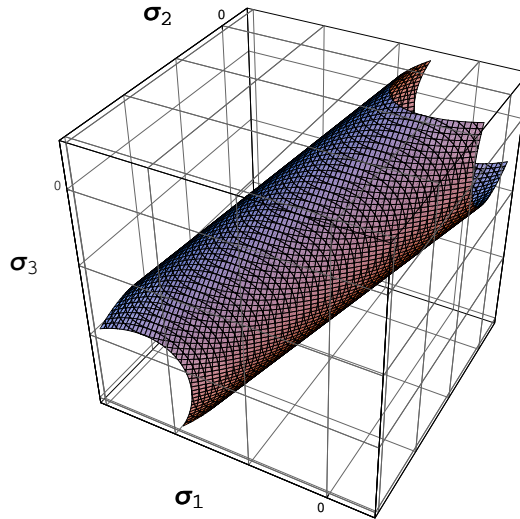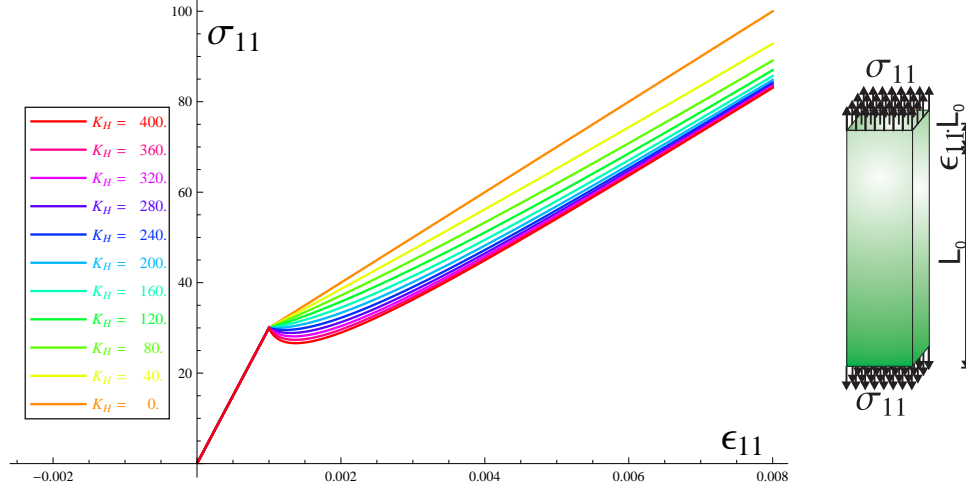In view of (3.45) and (3.42) the constitutive relations for the stress tensor $\boldsymbol{\sigma}$ and the thermo-dynamic driving forces $\boldsymbol{\sigma}_P$ and η_P become

$$\boldsymbol{\sigma} = \mathbb{C} : (\boldsymbol{\varepsilon} - \boldsymbol{\varepsilon}_P) = \operatorname{sph}\mathbb{C} : (\operatorname{tr}\boldsymbol{\varepsilon}\,\mathbf{I}) + \operatorname{dev}\mathbb{C} : (\operatorname{dev}\boldsymbol{\varepsilon} - \boldsymbol{\varepsilon}_P), \qquad (3.68)$$

$$\boldsymbol{\sigma}_P = \operatorname{dev}\mathbb{C} : (\operatorname{dev}\boldsymbol{\varepsilon} - \boldsymbol{\varepsilon}_P) = \operatorname{dev}\boldsymbol{\sigma}, \qquad \eta_P = -W'(\alpha_P). \qquad (3.69)$$

The dissipation potential (3.27) specified for the present case reads:

$$J(\dot{\boldsymbol{P}}) = \sup_{\boldsymbol{\sigma}_P, \eta_P} \left[\boldsymbol{\sigma}_P : \dot{\boldsymbol{\varepsilon}}_P + \eta_P\,\dot{\alpha}_P - I_K(\boldsymbol{\varepsilon}_P, \alpha_P, \boldsymbol{\sigma}_P, \eta_P, \boldsymbol{\varepsilon}) \right]. \qquad (3.70)$$

In order to complete the conjugate potential $J(\dot{\boldsymbol{P}})$, the set of inelastic constraints defining an elastic domain I_K (relations (3.23) and (3.25)) has to be specified, as well as the plastic potential $W(\alpha_P)$.

The plastic model used in this thesis employs a von-Mises yield function, cf. von Mises (1913). Two types of isotropic hardening and softening are investigated: a linear one in the *plastic model I* and a nonlinear one in saturation form in the *plastic model II*. The model quantities according to the consideration in sections 3.2.1 and 3.2.2 are summarized in Tables 3.3 and 3.4. The material parameter r_2 of the linear hardening law represents the plastic yield limit, while the parameters $r_{2,0}$ and $r_{2,\infty}$ of the nonlinear hardening law characterize the initial and the saturation value of the yield stress, respectively. Finally, the parameter K_H defines the rate of hardening. The term hardening is used here in generalized sense, denoting both softening and hardening behavior. Softening laws are obtained for appropriate values of material parameters, e.g. negative K_H in the plastic model I or including $r_{2,0} > r_{2,\infty}$ in the plastic model II.

Apart from the specification of the model quantities, Tables 3.3 and 3.4 contain the plot of the initial yield surface in principal stress space and the expressions for the inelastic tangents of the corresponding plastic models. Just like the *damage model I*, defined in the previous section, the plastic models in the Tables 3.3 and 3.4 belong to the category of generalized standard materials, cf. Halphen and Nguyen (1975); Hackl (1997), with the very nice property of symmetric inelastic tangent (3.62), (3.65). The behavior of a material described by the *plastic models I* and *II* in monotonic uniaxial tension tests and the dependence upon hardening modulus K_H is illustrated by resulting stress-strain diagrams.

3.2.4. Coupled damage-plastic material model

As it was discussed in the previous sections, plasticity and damage are dissipative material behaviors that are attributed to distinct microstructural phenomena. Plastic deformation is associated with dislocations along preferred slip planes or sliding over one another of grains and particles, while damage is related to nucleation and growth of microvoids or microcracks. However, a lot of non-metallic materials, in particular under compressive loading, develop both irreversible deformation as well as degradation of stiffness. In order to take both phenomena into consideration coupled theories are developed, which can be separated into two groups depending on the assumptions introduced in the modeling of coupling, cf. Grassl and Jirásek (2006); Al-Rub and Voyiadjis (2009). One type of combination relies on stress-based plasticity formulated in the effective (undamaged) space (e.g. Simo and Ju (1987); Ju (1990); Lee and Fenves (1998); Makowski et al. (2006)), where the effective

stress is defined as the average microscale stress acting on the undamaged material between microdefects. Another type is based on stress-based plasticity in the nominal (damaged) stress space (e.g. Ortiz (1985); Krätzig and Pölling (2004); Meschke et al. (1998) where the nominal stress is defined as the macroscale stress acting on both damaged and undamaged material. The later approach can be cast into a form involving the notion of *damage strains* ε_d, cf. Meschke et al. (1998); Ibrahimbegović et al. (2003), while the former one leads to the physical interpretation of undamaged material matrix prone to plastic deformation between microdefects. Such microdefects cause inevitably stress concentrations which can exceed by large the average stress in the material matrix. The illustration involving a case of spherical microvoids (Figure 3.3), which corresponds to the assumption of isotropic scalar damage made in section 3.2.2, shows clearly the amplifying influence of the microcracks on the actual "plastic" stress σ_P. Hence, the formulation of plasticity in the effective space describes the actual state of material more accurately, and is therefore favourable, cf. Olsson and Ristinmaa (2003). An additional advantage pointed out in Grassl and Jirásek (2006) is that formulation in effective stress space fulfills a priori the local uniqueness conditions, while these conditions put sometimes strict restrictions on the value of hardening parameter in the formulation in nominal macroscopic stress space. Consequently, the effective stress approach is followed in the formulation of coupled model.
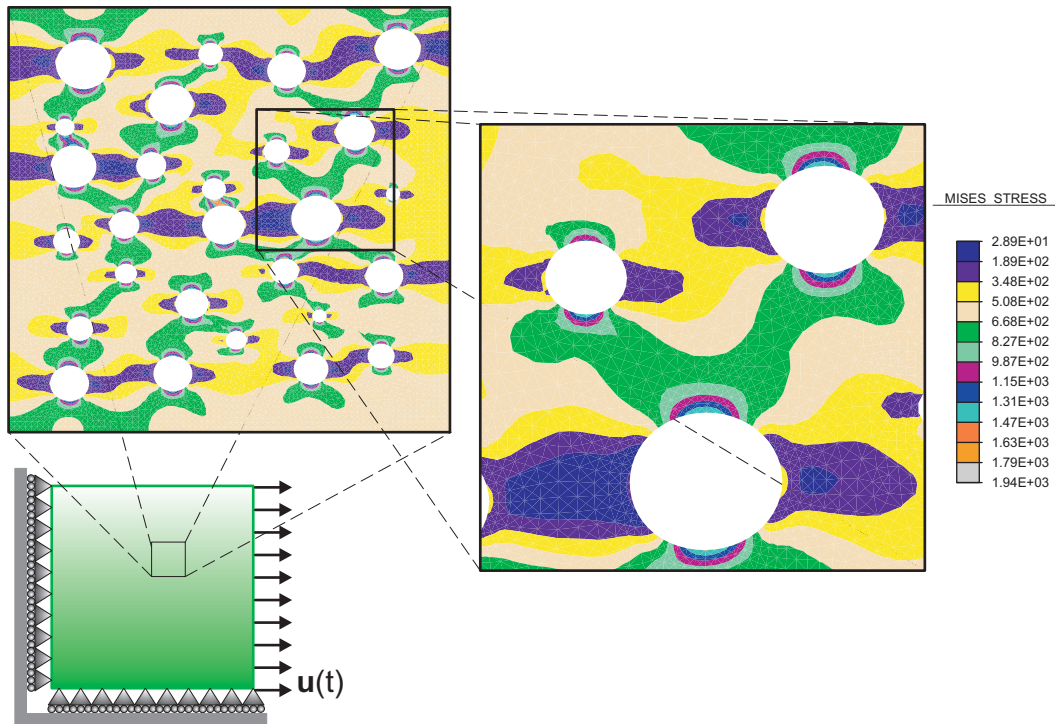
Figure 3.3.: Influence of microdefects on microscale stress

Assuming small strains, the decomposition of total strain in elastic ε_E and plastic ε_P parts (3.58) and the forms of the free-energy function accounting for damage (3.42) and plastic deformation (3.59), one can obtain the Helmholtz free-energy function of an material that develops both irreversible deformation as well as deterioration of stiffness as

$$\Psi = \frac{1}{2} f(d) \, (\varepsilon - \varepsilon_P) : \mathbb{C} : (\varepsilon - \varepsilon_P) \, + \, W(\boldsymbol{\alpha}_P) \, + \, g(d). \tag{3.71}$$

Restricting consideration to the case of purely deviatoric plasticity (3.66) it follows

$$\Psi = \frac{1}{2} f(d) \ ((\operatorname{tr} \boldsymbol{\varepsilon} \ \mathbf{I}) : \operatorname{sph} \mathbb{C} : (\operatorname{tr} \boldsymbol{\varepsilon} \ \mathbf{I}))$$

$$+ \ \frac{1}{2} f(d) \ (\operatorname{dev} \boldsymbol{\varepsilon} - \boldsymbol{\varepsilon}_P) : \operatorname{dev} \mathbb{C} : (\operatorname{dev} \boldsymbol{\varepsilon} - \boldsymbol{\varepsilon}_P) \ + \ W(\boldsymbol{\alpha}_P) \ + \ g(d). \quad (3.72)$$

The definition of the quantities involved in (3.71) and (3.72) is already given in sections 3.2.2 and 3.2.3. Hence, a free-energy function of a coupled material model merges the damage and plastic one by replacing the elastic material tensor $\mathbb{C}$ in the plastic model with the reduced one from the damage model. In addition, both plastic ($W(\boldsymbol{\alpha}_P)$) and damage ($g(d)$) potentials are included. Strictly speaking, one should consider an interaction between the micromechanical processes behind damage and plasticity (Figure 3.3). That will lead to the introduction of an additional coupling potential which is dependent on actual material. However, in the scope of this thesis we restrict ourselves to the consideration of uncoupled potentials only.

The lists of internal variables and their thermodynamic conjugates (3.26) involved in the formulation becomes

$$\boldsymbol{P} = \{d, \boldsymbol{\varepsilon}_P, \alpha_P\}, \qquad \boldsymbol{Q} = \{\eta_d, \boldsymbol{\sigma}_P, \eta_P\}. \quad (3.73)$$

In view of (3.72) and (3.73) the constitutive relations for the stress tensor $\boldsymbol{\sigma}$ and the thermo-dynamic driving forces η_d, $\boldsymbol{\sigma}_P$ and η_P become

$$\boldsymbol{\sigma} = f(d) \ \mathbb{C} : (\boldsymbol{\varepsilon} - \boldsymbol{\varepsilon}_P)$$

$$= f(d) \ \operatorname{sph} \mathbb{C} : (\operatorname{tr} \boldsymbol{\varepsilon} \ \mathbf{I}) \ + \ f(d) \ \operatorname{dev} \mathbb{C} : (\operatorname{dev} \boldsymbol{\varepsilon} - \boldsymbol{\varepsilon}_P), \quad (3.74)$$

$$\boldsymbol{\sigma}_P = f(d) \ \operatorname{dev} \mathbb{C} : (\operatorname{dev} \boldsymbol{\varepsilon} - \boldsymbol{\varepsilon}_P) = \operatorname{dev} \boldsymbol{\sigma}, \qquad \eta_P = -W'(\alpha_P), \quad (3.75)$$

$$\eta_d = -\frac{1}{2} f'(d) \ (\boldsymbol{\varepsilon} - \boldsymbol{\varepsilon}_P) : \mathbb{C} : (\boldsymbol{\varepsilon} - \boldsymbol{\varepsilon}_P) \ - \ g'(d). \quad (3.76)$$

The dissipation potential (3.27) specified for coupled model reads

$$J(\dot{\boldsymbol{P}}) = \sup_{\eta_d, \boldsymbol{\sigma}_P, \eta_P} \left[\eta_d \ \dot{d} \ + \ \boldsymbol{\sigma}_P : \dot{\boldsymbol{\varepsilon}}_P \ + \ \eta_P \ \dot{\alpha}_P - I_K(d, \boldsymbol{\varepsilon}_P, \alpha_P, \eta_d, \boldsymbol{\sigma}_P, \eta_P, \boldsymbol{\varepsilon}) \right]. \quad (3.77)$$

In order to complete the conjugate potential $J(\dot{\boldsymbol{P}})$, the set of inelastic constraints defining an elastic domain I_K (relations (3.23) and (3.25)) has to be specified, as well as plastic $W(\alpha_P)$ and damage $g(d)$ potentials .

Coupled models used in sequel combine the energetic damage threshold condition (*damage model I*) with the von-Mises plastic yield condition accounting for isotropic hardening (*plastic models I* and *II*). According to the type of plastic hardening (softening), one obtains two coupled models: the one including linear plastic hardening (denoted as *coupled model I*) and the one based on nonlinear saturation type plastic hardening (denoted as *coupled model II*). Both models involve exponential damage softening. The model quantities according to consideration in sections 3.2.1 and 3.2.2 are summarized in Tables 3.5 and 3.6. The material parameters of the models are already defined in sections 3.2.2 and 3.2.3 and are not going to be repeated here.

The plot of initial plastic yield and damage threshold surfaces in principal stress space in the Tables 3.5 and 3.6 represents one of the possible combinations, dependent on the actual values of the corresponding limits. In the current plot the yield stress is chosen such that

<div style="border:1px solid">

Coupled damage-plastic model I

(1) **Yield function ϕ_P, damage threshold function ϕ_d, damage and plastic potentials $g(d)$ and $W(\alpha_P)$ and damage softening function $f(d)$:**

$$\phi_P := \frac{1}{f(d)} \sqrt{\boldsymbol{\sigma}_P : \boldsymbol{\sigma}_P} - \eta_P \leq 0, \qquad \phi_d := \eta_d - r_1 \leq 0,$$

$$f(d) = e^{-d}, \quad g(d) = 0, \quad W_1(\alpha_P) = -r_2\,\alpha_P + \frac{1}{2}\,K_H\,\alpha_P^2 \quad (3.78)$$

(2) **Initial plastic and damage limit surfaces in principal stress space:**
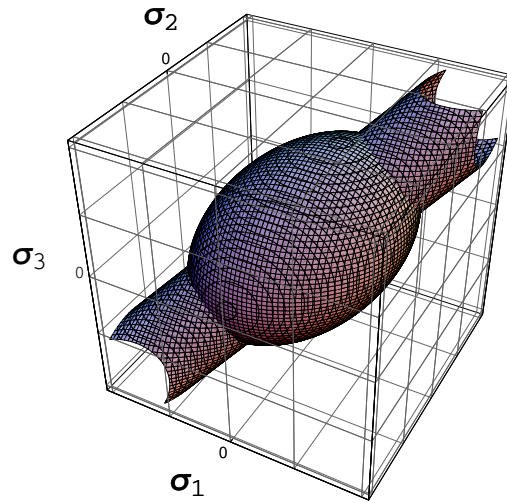
(3) **Stress tensor $\boldsymbol{\sigma}$ and the thermodynamic driving forces $\boldsymbol{\sigma}_P$, η_P and η_d:**

$$\boldsymbol{\sigma} = e^{-d}\,\mathbb{C} : (\boldsymbol{\varepsilon} - \boldsymbol{\varepsilon}_P), \quad \eta_d = \frac{1}{2}\,e^{-d}\,(\boldsymbol{\varepsilon} - \boldsymbol{\varepsilon}_P) : \mathbb{C} : (\boldsymbol{\varepsilon} - \boldsymbol{\varepsilon}_P),$$

$$\boldsymbol{\sigma}_P = e^{-d}\,\mathrm{dev}\,\mathbb{C} : (\mathrm{dev}\,\boldsymbol{\varepsilon} - \boldsymbol{\varepsilon}_P), \quad \eta_{P,1} = r_2 - K_H\,\alpha_P \quad (3.79)$$

(4) **Stress-strain curves in uniaxial tension:**

</div>
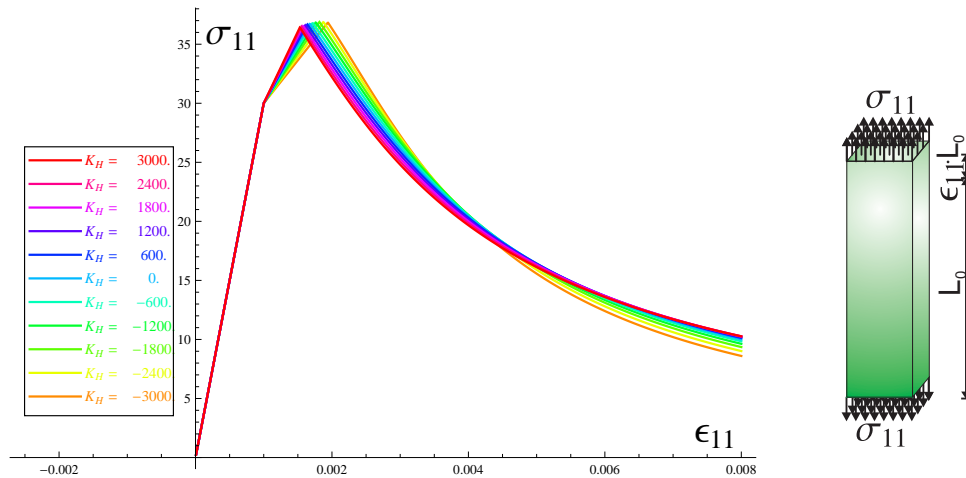
Table 3.5.: Summary of the coupled damage-plastic model I

Coupled damage-plastic model II

(1) Yield function ϕ_P, **damage threshold function** ϕ_d, **damage and plastic potentials** $g(d)$ **and** $W(\alpha_P)$ **and damage softening function** $f(d)$:

$$\phi_P := \frac{\sqrt{\boldsymbol{\sigma}_P : \boldsymbol{\sigma}_P}}{f(d)} - \eta_P \leq 0, \quad \phi_d := \eta_d - r_1 \leq 0, \quad f(d) = e^{-d} \quad (3.80)$$

$$g(d) = 0, \quad W_2(\alpha_P) = -r_{2,\infty}\,\alpha_P + \frac{r_{2,0} - r_{2,\infty}}{K_H}\left(\frac{1}{K_H\,\alpha_P - 1} - 1\right) \quad (3.81)$$

(2) Initial plastic and damage limit surfaces in principal stress space:

(3) Stress tensor $\boldsymbol{\sigma}$ **and the thermodynamic driving forces** $\boldsymbol{\sigma}_P$, η_P **and** η_d:

$$\boldsymbol{\sigma} = e^{-d}\,\mathbb{C} : (\boldsymbol{\varepsilon} - \boldsymbol{\varepsilon}_P), \quad \eta_d = \frac{1}{2}\,e^{-d}\,(\boldsymbol{\varepsilon} - \boldsymbol{\varepsilon}_P) : \mathbb{C} : (\boldsymbol{\varepsilon} - \boldsymbol{\varepsilon}_P), \quad (3.82)$$

$$\boldsymbol{\sigma}_P = e^{-d}\,\operatorname{dev}\mathbb{C} : (\operatorname{dev}\boldsymbol{\varepsilon} - \boldsymbol{\varepsilon}_P), \quad \eta_{P,2} = r_{2,\infty} + \frac{r_{2,0} - r_{2,\infty}}{(K_H\,\alpha_P - 1)^2} \quad (3.83)$$

(4) Stress-strain curves in uniaxial tension:
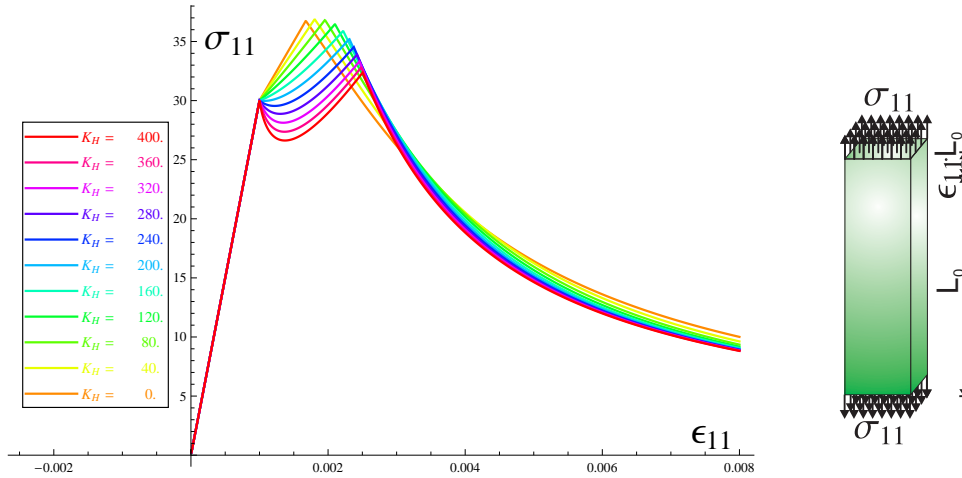
Table 3.6.: Summary of the coupled damage-plastic model II

Coupled damage-plastic model I

(5) **Inelastic tangent operator**:

$$\mathbb{C}^{IN} = e^{-d}\,\mathbb{C}\,-$$

$$\frac{H(\phi_d)\,e^{-d}\,\left[(\mathbb{C} : (\boldsymbol{\varepsilon} - \boldsymbol{\varepsilon}_P)) \otimes (\mathbb{C} : (\boldsymbol{\varepsilon} - \boldsymbol{\varepsilon}_P))\right]}{\frac{1}{2}\,(\boldsymbol{\varepsilon} - \boldsymbol{\varepsilon}_P) : \mathbb{C} : (\boldsymbol{\varepsilon} - \boldsymbol{\varepsilon}_P)}\,+$$
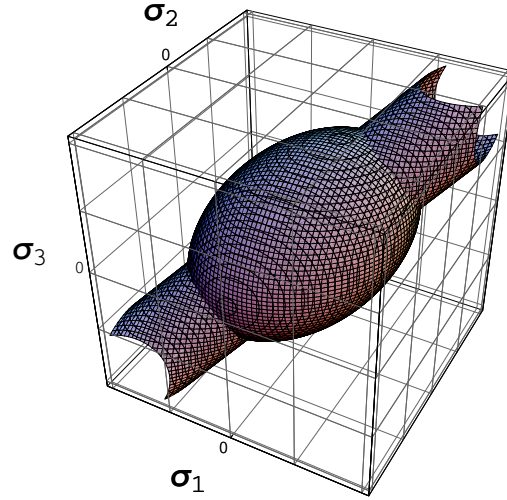
$$\frac{H(\phi_d)\,H(\phi_P)\,e^{-d}\,\left[(\mathbb{C} : (\boldsymbol{\varepsilon} - \boldsymbol{\varepsilon}_P)) \otimes (\mathrm{dev}\,\mathbb{C} : \boldsymbol{\sigma}_P)\right]}{\frac{1}{2}\,(\boldsymbol{\varepsilon} - \boldsymbol{\varepsilon}_P) : \mathbb{C} : (\boldsymbol{\varepsilon} - \boldsymbol{\varepsilon}_P)\,\left(\frac{1}{e^{-d}}\,\boldsymbol{\sigma}_P : \mathrm{dev}\,\mathbb{C} : \boldsymbol{\sigma}_P\,-\,K_H\,\boldsymbol{\sigma}_P : \boldsymbol{\sigma}_P\right)}\,-$$

$$\frac{H(\phi_P)\,\left[(\mathrm{dev}\,\mathbb{C} : \boldsymbol{\sigma}_P) \otimes (\mathrm{dev}\,\mathbb{C} : \boldsymbol{\sigma}_P)\right]}{\frac{1}{e^{-d}}\,\boldsymbol{\sigma}_P : \mathrm{dev}\,\mathbb{C} : \boldsymbol{\sigma}_P - K_H\,\boldsymbol{\sigma}_P : \boldsymbol{\sigma}_P} \tag{3.84}$$

Table 3.7.: Inelastic tangent operator of the coupled damage-plastic model I

Coupled damage-plastic model II

(5) **Inelastic tangent operator**:

$$\mathbb{C}^{IN} = e^{-d}\,\mathbb{C}\,-$$

$$\frac{H(\phi_d)\,e^{-d}\,\left[(\mathbb{C} : (\boldsymbol{\varepsilon} - \boldsymbol{\varepsilon}_P)) \otimes (\mathbb{C} : (\boldsymbol{\varepsilon} - \boldsymbol{\varepsilon}_P))\right]}{\frac{1}{2}\,(\boldsymbol{\varepsilon} - \boldsymbol{\varepsilon}_P) : \mathbb{C} : (\boldsymbol{\varepsilon} - \boldsymbol{\varepsilon}_P)}\,+$$

$$\frac{\dfrac{H(\phi_d)\,H(\phi_P)\,e^{-d}\,\left[(\mathbb{C} : (\boldsymbol{\varepsilon} - \boldsymbol{\varepsilon}_P)) \otimes (\mathrm{dev}\,\mathbb{C} : \boldsymbol{\sigma}_P)\right]}{\frac{1}{2}\,(\boldsymbol{\varepsilon} - \boldsymbol{\varepsilon}_P) : \mathbb{C} : (\boldsymbol{\varepsilon} - \boldsymbol{\varepsilon}_P)}}{\left(\frac{1}{e^{-d}}\,\boldsymbol{\sigma}_P : \mathrm{dev}\,\mathbb{C} : \boldsymbol{\sigma}_P\,-\,2K_H\,\dfrac{r_{2,0} - r_{2,\infty}}{(K_H\,\alpha_P - 1)^3}\,\boldsymbol{\sigma}_P : \boldsymbol{\sigma}_P\right)}\,-$$

$$\frac{H(\phi_P)\,\left[(\mathrm{dev}\,\mathbb{C} : \boldsymbol{\sigma}_P) \otimes (\mathrm{dev}\,\mathbb{C} : \boldsymbol{\sigma}_P)\right]}{\frac{1}{e^{-d}}\,\boldsymbol{\sigma}_P : \mathrm{dev}\,\mathbb{C} : \boldsymbol{\sigma}_P - 2K_H\,\dfrac{r_{2,0} - r_{2,\infty}}{(K_H\,\alpha_P - 1)^3}\,\boldsymbol{\sigma}_P : \boldsymbol{\sigma}_P} \tag{3.85}$$

Table 3.8.: Inelastic tangent operator of the coupled damage-plastic model II

plastic deformation occurs as first in the uniaxial tension test, followed by the evolution of damage which starts slightly later. The resulting stress-strain diagram are included in the Tables 3.5 and 3.6 as well, providing an insight on the effect of plastic hardening modulus K_H on the material response. Finally, the expressions for the inelastic tangents of the corresponding coupled models are presented in the Tables 3.7 and 3.8. Unlike the "ingredient" models, coupled damage-plastic models do not posses symmetric inelastic tangents (3.84), (3.85) due to formulation of the plastic yield functions in the effective stress space.

In order to illustrate elementary differences in the material response modeled by damage, plastic and coupled models a uniaxial tension tests are performed. In the first part of the test the test sample is loaded up to a strain value which is clearly in the inelastic range. The sample is then fully unloaded (up to zero stress). Material parameters of all models are calibrated such that the inelastic processes start at the same point (the same value of strain). The curves presented in Figure 3.4 correspond to *plastic model I* (Table 3.3), *damage model I* (Table 3.1) and their combination, *coupled model I* (Table 3.5). In the case of plastic model the total strain is, owing to the assumptions of small deformation, decomposed into elastic and plastic parts, relation (3.58). The elastic part of strain is recovered after unloading, with the stiffness (elastic modulus E) being unaffected by plastic deformation. The plastic part of strain (ε_P) remains unchanged after unloading, resulting in observable permanent deformation. In contrary to the plastic model, the damage model does not affect strains, but rather the elastic material tensor, represented by elastic modulus E, relations (3.42, 3.43). Hence, there is no residual deformation upon unloading. However, the unloading part of the response curve is not defined by the initial elastic modulus E_0 any more, but rather by the damage-influenced secant elastic modulus E_c. The coupled model combines both characteristic features of the ingredient models: residual strains upon unloading that proceeds along the path determined through damage-affected secant stiffness (modulus E_c). Consequently, the response of the coupled model resides in between the responses of plastic and damage models, depending on the type of loading.
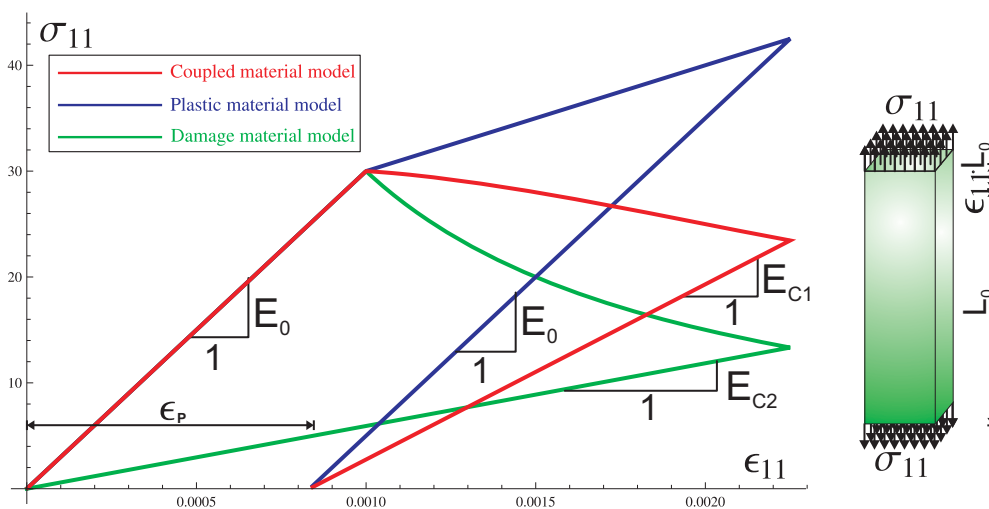
Figure 3.4.: Loading-unloading stress-strain curves of damage, plastic and coupled models

3.3. Localization

Utilization of material models with a softening phase is closely connected to the phenomenon of localization. Localization is characterized by the fact that the deformation tends to accumulate into narrow zones with high concentration of strains and in the development of internal variables, while the rest of the structure experiences unloading. The width of the localization zone is small, but finite and it is dependent on the material microstructure. Hence, it can be considered as a material-specific quantity called internal material length, determined by the size or spacing of dominant heterogeneities, cf. Jirásek (2002). Material models based on classical continuum considerations, like the ones discussed in the previous section, do not involve an internal material length and therefore fail to achieve an objective description of strain localization. In order to illustrate this fact, we start with an elucidative one-dimensional localization example.

3.3.1. One–dimensional example illustrating problems with an objective description of strain localization

Let us consider a straight bar with a constant cross section A and total length L under uniaxial tension, see Figure 3.5(a). The material behavior is described utilizing the *damage model I* (Table 3.1), resulting in the stress-strain dependence presented in Figure 3.5(b). The peak stress is developed at strain

$$\varepsilon_0 = \sqrt{\frac{2\,r_1}{E}}. \tag{3.86}$$

Recalling the local form of the balance of linear momentum (2.124), under vanishing volume forces one obtains that the stress state in the bar is homogeneous

$$\frac{\partial \sigma_{11}}{\partial X} = 0 \quad \Rightarrow \quad \sigma_{11}(X) = \sigma = const = \frac{P}{A}, \tag{3.87}$$

where P stands for the applied force and A for the cross-sectional area of the bar. The resulting displacement of the right end of the specimen is denoted as $u(X = L) = U$. In view of the relation (2.50) which defines the components of the strain tensor in terms of displacement derivatives a compatibility condition

$$\int_{X=0}^{L} \varepsilon_{11}\,dx = \int_{X=0}^{L} \varepsilon\,dx = U, \tag{3.88}$$

arises in the present one-dimensional case.

If the bar is monotonically loaded in tension the stress – strain relation remains linear up to the critical value of strain remains smaller than a critical value ε_0 defined in (3.86)

$$\sigma = E\,\varepsilon \quad \text{if } \varepsilon < \varepsilon_0. \tag{3.89}$$

Above the critical value the stress becomes decreasing function of the strain

$$\sigma = e^{-d}\,E\,\varepsilon \quad \text{if } \varepsilon > \varepsilon_0. \tag{3.90}$$
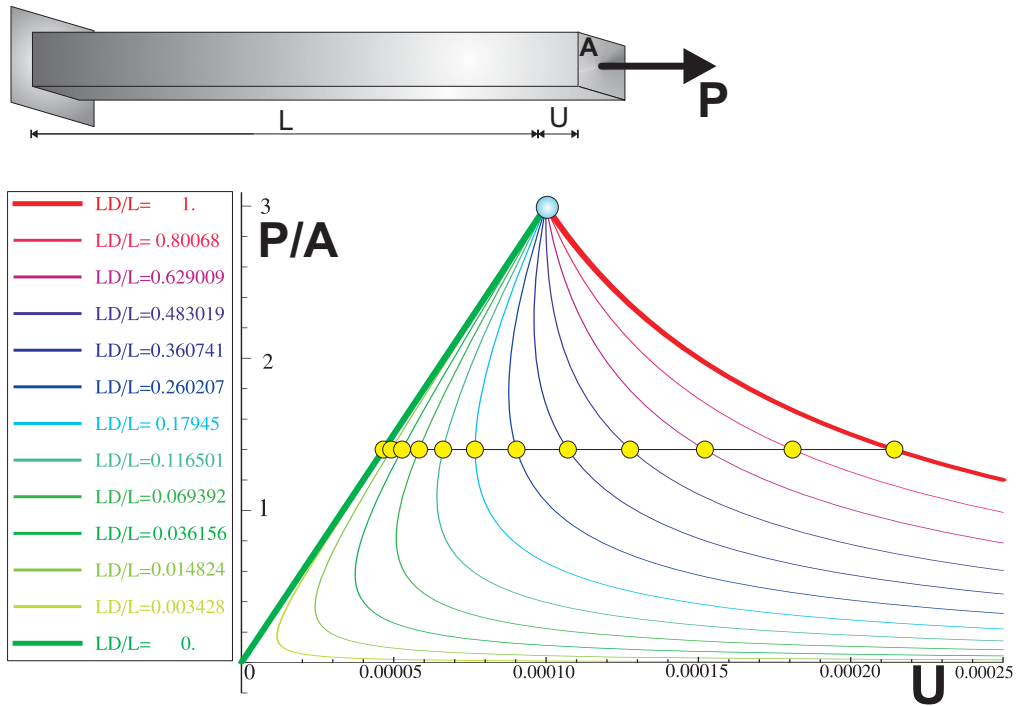
(a) Structural response of the specimen in dependence on the length of damaged zone
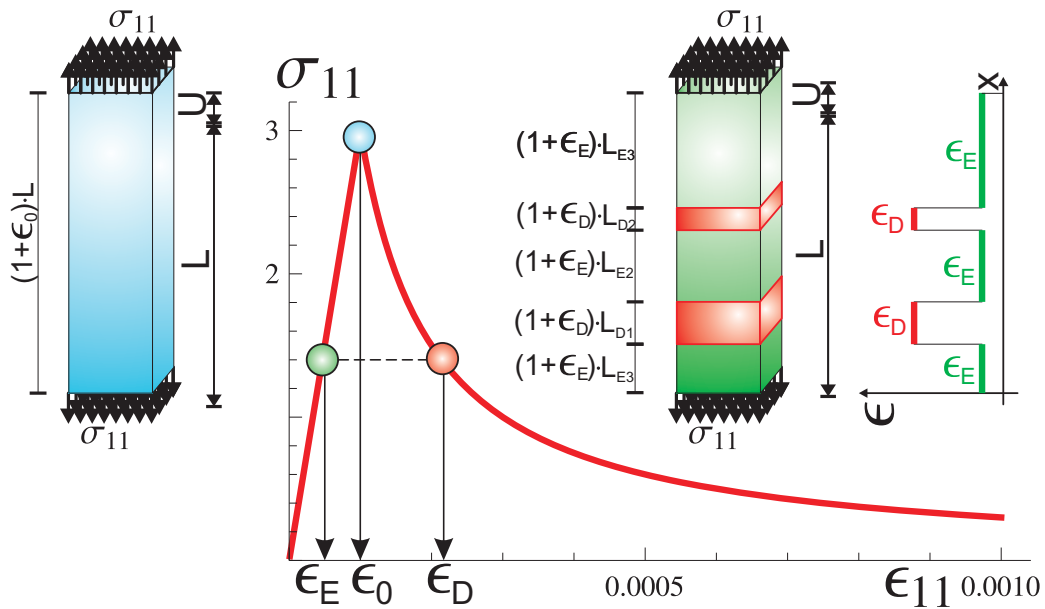
(b) Stress-strain curves resulting from the material model, development of damage zones in the specimen and corresponding strain distribution

Figure 3.5.: Localisation of deformation in uniaxial tension test

From the definitions of the damage threshold condition (3.48) and the damage driving force (3.49) one obtains for the monotonic tensile loading

$$d = -\ln\left(\frac{2\,r_1}{E\,\varepsilon^2}\right) \qquad \Rightarrow \qquad \sigma = \frac{2\,r_1}{\varepsilon} \quad \text{if } \varepsilon > \varepsilon_0. \tag{3.91}$$

In the solution of the problem one has to consider two stages. In the first stage of the test the response is linear elastic and therefore it follows from (3.89), (3.87) and (3.88) that the the strain field is homogeneous and given by

$$\varepsilon(X) = \frac{U}{L} \quad \forall\, X, \tag{3.92}$$

which results in the following relation between the applied force and the measured displacement at the right end of the specimen, Figure 3.5(a)

$$P = \frac{E\,A\,U}{L}. \tag{3.93}$$

The relation (3.92) is valid up to displacement $U_0 = L\,\varepsilon_0$ at which the peak stress (and consequently peak force) is reached, Figure 3.5(b). Then, stress cannot increase anymore and the second stage starts.

At each material point stress can decrease either with increasing strain and evolving damage (softening) or with decreasing strain (elastic unloading). That gives rise to the development of two regions (possibly containing several subregions): the damaged one Ω_D with cumulative length L_D and the elastic one Ω_E with cumulative length $L_E = L - L_D$. This situation is illustrated in the Figure 3.5(b), where the damaged subregions are colored in red, while the elastic regions are colored in green. Relation (3.87) implies that the stress has to remain homogeneous along the bar. However, every stress value between the peak one and zero corresponds to two values of the strain: the one attained in damaged region ε_D and the one realized in the elastic region ε_E

$$\varepsilon(X) = \begin{cases} \dfrac{\sigma}{E} & \forall\, X \in \Omega_E \\[2mm] \dfrac{2\,r_1}{\sigma} & \forall\, X \in \Omega_D \end{cases}. \tag{3.94}$$

Consequently, a piecewise constant distribution of strains is obtained, Figure 3.5(b). The compatibility condition (3.88) results in

$$\varepsilon_E\,L_E + \varepsilon_D\,L_D = U. \tag{3.95}$$

In view of (3.94) relation (3.95) becomes

$$L_E\,\frac{\sigma}{E} + L_D\,\frac{2\,r_1}{\sigma} = U, \tag{3.96}$$

and furthermore

$$L_E\,\frac{P}{E\,A} + L_D\,\frac{2\,r_1\,A}{P} = U. \tag{3.97}$$

The global responses of the structure in terms of the normalized applied load $\frac{P}{A}$ versus the displacement of the right end of the specimen U for several values of the normalized length of the damaged zone $\frac{L_D}{L}$ is presented in the Figure 3.5(a). For every value of the normalized
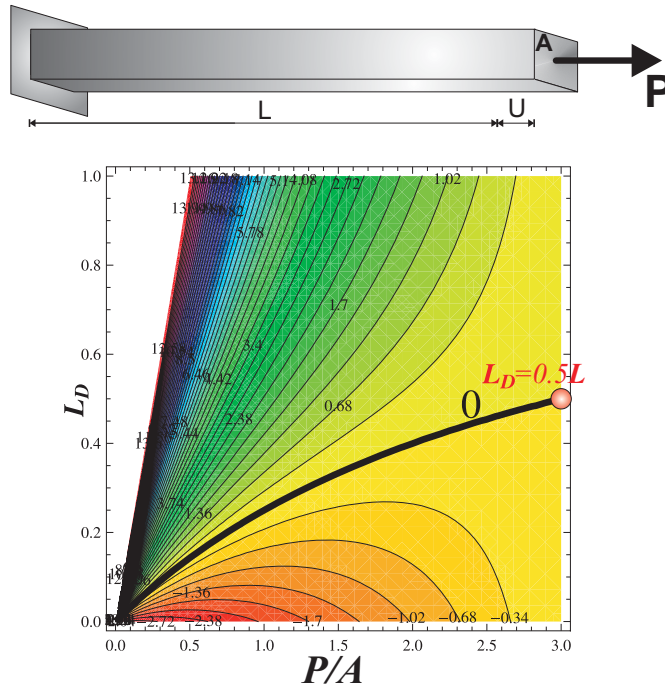
Figure 3.6.: Post-peak displacement of the end of the specimen scaled with the elasticity modulus ($E\bar{U}$) in dependence on the length of the damaged zone

load between the peak one and zero one can obtain displacement corresponding to a specific value of L_D (yellow points on the curves). Obviously, the response depends crucially on the size of the damaged zone and may even exhibit a snap-back behavior. In order to illustrate this possibility, a plot of the quantity

$$\bar{U} \;=\; U - U_0 \;=\; U - \varepsilon_0 L, \tag{3.98}$$

where U_0 stands for the displacement at limit of elastic behavior, is presented in the Figure 3.6. The black bold line in this figure represents the displacement equal to the one on the on-set of inelastic behavior ($U = U_0$). It can be observed that every length of the damaged zone shorter than a half of the specimen results in snap-back behaviour (the part of the diagram below the line $\bar{U} = 0$). Due to the fact that the length of the damage zone remains undetermined and can take any value between zero (corresponding to the limit case when the bar is unloaded just before any softening occurs) and the total length of the bar (corresponding to the limit case of uniformly damaged specimen), the discussed problem has infinitely many solutions. Without knowing the size of the damage zone one can not decide which of these solutions is the correct one. From the mathematical point of view, the problems involving materials with softening phase become ill-posed after the onset of softening and there does not exist a regular solution at all.

Taking into consideration small imperfections in geometry and material, the size of the softening zone is going to be governed by the size of the region with minimum strength. That region can be arbitrary small leading to the global response that tends to a pure elastic unloading, see Figure 3.5(a). Such behavior of material models with softening phase is particularly dangerous if numerical methods (e.g. FEM, Finite Difference Method) are used for the approximation of the solution of the problem, since numerical round-off errors act as imposed imperfections. Consequently, one obtains the solution governed solely by the properties of the numerical approximation of the problem variables, which is going to be illustrated later when we discus the implementation of material models within the finite element method.

3.3.2. Localization condition

In the one dimensional problems, localization occurs when the peak of the stress-strain diagram is reached, independently of the specific constitutive model used. In two- or three-dimensional problems the localization process is more complicated and one has to define conditions under which the strain can localize in one or more narrow bands separated from the remaining part of the body by weak discontinuity surfaces. The meaning of the adjective weak is that the displacement field remains continuous but the strain can have a jump, cf. Kuhl et al. (2000); Jirásek (2007).
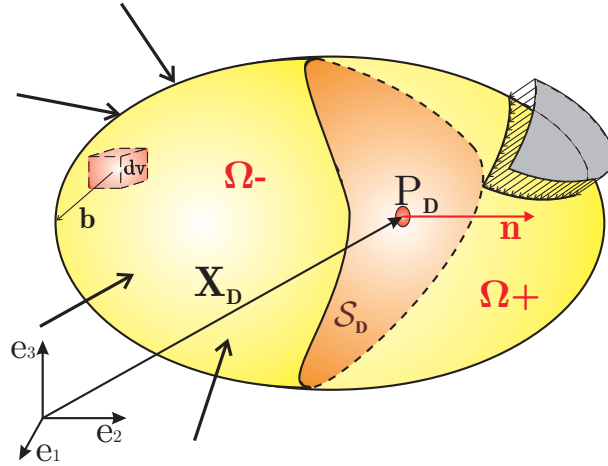
Figure 3.7.: Weak discontinuity surface in a deformed body

Let us consider a typical point P_D of the discontinuity surface $\mathcal{S}_D$ with the unit outward-normal vector $\boldsymbol{n}$, Figure 3.7, at the moment the strain continuity is lost. The body Ω is split by the discontinuity surface into two disjoint parts Ω^+ and Ω^-. If we approach the point P_D on the surface $\mathcal{S}_D$ separating Ω^+ and Ω^-, we obtain different limits for the fields characterizing localization

$$\boldsymbol{\xi}^+ = \lim_{\kappa \to 0^+} \boldsymbol{\xi}\left(\boldsymbol{X}_D + \kappa\boldsymbol{n}\right), \qquad \boldsymbol{\xi}^- = \lim_{\kappa \to 0^+} \boldsymbol{\xi}\left(\boldsymbol{X}_D - \kappa\boldsymbol{n}\right). \tag{3.99}$$

The jump in the corresponding fields is obtained as the difference between the values defined in (3.99) and is denoted as $[[\boldsymbol{\xi}]]$, i.e.

$$[[\boldsymbol{\xi}]] = \boldsymbol{\xi}^+ - \boldsymbol{\xi}^-. \tag{3.100}$$

At the onset of localization, the current strain and stress are still continuous and the jump appears only in their increments. However, these jumps cannot be completely arbitrary. Recalling the definition of the components of the stress tensor (2.97) and the Cauchy theorem (2.102), it has to hold

$$\Delta\boldsymbol{\sigma}^+ \cdot \boldsymbol{n} = \Delta\boldsymbol{\sigma}^- \cdot \boldsymbol{n}. \tag{3.101}$$

Additionally, the continuity of the displacement field imposes the condition that the gradients of the displacement increments on different sides of the discontinuity surface have to be rank-1 connected in the form

$$\left(\frac{\partial(\Delta\boldsymbol{u})}{\boldsymbol{X}}\right)^+ = \left(\frac{\partial(\Delta\boldsymbol{u})}{\boldsymbol{X}}\right)^- + \Delta\gamma_m \boldsymbol{m} \otimes \boldsymbol{n}. \tag{3.102}$$

Hence, the jump in the gradients of the displacement increments is defined by the rank-1 second order tensor dependent on the unit normal $\boldsymbol{n}$ on the surface $\mathcal{S}_D$, the so-called *polarization* unit vector $\boldsymbol{m}$ and the magnitude of the jump $\Delta\gamma_m$. The unit vectors $\boldsymbol{n}$ and $\boldsymbol{m}$ correlate to the failure mode of the structure: if they are parallel ($\boldsymbol{n} = \boldsymbol{m}$) a tensile splitting (mode I) is obtained, while the shear slip (mode II) results if they are perpendicular to each other ($\boldsymbol{n} \perp \boldsymbol{m}$). In view of the definition of the linearized strain tensor (2.85) the relation (3.102) can be rewritten as

$$\Delta\boldsymbol{\varepsilon}^+ = \Delta\boldsymbol{\varepsilon}^- + \frac{1}{2}\,\Delta\gamma_m\,(\boldsymbol{m}\otimes\boldsymbol{n} + \boldsymbol{n}\otimes\boldsymbol{m}). \tag{3.103}$$

In order to find the *necessary condition* (Jirásek (2007)) for the strain localization, the increments of strain and stress have to be connected to each other. For a given state at certain time $t = t^*$, defined by $\boldsymbol{\varepsilon}(\boldsymbol{X}, t) = \boldsymbol{\varepsilon}_0$ and $\boldsymbol{P}(\boldsymbol{X}, t) = \boldsymbol{P}_0$, one can relate increments of the stress tensor to increments of the strain tensor by

$$\Delta\boldsymbol{\sigma} = \mathbb{C}^{TAN}(\boldsymbol{\varepsilon}_0, \boldsymbol{P}_0) : \Delta\boldsymbol{\varepsilon}, \tag{3.104}$$

where $\mathbb{C}^{TAN}$ can be identified as inelastic tangent $\mathbb{C}^{IN}$, relation (3.41), in the case the evolution of inelastic processes takes place. In the case the elastic unloading does take place, the tangent stiffness is simply equal to the secant stiffness at the current state

$$\mathbb{C}^{TAN} = \begin{cases} \mathbb{C}^{IN}(\boldsymbol{\varepsilon}_0, \boldsymbol{P}_0) & \text{if } \Delta\boldsymbol{P} \neq \boldsymbol{0} \\ \left.\dfrac{\partial^2\Psi}{\partial\boldsymbol{\varepsilon}\,\partial\boldsymbol{\varepsilon}}\right|_{\boldsymbol{\varepsilon}_0, \boldsymbol{P}_0} & \text{if } \Delta\boldsymbol{P} = \boldsymbol{0}\,. \end{cases} \tag{3.105}$$

In general, although the current state of the material is initially the same on both sides of the initiating discontinuity, it is permitted that the evolution of internal variables progresses differently. In particular, one side can experience softening, while the other experiences elastic unloading. Hence, the tangent stiffness tensors can be different as well, leading to

$$\Delta\boldsymbol{\sigma}^+ = \left(\mathbb{C}^{TAN}\right)^+ : \Delta\boldsymbol{\varepsilon}^+, \qquad \Delta\boldsymbol{\sigma}^- = \left(\mathbb{C}^{TAN}\right)^- : \Delta\boldsymbol{\varepsilon}^-. \tag{3.106}$$

In view of (3.106) and (3.103), the continuity of the stress vector (3.101) can be rewritten as

$$\boldsymbol{n} \cdot \left[\left(\mathbb{C}^{TAN}\right)^+ : \left(\Delta\boldsymbol{\varepsilon}^- + \frac{1}{2}\,\Delta\gamma_m\,(\boldsymbol{m}\otimes\boldsymbol{n} + \boldsymbol{n}\otimes\boldsymbol{m})\right)\right] =$$
$$\boldsymbol{n} \cdot \left[\left(\mathbb{C}^{TAN}\right)^- : \Delta\boldsymbol{\varepsilon}^-\right]. \tag{3.107}$$

Taking into consideration minor symmetry of the tangent tensor $C_{ijkl}^{TAN} = C_{ijlk}^{TAN}$, one arrives after some manipulation at

$$\Delta\gamma_m\,\left(\boldsymbol{n} \cdot \left(\mathbb{C}^{TAN}\right)^+ \cdot \boldsymbol{n}\right) \cdot \boldsymbol{m} = \boldsymbol{n} \cdot \left(\left(\mathbb{C}^{TAN}\right)^+ - \left(\mathbb{C}^{TAN}\right)^-\right) : \Delta\boldsymbol{\varepsilon}^-. \tag{3.108}$$

This general equation can be significantly simplified if the tangent stiffness tensors on both sides of the discontinuity are the same, $\left(\mathbb{C}^{TAN}\right)^+ = \left(\mathbb{C}^{TAN}\right)^- = \mathbb{C}^{TAN}$, cf. Jirásek (2007). Considering the fact that a discontinuity is obtained only if the magnitude of the jump $\Delta\gamma_m > 0$, the relation (3.108) in this case reduces to

$$\left(\boldsymbol{n} \cdot \mathbb{C}^{TAN} \cdot \boldsymbol{n}\right) \cdot \boldsymbol{m} = \boldsymbol{0}. \tag{3.109}$$

The second order tensor

$$\mathcal{Q} \; = \; \boldsymbol{n} \cdot \mathbb{C}^{TAN} \cdot \boldsymbol{n} \tag{3.110}$$

is the so-called *localization (acoustic) tensor*. At the initiation of a weak discontinuity is the localization tensor singular

$$\det \mathcal{Q} \; = \; 0 \tag{3.111}$$

and its zero eigenvalue is associated to the eigenvector parallel to the polarization vector $\boldsymbol{m}$.

From the mathematical point of view, singularity of the localization tensor indicates the so-called loss of ellipticity of the governing system of differential equations which gives rise to the development of bifurcation modes. In Jirásek (2007) it is shown by an example involving damage model that (3.111) is stricter than (3.108). A similar statement regarding plastic models can be found in Forest and Lorentz (2004). Therefore, the simplified analysis based on the determinant of the localization tensor is fully sufficient. Since the tangent stiffness $\mathbb{C}^{TAN}$ is known for a given state, the relation (3.111) can be used to search for a unit vector that leads to a singular localization tensor $\mathcal{Q}$. A jump in the strain field across a surface with the normal $\boldsymbol{n}$ can develop only in the case that the unit vector $\boldsymbol{n}$ satisfying (3.111) exists. However, it is already stated that (3.111) represents the necessary local condition for the development of a localized deformation. Whether it indeed develops in a body depends on the state of the surrounding material and on the boundary conditions, cf. Forest and Lorentz (2004). Nevertheless, the analysis of localization tensors can be used as an important indicator of the occurrence of weak discontinuities.

3.4. Regularization strategies

It was already mentioned that classical continuum material models do not describe material microstructure and consequently do not involve characteristic internal material length scales into formulation. Whereas that property can rarely lead to problems in utilization of material models involving hardening (e.g. in the case of non-associated plasticity formulations with very low values of hardening parameter, cf. Kuhl et al. (2000)), it has devastating influence on the reliability of the results obtained employing material models involving softening effects (as it was illustrated in the one-dimensional example in section 3.3.1).

To achieve objective description of strain localization, one can follow several approaches based on a general idea that the displacement field remains continuous in the whole domain.[5]

3.4.1. Fracture energy approach

One approach is to consider a smeared inelastic process, distributed uniformly within the zone of a finite thickness l_i. Hence, the stress-strain softening law becomes the law connect-

---

[5]This is not the only possibility. Considering modeling of fracture and development of macroscopic cracks, one has to permit jumps in the displacement filed. The strategies following this path include so-called *strong discontinuity approach*, e.g. Oliver (2004); Jirásek (2000); Mosler (2005) and method-based X-FEM, e.g. Möes et al. (1999); Belytschko et al. (2001); Sukumar et al. (2003)
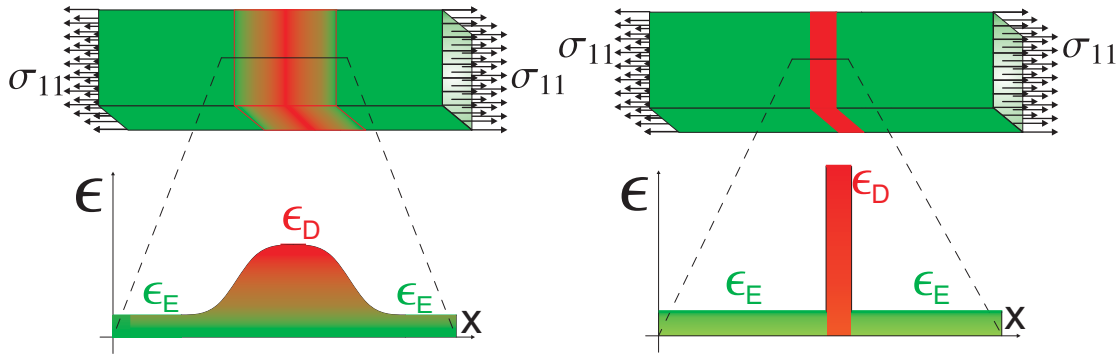
Figure 3.8.: Strain distribution in regularized continuum (left) and crack band (fracture energy) models (right)

ing the stress transmitted by the localization band to the average strain in that band. In order to fulfill the requirement that all the points within the zone dissipate the same amount of energy, one has to modify the softening law. That is done by making the softening parameter dependent on the fracture energy, cf. de Borst et al. (2004)

$$\mathcal{G}_C = \int \int \sigma \, d\varepsilon(x) \, dx = l_i \int \sigma \, d\varepsilon \tag{3.112}$$

necessary for the opening of a crack of a unit area. It is evident from (3.112) that a length scale is accounted for. The strain profile across the localization zone shows jumps characteristic for the localization, Figure 3.8, which matches the material behaviour. However, a stumbling block of the strategy is a length parameter l_i.

In order to circumvent the inherent property of common numerical approximation within the finite element method that the element size represents at the same time the length scale for the low-order-continuity approximation, one has to relate the material law (softening parameter) to numerical discretization (size of the elements). Moreover, this approach tweaks artificially the material law to force the structural response to be almost independent (cf. de Borst et al. (2004)) on the numerically introduced length parameter, but it does not change the fact that the underlying differential system of equations losses its ellipticity. As a consequence, the weak discontinuity surfaces still tend to align with numerical-method-specific discretization (e.g. to follow the boundaries of the finite elements thus leading to mesh-dependent development of the localized zone), cf. de Borst et al. (2004); Forest and Lorentz (2004); Feenstra and de Borst (1995).

3.4.2. Regularized continuum models

When adhering to a continuum concept, the only way to avoid the ill-posedness caused by the loss of ellipticity are various forms of *enhanced continuum theories*, which introduce intrinsically internal material length. In such theories strain field remains continuous even after the onset of localization, Figure 3.8. Moreover, the presence of an intrinsic length parameter results in models that are not invariant with respect to spatial scaling, in contrast to the classical models. As a consequence, regularized models are able to predict and describe the so-called *size effects* (dependence of the nominal stress on the size on the structure), cf. Fleck et al. (1994); Bažant and Jirásek (2002); Frantziskonis et al. (2001); Al-Rub et al. (2007).

In order to introduce the length scale into the model, one has to consider some form of non-locality, i.e. one has to consider interactions of the point under consideration with the points in its neighbourhood. The approach which is followed can be *weakly non-local*, typically described by differential equations containing derivatives of different orders (therefore involving implicit dependence on the neighbourhood) or *strongly non-local*, typically described by integro-differential equations (hence involving explicit dependence of the material response on the state of the neighboring points), cf. Bažant and Jirásek (2002). According to the character of the enhancement, regularization strategies can be classified into two groups, cf. Jirásek (2002): the one relying on enhanced kinematic relations and the one relying on enhanced constitutive relations.

Enhanced kinematic relations

The first strategy in the group of enhanced kinematic relations belongs to the category of *weakly non-local* models and it is based on the introduction of rotational degrees of freedom in addition to translational ones, leading to the so-called *micropolar (Cosserat) continuum*, cf. Cosserat and Cosserat (1909); Mindlin and Tiersten (1962a); Toupin (1962); Saczuk (1993). The characterization of deformation requires, besides the strain tensor, the knowledge about an additional second order tensor called curvature tensor. As an result of the enhanced kinematics one obtains unsymmetric stress and an additional (in general unsymmetric too) so-called couple stress tensor from the balance relations for linear and angular momentum. The constitutive relation relating the couple stress to the curvature has to be supplemented, requiring the specification of additional material parameters which implicitly introduce the internal length. Hence, the utilization of this strategy requires significant modification of the material model. Moreover, such modification influences elastic as well as inelastic behavior of a material.

The second *weakly non-local* strategy in the group of enhanced kinematic relations retains the displacement as the only independent kinematic field and introduces gradients of strain (i.e. higher order gradients of the displacement field) into the constitutive relations, cf. Toupin (1962); Mindlin and Tiersten (1962b); Aifantis (1999). The internal material length is implicitly introduced through the coefficients multiplying higher order gradients. Extensions in order to consider plastic material behaviour are presented in e.g. Aifantis (1984); Zbib and Aifantis (1988a,b,c); Fleck and Hutchinson (1993); Fleck et al. (1994); Huang et al. (1999, 2000). Due to existence of strain gradients, additional response functions for couple stresses (which are work-conjugates of the strain-gradient field) have to be defined. Consequently, equilibrium equations resulting from the balance of linear momentum have to be modified as well as constitutive equations. In application to plasticity the plastic yield function has to be formulated in dependence on the couple stress as well. In addition, higher order continuity (at least C^1) of the displacement field is required, which is possible without restrictions only in one-dimensional problems (see e.g. de Borst and Pamin (1996)). In two- or three-dimensional problems C^1 continuity is achievable only for special cases (as it is done in de Borst and Pamin (1996), Zhou et al. (2002), Zervos et al. (2001)). Hence, although the overall complexity of the modeling strategy is reduced in comparison to the micropolar continua, significant modifications in material models are still required.

Integral non-local models

The integral non-local strategy, which is categorized as *strongly non-local* introduces non-local variables as the weighted averages of the local variables over a neighborhood of the point under consideration, cf. Bažant and Jirásek (2002); Jirásek (2002). Internal material length is explicitly introduced as a parameter that defines the size of the averaging zone. Denoting a local field in the domain Ω as $\boldsymbol{\xi}(\boldsymbol{x})$, its non-local counterpart is defined as

$$\bar{\boldsymbol{\xi}}(\boldsymbol{x}) \;=\; \int_\Omega \alpha(\|\boldsymbol{x} - \boldsymbol{y}\|)\, \boldsymbol{\xi}(\boldsymbol{y})\, dy, \tag{3.113}$$

where $\alpha(\|\boldsymbol{x} - \boldsymbol{y}\|)$ represents the non-local weight function, which is usually taken either as Gaußfunction

$$\alpha(r) \;=\; \frac{1}{\left(l\,\sqrt{2\pi}\right)^3}\, e^{-\frac{r^2}{l^2}}, \tag{3.114}$$

or as Green function

$$\alpha(r) \;=\; \frac{1}{(4\pi\, l\, r)}\, e^{-\frac{r}{\sqrt{l}}}, \tag{3.115}$$

cf. Peerlings et al. (2001a); Jirásek and Rolshoven (2003), where the parameter l stands for the internal length of the nonlocal continuum. The non-local variables obtained this way replace the local counterparts in the constitutive equations.

Depending on the variables represented non-localy, enhancement of either kinematic or constitutive relation is obtained. In the former case some strain measure is enhanced, leading to non-local elasticity theories, cf. Kröner and Datta (1966); Edelen et al. (1971); Eringen and Edelen (1972). Much more popular is the latter approach, where internal variables or their thermodynamic conjugates are replaced in the constitutive relations by their non-local counterparts. Applications to damage mechanics are presented in e.g. Pijaudier-Cabot and Bažant (1988); Jirásek (1998); Comi (2001), while non-local plasticity can be found in e.g. Eringen (1981); Svedberg and Runesson (1998); Jirásek and Rolshoven (2003). That approach retains the balance equations and the kinematic relations, changing only the constitutive law, which constitutes considerable simplification in the application of the theory compared with micropolar or strain-gradient strategies. However, the application of non-local integral models together with inelastic materials has the drawback that global averaging procedure is required and consequently the resulting equations cannot easily be numerically approximated.

Gradient enhanced models

The gradient strategies introduce higher order gradient terms (mostly Laplacian) of non-local variables into the constitutive relations and belong to the group of *weakly non-local* strategies. They can be considered as the differential counterpart of integral nonlocal formulations. Moreover, first gradient models were derived from integral ones, see e.g. Mühlhaus and Aifantis (1991); Peerlings et al. (2001b), expanding generic variable $\boldsymbol{\xi}(\boldsymbol{x})$ introduced in (3.113) in Taylor-series around the material point $\boldsymbol{x}$

$$\boldsymbol{\xi}(\boldsymbol{y}) \;=\; \boldsymbol{\xi}(\boldsymbol{x}) + \frac{\partial \boldsymbol{\xi}}{\partial \boldsymbol{x}} \cdot (\boldsymbol{y} - \boldsymbol{x}) + \frac{1}{2}\, \frac{\partial^2 \boldsymbol{\xi}}{\partial \boldsymbol{x} \otimes \partial \boldsymbol{x}} : (\boldsymbol{y} - \boldsymbol{x}) \otimes (\boldsymbol{y} - \boldsymbol{x}) + \cdots . \tag{3.116}$$

Inserting (3.116) into (3.113) and integrating, it follows that only the gradient terms of even order remain due to the form of the weighting function (3.114). Truncating terms of higher order than two results in

$$\bar{\boldsymbol{\xi}}(\boldsymbol{x}) \,=\, \boldsymbol{\xi}(\boldsymbol{x}) \,+\, c(l)\,\nabla^2\boldsymbol{\xi}(\boldsymbol{x}).\tag{3.117}$$

Replacing the generic variable $\boldsymbol{\xi}(\boldsymbol{x})$ in the corresponding constitutive relations with the right-hand side of (3.117) one introduces an internal length parameter $(c(l))$ into the model thus regularizing it. However, not all gradient models can be derived from the non-local ones in such straight-forward way, e.g. Nedjar (1996); Makowski et al. (2006); Voyiadjis and Al-Rub (2005).

In general, models that involve explicit gradients (mostly Laplacian) of a certain problem variable in the formulation of the constitutive relations are called *explicit gradient* models. Their main advantage is that they can be formulated in thermodynamically consistent way (e.g. Nedjar (1996, 2001); Liebe et al. (2001); Liebe and Steinmann (2001); Makowski et al. (2006)) and offer simplification of the numerical treatment compared to non-local models. However, the explicit presence of higher order gradients in the generic variable demands higher-order continuity of its interpolation, which is, as we already discussed in the consideration of strain-gradient theories, achievable only for special cases. Therefore one has to resort to alternative methods for the calculation of the required gradients (for example simplified, but still relatively complicated super-element strategy found in Al-Rub and Voyiadjis (2005)), or to loosen the continuity requirements performing integration of the resulting equations using mixed method (e.g. Dorgan (2006)), generalized principle of virtual power (as in Nedjar (2001); Makowski et al. (2006)) or generalized principle of virtual work (as in Liebe et al. (2001); Liebe and Steinmann (2001)). The drawback of integrated techniques is that the description of the evolution of internal variables turns from a local system of differential-algebraic equations into a boundary value problem with a-priory unknown domain. Consequently, there emerge implementation difficulties related to the search for the inelastic domain (as it was done i.e. in Liebe et al. (2001); Liebe and Steinmann (2001)) and enforcement of the interface conditions at the evolving boundary of inelastic region.

An alternative approach, leading to the so-called *implicit gradient* models, which is followed by Peerlings et al. (1998); Peerlings (1999); Peerlings et al. (2001b); Simone et al. (2003) in the field of damage modeling and by Engelen et al. (2003, 2006) in the field of plasticity can be derived starting from the relation (3.117). Applying Laplace-operator on both sides, one obtains

$$\nabla^2\bar{\boldsymbol{\xi}}(\boldsymbol{x}) \,=\, \nabla^2\boldsymbol{\xi}(\boldsymbol{x}) \,+\, c(l)\,\nabla^4\boldsymbol{\xi}(\boldsymbol{x}).\tag{3.118}$$

In view of (3.118) the relation (3.117) can be written, under assumption that the subtracted coefficients multiplying terms of equal differential order are equal to zero, in the form

$$\bar{\boldsymbol{\xi}}(\boldsymbol{x}) - c(l)\nabla^2\bar{\boldsymbol{\xi}}(\boldsymbol{x}) \,=\, \boldsymbol{\xi}(\boldsymbol{x}).\tag{3.119}$$

The result is a Helmholtz-type differential equation for the non-local variable, which has to be supplemented with an appropriate boundary conditions in order to obtain a well-posed problem. Usually, a vanishing flux of the non-local variable across the boundary of a body is employed, cf. Peerlings et al. (2001b), which allows for a simple transformation of the differential equation (3.119) into a corresponding boundary value problem. As a result, the continuity requirement for the non-local field loosens to a simple C^0 continuity, which is

achievable without problems. Moreover, changes in the existing model are small due to the fact that the equations governing the evolution of inelastic variable remain quasi-local. One just replaces the generic variable $\boldsymbol{\xi}(\boldsymbol{x})$ in the equations by its non-local counterpart, as it was done in integral-type non-local models. It is even shown in Peerlings et al. (2001b) that *implicit gradient* models are equivalent to integral-type non-local models with special nonlocal weight functions (Green's function of the problem (3.119), given in (3.115)). Despite their simplicity and efficiency, the main disadvantage of *implicit gradient* models is that they are not formulated in a thermodynamically consistent way. Hence, common thermodynamics considerations are difficult to apply to such models.

Another strategy for gradient enhancement of inelastic material models will be discussed in the rest of the thesis. It unifies the simplicity and efficiency of *implicit gradient* models with the thermodynamically consistent formulation of some *explicit gradient* models.

4. A strategy for gradient enhancement of rate-independent inelastic material models

In this chapter a regularization strategy based on gradient enhancement of the free-energy function is in section 4.1 presented. The regularization is formulated by means of an interaction potential dependent on additional variables whose gradients play regularization role in the model, similar to implicit gradient models. The corresponding boundary value problem is further formulated in section 4.3 as a pure minimization of the potential functional with respect to displacements and additional non-local variables. Furthermore, thermodynamic aspects of the strategy are discussed and the constitutive update relations and algorithm are presented in section 4.4.

4.1. Gradient enhancement of the free-energy function

Let us consider a Helmholtz free-energy function of an isothermal deformation, defined per unit volume in the form

$$\Psi \;=\; \Psi(\boldsymbol{\varepsilon}, \boldsymbol{P}). \tag{4.1}$$

Following the definitions adopted in previous chapters, $\boldsymbol{\varepsilon}$ denotes the linearized strain tensor and $\boldsymbol{P}$ denotes a list of internal variables. The latter can include scalar as well as tensorial quantities and consists of two disjoint parts:

$$\boldsymbol{P} = \{\boldsymbol{P}_L, \boldsymbol{P}_{NL}\} . \tag{4.2}$$

The list $\boldsymbol{P}_L$ contains the variables which are treated in completely local manner, while the list $\boldsymbol{P}_{NL}$ comprises the variables included in the regularization procedure

$$\boldsymbol{P}_L = \{\boldsymbol{P}_{L\,1}, \, \dots \, , \boldsymbol{P}_{L\,nl}\}, \qquad \boldsymbol{P}_{NL} = \{\boldsymbol{P}_{NL\,1}, \, \dots \, , \boldsymbol{P}_{NL\,nnl}\} . \tag{4.3}$$

The parameters nl and nnl in the relation (4.3) stand for the number of elements of the corresponding lists, which can be scalar as well as tensorial fields. Following the discussion in sections 3.3 and 3.4, it is essential to account for the non-local interaction in order to attain well-posedness in the model. For that purpose a list of variables $\boldsymbol{\varphi}$ and a potential list $\boldsymbol{H}_{\boldsymbol{\varphi}}(\boldsymbol{P}_{NL})$ are introduced (as in Dimitrijević and Hackl (2006, 2008, 2009)), which enter the interaction potential in the form

$$\Psi_{intr}(\boldsymbol{P}_{NL}, \boldsymbol{\varphi}, \boldsymbol{\nabla}\boldsymbol{\varphi}) \;=\; \frac{1}{2} \left\langle \, \boldsymbol{\varphi} - \boldsymbol{H}_{\boldsymbol{\varphi}}(\boldsymbol{P}_{NL}), \, \boldsymbol{\beta}\left(\boldsymbol{\varphi} - \boldsymbol{H}_{\boldsymbol{\varphi}}(\boldsymbol{P}_{NL})\right) \, \right\rangle_{NL}$$
$$+ \; \frac{1}{2} \left\langle \, \boldsymbol{\nabla}\boldsymbol{\varphi}, \, \mathbf{c}\left(\boldsymbol{\nabla}\boldsymbol{\varphi}\right) \, \right\rangle_{GNL} . \tag{4.4}$$

We start the consideration of the relation (4.4) by discussing a potential list $\boldsymbol{H}_{\boldsymbol{\varphi}}(\boldsymbol{P}_{NL})$. It consists of several scalar or tensorial functions $\boldsymbol{H}_{\boldsymbol{\varphi}\,i}$ dependent on the sublist of internal

variables $\boldsymbol{P}_{NL}$. Although it is possible that any function $\boldsymbol{H}_{\varphi i}$ depends on several variables $\boldsymbol{P}_{NL\,i}$ of the list $\boldsymbol{P}_{NL}$, we restrict our attention to the cases where an one-to-one correspondence between the elements of both lists is established

$$\boldsymbol{H}_{\varphi} = \{\boldsymbol{H}_{\varphi 1}(\boldsymbol{P}_{NL\,1}),\ \dots\ ,\boldsymbol{H}_{\varphi\,nnl}(\boldsymbol{P}_{NL\,nnl})\}\,. \tag{4.5}$$

As an example of the function $\boldsymbol{H}_{\varphi i}$ in the case of a plastic material model, one may think of an increment of the plastic strain tensor $\boldsymbol{H}_{\varphi i}(\varepsilon_P) = \Delta\varepsilon_P$, which was used e.g. in Zervos et al. (2001), but one may as well utilize the effective plastic strain $\boldsymbol{H}_{\varphi i}(\varepsilon_P) = \sqrt{\frac{2}{3}\varepsilon_P : \varepsilon_P}$, used e.g. in Mühlhaus and Aifantis (1991). In view of (4.5), the field φ should be understood as a list of variables rather than a single one, including possibly subsets of different nature (scalars or tensors). In order to comply with the relation (4.5) the list φ has to be structured in the same way as $\boldsymbol{H}_{\varphi i}$. The gradients of the elements of φ are gathered in the list $\nabla\varphi$

$$\nabla\varphi = \{\nabla\varphi_1,\ \dots\ ,\nabla\varphi_{nnl}\}\,. \tag{4.6}$$

In general, the operator $\boldsymbol{\beta}$ in (4.4) can be non-linear and can depend on both lists φ and $\boldsymbol{P}_{NL}$ (or more precisely on the elements of both lists). However, in this thesis we restrict ourselves on the linear operator $\boldsymbol{\beta}$, which renders the expression $\boldsymbol{\beta}\,(\varphi - \boldsymbol{H}_{\varphi})$ a linear form of the difference between the elements of the lists φ and $\boldsymbol{H}_{\varphi}$. In the simplest case one may think of a diagonal operator $\boldsymbol{\beta}$, resulting in

$$\boldsymbol{\beta}\,(\varphi - \boldsymbol{H}_{\varphi}(\boldsymbol{P}_{NL})) = \{\beta_1\,(\varphi_1 - \boldsymbol{H}_{\varphi 1}),\ \dots\ ,\beta_{nnl}\,(\varphi_{nnl} - \boldsymbol{H}_{\varphi\,nnl})\}\,. \tag{4.7}$$

Furthermore, the bilinear product operator $\left\langle\,(\varphi - \boldsymbol{H}_{\varphi})\,,\boldsymbol{\beta}\,(\varphi - \boldsymbol{H}_{\varphi})\,\right\rangle_{NL}$ becomes

$$\left\langle\,\varphi - \boldsymbol{H}_{\varphi}(\boldsymbol{P}_{NL}),\boldsymbol{\beta}\,(\varphi - \boldsymbol{H}_{\varphi}(\boldsymbol{P}_{NL}))\,\right\rangle_{NL} = $$
$$\sum_{i=1}^{nnl}\beta_i\,(\varphi_i - \boldsymbol{H}_{\varphi i}) : (\varphi_i - \boldsymbol{H}_{\varphi i})\,. \tag{4.8}$$

Since the elements φ_i of the list of non-local variables φ can be a scalars or tensors of arbitrary order, the double dot product they are is involved at in (4.8) has to be understood as the scalar product between equally structured objects. Once the structure of φ_i is known, the operator (:) may be interpreted accordingly (as a simple contraction of vectors, double contraction of second order tensors etc.).

Similar consideration applies to the operator $\mathbf{c}$: generally it can be be non-linear and dependent on the elements of the lists φ and $\boldsymbol{P}_{NL}$ (such approach is advocated in e.g. Voyiadjis and Al-Rub (2005) and Geers (1997); Geers et al. (1998)), but in the scope of this thesis is only a linear operator $\mathbf{c}$ considered. Nevertheless, the present work can be easily extended to account for such dependence. The choice of linear $\mathbf{c}$ leads to bilinear product operator $\left\langle\,\nabla\varphi,\,\mathbf{c}\,(\nabla\varphi)\,\right\rangle_{GNL}$. In the simplest case where it is assumed that whether interaction between the gradients of the individual elements of the list of non-local variables φ_i nor preferable direction for their development exist, one obtains

$$\mathbf{c}\,(\nabla\varphi) = \{c_1\,\nabla\varphi_1,\ \dots\ ,c_{nnl}\,\nabla\varphi_{nnl}\}\,, \tag{4.9}$$

and consequently

$$\left\langle\,\nabla\varphi,\,\mathbf{c}\,(\nabla\varphi)\,\right\rangle_{GNL} = \sum_{i=1}^{nnl}c_i\,\nabla\varphi_i \vdots \nabla\varphi_i. \tag{4.10}$$

Discussion above concerning the double dot product applies at triple dot product in (4.10) as well. Once the structure of the lists φ_i is known, the operator $(\vdots)$ may be interpreted as a simple contraction in the case φ_i is a scalar, double contraction if φ_i is a vector etc.

The enhanced Helmholtz free-energy function of a small strain isothermal problem is obtained by adding the interaction potential (4.4) to the standard form (4.1), leading to

$$\tilde{\Psi} = \tilde{\Psi}(\boldsymbol{\varepsilon}, \boldsymbol{P}, \boldsymbol{\varphi}, \boldsymbol{\nabla\varphi}) = \Psi(\boldsymbol{\varepsilon}, \boldsymbol{P}) + \Psi_{intr}(\boldsymbol{P}_{NL}, \boldsymbol{\varphi}, \boldsymbol{\nabla\varphi}). \tag{4.11}$$

The meaning and the influence of the operators $\boldsymbol{\beta}$ and $\mathbf{c}$ will be discussed later in details. At this point we just mention that the interaction between them introduces the necessary length scale in the material models, as it is discussed by Forest (2009) in his work that shares the same spirit with the current contribution.

4.2. Variational formulation of the problem

Before proceeding with the variational formulation of the problem, we repeat the relations defined or derived in the previous chapters that constitute the boundary value problem of an inelastic-deformable solid under assumption of quasi-static small deformation and isothermal conditions.

4.2.1. Boundary value problem
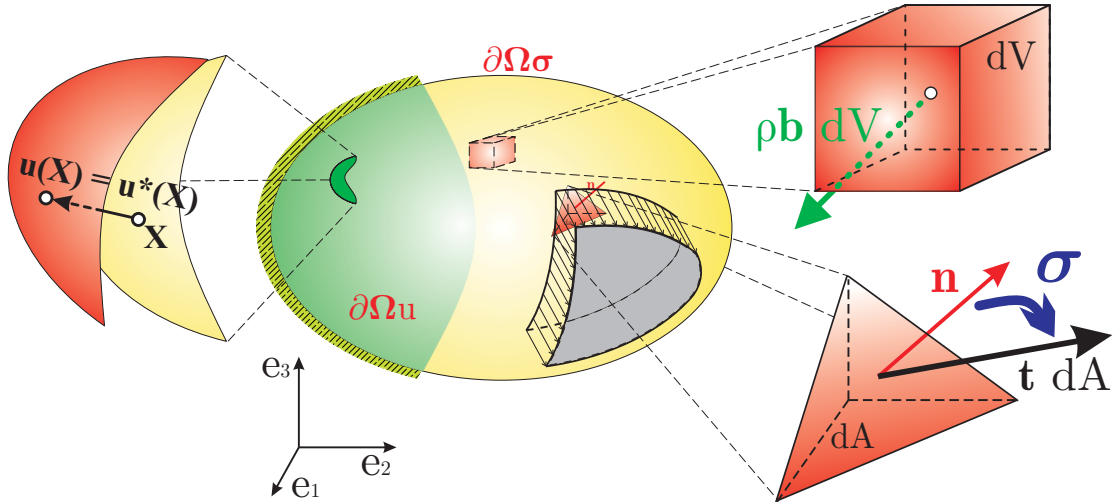
Figure 4.1.: Boundary value problem

Let us consider a body occupying the domain Ω, Figure 4.1, limited by the boundary $\partial\Omega$, which consists of two non-overlapping parts: a so-caled *Dirichlet* boundary $\partial\Omega_u$ and a so-called *Neumann* boundary of the body $\partial\Omega_\sigma$

$$\partial\Omega = \partial\Omega_u \cup \partial\Omega_\sigma, \qquad \partial\Omega_u \cap \partial\Omega_\sigma = \emptyset. \tag{4.12}$$

As a rule, primary variables (in the classical mechanical setting displacements) are prescribed on the Dirichlet boundary

$$\boldsymbol{u} = \boldsymbol{u}^* \quad \text{on } \partial\Omega_u, \tag{4.13}$$

and the fluxes of the dependent quantities (in the classical mechanical setting Cauchy stress vector using the Cauchy-theorem (2.102)) are prescribed on the Neumann boundary

$$t = \boldsymbol{\sigma} \cdot \boldsymbol{n} \quad \text{on } \partial\Omega_\sigma. \tag{4.14}$$

In order to formulate the boundary value problem, apart from the boundary conditions specified in (4.13) and (4.14), one has to include the kinematic relations, i.e. the definition of the linearized strain tensor (2.85)

$$\boldsymbol{\varepsilon} = \frac{1}{2}\left(\nabla\boldsymbol{u} + (\nabla\boldsymbol{u})^T\right). \tag{4.15}$$

Furthermore, the local forms of the balance of linear (2.122) and angular (2.131) momentum

$$\operatorname{div}\boldsymbol{\sigma} + \rho\,\boldsymbol{b} = \boldsymbol{0}, \qquad \boldsymbol{\sigma} = \boldsymbol{\sigma}^T, \tag{4.16}$$

delivering kinetic relations have to be supplemented. Finally, the balance of entropy and the discussion of its consequences in the section 2.4.1 delivers the constitutive relation for the stress tensor (3.2)

$$\boldsymbol{\sigma} = \frac{\partial\Psi}{\partial\boldsymbol{\varepsilon}} \tag{4.17}$$

and the list of driving forces thermodynamically conjugated to the internal variables (3.26)

$$\boldsymbol{Q} = -\frac{\partial\Psi}{\partial\boldsymbol{P}}. \tag{4.18}$$

In order to close the formulation of the problem, the evolution of the internal variables is specified through the dissipation potential (3.27)

$$J(\dot{\boldsymbol{P}}) = \sup_{\boldsymbol{Q}}\left[\boldsymbol{Q}:\dot{\boldsymbol{P}} - I_K(\boldsymbol{P},\boldsymbol{Q},\boldsymbol{\varepsilon})\right]. \tag{4.19}$$

In the equations above $\boldsymbol{u}$ stands for the displacement vector, $\boldsymbol{\varepsilon}$ for the linearized strain tensor, $\boldsymbol{P}$ denotes the list of the internal variables, $\rho\boldsymbol{b}$ stands for the force per unit volume of the body Ω and $\mathbf{t}$ for the external loading per unit surface of the Neumann boundary $\partial\Omega_\sigma$, Figure 4.1.

In view of relation (4.11) that defines the enhanced form of the free-energy function it is obvious that the introduced enhancement does not cause any changes to the stress tensor $\boldsymbol{\sigma}$ given by (4.17). Hence, it can be written

$$\boldsymbol{\sigma} = \frac{\partial\Psi}{\partial\boldsymbol{\varepsilon}} = \frac{\partial\tilde{\Psi}}{\partial\boldsymbol{\varepsilon}}. \tag{4.20}$$

However, that is not the case with the list of the conjugate microforces $\boldsymbol{Q}$, due to the presence of the sublist of internal variables $\boldsymbol{P}_{NL}$ within the interaction potential (4.4). This issue is going to be addressed later in the section (4.4).

The system of differential equations (4.15)-(4.19) subjected to the boundary conditions (4.13) and (4.14) constitutes the boundary value problem which should be solved for the displacement, strain, stress and internal variable fields. The enhancement of the free-energy function defined in (4.11) introduces an additional field φ (or more precisely a list of additional fields) that have to be accounted for as well. The solution is obtained through two variational principles coupled to each other. The first one unifies the relations (4.13)-(4.16) and the definition of the stress tensor utilizing the enhanced free-energy into an extended principle of minimum of potential energy and it is time-independent. It is presented in the section 4.3. The second one is time-dependent minimum principle for the dissipation potential, already discussed in the section 3.2.1. It handles the remaining equations (4.18) and (4.19) and its modified formulation resulting from the ehnacement of the free-energy is presented in the section 4.4.

4.3. Potential functional and the variational (minimum) principle

With the definition of the enhanced free-energy function (4.11) at hands, one can define the potential of internal forces

$$\Pi_{int} := \int_{\Omega} \tilde{\Psi}(\boldsymbol{\varepsilon}(\boldsymbol{u}), \boldsymbol{P}, \boldsymbol{\varphi}, \boldsymbol{\nabla}\boldsymbol{\varphi}) dV \tag{4.21}$$

as an integral of the free-energy over the domain Ω occupied by the body. The kinematic relation (4.15) is explicitly taken into account in (4.21). The potential energy of the external forces can be obtained in a classical manner, integrating the work performed on the deformation by the volume $\boldsymbol{f}$ and surface $\boldsymbol{t}$ forces

$$\Pi_{ext} = -\int_{\Omega} \boldsymbol{u} \cdot \boldsymbol{f} \, dV - \int_{\partial\Omega_{\sigma}} \boldsymbol{u} \cdot \boldsymbol{t} \, dA. \tag{4.22}$$

Here $\boldsymbol{f} = \rho\boldsymbol{b}$ denotes the force per unit volume of the body Ω. One can furthermore define the global potential functional as a sum of the potentials of internal and external forces, cf. Washizu (1982); Hackl (1997)

$$\Pi = \Pi_{int} + \Pi_{ext} = \int_{\Omega} \tilde{\Psi}(\boldsymbol{\varepsilon}(\boldsymbol{u}), \boldsymbol{P}, \boldsymbol{\varphi}, \boldsymbol{\nabla}\boldsymbol{\varphi}) dV - \int_{\Omega} \boldsymbol{u} \cdot \boldsymbol{f} dV - \int_{\partial\Omega_{\sigma}} \boldsymbol{u} \cdot \mathbf{t} dA. \tag{4.23}$$

The corresponding variational problem is stated in the form:

$$\text{find } \{\mathbf{u}, \boldsymbol{\varphi}\} = \operatorname{argmin} \left\{\Pi(\mathbf{u}, \boldsymbol{\varphi}) \,|\, \mathbf{u} = \mathbf{u}^* \text{ on } \partial\Omega_u\right\}. \tag{4.24}$$

The primal variables of the variational problem are displacements $\mathbf{u}$ and the non-local field $\boldsymbol{\varphi}$, while the internal variable set $\boldsymbol{P}$ is considered constant with respect to variation. The body $\boldsymbol{f}$ and the surface $\boldsymbol{t}$ forces are assumed to be independent on the actual state of the body, i.e. only conservative loading is considered here.

Variation of the potential functional (4.23) with respect to the variables $\boldsymbol{u}$ and $\boldsymbol{\varphi}$, defined by the Gâteaux-derivative[1] of the potential

$$\delta\Pi := D\Pi(\boldsymbol{u}, \boldsymbol{\varphi})(\delta\boldsymbol{u}) + D\Pi(\boldsymbol{u}, \boldsymbol{\varphi})(\delta\boldsymbol{\varphi}) \tag{4.25}$$

yields the following expression

$$\begin{aligned}
\delta\Pi = &\int_{\Omega} \delta\boldsymbol{\varepsilon}(\boldsymbol{u}) : \boldsymbol{\sigma} \, dV - \int_{\Omega} \delta\boldsymbol{u} \cdot \boldsymbol{f} \, dV - \int_{\partial\Omega_{\sigma}} \delta\boldsymbol{u} \cdot \boldsymbol{t} \, dA \\
&+ \int_{\Omega} \left[\frac{\partial\tilde{\Psi}}{\partial\boldsymbol{\varphi}} \delta\boldsymbol{\varphi} + \frac{\partial\tilde{\Psi}}{\partial(\boldsymbol{\nabla}\boldsymbol{\varphi})} \boldsymbol{\nabla}\delta\boldsymbol{\varphi} \right] dV.
\end{aligned} \tag{4.26}$$

---

[1]For details on linearization and the *Gâteaux-derivative* see the section A.1.

The stationary point (in the present case a minimum point) of the functional Π, relation (4.23) is achieved by demanding the vanishing variation ($\delta\Pi = 0$). Hence, minimization of the potential (4.23) leads to the system of variational equations that has to be solved

$$\int_\Omega \delta\boldsymbol{\varepsilon}(\boldsymbol{u}) : \boldsymbol{\sigma}\,dV - \int_\Omega \delta\boldsymbol{u} \cdot \boldsymbol{f}\,dV - \int_{\partial\Omega_\sigma} \delta\boldsymbol{u} \cdot \boldsymbol{t}\,dA = 0 \quad \forall\,\delta\boldsymbol{u}\,|\,\delta\boldsymbol{u} = \boldsymbol{0} \text{ on } \partial\Omega_u, \quad (4.27)$$

$$\int_\Omega \left[\frac{\partial\tilde{\Psi}}{\partial\boldsymbol{\varphi}}\,\delta\boldsymbol{\varphi} + \frac{\partial\tilde{\Psi}}{\partial(\boldsymbol{\nabla}\boldsymbol{\varphi})}\,\boldsymbol{\nabla}\delta\boldsymbol{\varphi}\right] dV = 0 \quad \forall\,\delta\boldsymbol{\varphi}\,|\,\delta\boldsymbol{\varphi} = \boldsymbol{0} \text{ on } \partial\Omega. \quad (4.28)$$

The first equation (4.27) is the so-called *principle of virtual work* and it represents the most common basis for the numerical solution of the underlying boundary value problem. It contains no changes compared with the form obtained using standard (unenhanced) form of the free energy function. However, the second equation (4.28) is a direct consequence of the introduced enhancement. It consists of two terms: the one representing a variation with respect to the list of non-local variables $\boldsymbol{\varphi}$ and the one representing a variation with respect to the list of the gradients of non-local variables $\boldsymbol{\nabla}\boldsymbol{\varphi}$. In view of the relation (4.4) and the assumption of linearity of the operators $\boldsymbol{\beta}$ and $\boldsymbol{c}$ therein, one obtains from (4.28)

$$\int_\Omega \Big[\big\langle\, \delta\boldsymbol{\varphi},\, \boldsymbol{\beta}\,(\boldsymbol{\varphi} - \boldsymbol{H}_{\boldsymbol{\varphi}}(\boldsymbol{P}_{NL}))\, \big\rangle_{NL}$$

$$+ \big\langle\, \boldsymbol{\nabla}\delta\boldsymbol{\varphi},\, \boldsymbol{c}\,(\boldsymbol{\nabla}\boldsymbol{\varphi})\, \big\rangle_{GNL}\Big] dV = 0 \quad \forall\,\delta\boldsymbol{\varphi}\,|\,\delta\boldsymbol{\varphi} = \boldsymbol{0} \text{ on } \partial\Omega. \quad (4.29)$$

The relations (4.27) and (4.28) (or consequently (4.29)) constitute two boundary-value subproblems coupled to each other, formulated on the whole domain of the body Ω. Consequently, the implementation difficulties of the explicit gradient models related to the search for the inelastic domain (as it was done e.g. in Liebe et al. (2001); Liebe and Steinmann (2001)) and enforcement of the interface conditions at the evolving boundary of inelastic region are eliminated.

Let us focus on the second term in (4.28) and (4.29). This volume integral can be transformed using the divergence theorem of Gauß-Ostrogradski[2] into one integral over boundary of the body and one volume integral involving a second order differential term

$$\int_\Omega \big\langle\, \boldsymbol{\nabla}\delta\boldsymbol{\varphi},\, \boldsymbol{c}\,(\boldsymbol{\nabla}\boldsymbol{\varphi})\, \big\rangle_{GNL}\,dV =$$

$$\int_{\partial\Omega} \big\langle\, \delta\boldsymbol{\varphi},\, (\boldsymbol{c}\,(\boldsymbol{\nabla}\boldsymbol{\varphi}))_{\boldsymbol{n}}\, \big\rangle_{NL}\,dA - \int_\Omega \big\langle\, \delta\boldsymbol{\varphi},\, \boldsymbol{\nabla}\cdot(\boldsymbol{c}\,(\boldsymbol{\nabla}\boldsymbol{\varphi}))\, \big\rangle_{NL}\,dV. \quad (4.30)$$

Here the following notation has been introduced

$$(\boldsymbol{c}\,(\boldsymbol{\nabla}\boldsymbol{\varphi}))_{\boldsymbol{n}} = \{\boldsymbol{c}\,(\boldsymbol{\nabla}\varphi_1)\cdot\boldsymbol{n},\, \ldots,\, \boldsymbol{c}\,(\boldsymbol{\nabla}\varphi_{nnl})\cdot\boldsymbol{n}\}. \quad (4.31)$$

The vector $\boldsymbol{n}$ in the expression above stands for the outward unit normal to the infinitesimal surface element of the domain boundary $dA \subset \partial\Omega$. The requirement of the vanishing variation together with the absence of other boundary terms in (4.23) results in vanishing boundary integral

$$\int_{\partial\Omega} \big\langle\, \delta\boldsymbol{\varphi},\, (\boldsymbol{c}\,(\boldsymbol{\nabla}\boldsymbol{\varphi}))_{\boldsymbol{n}}\, \big\rangle_{NL}\,dA = 0 \quad \forall\,\delta\boldsymbol{\varphi}\,|\,\delta\boldsymbol{\varphi} = \boldsymbol{0} \text{ on } \partial\Omega. \quad (4.32)$$

---

[2]For details on theorem of Gauß-Ostrogradski see the section A.2

If it is moreover assumed that the operator $\boldsymbol{c}$ has diagonal structure (as in the relation (4.9)), which is the case with the models used in this thesis, the condition (4.32) reduces to a vanishing flux of the non-local variable field across the boundary

$$\int_{\partial\Omega} \sum_{i=1}^{nnl} c_i\, \delta\boldsymbol{\varphi}_i : (\boldsymbol{\nabla}\boldsymbol{\varphi}_i \cdot \mathbf{n})\, dA \;=\; 0 \quad \forall\, \delta\boldsymbol{\varphi}\,|\, \delta\boldsymbol{\varphi} = \mathbf{0} \text{ on } \partial\Omega. \tag{4.33}$$

As a consequence of the arbitrariness of $\delta\boldsymbol{\varphi}$, the gradients of the non-local variables at every point of the boundary of the body $\partial\Omega$ have to lie in the tangent plane on the boundary at that point:

$$\boldsymbol{\nabla}\boldsymbol{\varphi}_i \cdot \mathbf{n} = 0 \quad \text{on } \partial\Omega \quad i = 1, \ldots, nnl. \tag{4.34}$$

In view of the results (4.32) and (4.30), the relation (4.29) becomes

$$\int_{\Omega} \big\langle\, \delta\boldsymbol{\varphi}, \boldsymbol{\beta}\,(\boldsymbol{\varphi} - \boldsymbol{H}_{\boldsymbol{\varphi}}(\boldsymbol{P}_{NL})) - \boldsymbol{\nabla}\cdot(\mathbf{c}\,(\boldsymbol{\nabla}\boldsymbol{\varphi}))\, \big\rangle_{NL}\, dV = 0 \quad \forall\, \delta\boldsymbol{\varphi}\,|\,\delta\boldsymbol{\varphi} = \mathbf{0} \text{ on } \partial\Omega. \tag{4.35}$$

Owing to arbitrariness of $\delta\boldsymbol{\varphi}$ and the linearity of the operator $\boldsymbol{c}$, the integral variational equation (4.35) can be transformed into its strong (differential) form

$$\boldsymbol{\beta}\,(\boldsymbol{\varphi} - \boldsymbol{H}_{\boldsymbol{\varphi}}(\boldsymbol{P}_{NL})) - \mathbf{c}\,(\boldsymbol{\nabla}\cdot\boldsymbol{\nabla}\boldsymbol{\varphi}) = \mathbf{0}. \tag{4.36}$$

The choice of diagonal operators $\boldsymbol{\beta}$ and $\boldsymbol{c}$ leads to further simplification and to the system of uncoupled second order partial differential equations

$$\beta_i\,(\boldsymbol{\varphi}_i - \boldsymbol{H}_{\boldsymbol{\varphi}\,i}(\boldsymbol{P}_{NL\,i})) - c_i\,\nabla^2\boldsymbol{\varphi}_i = \mathbf{0} \qquad i = 1, \ldots, nnl. \tag{4.37}$$

Comparison of the differential equations governing the distribution and evolution of non-local variables resulting from the present strategy (4.37) with the one of the implicit gradient models (3.119) reveals that the later one can be recovered from the former one for a specific choice of the model parameters $\beta_i = 1$ and $c_i = c(l)$. Hence, the particularly convenient properties of the implicit models (low-order continuity requirement for the primary variable fields and quasi-local evolution equations for internal variables) are kept by the strategy that is investigated in the thesis. Moreover, one can state that it represents a generalization of the implicit gradient models.

4.3.1. Linearization of the potential variation

The variation of the potential functional $\delta\Pi$, given in (4.26), is a non-linear functional itself. For the application in numerical procedures, which typically make use of linearized quantities, its linearization around a current variable state $\{\boldsymbol{u}_0, \boldsymbol{\varphi}_0\}$ has to be performed, cf. Başar and Weichert (2000). Denoting the increments of the displacement and non-local fields $\Delta\boldsymbol{u}$ and $\Delta\boldsymbol{\varphi}$ respectively, one one can perform a linearization of all dependent quantities using the Gâteaux-derivative

$$\mathcal{L}\delta\Pi := \delta\Pi(\boldsymbol{u}_0, \boldsymbol{\varphi}_0) + D\delta\Pi(\boldsymbol{u}_0, \boldsymbol{\varphi}_0)(\Delta\boldsymbol{u}) + D\delta\Pi(\boldsymbol{u}_0, \boldsymbol{\varphi}_0)(\Delta\boldsymbol{\varphi}). \tag{4.38}$$

For notational simplification the last two summands in (4.38) are denoted as

$$\Delta\delta\Pi := D\delta\Pi(\boldsymbol{u}_0, \boldsymbol{\varphi}_0)(\Delta\boldsymbol{u}) + D\delta\Pi(\boldsymbol{u}_0, \boldsymbol{\varphi}_0)(\Delta\boldsymbol{\varphi}). \tag{4.39}$$

Applying the definition (4.39) on the relation (4.26) under consideration of (4.29) and assumed linearity of the operators $\boldsymbol{\beta}$ and $\boldsymbol{c}$, one ends up with the following expression for the incrementation of $\delta\Pi$

$$
\begin{aligned}
\Delta\delta\Pi \;=\; & \int_\Omega \delta\boldsymbol{\varepsilon} : \frac{\partial\boldsymbol{\sigma}}{\partial\boldsymbol{\varepsilon}} : \Delta\boldsymbol{\varepsilon}\,dV + \int_\Omega \delta\boldsymbol{\varepsilon} : \frac{\partial\boldsymbol{\sigma}}{\partial\boldsymbol{\varphi}}\,\Delta\boldsymbol{\varphi}\,dV \\[2mm]
& + \int_\Omega \Big\langle\, \delta\boldsymbol{\varphi}, \frac{\partial}{\partial\boldsymbol{\varepsilon}}\left[\boldsymbol{\beta}\left(\boldsymbol{\varphi}-\boldsymbol{H}_\varphi(\boldsymbol{P}_{NL})\right)\right] : \Delta\boldsymbol{\varepsilon} \,\Big\rangle_{NL}\,dV \\[2mm]
& + \int_\Omega \Big\langle\, \delta\boldsymbol{\varphi}, \frac{\partial}{\partial\boldsymbol{\varphi}}\left[\boldsymbol{\beta}\left(\boldsymbol{\varphi}-\boldsymbol{H}_\varphi(\boldsymbol{P}_{NL})\right)\right]\Delta\boldsymbol{\varphi} \,\Big\rangle_{NL}\,dV \\[2mm]
& + \int_\Omega \Big\langle\, \boldsymbol{\nabla}\delta\boldsymbol{\varphi},\, \mathbf{c}\,(\boldsymbol{\nabla}\Delta\boldsymbol{\varphi}) \,\Big\rangle_{GNL}\,dV.
\end{aligned}
\tag{4.40}
$$

If, additionally, operators $\boldsymbol{\beta}$ and $\boldsymbol{c}$ possess a diagonal structure in the sense that they couple neither elements of the non-local list $\boldsymbol{\varphi}_i$ and $\boldsymbol{\nabla}\boldsymbol{\varphi}_i$, respectively, nor their components, i.e.

$$
\boldsymbol{\beta}(\boldsymbol{\varphi}_i) \;=\; \beta_i\boldsymbol{\varphi}_i, \qquad \boldsymbol{c}(\boldsymbol{\nabla}\boldsymbol{\varphi}_i) \;=\; c_i\boldsymbol{\nabla}\boldsymbol{\varphi}_i
\tag{4.41}
$$

(as it is the case with the models in this thesis), the relation (4.40) attains the form

$$
\begin{aligned}
\Delta\delta\Pi \;=\; & \int_\Omega \delta\boldsymbol{\varepsilon} : \frac{\partial\boldsymbol{\sigma}}{\partial\boldsymbol{\varepsilon}} : \Delta\boldsymbol{\varepsilon}\,dV + \int_\Omega \sum_{i=1}^{nnl} \delta\boldsymbol{\varepsilon} : \frac{\partial\boldsymbol{\sigma}}{\partial\boldsymbol{\varphi}_i} : \Delta\boldsymbol{\varphi}_i\,dV \\[2mm]
& + \int_\Omega \sum_{i=1}^{nnl} \delta\boldsymbol{\varphi}_i : \frac{\partial}{\partial\boldsymbol{\varepsilon}}\left[\beta_i\left(\boldsymbol{\varphi}_i-\boldsymbol{H}_{\varphi\,i}(\boldsymbol{P}_{NL\,i})\right)\right] : \Delta\boldsymbol{\varepsilon}\,dV \\[2mm]
& + \int_\Omega \sum_{i=1}^{nnl} \delta\boldsymbol{\varphi}_i : \frac{\partial}{\partial\boldsymbol{\varphi}_i}\left[\beta_i\left(\boldsymbol{\varphi}_i-\boldsymbol{H}_{\varphi\,i}(\boldsymbol{P}_{NL\,i})\right)\right] : \Delta\boldsymbol{\varphi}_i\,dV \\[2mm]
& + \int_\Omega \sum_{i=1}^{nnl} c_i\,\boldsymbol{\nabla}\delta\boldsymbol{\varphi}_i \vdots \boldsymbol{\nabla}\Delta\boldsymbol{\varphi}_i\,dV.
\end{aligned}
\tag{4.42}
$$

The discussion within this section was based on the consideration of the internal variable set $\boldsymbol{P}$ as constant with respect to variation of the potential functional (4.23), which left us with displacement $\boldsymbol{u}$ and non-local variables $\boldsymbol{\varphi}$ as problem unknowns. However, internal variables are not constant, but rather dependent on the history of deformation. In the following section the evolution of internal variables and its consequences on the variational problem defined in this section is discussed.

4.4. Constitutive model

The evolution of internal variables, which is connected to the history of deformation, has to be specified in a way consistent with the physical laws derived in chapter 2. That task was

accomplished in the case of a classical theory introducing a dissipation potential given in (4.19). In order to follow the same approach in conjunction with the investigated regularization strategy, we first discuss the thermodynamic applicability and consequences of the gradient enhancement of the free-energy function (4.11) in the section 4.4.1. Afterwards, the formulation of the constitutive update is presented in the section 4.4.3 and its consistent linearization in the section 4.4.4. Finally, some remarks about the application of the strategy are given in the section 4.4.5.

4.4.1. Thermodynamic consistency of the enhanced strategy

The balance of entropy, derived in the section 2.3.5, leads to the Clausius-Plank inequality in the small-deformation setting (2.166), (2.167). Assuming isothermal deformation, it is expressed in its global form in terms of free-energy function per unit volume (3.1) as

$$\dot{\mathcal{S}}_{irr} = \int_{\Omega} \boldsymbol{\sigma} : \dot{\boldsymbol{\varepsilon}} - \dot{\Psi} \, dV \geq 0. \tag{4.43}$$

The local form is deduced from (4.43) demanding that it has to hold for every subdomain $\bar{\Omega} \in \Omega$ as well, leading to

$$\mathcal{D}_{int} = \boldsymbol{\sigma} : \dot{\boldsymbol{\varepsilon}} - \dot{\Psi} \geq 0. \tag{4.44}$$

Inserting the enhanced Helmholtz free-energy function (4.11) into (4.43) it follows

$$\dot{\mathcal{S}}_{irr} = \int_{\Omega} \boldsymbol{\sigma} : \dot{\boldsymbol{\varepsilon}} - \dot{\tilde{\Psi}}(\boldsymbol{\varepsilon}, \boldsymbol{P}, \varphi, \boldsymbol{\nabla}\varphi) \, dV \geq 0. \tag{4.45}$$

In view of the relation (4.11) and the decomposition of the list of internal variables (4.2), the rate of the enhanced free energy function is obtained as

$$\dot{\tilde{\Psi}} = \dot{\Psi}(\boldsymbol{\varepsilon}, \boldsymbol{P}_L, \boldsymbol{P}_{NL}) + \dot{\Psi}_{intr}(\boldsymbol{P}_{NL}, \varphi, \boldsymbol{\nabla}\varphi), \tag{4.46}$$

and consequently as

$$\dot{\tilde{\Psi}} = \frac{\partial \Psi}{\partial \boldsymbol{\varepsilon}} : \dot{\boldsymbol{\varepsilon}} + \frac{\partial \Psi}{\partial \boldsymbol{P}_L} : \dot{\boldsymbol{P}}_L + \frac{\partial \Psi}{\partial \boldsymbol{P}_{NL}} : \dot{\boldsymbol{P}}_{NL} +$$
$$\frac{\partial \Psi_{intr}}{\partial \boldsymbol{P}_{NL}} : \dot{\boldsymbol{P}}_{NL} + \frac{\partial \Psi_{intr}}{\partial \varphi} \dot{\varphi} + \frac{\partial \Psi_{intr}}{\partial (\boldsymbol{\nabla}\varphi)} (\dot{\boldsymbol{\nabla}\varphi}). \tag{4.47}$$

Non-negativity of the internal dissipation in a process of elastic deformation (4.44) for arbitrary rates of strain tensor results in the constitutive relation for the stress tensor identical to the one of classical theory

$$\boldsymbol{\sigma} := \frac{\partial \Psi}{\partial \boldsymbol{\varepsilon}} = \frac{\partial \tilde{\Psi}}{\partial \boldsymbol{\varepsilon}}. \tag{4.48}$$

In view of (4.48) and (4.47), the global form of Clausius-Planck inequality (4.43) becomes

$$\dot{\mathcal{S}}_{irr} = \int_{\Omega} -\frac{\partial \Psi}{\partial \boldsymbol{P}_L} : \dot{\boldsymbol{P}}_L - \frac{\partial \Psi}{\partial \boldsymbol{P}_{NL}} : \dot{\boldsymbol{P}}_{NL} -$$
$$\frac{\partial \Psi_{intr}}{\partial \boldsymbol{P}_{NL}} : \dot{\boldsymbol{P}}_{NL} - \frac{\partial \Psi_{intr}}{\partial \varphi} \dot{\varphi} - \frac{\partial \Psi_{intr}}{\partial (\boldsymbol{\nabla}\varphi)} (\dot{\boldsymbol{\nabla}\varphi}) \, dV \geq 0. \tag{4.49}$$

Recalling the variational equation (4.28) and the arbitrariness of the variation of the list of non-local variables φ therein, the last two integrals in (4.49) vanish

$$
\int_\Omega - \frac{\partial \Psi_{intr}}{\partial \varphi} \, \dot{\varphi} - \frac{\partial \Psi_{intr}}{\partial (\boldsymbol{\nabla} \varphi)} \, (\dot{\boldsymbol{\nabla} \varphi}) dV = 0, \tag{4.50}
$$

so that one obtains

$$
\dot{\mathcal{S}}_{irr} = \int_\Omega - \frac{\partial \Psi}{\partial \boldsymbol{P}_L} : \dot{\boldsymbol{P}}_L - \frac{\partial \Psi}{\partial \boldsymbol{P}_{NL}} : \dot{\boldsymbol{P}}_{NL} - \frac{\partial \Psi_{intr}}{\partial \boldsymbol{P}_{NL}} : \dot{\boldsymbol{P}}_{NL} \; dV \; \geq 0. \tag{4.51}
$$

The global form of Clausius-Planck inequality (4.51) results from the proposed gradient-enhancement strategy, and its local form can be deduced as

$$
\mathcal{D}_{int} = - \frac{\partial \Psi}{\partial \boldsymbol{P}_L} : \dot{\boldsymbol{P}}_L - \frac{\partial \Psi}{\partial \boldsymbol{P}_{NL}} : \dot{\boldsymbol{P}}_{NL} - \frac{\partial \Psi_{intr}}{\partial \boldsymbol{P}_{NL}} : \dot{\boldsymbol{P}}_{NL} \; \geq 0. \tag{4.52}
$$

Motivated by the split of the list of internal variables (4.2) into two sublists $\boldsymbol{P}_L$ and $\boldsymbol{P}_{NL}$, one can define two lists of their thermodynamical conjugates $\boldsymbol{Q}_L$ and $\boldsymbol{Q}_{NL}$ as well

$$
\boldsymbol{Q}_L := - \frac{\partial \Psi}{\partial \boldsymbol{P}_L}, \qquad \boldsymbol{Q}_{NL} := - \frac{\partial \Psi}{\partial \boldsymbol{P}_{NL}} - \frac{\partial \Psi_{intr}}{\partial \boldsymbol{P}_{NL}}, \tag{4.53}
$$

which are structured in the same way as corresponding lists of internal variables

$$
\boldsymbol{Q}_L = \{\boldsymbol{Q}_{L\,1}, \, \ldots \, , \boldsymbol{Q}_{L\,nl}\}, \qquad \boldsymbol{Q}_{L\,i} := - \frac{\partial \Psi}{\partial \boldsymbol{P}_{L\,i}}, \tag{4.54}
$$

$$
\boldsymbol{Q}_{NL} = \{\boldsymbol{Q}_{NL\,1}, \, \ldots \, , \boldsymbol{Q}_{NL\,nnl}\}, \qquad \boldsymbol{Q}_{NL\,i} := - \frac{\partial \Psi}{\partial \boldsymbol{P}_{NL\,i}} - \frac{\partial \Psi_{intr}}{\partial \boldsymbol{P}_{NL\,i}}. \tag{4.55}
$$

The parameters nl and nnl in the relations (4.54) and (4.55) respectively, stand for the number of elements of the corresponding lists, which can be scalar as well as tensorial fields. Hence, the internal dissipation attains the form

$$
\mathcal{D}_{int} = \boldsymbol{Q}_L : \dot{\boldsymbol{P}}_L + \boldsymbol{Q}_{NL} : \dot{\boldsymbol{P}}_{NL} \; \geq 0. \tag{4.56}
$$

4.4.2. Consequences of the enhancement strategy on the micromechanical driving forces

Comparing the relations (4.54) and (4.55) with the one derived within a classical (local) model (3.26), one can notice that the only difference represents the presence of an additional conjugate term in the list $\boldsymbol{Q}_{NL}$. This outcome is in agreement with the fact that the list $\boldsymbol{P}_{NL}$ comprises the variables included in the regularization procedure, while list $\boldsymbol{P}_L$ contains the variables which are treated in classical (local) manner. Let us furthermore consider the interaction potential presented in (4.4) in conjunction with the assumption of the linear operator $\boldsymbol{\beta}$ therein. The derivative of Ψ_{intr} with respect to the internal variables $\boldsymbol{P}_{NL}$ turns out to be

$$
\frac{\partial \Psi_{intr}}{\partial \boldsymbol{P}_{NL}} = \frac{\partial}{\partial \boldsymbol{P}_{NL}} \left(\frac{1}{2} \left\langle \varphi - \boldsymbol{H}_\varphi(\boldsymbol{P}_{NL}), \, \boldsymbol{\beta} \left(\varphi - \boldsymbol{H}_\varphi(\boldsymbol{P}_{NL}) \right) \right\rangle_{NL} \right) =
$$
$$
- \boldsymbol{\beta} \left(\varphi - \boldsymbol{H}_\varphi(\boldsymbol{P}_{NL}) \right) \frac{\partial \boldsymbol{H}_\varphi}{\partial \boldsymbol{P}_{NL}}. \tag{4.57}
$$

Utilization of operators $\boldsymbol{\beta}$ satisfying the condition (4.41), which is the case investigated in this thesis, leads to

$$\frac{\partial \Psi_{intr}}{\partial \boldsymbol{P}_{NL}} = \left\{ \frac{\partial \Psi_{intr}}{\partial \boldsymbol{P}_{NL\,1}}, \cdots, \frac{\partial \Psi_{intr}}{\partial \boldsymbol{P}_{NL\,nnl}} \right\},$$

$$\frac{\partial \Psi_{intr}}{\partial \boldsymbol{P}_{NL\,i}} = -\beta_i \left(\boldsymbol{\varphi}_i - \boldsymbol{H}_{\boldsymbol{\varphi}\,i}(\boldsymbol{P}_{NL\,i}) \right) : \frac{\partial \boldsymbol{H}_{\boldsymbol{\varphi}\,i}}{\partial \boldsymbol{P}_{NL\,i}}. \quad (4.58)$$

Since the elements $\boldsymbol{\varphi}_i$ and $\boldsymbol{H}_{\boldsymbol{\varphi}\,i}$ of the corresponding lists can be scalars or tensors of arbitrary order, the double dot product has to be understood as the scalar product between equally structured objects.

In view of (4.57), the thermodynamic conjugates $\boldsymbol{Q}_{NL}$ of the list of internal variables $\boldsymbol{P}_{NL}$, defined in (4.55), can be written as

$$\boldsymbol{Q}_{NL} = \underbrace{-\frac{\partial \Psi}{\partial \boldsymbol{P}_{NL}}}_{\widehat{\boldsymbol{Q}}_{NL}} + \underbrace{\boldsymbol{\beta} \left(\boldsymbol{\varphi} - \boldsymbol{H}_{\boldsymbol{\varphi}}(\boldsymbol{P}_{NL}) \right) \frac{\partial \boldsymbol{H}_{\boldsymbol{\varphi}}}{\partial \boldsymbol{P}_{NL}}}_{\widetilde{\boldsymbol{Q}}_{NL}}. \quad (4.59)$$

The first part ($\widehat{\boldsymbol{Q}}_{NL}$) on the right-hand side in (4.59) comes from a classical (local) inelastic consideration. The second one ($\widetilde{\boldsymbol{Q}}_{NL}$), on the other hand, is a direct consequence of the gradient enhancement of the free-energy function (4.11). It introduces non-local interaction into the definition of the micromechanical driving forces $\boldsymbol{Q}_{NL}$ and consequently into the evolution of corresponding internal variables $\boldsymbol{P}_{NL}$, as it will be shown later. Recalling the relation (4.36) and rewriting it as

$$\boldsymbol{\beta} \left(\boldsymbol{\varphi} - \boldsymbol{H}_{\boldsymbol{\varphi}}(\boldsymbol{P}_{NL}) \right) = \mathbf{c} \left(\boldsymbol{\nabla} \cdot \boldsymbol{\nabla} \boldsymbol{\varphi} \right), \quad (4.60)$$

one can express the non-local interaction part ($\widetilde{\boldsymbol{Q}}_{NL}$) in an equivalent form that involves the second order derivative (Laplacian) term in the non-local variable $\boldsymbol{\varphi}$

$$\boldsymbol{Q}_{NL} = \mathbf{c} \left(\boldsymbol{\nabla} \cdot \boldsymbol{\nabla} \boldsymbol{\varphi} \right) \frac{\partial \boldsymbol{H}_{\boldsymbol{\varphi}}}{\partial \boldsymbol{P}_{NL}}. \quad (4.61)$$

The result (4.62) can be used to transform the equation (4.59), leading to the following expression

$$\boldsymbol{Q}_{NL} = \underbrace{-\frac{\partial \Psi}{\partial \boldsymbol{P}_{NL}}}_{\widehat{\boldsymbol{Q}}_{NL}} + \underbrace{\mathbf{c} \left(\boldsymbol{\nabla} \cdot \boldsymbol{\nabla} \boldsymbol{\varphi} \right) \frac{\partial \boldsymbol{H}_{\boldsymbol{\varphi}}}{\partial \boldsymbol{P}_{NL}}}_{\widetilde{\boldsymbol{Q}}_{NL}}. \quad (4.62)$$

Hence, one can consider the driving forces $\boldsymbol{Q}_{NL}$ as being dependent on the second order derivatives of the non-local variable field $\boldsymbol{\varphi}$ in addition to the strain tensor $\boldsymbol{\varepsilon}$ and internal variables $\boldsymbol{P}$. If the specific form of the enhanced free-energy function (4.11) employs the operator $\boldsymbol{\beta}$ satisfying the condition (4.41), the micromechanical driving force $\boldsymbol{Q}_{NL}$ becomes

$$\boldsymbol{Q}_{NL} = \left\{ \boldsymbol{Q}_{NL\,1}, \cdots, \boldsymbol{Q}_{NL\,nnl} \right\},$$

$$\boldsymbol{Q}_{NL\,i} = \underbrace{-\frac{\partial \Psi}{\partial \boldsymbol{P}_{NL\,i}}}_{\widehat{\boldsymbol{Q}}_{NL\,i}} + \underbrace{c_i \left(\nabla^2 \boldsymbol{\varphi}_i \right) \frac{\partial \boldsymbol{H}_{\boldsymbol{\varphi}\,i}}{\partial \boldsymbol{P}_{NL\,i}}}_{\widetilde{\boldsymbol{Q}}_{NL\,i}}. \quad (4.63)$$

4.4.3. Evolution of inelastic variables

The evolution of inelastic variables is described following the lines defined in the section 3.2.1. A particularly suitable property of the proposed enhancement strategy is that, in view of (4.56), the *dissipation potential* $J(\dot{\boldsymbol{P}})$ retains its common form (cf. Dimitrijević and Hackl (2006, 2008, 2009)). Following the discussion in the 3.2.1, the dissipation potential

$$
\begin{aligned}
J(\dot{\boldsymbol{P}}) \;&=\; \sup_{\boldsymbol{Q}} \left[\boldsymbol{Q} : \dot{\boldsymbol{P}} \;-\; I_K(\boldsymbol{P},\boldsymbol{Q},\boldsymbol{\varepsilon}) \right] \\
&=\; \sup_{\boldsymbol{Q}_L,\boldsymbol{Q}_{NL}} \left[\boldsymbol{Q}_L : \dot{\boldsymbol{P}}_L \;+\; \boldsymbol{Q}_{NL} : \dot{\boldsymbol{P}}_{NL} \;-\; I_K(\boldsymbol{P}_L,\boldsymbol{P}_{NL},\boldsymbol{Q},\boldsymbol{\varepsilon}) \right].
\end{aligned}
\tag{4.64}
$$

is utilized in the subsequent considerations. The quantity I_K in (4.64) represents the characteristic function of a domain K and is already defined in (3.24). The domain K is assumed to be defined through the set of m inelastic constraints, as it was done in the discussion of classical (local) models (section 3.2.1)

$$
K = \left\{ \boldsymbol{Q}_L, \boldsymbol{Q}_{NL} \;\middle|\; \phi_i(\boldsymbol{P}_L, \boldsymbol{P}_{NL}, \boldsymbol{Q}_L, \boldsymbol{Q}_{NL}, \boldsymbol{\varepsilon}) \leq 0, \;\; i = 1, ..., m \right\}.
\tag{4.65}
$$

The definition of the dissipation potential (4.65) results in a (possibly multiple) constrained optimization problem, cf. Simo and Hughes (1998), whose solution are the evolution equations for the internal variables:

$$
\dot{\boldsymbol{P}}_L = \sum_{i=1}^{m} \dot{\lambda}_i \, \frac{\partial \phi_i}{\partial \boldsymbol{Q}_L}; \qquad \dot{\boldsymbol{P}}_{NL} = \sum_{i=1}^{m} \dot{\lambda}_i \, \frac{\partial \phi_i}{\partial \boldsymbol{Q}_{NL}}
\tag{4.66}
$$

subjected to corresponding Kuhn-Karush-Tucker optimality conditions:

$$
\dot{\lambda}_i \geq 0, \;\; \phi_i \leq 0, \;\; \dot{\lambda}_i \phi_i = 0, \qquad \forall \, i = 1, ..., m
\tag{4.67}
$$

From the optimality conditions (4.67) one can define the set of indices of *active inelastic constraints*

$$
\mathbb{S}_{act} = \left\{ j \in 1, ..., m \;\middle|\; \phi_j = 0, \; \dot{\lambda}_j > 0 \right\}.
\tag{4.68}
$$

Owing to the fact that only activated inelastic constrains contribute to the evolution of the internal variables, the set $\mathbb{S}_{act}$ can be used to modify the relation (4.66) into

$$
\dot{\boldsymbol{P}}_L = \sum_{j \in \mathbb{S}_{act}} \dot{\lambda}_j \, \frac{\partial \phi_j}{\partial \boldsymbol{Q}_L}, \qquad \dot{\boldsymbol{P}}_{NL} = \sum_{j \in \mathbb{S}_{act}} \dot{\lambda}_j \, \frac{\partial \phi_j}{\partial \boldsymbol{Q}_{NL}}.
\tag{4.69}
$$

Relations (4.67)-(4.69) constitute the differential-algebraic system of equations driving the evolution of internal variables and therefore closing the formulation of the problem. For the implementation within the numerical procedure this system has to be discretized in time and in that purpose unconditionally stable Backward-Euler discretization is employed, cf. Hackl and Schmidt-Baldassari (2001); Hackl (2001). The constitutive update is formulated through the *elastic predictor-inelastic corrector* scheme, cf. Simo and Hughes (1998), and it is summarized in the Tables 4.1 and 4.2.

Elastic predictor step

(1) Initialize the variables:

Given: $\quad t = t_{n+1},\ \boldsymbol{\varepsilon}_{n+1},\ \boldsymbol{\varphi}_{n+1},\ \boldsymbol{P}_n$,

Set: $\quad it = 0,\ \boldsymbol{P}_{n+1}^{(it)} = \boldsymbol{P}_n,\ inel = 0$,

Calculate: $\quad \boldsymbol{Q}_{L,\,n+1}^{(it)} = -\dfrac{\partial \Psi\left(\boldsymbol{\varepsilon}, \boldsymbol{P}_L^{(it)}, \boldsymbol{P}_{NL}^{(it)}\right)_{n+1}}{\partial \boldsymbol{P}_L}$,

$\quad \boldsymbol{Q}_{NL,\,n+1}^{(it)} = -\dfrac{\partial \Psi\left(\boldsymbol{\varepsilon}, \boldsymbol{P}_L^{(it)}, \boldsymbol{P}_{NL}^{(it)}\right)_{n+1}}{\partial \boldsymbol{P}_{NL}} - \dfrac{\partial \Psi_{intr}\left(\boldsymbol{\varphi}, \boldsymbol{P}_{NL}^{(it)}\right)_{n+1}}{\partial \boldsymbol{P}_{NL}}$,

$\quad \phi_i = \phi_i\left(\boldsymbol{P}_L, \boldsymbol{P}_{NL}, \boldsymbol{Q}_L, \boldsymbol{Q}_{NL}, \boldsymbol{\varepsilon}\right)_{n+1}^{(it)}, \quad i = 1, ..., m$.

(2) Check for inelastic processes:

IF $\phi_i \leq 0\ \ \forall\, i = 1, ..., m$ THEN:

Set: $\quad \boldsymbol{P}_{L,\,n+1} = \boldsymbol{P}_{L,\,n+1}^{(it)},\ \boldsymbol{P}_{NL,\,n+1} = \boldsymbol{P}_{NL,\,n+1}^{(it)}$,

$\quad \boldsymbol{Q}_{L,\,n+1} = \boldsymbol{Q}_{L,\,n+1}^{(it)},\ \boldsymbol{Q}_{NL,\,n+1} = \boldsymbol{Q}_{NL,\,n+1}^{(it)}$.

GO TO 11.

ELSE

Extract active set: $\quad \mathbb{S}_{act} = \{j \in 1, ..., m \mid \phi_j > 0\}$,

Set: $\quad it = 1,\ \Delta\lambda_j = 0\ \forall\, j \in \mathbb{S}_{act},\ inel = 1$,

GO TO 3.

ENDIF

Table 4.1.: Constitutive update algorithm I

4.4.4. Linerization of the update algorithm

The important difference between the classical (local) inelastic material models and the gradient enhanced models based on the presented strategy is that in the latter case the constitutive update algorithm is not only strain-driven, but additionally driven by the set of additional non-local variables $\boldsymbol{\varphi}$ as well. Hence, for the solution of the system of variational equations (4.27) and (4.28) it has to provide, in addition to the commonly required stress tensor $\boldsymbol{\sigma}$, the value of the updated quantity $\boldsymbol{\beta}\left(\boldsymbol{\varphi} - \boldsymbol{H}_{\boldsymbol{\varphi}}(\boldsymbol{P}_{NL})\right)$ at the end of the current time step t_{n+1}. In order to notationally simplify forthcoming derivation, let us denote

$$\boldsymbol{L}_{\boldsymbol{\varphi}} := \boldsymbol{\beta}\left(\boldsymbol{\varphi} - \boldsymbol{H}_{\boldsymbol{\varphi}}(\boldsymbol{P}_{NL})\right). \tag{4.70}$$

Furthermore, the constitutive update has to supply the tangent moduli occurring in the linearization of the potential variation (equation (4.40)), since their utilization is crucial in the numerical approximation of the problem. As a consequence, consistent linearization of the update algorithm has to be performed. Due to additional driving variables additional tangent moduli are required as well, and they present the most significant difference in the treatment of the constitutive update between the local and enhanced model. For the sake of notational clarity, a use of the relation (4.70) is made, leading to

$$\frac{\partial \boldsymbol{L}_{\boldsymbol{\varphi}}}{\partial \boldsymbol{\varepsilon}} = \frac{\partial}{\partial \boldsymbol{\varepsilon}}\left[\boldsymbol{\beta}\left(\boldsymbol{\varphi} - \boldsymbol{H}_{\boldsymbol{\varphi}}(\boldsymbol{P}_{NL})\right)\right], \qquad \frac{\partial \boldsymbol{L}_{\boldsymbol{\varphi}}}{\partial \boldsymbol{\varphi}} = \frac{\partial}{\partial \boldsymbol{\varphi}}\left[\boldsymbol{\beta}\left(\boldsymbol{\varphi} - \boldsymbol{H}_{\boldsymbol{\varphi}}(\boldsymbol{P}_{NL})\right)\right]. \tag{4.71}$$

Let us consider the state $\boldsymbol{\varepsilon}(\boldsymbol{X}, t) = \boldsymbol{\varepsilon}_0$, $\boldsymbol{\varphi}(\boldsymbol{X}, t) = \boldsymbol{\varphi}_0$ and $\boldsymbol{P}(\boldsymbol{X}, t) = \boldsymbol{P}_0$ at certain time $t = t^*$. Denoting the increments of strain , non-local variable list and internal variable list

---

General multiple-constrained update iteration

(3) Calculate residuals and inelastic constraints:

$$\boldsymbol{Q}_{L,\,n+1}^{(it)} = -\frac{\partial \Psi \left(\boldsymbol{\varepsilon}, \boldsymbol{P}_L^{(it)}, \boldsymbol{P}_{NL}^{(it)} \right)_{n+1}}{\partial \boldsymbol{P}_L}, \; \boldsymbol{Q}_{NL,\,n+1}^{(it)} = -\frac{\partial \Psi \left(\boldsymbol{\varepsilon}, \boldsymbol{P}_L^{(it)}, \boldsymbol{P}_{NL}^{(it)} \right)_{n+1}}{\partial \boldsymbol{P}_{NL}} - \frac{\partial \Psi_{intr} \left(\boldsymbol{\varphi}, \boldsymbol{P}_{NL}^{(it)} \right)_{n+1}}{\partial \boldsymbol{P}_{NL}} \, ,$$

$$\phi_j^{(it)} = \phi_j \left(\boldsymbol{P}_L, \boldsymbol{P}_{NL}, \boldsymbol{Q}_L, \boldsymbol{Q}_{NL}, \boldsymbol{\varepsilon} \right)_{n+1}^{(it)}, \quad \forall \, j \in \mathbb{S}_{act} \, ,$$

$$\mathbf{R}^{(it)} = \left\{ \begin{array}{c} \mathbf{R}_{P_L}^{(it)} \\ \mathbf{R}_{P_{NL}}^{(it)} \end{array} \right\} = \left\{ \begin{array}{c} -\boldsymbol{P}_{L,\,n+1}^{(it)} + \boldsymbol{P}_{L,\,n} \\ -\boldsymbol{P}_{NL,\,n+1}^{(it)} + \boldsymbol{P}_{NL,\,n} \end{array} \right\} + \sum_{j \in \mathbb{S}_{act}} \Delta\lambda_j^{(it)} \left\{ \begin{array}{c} \frac{\partial \phi_j}{\partial \boldsymbol{Q}_L} \\ \frac{\partial \phi_j}{\partial \boldsymbol{Q}_{NL}} \end{array} \right\}^{(it)} .$$

(4) Check for convergence:

IF $\phi_j^{(it)} \leq TOL_1 \; \forall \, j \in \mathbb{S}_{act}$ and $\left\| \mathbf{R}^{(it)} \right\| \leq TOL_2$ THEN:

  GO TO 9.

ENDIF

(5) Calculate derivatives for the local Newton update:

$$\mathbb{D}^{(it)} = \left[\begin{array}{cc} -\frac{\partial^2 \Psi}{\partial \boldsymbol{P}_L \partial \boldsymbol{P}_L} & -\frac{\partial^2 \Psi}{\partial \boldsymbol{P}_L \partial \boldsymbol{P}_{NL}} \\ -\frac{\partial^2 \Psi}{\partial \boldsymbol{P}_{NL} \partial \boldsymbol{P}_L} & -\frac{\partial^2 \Psi}{\partial \boldsymbol{P}_{NL} \partial \boldsymbol{P}_{NL}} - \frac{\partial^2 \Psi_{intr}}{\partial \boldsymbol{P}_{NL} \partial \boldsymbol{P}_{NL}} \end{array} \right]^{(it)} ,$$

$$\mathbb{A}^{(it)} = - \left(\mathbb{D}^{(it)} \right)^{-1} + \sum_{j \in \mathbb{S}_{act}} \Delta\lambda_j \left[\begin{array}{cc} \frac{\partial^2 \phi_j}{\partial \boldsymbol{Q}_L \partial \boldsymbol{Q}_L} & \frac{\partial^2 \phi_j}{\partial \boldsymbol{Q}_L \partial \boldsymbol{Q}_{NL}} \\ \frac{\partial^2 \phi_j}{\partial \boldsymbol{Q}_{NL} \partial \boldsymbol{Q}_L} & \frac{\partial^2 \phi_j}{\partial \boldsymbol{Q}_{NL} \partial \boldsymbol{Q}_{NL}} \end{array} \right]^{(it)} ,$$

$$[G_{jk}]^{(it)} = \left\{ \begin{array}{cc} \frac{\partial \phi_j}{\partial \boldsymbol{Q}_L} & \frac{\partial \phi_j}{\partial \boldsymbol{Q}_{NL}} \end{array} \right\}^{(it)} : \mathbb{A}^{(it)} : \left\{ \begin{array}{c} \frac{\partial \phi_k}{\partial \boldsymbol{Q}_L} \\ \frac{\partial \phi_k}{\partial \boldsymbol{Q}_{NL}} \end{array} \right\}^{(it)} ,$$

$$\left[G^{jk} \right]^{(it)} = \left([G_{jk}]^{(it)} \right)^{-1} .$$

(6) Obtain increment to consistency parameters:

$$\Delta\Delta\lambda_j^{(it)} = \sum_{k \in \mathbb{S}_{act}} \left[G^{jk} \right]^{(it)} \left\{ \phi_k - \left[\begin{array}{cc} \frac{\partial \phi_k}{\partial \boldsymbol{Q}_L} & \frac{\partial \phi_k}{\partial \boldsymbol{Q}_{NL}} \end{array} \right] : (\mathbb{A})^{-1} : \mathbf{R} \right\}^{(it)} ,$$

$$\Delta\bar{\lambda}_j^{(it+1)} = \Delta\lambda_j^{(it)} + \Delta\Delta\lambda_j^{(it)} ,$$

IF $\Delta\bar{\lambda}_j^{(it+1)} \leq 0$ for some $k \in \mathbb{S}_{act}$ THEN:

  Update active set $\mathbb{S}_{act} = \left\{ j \in 1, ..., m \mid \Delta\bar{\lambda}_j > 0 \right\} ,$

  GO TO 3.

ELSE

  GO TO 7.

ENDIF

(7) Obtain increment to internal variables:

$$\left\{ \begin{array}{c} \Delta\boldsymbol{P}_L \\ \Delta\boldsymbol{P}_{NL} \end{array} \right\}^{(it)} = \left(\mathbb{A}^{(it)} \right)^{-1} : \left(-\mathbf{R} - \sum_{j \in \mathbb{S}_{act}} \Delta\Delta\lambda_j \left\{ \begin{array}{c} \frac{\partial \phi_j}{\partial \boldsymbol{Q}_L} \\ \frac{\partial \phi_j}{\partial \boldsymbol{Q}_{NL}} \end{array} \right\} \right)^{(it)} .$$

(8) Update internal variables and continue the loop:

$$\left\{ \begin{array}{c} \boldsymbol{P}_L \\ \boldsymbol{P}_{NL} \\ \Delta\lambda_j \end{array} \right\}^{(it+1)} = \left\{ \begin{array}{c} \boldsymbol{P}_L \\ \boldsymbol{P}_{NL} \\ \Delta\lambda_j \end{array} \right\}^{(it)} + \left\{ \begin{array}{c} \Delta\boldsymbol{P}_L \\ \Delta\boldsymbol{P}_{NL} \\ \Delta\Delta\lambda_j \end{array} \right\}^{(it)} ,$$

  Set $it \leftarrow it + 1 ,$

  GO TO 3.

Table 4.2.: Constitutive update algorithm II

$\Delta\varepsilon$, $\Delta\varphi$ and $\Delta\boldsymbol{P}$ respectively, one can perform linearization of the stress tensor $\boldsymbol{\sigma}$ and the response function $\boldsymbol{L}_\varphi$ about the state ε_0, φ_0, $\boldsymbol{P}_0$ using the Gâteaux-derivative[3]

$$\mathcal{L}\boldsymbol{\sigma} = \boldsymbol{\sigma}_0 + D\boldsymbol{\sigma}(\varepsilon,\varphi,\boldsymbol{P})(\Delta\varepsilon) + D\boldsymbol{\sigma}(\varepsilon,\varphi,\boldsymbol{P})(\Delta\varphi) + D\boldsymbol{\sigma}(\varepsilon,\varphi,\boldsymbol{P})(\Delta\boldsymbol{P}) =$$

$$\boldsymbol{\sigma}_0 + \left.\frac{\partial^2\tilde{\Psi}}{\partial\varepsilon\,\partial\varepsilon}\right|_{\varepsilon_0,\varphi_0,\boldsymbol{P}_0} : \Delta\varepsilon + \left.\frac{\partial^2\tilde{\Psi}}{\partial\varepsilon\,\partial\varphi}\right|_{\varepsilon_0,\varphi_0,\boldsymbol{P}_0} : \Delta\varphi +$$

$$\left.\frac{\partial^2\tilde{\Psi}}{\partial\varepsilon\,\partial\boldsymbol{P}_L}\right|_{\varepsilon_0,\varphi_0,\boldsymbol{P}_0} : \Delta\boldsymbol{P}_L + \left.\frac{\partial^2\tilde{\Psi}}{\partial\varepsilon\,\partial\boldsymbol{P}_{NL}}\right|_{\varepsilon_0,\varphi_0,\boldsymbol{P}_0} : \Delta\boldsymbol{P}_{NL}. \quad (4.72)$$

$$\mathcal{L}\boldsymbol{L}_\varphi = \boldsymbol{L}_{\varphi\,0} + D\boldsymbol{L}_\varphi(\varepsilon,\varphi,\boldsymbol{P})(\Delta\varepsilon) + D\boldsymbol{L}_\varphi(\varepsilon,\varphi,\boldsymbol{P})(\Delta\varphi) + D\boldsymbol{L}_\varphi(\varepsilon,\varphi,\boldsymbol{P})(\Delta\boldsymbol{P}) =$$

$$\boldsymbol{L}_{\varphi\,0} + \left.\frac{\partial^2\tilde{\Psi}}{\partial\varphi\,\partial\varepsilon}\right|_{\varepsilon_0,\varphi_0,\boldsymbol{P}_0} : \Delta\varepsilon + \left.\frac{\partial^2\tilde{\Psi}}{\partial\varphi\,\partial\varphi}\right|_{\varepsilon_0,\varphi_0,\boldsymbol{P}_0} : \Delta\varphi +$$

$$\left.\frac{\partial^2\tilde{\Psi}}{\partial\varphi\,\partial\boldsymbol{P}_{NL}}\right|_{\varepsilon_0,\varphi_0,\boldsymbol{P}_0} : \Delta\boldsymbol{P}_{NL}. \quad (4.73)$$

In the case that an evolution of inelastic variables takes place, from (4.67) we have $\phi_j = 0 \; \forall \; j \in \mathbb{S}_{act}$ and therefore the consistency condition

$$\Delta\phi_j = \frac{\partial\phi_j}{\partial\boldsymbol{P}_L} : \Delta\boldsymbol{P}_L + \frac{\partial\phi_j}{\partial\boldsymbol{P}_{NL}} : \Delta\boldsymbol{P}_{NL} + \frac{\partial\phi_j}{\partial\boldsymbol{Q}_L} : \Delta\boldsymbol{Q}_L + \frac{\partial\phi_j}{\partial\boldsymbol{Q}_{NL}} : \Delta\boldsymbol{Q}_{NL} +$$

$$\frac{\partial\phi_j}{\partial\varepsilon} : \Delta\varepsilon = 0 \quad \forall \; j \in \mathbb{S}_{act} \quad (4.74)$$

has to be fulfilled. In view of (4.53), incrementation of the lists $\boldsymbol{Q}_L$ and $\boldsymbol{Q}_{NL}$ becomes

$$\Delta\boldsymbol{Q}_L = -\frac{\partial^2\tilde{\Psi}}{\partial\boldsymbol{P}_L\,\partial\boldsymbol{P}_L} : \Delta\boldsymbol{P}_L - \frac{\partial^2\tilde{\Psi}}{\partial\boldsymbol{P}_L\,\partial\boldsymbol{P}_{NL}} : \Delta\boldsymbol{P}_{NL} - \frac{\partial^2\tilde{\Psi}}{\partial\boldsymbol{P}_L\,\partial\varepsilon} : \Delta\varepsilon, \quad (4.75)$$

$$\Delta\boldsymbol{Q}_{NL} = -\frac{\partial^2\tilde{\Psi}}{\partial\boldsymbol{P}_{NL}\,\partial\boldsymbol{P}_L} : \Delta\boldsymbol{P}_L - \frac{\partial^2\tilde{\Psi}}{\partial\boldsymbol{P}_{NL}\,\partial\boldsymbol{P}_{NL}} : \Delta\boldsymbol{P}_{NL} -$$

$$\frac{\partial^2\tilde{\Psi}}{\partial\boldsymbol{P}_{NL}\,\partial\varepsilon} : \Delta\varepsilon - \frac{\partial^2\tilde{\Psi}}{\partial\boldsymbol{P}_{NL}\,\partial\varphi} : \Delta\varphi, \quad (4.76)$$

which, taking into consideration the evolution equations for internal variable lists (4.66),

---

[3]For details on linearization and the *Gâteaux-derivative* see the section A.1.

allows to express the consistency condition in the form

$$
\begin{aligned}
\Delta\phi_j \;=\; &\sum_{k\in\mathbb{S}_{act}} \Delta\lambda_k \left(\frac{\partial\phi_j}{\partial\boldsymbol{P}_L} : \frac{\partial\phi_k}{\partial\boldsymbol{Q}_L} + \frac{\partial\phi_j}{\partial\boldsymbol{P}_{NL}} : \frac{\partial\phi_k}{\partial\boldsymbol{Q}_{NL}} - \right.\\
&\frac{\partial\phi_j}{\partial\boldsymbol{Q}_L} : \frac{\partial^2\tilde{\Psi}}{\partial\boldsymbol{P}_L\,\partial\boldsymbol{P}_L} : \frac{\partial\phi_k}{\partial\boldsymbol{Q}_L} - \frac{\partial\phi_j}{\partial\boldsymbol{Q}_L} : \frac{\partial^2\tilde{\Psi}}{\partial\boldsymbol{P}_L\,\partial\boldsymbol{P}_{NL}} : \frac{\partial\phi_k}{\partial\boldsymbol{Q}_{NL}} - \\
&\left.\frac{\partial\phi_j}{\partial\boldsymbol{Q}_{NL}} : \frac{\partial^2\tilde{\Psi}}{\partial\boldsymbol{P}_{NL}\,\partial\boldsymbol{P}_L} : \frac{\partial\phi_k}{\partial\boldsymbol{Q}_L} - \frac{\partial\phi_j}{\partial\boldsymbol{Q}_{NL}} : \frac{\partial^2\tilde{\Psi}}{\partial\boldsymbol{P}_{NL}\,\partial\boldsymbol{P}_{NL}} : \frac{\partial\phi_k}{\partial\boldsymbol{Q}_{NL}} \right) + \\
&\left(\frac{\partial\phi_j}{\partial\boldsymbol{\varepsilon}} - \frac{\partial\phi_j}{\partial\boldsymbol{Q}_L} : \frac{\partial^2\tilde{\Psi}}{\partial\boldsymbol{P}_L\,\partial\boldsymbol{\varepsilon}} - \frac{\partial\phi_j}{\partial\boldsymbol{Q}_{NL}} : \frac{\partial^2\tilde{\Psi}}{\partial\boldsymbol{P}_{NL}\,\partial\boldsymbol{\varepsilon}} \right) : \Delta\boldsymbol{\varepsilon} - \\
&\left(\frac{\partial\phi_j}{\partial\boldsymbol{Q}_{NL}} : \frac{\partial^2\tilde{\Psi}}{\partial\boldsymbol{P}_{NL}\,\partial\boldsymbol{\varphi}} \right) : \Delta\boldsymbol{\varphi} \;=\; 0 \quad \forall\, j \in \mathbb{S}_{act}. \quad (4.77)
\end{aligned}
$$

Collecting the coefficients multiplying incrementation of inelastic consistency parameters $\Delta\lambda_k$ into a matrix

$$
\begin{aligned}
\tilde{G}_{jk} \;=\; &\frac{\partial\phi_j}{\partial\boldsymbol{P}_L} : \frac{\partial\phi_k}{\partial\boldsymbol{Q}_L} + \frac{\partial\phi_j}{\partial\boldsymbol{P}_{NL}} : \frac{\partial\phi_k}{\partial\boldsymbol{Q}_{NL}} + \\
&\frac{\partial\phi_j}{\partial\boldsymbol{Q}_L} : \frac{\partial^2\tilde{\Psi}}{\partial\boldsymbol{P}_L\,\partial\boldsymbol{P}_L} : \frac{\partial\phi_k}{\partial\boldsymbol{Q}_L} - \frac{\partial\phi_j}{\partial\boldsymbol{Q}_L} : \frac{\partial^2\tilde{\Psi}}{\partial\boldsymbol{P}_L\,\partial\boldsymbol{P}_{NL}} : \frac{\partial\phi_k}{\partial\boldsymbol{Q}_{NL}} - \\
&\frac{\partial\phi_j}{\partial\boldsymbol{Q}_{NL}} : \frac{\partial^2\tilde{\Psi}}{\partial\boldsymbol{P}_{NL}\,\partial\boldsymbol{P}_L} : \frac{\partial\phi_k}{\partial\boldsymbol{Q}_L} - \frac{\partial\phi_j}{\partial\boldsymbol{Q}_{NL}} : \frac{\partial^2\tilde{\Psi}}{\partial\boldsymbol{P}_{NL}\,\partial\boldsymbol{P}_{NL}} : \frac{\partial\phi_k}{\partial\boldsymbol{Q}_{NL}} \quad (4.78)
\end{aligned}
$$

and inverting it

$$
\tilde{G}^{jk} \;=\; \left(\tilde{G}_{jk} \right)^{-1}, \tag{4.79}
$$

one can solve (4.77) for the increments of the inelastic consistency parameters

$$
\begin{aligned}
\Delta\lambda_j \;=\; \sum_{k\in\mathbb{S}_{act}} \tilde{G}^{jk} \cdot \Bigg[&\left(\frac{\partial\phi_k}{\partial\boldsymbol{Q}_L} : \frac{\partial^2\tilde{\Psi}}{\partial\boldsymbol{P}_L\,\partial\boldsymbol{\varepsilon}} + \frac{\partial\phi_k}{\partial\boldsymbol{Q}_{NL}} : \frac{\partial^2\tilde{\Psi}}{\partial\boldsymbol{P}_{NL}\,\partial\boldsymbol{\varepsilon}} - \frac{\partial\phi_k}{\partial\boldsymbol{\varepsilon}} \right) : \Delta\boldsymbol{\varepsilon} + \\
&\left(\frac{\partial\phi_k}{\partial\boldsymbol{Q}_{NL}} : \frac{\partial^2\tilde{\Psi}}{\partial\boldsymbol{P}_{NL}\,\partial\boldsymbol{\varphi}} \right) : \Delta\boldsymbol{\varphi} \Bigg]. \quad (4.80)
\end{aligned}
$$

In view of (4.80) and (4.69) the linearization of the stress tensor (4.72) becomes

$$
\begin{aligned}
\mathcal{L}\boldsymbol{\sigma} = {}& \boldsymbol{\sigma}_0 \,+\, \frac{\partial^2 \tilde{\Psi}}{\partial \boldsymbol{\varepsilon}\, \partial \boldsymbol{\varepsilon}} : \Delta\boldsymbol{\varepsilon} \,+\, \frac{\partial^2 \tilde{\Psi}}{\partial \boldsymbol{\varepsilon}\, \partial \boldsymbol{\varphi}} : \Delta\boldsymbol{\varphi} \\
&+ \sum_{j\in\mathbb{S}_{act}} \sum_{k\in\mathbb{S}_{act}} \tilde{G}^{jk} \left[\left(\frac{\partial^2 \tilde{\Psi}}{\partial \boldsymbol{\varepsilon}\, \partial \boldsymbol{P}_L} : \frac{\partial \phi_j}{\partial \boldsymbol{Q}_L} \right) \otimes \left(\frac{\partial \phi_k}{\partial \boldsymbol{Q}_L} : \frac{\partial^2 \tilde{\Psi}}{\partial \boldsymbol{P}_L\, \partial \boldsymbol{\varepsilon}} \right) \right. \\
&+ \left(\frac{\partial^2 \tilde{\Psi}}{\partial \boldsymbol{\varepsilon}\, \partial \boldsymbol{P}_{NL}} : \frac{\partial \phi_j}{\partial \boldsymbol{Q}_{NL}} \right) \otimes \left(\frac{\partial \phi_k}{\partial \boldsymbol{Q}_L} : \frac{\partial^2 \tilde{\Psi}}{\partial \boldsymbol{P}_L\, \partial \boldsymbol{\varepsilon}} \right) \\
&+ \left(\frac{\partial^2 \tilde{\Psi}}{\partial \boldsymbol{\varepsilon}\, \partial \boldsymbol{P}_L} : \frac{\partial \phi_j}{\partial \boldsymbol{Q}_L} \right) \otimes \left(\frac{\partial \phi_k}{\partial \boldsymbol{Q}_{NL}} : \frac{\partial^2 \tilde{\Psi}}{\partial \boldsymbol{P}_{NL}\, \partial \boldsymbol{\varepsilon}} \right) \\
&+ \left(\frac{\partial^2 \tilde{\Psi}}{\partial \boldsymbol{\varepsilon}\, \partial \boldsymbol{P}_{NL}} : \frac{\partial \phi_j}{\partial \boldsymbol{Q}_{NL}} \right) \otimes \left(\frac{\partial \phi_k}{\partial \boldsymbol{Q}_{NL}} : \frac{\partial^2 \tilde{\Psi}}{\partial \boldsymbol{P}_{NL}\, \partial \boldsymbol{\varepsilon}} \right) \\
&- \left. \left(\frac{\partial^2 \tilde{\Psi}}{\partial \boldsymbol{\varepsilon}\, \partial \boldsymbol{P}_L} : \frac{\partial \phi_j}{\partial \boldsymbol{Q}_L} + \frac{\partial^2 \tilde{\Psi}}{\partial \boldsymbol{\varepsilon}\, \partial \boldsymbol{P}_{NL}} : \frac{\partial \phi_j}{\partial \boldsymbol{Q}_{NL}} \right) \otimes \frac{\partial \phi_k}{\partial \boldsymbol{\varepsilon}} \right] : \Delta\boldsymbol{\varepsilon} \\
&+ \sum_{j\in\mathbb{S}_{act}} \sum_{k\in\mathbb{S}_{act}} \tilde{G}^{jk} \left[\left(\frac{\partial^2 \tilde{\Psi}}{\partial \boldsymbol{\varepsilon}\, \partial \boldsymbol{P}_L} : \frac{\partial \phi_j}{\partial \boldsymbol{Q}_L} \right) \otimes \left(\frac{\partial \phi_k}{\partial \boldsymbol{Q}_{NL}} : \frac{\partial^2 \tilde{\Psi}}{\partial \boldsymbol{P}_{NL}\, \partial \boldsymbol{\varphi}} \right) \right. \\
&+ \left. \left(\frac{\partial^2 \tilde{\Psi}}{\partial \boldsymbol{\varepsilon}\, \partial \boldsymbol{P}_{NL}} : \frac{\partial \phi_j}{\partial \boldsymbol{Q}_{NL}} \right) \otimes \left(\frac{\partial \phi_k}{\partial \boldsymbol{Q}_{NL}} : \frac{\partial^2 \tilde{\Psi}}{\partial \boldsymbol{P}_{NL}\, \partial \boldsymbol{\varphi}} \right) \right] : \Delta\boldsymbol{\varphi}, \quad (4.81)
\end{aligned}
$$

while the linearization of the response function $\boldsymbol{L}_{\boldsymbol{\varphi}}$ (4.73) is obtained as

$$
\begin{aligned}
\mathcal{L}\boldsymbol{L}_{\boldsymbol{\varphi}} = {}& \boldsymbol{L}_{\boldsymbol{\varphi}\,0} \,+\, \frac{\partial^2 \tilde{\Psi}}{\partial \boldsymbol{\varphi}\, \partial \boldsymbol{\varepsilon}} : \Delta\boldsymbol{\varepsilon} \,+\, \frac{\partial^2 \tilde{\Psi}}{\partial \boldsymbol{\varphi}\, \partial \boldsymbol{\varphi}} : \Delta\boldsymbol{\varphi} \\
&+ \sum_{j\in\mathbb{S}_{act}} \sum_{k\in\mathbb{S}_{act}} \tilde{G}^{jk} \left[\left(\frac{\partial^2 \tilde{\Psi}}{\partial \boldsymbol{\varphi}\, \partial \boldsymbol{P}_{NL}} : \frac{\partial \phi_j}{\partial \boldsymbol{Q}_{NL}} \right) \otimes \left(\frac{\partial \phi_k}{\partial \boldsymbol{Q}_L} : \frac{\partial^2 \tilde{\Psi}}{\partial \boldsymbol{P}_L\, \partial \boldsymbol{\varepsilon}} \right) \right. \\
&+ \left(\frac{\partial^2 \tilde{\Psi}}{\partial \boldsymbol{\varphi}\, \partial \boldsymbol{P}_{NL}} : \frac{\partial \phi_j}{\partial \boldsymbol{Q}_{NL}} \right) \otimes \left(\frac{\partial \phi_k}{\partial \boldsymbol{Q}_{NL}} : \frac{\partial^2 \tilde{\Psi}}{\partial \boldsymbol{P}_{NL}\, \partial \boldsymbol{\varepsilon}} \right) \\
&- \left. \left(\frac{\partial^2 \tilde{\Psi}}{\partial \boldsymbol{\varphi}\, \partial \boldsymbol{P}_{NL}} : \frac{\partial \phi_j}{\partial \boldsymbol{Q}_{NL}} \right) \otimes \frac{\partial \phi_k}{\partial \boldsymbol{\varepsilon}} \right] : \Delta\boldsymbol{\varepsilon} \\
&+ \sum_{j\in\mathbb{S}_{act}} \sum_{k\in\mathbb{S}_{act}} \tilde{G}^{jk} \left[\left(\frac{\partial^2 \tilde{\Psi}}{\partial \boldsymbol{\varphi}\, \partial \boldsymbol{P}_{NL}} : \frac{\partial \phi_j}{\partial \boldsymbol{Q}_{NL}} \right) \otimes \left(\frac{\partial \phi_k}{\partial \boldsymbol{Q}_{NL}} : \frac{\partial^2 \tilde{\Psi}}{\partial \boldsymbol{P}_{NL}\, \partial \boldsymbol{\varphi}} \right) \right] : \Delta\boldsymbol{\varphi}.
\end{aligned}
$$
$$(4.82)$$

Hence, one can relate increments of the stress tensor to increments of the strain tensor and the non-local variable field in a manner analogous to the classical (local) theory (3.40), except for the additional term which is a consequence of the gradient enhancement

$$
\mathcal{L}\boldsymbol{\sigma} = \boldsymbol{\sigma}_0 + \mathbb{C}^{IN}(\boldsymbol{\varepsilon}_0, \boldsymbol{\varphi}_0, \boldsymbol{P}_0) : \Delta\boldsymbol{\varepsilon} + \frac{\partial \boldsymbol{\sigma}}{\partial \boldsymbol{\varphi}}(\boldsymbol{\varepsilon}_0, \boldsymbol{\varphi}_0, \boldsymbol{P}_0) : \Delta\boldsymbol{\varphi}. \tag{4.83}
$$

The increments of the response function $\boldsymbol{L}_{\boldsymbol{\varphi}}$ are related to increments of the strain tensor and the non-local variable field as

$$
\mathcal{L}\boldsymbol{L}_{\boldsymbol{\varphi}} = \boldsymbol{L}_{\boldsymbol{\varphi}\,0} + \frac{\partial \boldsymbol{L}_{\boldsymbol{\varphi}}}{\partial \boldsymbol{\varepsilon}}(\boldsymbol{\varepsilon}_0, \boldsymbol{\varphi}_0, \boldsymbol{P}_0) : \Delta\boldsymbol{\varepsilon} + \frac{\partial \boldsymbol{L}_{\boldsymbol{\varphi}}}{\partial \boldsymbol{\varphi}}(\boldsymbol{\varepsilon}_0, \boldsymbol{\varphi}_0, \boldsymbol{P}_0) : \Delta\boldsymbol{\varphi}. \tag{4.84}
$$

The tangent moduli $\mathbb{C}^{IN}$ and $\frac{\partial \boldsymbol{L}_\varphi}{\partial \boldsymbol{\varepsilon}}$ can be extracted from the relations (4.81) and (4.82) as the quantities multiplying the increment of the strain tensor $\Delta \boldsymbol{\varepsilon}$, respectively. Analogous holds for the moduli $\frac{\partial \boldsymbol{\sigma}}{\partial \varphi}$ and $\frac{\partial \boldsymbol{L}_\varphi}{\partial \varphi}$. The results of the linearization procedure are summarized in the Table 4.3. It contains the description of quantities obtained from the constitutive update, which are used in the solution of the boundary value problems (4.27) and (4.28).

4.4.5. Portability of the strategy

The utilization of the investigated regularization strategy results in the constitutive update whose structure is very similar to the one of the local model. Hence, the implementation within numerical schemes is particularly convenient and does not increase computational effort significantly, due to a very few differences compared to the classical (local) models. The question that naturally arises in practical application is whether it is possible to employ the strategy on the material models whose numerical implementation is already done without performing tedious derivation and coding from the beginning. This is indeed possible for the models developed within the concept of generalized standard media or its extended version used in this thesis (which considers explicit dependence of the boundaries of the elastic range on the linearized strain tensor (3.27)). The changes to be made are highlighted in red in the Tables 4.1, 4.2 and 4.3 that contain summarized algorithm of the local constitutive update. First, the local micro structural driving force $\boldsymbol{Q}_{NL}$ has to be replaced by the enhanced one, relation (4.59). Next, the intermediate algorithmic modulus $(\mathbb{D}^{(it)})_{local}$ of the local model has to be replaced by the enhanced one as well

$$\mathbb{D}^{(it)} = (\mathbb{D}^{(it)})_{local} + \begin{bmatrix} \boldsymbol{0} & \boldsymbol{0} \\ \boldsymbol{0} & -\dfrac{\partial^2 \Psi_{intr}}{\partial \boldsymbol{P}_{NL} \partial \boldsymbol{P}_{NL}} \end{bmatrix} . \tag{4.85}$$

After the constitutive update has been made, one needs to introduce changes in the calculation of the stress-strain derivative (inelastic tangent). This is accomplished by modification of the corresponding metric coefficients of the local model

$$\tilde{G}_{jk} = (\tilde{G}_{jk})_{local} - \frac{\partial \phi_j}{\partial \boldsymbol{Q}_{NL}} : \frac{\partial^2 \Psi_{intr}}{\partial \boldsymbol{P}_{NL} \partial \boldsymbol{P}_{NL}} : \frac{\partial \phi_k}{\partial \boldsymbol{Q}_{NL}} . \tag{4.86}$$

Utilizing these metric coefficients in the calculation of the inelastic tangent $\mathbb{C}^{IN}$ within the local model results in the correct stress-strain tangent modulus of the enhanced model. Finally, there are additional tangent operators emerging from the linearization of the stress tensor (4.83) and the conjugate of the non-local variable list (4.84) that have to be evaluated. They are specified in the Table 4.3 as well, together with the list of conjugates of the non-local variable $\boldsymbol{L}_\varphi$.

Obviously, an implementation of the proposed gradient enhancement strategy requires relatively little modifications of the classical (local) material models developed within the concept of generalized standard media (Halphen and Nguyen (1975); Hackl (1997); Lorentz and Benallal (2005)), thus making its application attractive.

Calculation of the updated quantities and the tangent moduli

(9) Calculate metric coefficients:

$$\tilde{G}_{jk} = -\left\{ \begin{array}{cc} \frac{\partial\phi_j}{\partial\boldsymbol{Q}_L} & \frac{\partial\phi_j}{\partial\boldsymbol{Q}_{NL}} \end{array} \right\} : \left[\begin{array}{cc} \frac{\partial^2\Psi}{\partial\boldsymbol{P}_L\partial\boldsymbol{P}_L} & \frac{\partial^2\Psi}{\partial\boldsymbol{P}_L\partial\boldsymbol{P}_{NL}} \\ \frac{\partial^2\Psi}{\partial\boldsymbol{P}_{NL}\partial\boldsymbol{P}_L} & \frac{\partial^2\Psi}{\partial\boldsymbol{P}_{NL}\partial\boldsymbol{P}_{LN}} + \frac{\partial^2\Psi_{intr}}{\partial\boldsymbol{P}_{NL}\partial\boldsymbol{P}_{NL}} \end{array} \right] : \left\{ \begin{array}{c} \frac{\partial\phi_k}{\partial\boldsymbol{Q}_L} \\ \frac{\partial\phi_k}{\partial\boldsymbol{Q}_{NL}} \end{array} \right\}$$

$$+ \left\{ \begin{array}{cc} \frac{\partial\phi_j}{\partial\boldsymbol{P}_L} & \frac{\partial\phi_j}{\partial\boldsymbol{P}_{NL}} \end{array} \right\} : \left\{ \begin{array}{c} \frac{\partial\phi_k}{\partial\boldsymbol{Q}_L} \\ \frac{\partial\phi_k}{\partial\boldsymbol{Q}} \end{array} \right\},$$

$$\tilde{G}^{jk} = \left(\tilde{G}_{jk}\right)^{-1}.$$

(10) Calculate intermediate moduli:

$$\mathbb{A}_{jk}^{(\boldsymbol{\varepsilon},\boldsymbol{\varepsilon})} = \left(\left[\begin{array}{cc} \frac{\partial^2\Psi}{\partial\boldsymbol{\varepsilon}\partial\boldsymbol{P}_L} & \frac{\partial^2\Psi}{\partial\boldsymbol{\varepsilon}\partial\boldsymbol{P}_{NL}} \end{array} \right] : \left\{ \begin{array}{c} \frac{\partial\phi_j}{\partial\boldsymbol{Q}_L} \\ \frac{\partial\phi_j}{\partial\boldsymbol{Q}_{NL}} \end{array} \right\} \right) \otimes \left(\left\{ \begin{array}{cc} \frac{\partial\phi_k}{\partial\boldsymbol{Q}_L} & \frac{\partial\phi_k}{\partial\boldsymbol{Q}_{NL}} \end{array} \right\} : \left[\begin{array}{c} \frac{\partial^2\Psi}{\partial\boldsymbol{P}_L\partial\boldsymbol{\varepsilon}} \\ \frac{\partial^2\Psi}{\partial\boldsymbol{P}_{NL}\partial\boldsymbol{\varepsilon}} \end{array} \right] \right)$$

$$- \left(\left[\begin{array}{cc} \frac{\partial^2\Psi}{\partial\boldsymbol{\varepsilon}\partial\boldsymbol{P}_L} & \frac{\partial^2\Psi}{\partial\boldsymbol{\varepsilon}\partial\boldsymbol{P}_{NL}} \end{array} \right] : \left\{ \begin{array}{c} \frac{\partial\phi_j}{\partial\boldsymbol{Q}_L} \\ \frac{\partial\phi_j}{\partial\boldsymbol{Q}_{NL}} \end{array} \right\} \right) \otimes \frac{\partial\phi_k}{\partial\boldsymbol{\varepsilon}},$$

$$\textcolor{red}{\mathbb{A}_{jk}^{(\boldsymbol{\varepsilon},\boldsymbol{\varphi})} = \left(\left[\begin{array}{cc} \frac{\partial^2\Psi}{\partial\boldsymbol{\varepsilon}\partial\boldsymbol{P}_L} & \frac{\partial^2\Psi}{\partial\boldsymbol{\varepsilon}\partial\boldsymbol{P}_{NL}} \end{array} \right] : \left\{ \begin{array}{c} \frac{\partial\phi_j}{\partial\boldsymbol{Q}_L} \\ \frac{\partial\phi_j}{\partial\boldsymbol{Q}_{NL}} \end{array} \right\} \right) \otimes \left(\frac{\partial\phi_k}{\partial\boldsymbol{Q}_{NL}} : \frac{\partial^2\Psi_{intr}}{\partial\boldsymbol{P}_{NL}\partial\boldsymbol{\varphi}} \right),}$$

$$\textcolor{red}{\mathbb{A}_{jk}^{(\boldsymbol{\varphi},\boldsymbol{\varepsilon})} = \left(\frac{\partial^2\Psi_{intr}}{\partial\boldsymbol{\varphi}\partial\boldsymbol{P}_{NL}} : \frac{\partial\phi_j}{\partial\boldsymbol{Q}_{NL}} \right) \otimes \left(\left\{ \begin{array}{cc} \frac{\partial\phi_k}{\partial\boldsymbol{Q}_L} & \frac{\partial\phi_k}{\partial\boldsymbol{Q}_{NL}} \end{array} \right\} : \left[\begin{array}{c} \frac{\partial^2\Psi}{\partial\boldsymbol{P}_L\partial\boldsymbol{\varepsilon}} \\ \frac{\partial^2\Psi}{\partial\boldsymbol{P}_{NL}\partial\boldsymbol{\varepsilon}} \end{array} \right] \right)}$$

$$\textcolor{red}{- \left(\frac{\partial^2\Psi_{intr}}{\partial\boldsymbol{\varphi}\partial\boldsymbol{P}_{NL}} : \frac{\partial\phi_j}{\partial\boldsymbol{Q}_{NL}} \right) \otimes \frac{\partial\phi_k}{\partial\boldsymbol{\varepsilon}},}$$

$$\textcolor{red}{\mathbb{A}_{jk}^{(\boldsymbol{\varphi},\boldsymbol{\varphi})} = \left(\frac{\partial^2\Psi_{intr}}{\partial\boldsymbol{\varphi}\partial\boldsymbol{P}_{NL}} : \frac{\partial\phi_j}{\partial\boldsymbol{Q}_{NL}} \right) \otimes \left(\frac{\partial\phi_k}{\partial\boldsymbol{Q}_{NL}} : \frac{\partial^2\Psi_{intr}}{\partial\boldsymbol{P}_{NL}\partial\boldsymbol{\varphi}} \right).}$$

(11) Calculate tangent moduli:

IF $inel = 0$ THEN:

$$\mathbb{C}^{IN} = \frac{\partial^2\Psi}{\partial\boldsymbol{\varepsilon}\partial\boldsymbol{\varepsilon}}, \qquad \textcolor{red}{\frac{\partial\boldsymbol{\sigma}}{\partial\boldsymbol{\varphi}} = \boldsymbol{0}}, \qquad \textcolor{red}{\frac{\partial\boldsymbol{L}_{\boldsymbol{\varphi}}}{\partial\boldsymbol{\varepsilon}} = \boldsymbol{0}}, \qquad \textcolor{red}{\frac{\partial\boldsymbol{L}_{\boldsymbol{\varphi}}}{\partial\boldsymbol{\varphi}} = \frac{\partial^2\Psi_{intr}}{\partial\boldsymbol{\varphi}\partial\boldsymbol{\varphi}}}.$$

ELSE

$$\mathbb{C}^{IN} = \frac{\partial^2\Psi}{\partial\boldsymbol{\varepsilon}\partial\boldsymbol{\varepsilon}} + \sum_{j\in\mathbb{S}_{act}}\sum_{k\in\mathbb{S}_{act}} \tilde{G}^{jk}\,\mathbb{A}_{jk}^{(\boldsymbol{\varepsilon},\boldsymbol{\varepsilon})}, \qquad \textcolor{red}{\frac{\partial\boldsymbol{\sigma}}{\partial\boldsymbol{\varphi}} = \sum_{j\in\mathbb{S}_{act}}\sum_{k\in\mathbb{S}_{act}} \tilde{G}^{jk}\,\mathbb{A}_{jk}^{(\boldsymbol{\varepsilon},\boldsymbol{\varphi})}},$$

$$\textcolor{red}{\frac{\partial\boldsymbol{L}_{\boldsymbol{\varphi}}}{\partial\boldsymbol{\varepsilon}} = \sum_{j\in\mathbb{S}_{act}}\sum_{k\in\mathbb{S}_{act}} \tilde{G}^{jk}\,\mathbb{A}_{jk}^{(\boldsymbol{\varphi},\boldsymbol{\varepsilon})}, \qquad \frac{\partial\boldsymbol{L}_{\boldsymbol{\varphi}}}{\partial\boldsymbol{\varphi}} = \frac{\partial^2\Psi_{intr}}{\partial\boldsymbol{\varphi}\partial\boldsymbol{\varphi}} + \sum_{j\in\mathbb{S}_{act}}\sum_{k\in\mathbb{S}_{act}} \tilde{G}^{jk}\,\mathbb{A}_{jk}^{(\boldsymbol{\varphi},\boldsymbol{\varphi})}}.$$

ENDIF

(12) Calculate dependent variables and exit:

Calculate: $\boldsymbol{\sigma}_{n+1} = \dfrac{\partial\Psi}{\partial\boldsymbol{\varepsilon}}\left(\boldsymbol{\varepsilon}_{n+1}, \boldsymbol{P}_{L,n+1}, \boldsymbol{P}_{NL,n+1}\right),$

$$\textcolor{red}{\boldsymbol{L}_{\boldsymbol{\varphi},n+1} = \frac{\partial\Psi_{intr}}{\partial\boldsymbol{\varphi}}\left(\boldsymbol{P}_{L,n+1}, \boldsymbol{P}_{NL,n+1}, \boldsymbol{\varphi}_{n+1}\right).}$$

EXIT

Table 4.3.: Constitutive update algorithm III

5. Application of the gradient enhancement strategy

In this chapter the gradient regularization strategy described in the previous chapter will be applied to several rate-independent inelastic material models. The section 5.1 deals with the gradient enhancement of damage models, while the application on the plastic model is given in the section 5.2. Finally, section 5.3 utilizes the gradient-enhancement strategy in conjunction with the coupled damage-plastic model.

5.1. Gradient enhancement of damage material models

In this section is the application of the investigated gradient regularization strategy on the damage material models described in the section 3.2.2 presented. We first consider the regularization of the *damage model I*, with the quantities arising in this process gathered in the Table 5.1. In order to perform the gradient enhancement within the present framework, one has to specify the elements of the internal variable lists $\boldsymbol{P}$, $\boldsymbol{P}_{NL}$ and $\boldsymbol{P}_L$, see equation (5.1). This task is trivial, since the only internal variable in the model is the damage parameter d. Hence, it is automatically the variable which is used in the definition of the interaction potential. Utilizing the simplest choice for the potential $\boldsymbol{H}_{\varphi}$ by taking it to be equal to the damage parameter d, relation (5.3), the non-local variable list $\boldsymbol{\varphi}$ degenerates to a single variable φ_d, see (5.2). The micromechanical driving forces are specified in (5.6) and (5.7), while the inelastic tangent operators originating from the linearisation of the variation of the potential functional (4.42) are given in (5.8)-(5.11).

Let us now focus on the thermodynamical conjugate of the damage variable (5.7). As it is already discussed in the section 4.4.2, it contains two types of contribution: the purely local one $\hat{\eta}_d$ and the one that introduces non-local interaction into the definition of the micromechanical driving forces $\tilde{\eta}_d$. Recalling the expression of the internal dissipation of the gradient-enhanced model (4.56), it follows

$$\mathcal{D}_{int} \;=\; \eta_d \, \dot{d} \;=\; \hat{\eta}_d \, \dot{d} \;+\; \tilde{\eta}_d \, \dot{d}. \tag{5.12}$$

Analyzing (5.12) in view of (5.7), one can state that the first part ($\hat{\eta}_d \, \dot{d}$) represents the dissipation of energy resulting from the local deformation at the considered point. The second part ($\tilde{\eta}_d \, \dot{d}$) is a result of the interaction between the neighboring points and therefore describes the transfer of energy within the body due to inelastic processes. Focusing on the second term and utilizing the relation (4.63) it is obtained

$$\tilde{\eta}_d \, \dot{d} \;=\; \beta_d \, (\varphi_d - d) \, \dot{d} \;=\; c_d \, \nabla^2 \varphi_d \, \dot{d}. \tag{5.13}$$

Owing to the fact that the non-local variable φ_d is a solution of the differential equation

$$\beta_d \, (\varphi_d - d) - c_d \, \nabla^2 \varphi_d \;=\; 0, \tag{5.14}$$

Damage model I

(1) Internal variable lists:

$$\boldsymbol{P} = \{d\}, \quad \boldsymbol{P}_{NL} = \{d\}, \quad \boldsymbol{P}_L = \{\varnothing\} \tag{5.1}$$

(2) Non-local variable list φ and the potential $\boldsymbol{H}_{\boldsymbol{\varphi}}(\boldsymbol{P}_{NL})$:

$$\boldsymbol{\varphi} = \{\varphi_d\}, \quad \boldsymbol{H}_{\boldsymbol{\varphi}}(\boldsymbol{P}_{NL}) = \{H_{\boldsymbol{\varphi}}(d)\}, \tag{5.2}$$

$$H_{\boldsymbol{\varphi}}(d) = d \tag{5.3}$$

(3) Interaction potential Ψ_{intr} and the operators $\boldsymbol{\beta}$ and c:

$$\Psi_{intr} = \frac{1}{2}\beta_d \, (\varphi_d - d)^2 \; + \; \frac{1}{2} \, c_d \, \nabla\varphi_d \cdot \nabla\varphi_d, \tag{5.4}$$

$$\boldsymbol{L}_{\boldsymbol{\varphi}} = \beta_d \, (\varphi_d - d), \quad \mathbf{c} \, (\boldsymbol{\nabla\varphi}) = c_d \, \nabla\varphi_d \tag{5.5}$$

(4) Lists of the micromechanical driving forces:

$$\boldsymbol{Q}_L = \{\varnothing\}, \quad \boldsymbol{Q}_{NL} = \{\eta_d\}, \tag{5.6}$$

$$\eta_d \; = \; \underbrace{\frac{1}{2} \, e^{-d} \, (\boldsymbol{\varepsilon} : \mathbb{C} : \boldsymbol{\varepsilon})}_{\hat{\eta}_d} - \underbrace{\beta_d \, (\varphi_d - d)}_{\tilde{\eta}_d} \tag{5.7}$$

(5) Inelastic tangent moduli:

$$\mathbb{C}^{IN} = e^{-d} \left(\mathbb{C} \; - \; \frac{1}{\frac{1}{2} \, (\boldsymbol{\varepsilon} : \mathbb{C} : \boldsymbol{\varepsilon}) + \frac{\beta_d}{e^{-d}}} \; (\mathbb{C} : \boldsymbol{\varepsilon}) \otimes (\mathbb{C} : \boldsymbol{\varepsilon}) \right), \tag{5.8}$$

$$\frac{\partial\boldsymbol{\sigma}}{\partial\boldsymbol{\varphi}} = \frac{\beta_d}{\frac{1}{2} \, (\boldsymbol{\varepsilon} : \mathbb{C} : \boldsymbol{\varepsilon}) + \frac{\beta_d}{e^{-d}}} \; (\mathbb{C} : \boldsymbol{\varepsilon}), \tag{5.9}$$

$$\frac{\partial\boldsymbol{L}_{\boldsymbol{\varphi}}}{\partial\boldsymbol{\varepsilon}} = \frac{\beta_d}{\frac{1}{2} \, (\boldsymbol{\varepsilon} : \mathbb{C} : \boldsymbol{\varepsilon}) + \frac{\beta_d}{e^{-d}}} \; (\mathbb{C} : \boldsymbol{\varepsilon}), \tag{5.10}$$

$$\frac{\partial\boldsymbol{L}_{\boldsymbol{\varphi}}}{\partial\boldsymbol{\varphi}} = \beta_d \left(1 - \frac{\beta_d}{\frac{1}{2} \, e^{-d} \, (\boldsymbol{\varepsilon} : \mathbb{C} : \boldsymbol{\varepsilon}) + \beta_d} \right) \tag{5.11}$$

Table 5.1.: Gradient enhancement of the *damage model I*

relation (4.63), it follows that the φ_d has to have lower values than the damage parameter d within the zone of the concentrated damaging and consequently a negative Laplacian $\nabla^2\varphi_d < 0$, cf. Liebe (2003), Dorgan (2006). Outside of the process zone is the situation opposite: the non-local variable has to have higher values than d resulting in positive Laplacian $\nabla^2\varphi_d > 0$. Hence, the interaction part of the micromechanical driving force $\tilde{\eta}_d$ follows the same pattern: it is negative within the localization zone and positive elsewhere, Figure 5.1
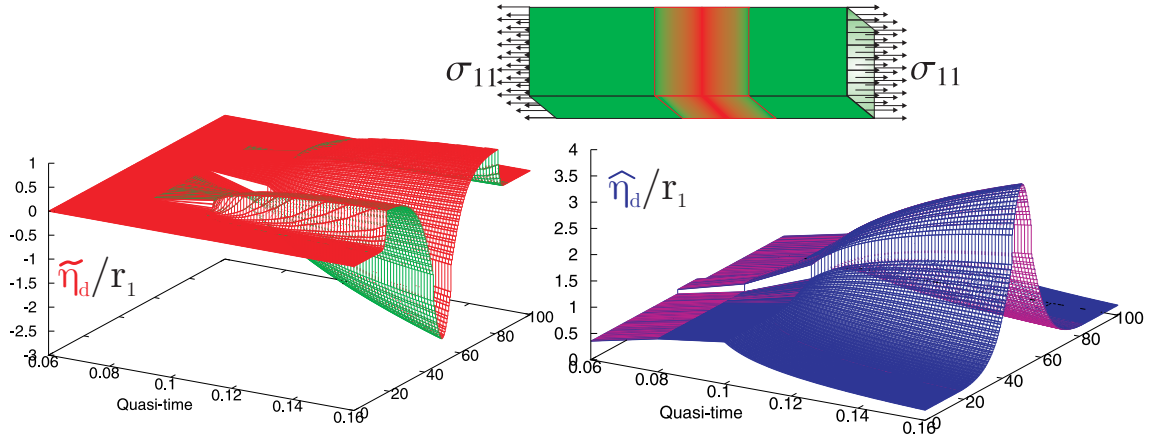
Figure 5.1.: Evolution of a distribution of local ($\hat{\eta}_d$) and interaction ($\tilde{\eta}_d$) part of the micromechanical driving force normalized with the damage threshold r_1

Having this in mind, one can conclude from (5.12) that the second part ($\tilde{\eta}_d\,\dot{d}$) of the internal dissipation reduces the dissipation within the zone of excessive deformation thus slowing down the evolution of the internal variable d. Outside of this zone, on the contrary, it increases the dissipation thus forcing the spreading of the region in which the damage variable evolves. This implies additionally, in view of (3.48) that the higher values of the purely local part of the micromechanical driving force will be allowed then in the unregularized model. In order to illustrate this point, let us repeat the damage threshold condition of the *damage model I*, accounting for (5.7)

$$\phi_d \ := \ \eta_d - r_1 \ = \ \hat{\eta}_d + \tilde{\eta}_d - r_1 \ \leq \ 0. \tag{5.15}$$

Collecting last two terms into a quantity we are going to name the *non-local damage threshold*

$$r_{1\,NL} \ := \ r_1 - \tilde{\eta}_d \ = \ r_1 - \beta_d\,(\varphi_d - d), \tag{5.16}$$

the relation (5.15) attains the form

$$\phi_d \ := \ \hat{\eta}_d - r_{1\,NL} \ \leq \ 0. \tag{5.17}$$

Adhering to the discussion above, it follows from (5.16) that the damage threshold will be effectively increased within the localization zone ($r_{1\,NL} > r_1$) and decreased outside ($r_{1\,NL} < r_1$), Figure 5.2.

In the gradient enhancement of the *damage model II*, Table 5.2, a slightly different approach is used. The difference is in the definition of the potential $\boldsymbol{H}_\varphi$, which is taken here to be equal to the cumulative change in the damage potential $g(d)$, equation (5.20). Due to

---

Damage model II

(1) Internal variable lists:

$$\boldsymbol{P} = \{d\}, \quad \boldsymbol{P}_{NL} = \{d\}, \quad \boldsymbol{P}_L = \{\varnothing\} \tag{5.18}$$

(2) Non-local variable list $\boldsymbol{\varphi}$ and the potential $\boldsymbol{H_\varphi}(\boldsymbol{P}_{NL})$:

$$\boldsymbol{\varphi} = \{\varphi_d\}, \quad \boldsymbol{H_\varphi}(\boldsymbol{P}_{NL}) = \{H_\varphi(d)\}, \tag{5.19}$$

$$H_\varphi(d) = g(0) - g(d) \tag{5.20}$$

(3) Interaction potential Ψ_{intr} and the operators $\boldsymbol{\beta}$ and c:

$$\Psi_{intr} = \frac{1}{2}\beta_d \left(\varphi_d - g(0) + g(d)\right)^2 + \frac{1}{2} c_d \nabla\varphi_d \cdot \nabla\varphi_d, \tag{5.21}$$

$$\boldsymbol{L_\varphi} = \beta_d \left(\varphi_d - g(0) + g(d)\right), \quad \mathbf{c}\left(\boldsymbol{\nabla\varphi}\right) = c_d \nabla\varphi_d \tag{5.22}$$

(4) Lists of the micromechanical driving forces:

$$\boldsymbol{Q}_L = \{\varnothing\}, \quad \boldsymbol{Q}_{NL} = \{\eta_d\}, \tag{5.23}$$

$$\eta_d = \underbrace{(1-d)^2 \left(\boldsymbol{\varepsilon} : \mathbb{C} : \boldsymbol{\varepsilon}\right) - g'(d)}_{\hat{\eta}_d} + \underbrace{\beta_d\, g'(d) \left(\varphi_d - g(0) + g(d)\right)}_{\tilde{\eta}_d} \tag{5.24}$$

(5) Inelastic tangent moduli:

$$G_{dd} = -\boldsymbol{\varepsilon}^+ : \mathbb{C} : \boldsymbol{\varepsilon}^+ -$$
$$g''(d) \left[1 + \beta_d \left(\varphi_d - g(0) + g(d)\right)\right] - \beta_d \left(g'(d)\right)^2 \tag{5.25}$$

$$\mathbb{C}^{IN} = (1-d)^2\, \mathbb{C} +$$
$$\frac{4(1-d)^2}{G_{dd}} \left[(\mathbb{C} : \boldsymbol{\varepsilon}) \otimes \left(\sum_{i=1}^{3} H(\varepsilon_i) \left(\boldsymbol{N}_i : \mathbb{C} : \boldsymbol{\varepsilon}^+\right) \boldsymbol{N}_i\right)\right], \tag{5.26}$$

$$\frac{\partial\boldsymbol{\sigma}}{\partial\boldsymbol{\varphi}} = -\frac{2(1-d)\,\beta_d\, g'(d)}{G_{dd}}\, (\mathbb{C} : \boldsymbol{\varepsilon}), \tag{5.27}$$

$$\frac{\partial\boldsymbol{L_\varphi}}{\partial\boldsymbol{\varepsilon}} = -\frac{2(1-d)\,\beta_d\, g'(d)}{G_{dd}}\, (\mathbb{C} : \boldsymbol{\varepsilon}), \tag{5.28}$$

$$\frac{\partial\boldsymbol{L_\varphi}}{\partial\boldsymbol{\varphi}} = \beta_d \left(1 + \frac{(\beta_d\, g'(d))^2}{G_{dd}}\right) \tag{5.29}$$

Table 5.2.: Gradient enhancement of the *damage model II*
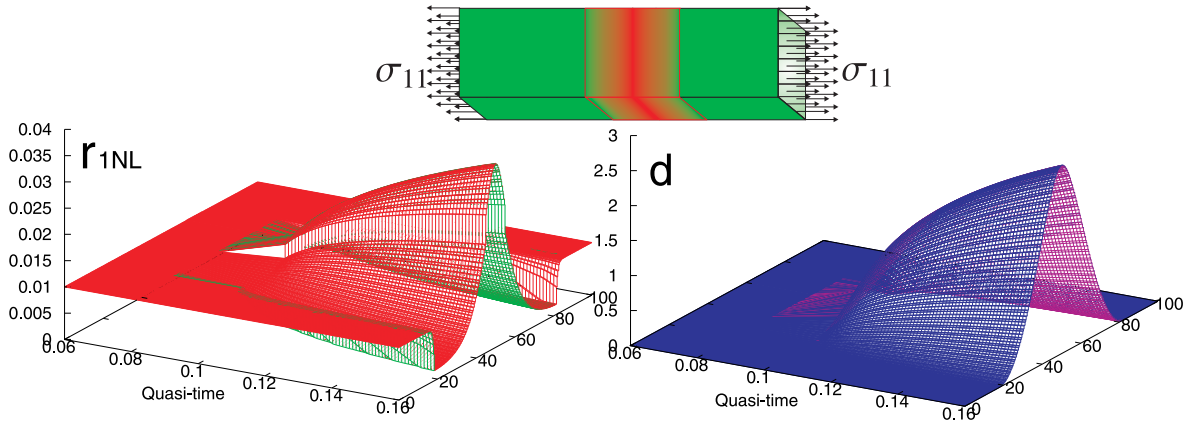
Figure 5.2.: Evolution of a distribution of the non-local damage threshold $r_{1\,NL}$ (left) and the damage parameter d (right) in uniaxial tension problem.

the fact that the corresponding damage potential defines the damage threshold and controls the softening response, relation (3.51), it fits perfectly into the non-local damage threshold interpretation discussed above. Denoting the damage-parameter-dependent quantity which determines the limits of the elastic range

$$R_1(d) = g'(d), \tag{5.30}$$

one can introduce its counterpart arising from the non-local interaction

$$R_{1\,NL}(d) = g'(d) \; [1 + \beta_d \, (\varphi_d - g(0) + g(d))] \,. \tag{5.31}$$

In view of (4.37) the non-local variable φ_d has to satisfy the condition

$$\beta_d \, (\varphi_d - H_{\boldsymbol{\varphi}}(d)) - c_d \, \nabla^2 \varphi_d \; = \; 0. \tag{5.32}$$

Taking into consideration positivity of the parameters β_d and c_d, and the fact that $H_{\boldsymbol{\varphi}}(d)$ is a monotonically decreasing function of the damage variable, Figure 5.3, it follows that term in the brackets $(\varphi_d - H_{\boldsymbol{\varphi}}(d))$ has to be positive in the localization zone. Consequently, the term $\nabla^2 \varphi_d > 0$ is positive in this zone as well, in contrast to the *damage model I*. That is due to the monotonically increasing potential function employed in the regularization of the *damage model I*. The potential function chosen in conjunction with the *damage model II* therefore yields higher values of the non-local variable than the corresponding potential within the localization zone, while is convers outside of this zone. Hence, the term in square brackets in the relation (5.31) is going to be greater than one in the process zone, leading to the increase of the elastic limit value due to non-local interaction and accordingly to damping of the damage evolution. Interestingly, the regularization procedure produces the same effect as the increase of the softening model parameter a_1 in the localization zone, Figure 5.3. However, outside of this zone is $R_{1\,NL}(d) < R_1(d)$, which is an equivalent of decreasing the value of a_1, thus leading to the acceleration of damage evolution.

5.2. Gradient enhancement of a plastic material model

This section deals with the application of the investigated gradient regularization strategy on the plastic models described in the section 3.2.3. The details on the application are
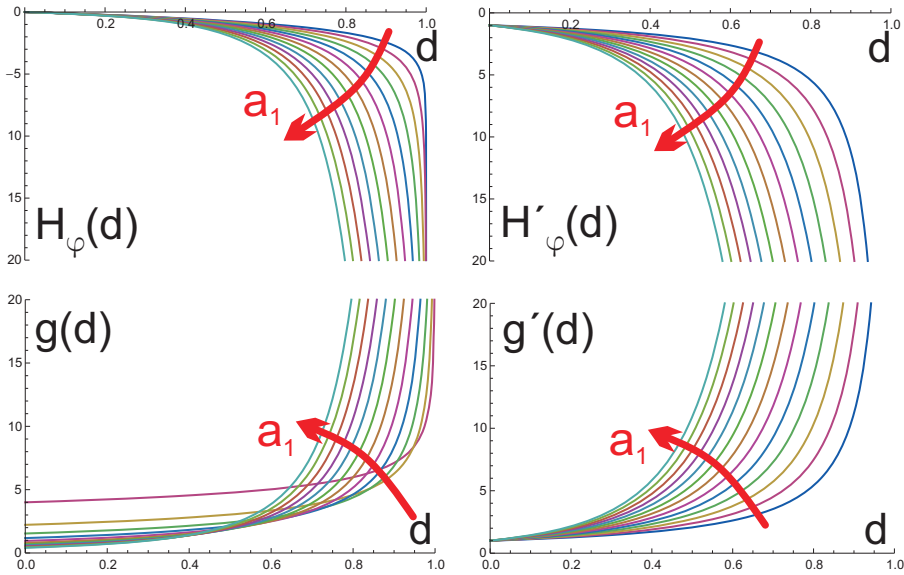
Figure 5.3.: Potential functions $g(d)$ and $H_\varphi(d)$ and their derivatives. The red arrow shows the direction in which the parameter a_1 increases.

summarized in the Tables 5.3 and 5.4. The internal variable lists $\boldsymbol{P}$, $\boldsymbol{P}_{NL}$ and $\boldsymbol{P}_L$ are specified in the equations (5.33) and (5.45), and they are equal in both cases. The potential $\boldsymbol{H}_\varphi$ is chosen to be a function of the hardening (softening) variable α_P. Two different forms of the corresponding potential function are investigated. In the first one, the simplest choice is made by taking it to be equal to the hardening variable itself, relation (5.35). In the second case the total change in the plastic hardening (softening) potential $W(\alpha_P)$ is utilized in the regularization procedure, expression (5.47). Both approaches result in a single scalar non-local variable φ_P, equations (5.34) and (5.46), respectively. The micromechanical driving forces are specified in (5.38) and (5.39) for the first case , and in (5.50) and (5.51) for the second case. The plastic stress tensor retains its local form (3.69) and it is therefore not repeated here. Finally, the inelastic tangent operators related to both approaches are presented in (5.41)-(5.44) and (5.53)-(5.56) respectively.

In view of (5.39) the internal dissipation of the gradient-enhanced model (4.56) becomes

$$\mathcal{D}_{int} \;=\; \boldsymbol{\sigma}_P : \dot{\boldsymbol{\varepsilon}}_P + \eta_P\,\dot{\alpha}_P \;=\; \boldsymbol{\sigma}_P : \dot{\boldsymbol{\varepsilon}}_P \;+\; \hat{\eta}_P\,\dot{\alpha}_P \;+\; \tilde{\eta}_P\,\dot{\alpha}_P. \tag{5.57}$$

Therefore one may, as in the case of damage material models, identify the part coming from non-local interaction as

$$\tilde{\mathcal{D}}_{int} \;=\; H'_{\boldsymbol{\varphi}}(\alpha_P)\,\beta_P\,(\varphi_P - H_{\boldsymbol{\varphi}}(\alpha_P))\,\dot{\alpha}_P. \tag{5.58}$$

In order to reduce the overall dissipation at the current point in the localization zone, the non-local interaction part has to be negative. Outside of the zone, however, the situation is converse: $\tilde{\mathcal{D}}_{int}$ has to be positive in order to accelerate the inelastic evolution process. Owing to negativity of the rate of the plastic hardening variable, it follows that $H'_\varphi(\alpha_P)$ has to have the same sign as the bracketed term in (5.58) within the localization zone and vice versa. Since it is assumed that in the initial state the non-local variable has zero value, one has to choose either the potential function with negative values and positive first derivative or the positive function with negative first derivative. All three functions used in the enhancement procedure, e.g. (5.35) in the first approach and (5.47) in the second approach[1], fulfill this

---

[1]Since the procedure is applied onto two models with different softening functions (3.60) and (3.63), one has actually two different potential functions $H_\varphi(\alpha_P)$.

Plastic models

---

(1) Internal variable lists:

$$\boldsymbol{P} = \{\boldsymbol{\varepsilon}_P, \alpha_P\}, \quad \boldsymbol{P}_{NL} = \{\alpha_P\}, \quad \boldsymbol{P}_L = \{\boldsymbol{\varepsilon}_P\} \tag{5.33}$$

(2) Non-local variable list $\boldsymbol{\varphi}$ and the potential $\boldsymbol{H}_{\boldsymbol{\varphi}}(\boldsymbol{P}_{NL})$:

$$\boldsymbol{\varphi} = \{\varphi_P\}, \quad \boldsymbol{H}_{\boldsymbol{\varphi}}(\boldsymbol{P}_{NL}) = \{H_{\boldsymbol{\varphi}}(\alpha_P)\}, \tag{5.34}$$

$$H_{\boldsymbol{\varphi}}(\alpha_P) = \alpha_P \tag{5.35}$$

(3) Interaction potential Ψ_{intr} and the operators $\boldsymbol{\beta}$ and c:

$$\Psi_{intr} = \frac{1}{2}\beta_P \left(\varphi_P - \alpha_P\right)^2 + \frac{1}{2} c_P \nabla\varphi_P \cdot \nabla\varphi_P, \tag{5.36}$$

$$\boldsymbol{L}_{\boldsymbol{\varphi}} = \beta_P \left(\varphi_P - \alpha_P\right), \quad \mathbf{c}\left(\boldsymbol{\nabla}\boldsymbol{\varphi}\right) = c_P \nabla\varphi_P \tag{5.37}$$

(4) Lists of the micromechanical driving forces:

$$\boldsymbol{Q}_L = \{\boldsymbol{\sigma}_P\}, \quad \boldsymbol{Q}_{NL} = \{\eta_P\}, \tag{5.38}$$

$$\eta_P = \underbrace{-W'(\alpha_P)}_{\hat{\eta}_P} + \underbrace{\beta_P \left(\varphi_P - \alpha_P\right)}_{\tilde{\eta}_P} \tag{5.39}$$

(5) Inelastic tangent moduli:

$$G_{PP} = -\frac{\boldsymbol{\sigma}_P : \boldsymbol{\sigma}_P}{\boldsymbol{\sigma}_P : \mathrm{dev}\,\mathbb{C} : \boldsymbol{\sigma}_P + (W''(\alpha_P) + \beta_P)\ \boldsymbol{\sigma}_P : \boldsymbol{\sigma}_P} \tag{5.40}$$

$$\mathbb{C}^{IN} = \mathbb{C} + \frac{1}{G_{PP}} \left[(\mathrm{dev}\,\mathbb{C} : \boldsymbol{\sigma}_P) \otimes (\mathrm{dev}\,\mathbb{C} : \boldsymbol{\sigma}_P)\right] \tag{5.41}$$

$$\frac{\partial\boldsymbol{\sigma}}{\partial\boldsymbol{\varphi}} = -\frac{\beta_P}{G_{PP}} \frac{1}{\boldsymbol{\sigma}_P : \boldsymbol{\sigma}_P} \left(\mathrm{dev}\,\mathbb{C} : \boldsymbol{\sigma}_P\right), \tag{5.42}$$

$$\frac{\partial\boldsymbol{L}_{\boldsymbol{\varphi}}}{\partial\boldsymbol{\varepsilon}} = -\frac{\beta_P}{G_{PP}} \frac{1}{\boldsymbol{\sigma}_P : \boldsymbol{\sigma}_P} \left(\mathrm{dev}\,\mathbb{C} : \boldsymbol{\sigma}_P\right), \tag{5.43}$$

$$\frac{\partial\boldsymbol{L}_{\boldsymbol{\varphi}}}{\partial\boldsymbol{\varphi}} = \beta_P \left(1 + \frac{\beta_P}{G_{PP}}\right) \tag{5.44}$$

Table 5.3.: Gradient enhancement of the plastic models - variant I

Plastic models

(1) Internal variable lists:

$$\boldsymbol{P} = \{\boldsymbol{\varepsilon}_P, \alpha_P\}, \quad \boldsymbol{P}_{NL} = \{\alpha_P\}, \quad \boldsymbol{P}_L = \{\boldsymbol{\varepsilon}_P\} \tag{5.45}$$

(2) Non-local variable list $\boldsymbol{\varphi}$ and the potential $\boldsymbol{H}_{\boldsymbol{\varphi}}(\boldsymbol{P}_{NL})$:

$$\boldsymbol{\varphi} = \{\varphi_P\}, \quad \boldsymbol{H}_{\boldsymbol{\varphi}}(\boldsymbol{P}_{NL}) = \{H_{\boldsymbol{\varphi}}(\alpha_P)\}, \tag{5.46}$$

$$H_{\boldsymbol{\varphi}}(\alpha_P) = W(\alpha_P) - W(0) \tag{5.47}$$

(3) Interaction potential Ψ_{intr} and the operators $\boldsymbol{\beta}$ and c:

$$\Psi_{intr} = \frac{1}{2}\beta_P \ (\varphi_P - W(\alpha_P) + W(0))^2 + \frac{1}{2}\, c_P \ \nabla\varphi_P \cdot \nabla\varphi_P, \tag{5.48}$$

$$\boldsymbol{L}_{\boldsymbol{\varphi}} = \beta_P \ (\varphi_P - W(\alpha_P) + W(0)), \quad \mathbf{c}(\boldsymbol{\nabla}\boldsymbol{\varphi}) = c_P \ \nabla\varphi_P \tag{5.49}$$

(4) Lists of the micromechanical driving forces:

$$\boldsymbol{Q}_L = \{\boldsymbol{\sigma}_P\}, \quad \boldsymbol{Q}_{NL} = \{\eta_P\}, \tag{5.50}$$

$$\eta_P = \underbrace{-W'(\alpha_P)}_{\hat{\eta}_P} + \underbrace{\beta_P \ W'(\alpha_P) \ (\varphi_P - W(\alpha_P) + W(0))}_{\tilde{\eta}_P} \tag{5.51}$$

(5) Inelastic tangent moduli:

$$G_{PP} = -\frac{1}{\boldsymbol{\sigma}_P : \boldsymbol{\sigma}_P}\,\boldsymbol{\sigma}_P : \operatorname{dev}\mathbb{C} : \boldsymbol{\sigma}_P - $$
$$W''(\alpha_P)\left[1 + \beta_P\left(\varphi_P - W(\alpha_P) + W(0)\right)\right] + \beta_P \ (W'(\alpha_P))^2 \tag{5.52}$$

$$\mathbb{C}^{IN} = \mathbb{C} + \frac{1}{G_{PP}} \left[(\operatorname{dev}\mathbb{C} : \boldsymbol{\sigma}_P) \otimes (\operatorname{dev}\mathbb{C} : \boldsymbol{\sigma}_P)\right] \tag{5.53}$$

$$\frac{\partial\boldsymbol{\sigma}}{\partial\boldsymbol{\varphi}} = -\frac{\beta_P \ W'(\alpha_P)}{G_{PP}} \ \frac{1}{\boldsymbol{\sigma}_P : \boldsymbol{\sigma}_P} \ (\operatorname{dev}\mathbb{C} : \boldsymbol{\sigma}_P), \tag{5.54}$$

$$\frac{\partial\boldsymbol{L}_{\boldsymbol{\varphi}}}{\partial\boldsymbol{\varepsilon}} = -\frac{\beta_P \ W'(\alpha_P)}{G_{PP}} \ \frac{1}{\boldsymbol{\sigma}_P : \boldsymbol{\sigma}_P} \ (\operatorname{dev}\mathbb{C} : \boldsymbol{\sigma}_P), \tag{5.55}$$

$$\frac{\partial\boldsymbol{L}_{\boldsymbol{\varphi}}}{\partial\boldsymbol{\varphi}} = \beta_P \ \left(1 + \frac{\beta_P \ (W'(\alpha_P))^2}{G_{PP}}\right) \tag{5.56}$$

Table 5.4.: Gradient enhancement of the plastic models - variant II

requirement. Since φ_P is a solution of the differential equation

$$\beta_P \left(\varphi_P - H_{\boldsymbol{\varphi}}(\alpha_P) \right) - c_P \nabla^2 \varphi_P = 0, \tag{5.59}$$

its Laplacian in the localization zone will be negative in conjunction with the positive plastic interaction potential function $H_{\boldsymbol{\varphi}}(\alpha_P)$ and positive if the negative function is employed. In view of (5.59) the hardening (softening) driving force becomes

$$\eta_P = \hat{\eta}_P + H'_{\boldsymbol{\varphi}}(\alpha_P)\, \beta_P \left(\varphi_P - H_{\boldsymbol{\varphi}}(\alpha_P) \right) = \hat{\eta}_P + H'_{\boldsymbol{\varphi}}(\alpha_P)\, c_P \nabla^2 \varphi_P. \tag{5.60}$$

Recalling the definitions (3.60) and (3.63) of the yield function utilized in *plastic models I and II*, respectively, one can interpret $\tilde{\eta}_P$ as a contribution to the yield strength coming from non-local interactions

$$\tilde{\eta}_P = H'_{\boldsymbol{\varphi}}(\alpha_P)\, c_P \nabla^2 \varphi_P. \tag{5.61}$$

From the discussion in this section it follows that $\tilde{\eta}_P$ attains positive values in the localization zone, thus increasing the yield limit and consequently damping the evolution of inelastic variables. Outside of this zone the converse holds: the yield limit is decreased and therefore the evolution of inelastic variables is accelerated.

In this context, let us consider the regularization of the *plastic model II* employing the second approach, e.g. taking

$$H_{\boldsymbol{\varphi}}(\alpha_P) = W_2(\alpha_P) - W_2(0) = -r_{2,\infty}\, \alpha_P + \frac{r_{2,0} - r_{2,\infty}}{K_H}\, \frac{1}{K_H\, \alpha_P - 1}. \tag{5.62}$$

The plots of this function and its derivative are presented in the Figure 5.4. As it is obvious,
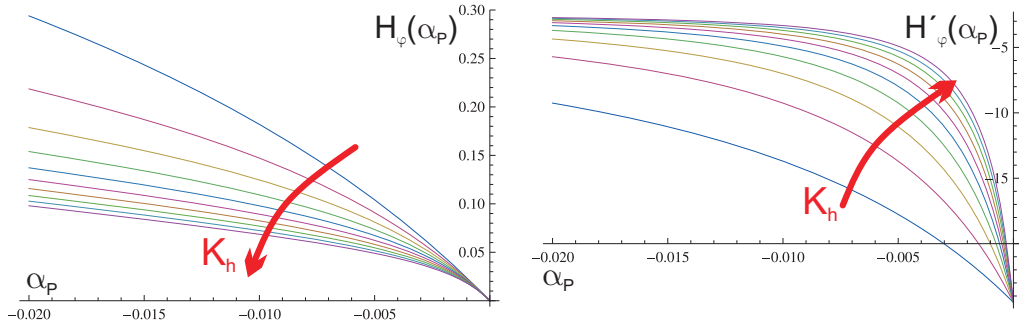
Figure 5.4.: Potential function $H_{\boldsymbol{\varphi}}(\alpha_P)$ and its derivatives based on the plastic potential $W_2(\alpha_P)$. The red arrow shows the direction in which the parameter K_H increases.

the derivative $H'_{\boldsymbol{\varphi}}(\alpha_P)$ decreases in the absolute value with the evolution of the softening variable

$$\left| H'_{\boldsymbol{\varphi}}(\alpha_P(t_{n+1})) \right| \leq \left| H'_{\boldsymbol{\varphi}}(\alpha_P(t_n)) \right| \quad \forall\, t_{n+1} > t_n. \tag{5.63}$$

In view of (5.61), the relation (5.63) implies that the influence of non-local interaction declines with evolving plastic process. Hence, utilizing (5.62) in the regularization of the *plastic model II* will lead to problems if used with small values of the parameter $r_{2,\infty}$, as it is going to be demonstrated by suitable example in the next chapter.

5.3. Gradient enhancement of a coupled damage-plastic material model

In this section the application of the investigated gradient regularization strategy on the coupled damage-plastic model (which is described in the section 3.2.3) is presented and its details are summarized in the Tables 5.5 and 5.6.

Coupled damage-plastic models

(1) **Internal variable lists**:

$$\boldsymbol{P} = \{d, \boldsymbol{\varepsilon}_P, \alpha_P\}, \quad \boldsymbol{P}_{NL} = \{d, \alpha_P\}, \quad \boldsymbol{P}_L = \{\boldsymbol{\varepsilon}_P\} \tag{5.64}$$

(2) **Non-local variable list $\boldsymbol{\varphi}$ and the potential $\boldsymbol{H}_{\boldsymbol{\varphi}}(\boldsymbol{P}_{NL})$**:

$$\boldsymbol{\varphi} = \{\varphi_d, \varphi_P\}, \quad \boldsymbol{H}_{\boldsymbol{\varphi}}(\boldsymbol{P}_{NL}) = \{H_{\boldsymbol{\varphi}\,d}(d), H_{\boldsymbol{\varphi}\,P}(\alpha_P)\}, \tag{5.65}$$

$$H_{\boldsymbol{\varphi}\,d}(d) = d, \qquad H_{\boldsymbol{\varphi}\,P}(\alpha_P) = \alpha_P \tag{5.66}$$

(3) **Interaction potential Ψ_{intr} and the operators $\boldsymbol{\beta}$ and c**:

$$\Psi_{intr} = \frac{1}{2}\left(\beta_d\,(\varphi_d - d)^2 + \beta_P\,(\varphi_P - \alpha_P)^2\right) +$$
$$\frac{1}{2}\left(c_d\,\nabla\varphi_d \cdot \nabla\varphi_d + c_P\,\nabla\varphi_P \cdot \nabla\varphi_P\right), \tag{5.67}$$

$$\boldsymbol{L}_{\boldsymbol{\varphi}} = \{\beta_d\,(\varphi_d - d),\ \ \beta_P\,(\varphi_P - \alpha_P)\}, \tag{5.68}$$

$$\mathbf{c}\,(\boldsymbol{\nabla\varphi}) = \{c_d\,\nabla\varphi_d,\ \ c_P\,\nabla\varphi_P\} \tag{5.69}$$

(4) **Lists of the micromechanical driving forces**:

$$\boldsymbol{Q}_L = \{\boldsymbol{\sigma}_P\}, \quad \boldsymbol{Q}_{NL} = \{\eta_d, \eta_P\}, \tag{5.70}$$

$$\eta_d = \underbrace{\frac{1}{2}\,e^{-d}\,(\boldsymbol{\varepsilon} - \boldsymbol{\varepsilon}_P) : \mathbb{C} : (\boldsymbol{\varepsilon} - \boldsymbol{\varepsilon}_P)}_{\hat{\eta}_d} + \underbrace{\beta_d\,(\varphi_d - d)}_{\tilde{\eta}_d} \tag{5.71}$$

$$\eta_P = \underbrace{-W'(\alpha_P)}_{\hat{\eta}_P} + \underbrace{\beta_P\,(\varphi_P - \alpha_P)}_{\tilde{\eta}_P} \tag{5.72}$$

Table 5.5.: Gradient enhancement of the coupled damage-plastic models

---

The internal variable lists $\boldsymbol{P}$, $\boldsymbol{P}_{NL}$ and $\boldsymbol{P}_L$ are specified in (5.64). Since $\boldsymbol{P}_{NL}$ contains two scalar variables, one has to define two potential functions that are the elements of the list $\boldsymbol{H}_{\boldsymbol{\varphi}}$, relation (5.65). They are chosen to be equal to the variables themselfs, equation (5.66). Hence, the non-local variable list $\boldsymbol{\varphi}$ contains two elements, see (5.65), and the interaction potential is obtained as a sum of the interaction potentials of constituent models, relation (5.67). The micromechanical driving forces are specified in (5.70)-(5.72) and their interaction parts are identical with the ones occurring in the damage model (5.7) and the plastic model (5.39). Finally, the inelastic tangent operators are presented in the Table 5.6. As it is

---

Coupled damage-plastic models

(5) Metric coefficients:

$$\tilde{G}^{dd} = -\frac{1}{\frac{1}{2}\,e^{-d}\,(\boldsymbol{\varepsilon}-\boldsymbol{\varepsilon}_P):\mathbb{C}:(\boldsymbol{\varepsilon}-\boldsymbol{\varepsilon}_P)} \tag{5.73}$$

$$\tilde{G}^{PP} = -\frac{1}{\frac{1}{e^{-d}\,\boldsymbol{\sigma}_P:\boldsymbol{\sigma}_P}\,\boldsymbol{\sigma}_P:\mathbb{C}:\boldsymbol{\sigma}_P\,+\,W''(\alpha_P)\,+\,\beta_P} \tag{5.74}$$

$$\tilde{G}^{dP} = -\frac{-e^{-d}\,\sqrt{\boldsymbol{\sigma}_P:\boldsymbol{\sigma}_P}}{\frac{1}{e^{-d}\,\boldsymbol{\sigma}_P:\boldsymbol{\sigma}_P}\,\boldsymbol{\sigma}_P:\mathbb{C}:\boldsymbol{\sigma}_P\,+\,W''(\alpha_P)\,+\,\beta_P}$$

$$\frac{1}{\frac{1}{2}\,e^{-d}\,(\boldsymbol{\varepsilon}-\boldsymbol{\varepsilon}_P):\mathbb{C}:(\boldsymbol{\varepsilon}-\boldsymbol{\varepsilon}_P)} \tag{5.75}$$

(6) Inelastic tangent moduli:

$$\mathbb{C}^{IN} = \mathbb{C}\,-\,e^{-2d}\,\tilde{G}^{dd}\,[\mathbb{C}:(\boldsymbol{\varepsilon}-\boldsymbol{\varepsilon}_P)]\otimes[\mathbb{C}:(\boldsymbol{\varepsilon}-\boldsymbol{\varepsilon}_P)]\,+$$
$$\frac{e^{-d}}{\sqrt{\boldsymbol{\sigma}_P:\boldsymbol{\sigma}_P}}\,\tilde{G}^{dP}\,[\mathbb{C}:(\boldsymbol{\varepsilon}-\boldsymbol{\varepsilon}_P)]\otimes[\mathbb{C}:\boldsymbol{\sigma}_P]\,-$$
$$\frac{1}{\boldsymbol{\sigma}_P:\boldsymbol{\sigma}_P}\,\tilde{G}^{PP}\,[\mathbb{C}:\boldsymbol{\sigma}_P]\otimes[\mathbb{C}:\boldsymbol{\sigma}_P], \tag{5.76}$$

$$\frac{\partial\boldsymbol{\sigma}}{\partial\boldsymbol{\varphi}} = \left\{ e^{-d}\,\beta_d\,\tilde{G}^{dd}\,\mathbb{C}:(\boldsymbol{\varepsilon}-\boldsymbol{\varepsilon}_P),\right.$$
$$\left. -e^{-d}\,\beta_P\,\tilde{G}^{dP}\,\mathbb{C}:(\boldsymbol{\varepsilon}-\boldsymbol{\varepsilon}_P)-\frac{\beta_P}{\sqrt{\boldsymbol{\sigma}_P:\boldsymbol{\sigma}_P}}\,\mathbb{C}:\boldsymbol{\sigma}_P\right\}, \tag{5.77}$$

$$\frac{\partial\boldsymbol{L}_\varphi}{\partial\boldsymbol{\varepsilon}} = \left\{ \begin{array}{c} e^{-d}\,\beta_d\,\tilde{G}^{dd}\,\mathbb{C}:(\boldsymbol{\varepsilon}-\boldsymbol{\varepsilon}_P) \\ -e^{-d}\,\beta_P\,\tilde{G}^{dP}\,\mathbb{C}:(\boldsymbol{\varepsilon}-\boldsymbol{\varepsilon}_P)-\frac{\beta_P}{\sqrt{\boldsymbol{\sigma}_P:\boldsymbol{\sigma}_P}}\,\mathbb{C}:\boldsymbol{\sigma}_P \end{array}\right\}, \tag{5.78}$$

$$\frac{\partial\boldsymbol{L}_\varphi}{\partial\boldsymbol{\varphi}} = \left[\begin{array}{cc} \beta_d^2\,\tilde{G}^{dd} & -\beta_d\,\beta_P\,\tilde{G}^{dP} \\ 0 & \beta_P^2\,\tilde{G}^{PP} \end{array}\right] \tag{5.79}$$

Table 5.6.: Inelastic tangent moduli of the coupled damage-plastic models

already stated, there are no differences in the interaction parts between the coupled damage-plastic model and the constituent models. Hence, the discussions made in the sections 5.2 and 5.1 apply here as well.

This section completes the presentation of the application of the gradient regularization strategy onto investigated material models completed and we proceed to the numerical solution of the boundary value problem posed in the section 4.3.

6. Finite Element implementation

In this chapter we discuss the numerical solution of the boundary value problem posed in the section 4.3 utilizing *finite element method*. After some introductory remarks about the finite element method presented in the section 6.1, we continue by presenting the discretization of the boundary value problem in the section 6.2. Finally, the solution of the discretized problem is discussed in the section 6.3.

6.1. Finite element method

Mathematical modeling of physical problems in engineering results often in the system of partial differential equations which cannot be solved analytically due to complicated geometry of the domain of the problem, highly nonlinear relations describing the model etc.. An example of such system is a boundary value problem defined in the section 4.3. In order to find an appropriate solution of a posed problem one typically has to resort to numerical approximation methods. Although it is possible to apply numerical approximation to differential equations directly using the method of finite differences, cf. Orkisz (1998), it is much more common and suitable to utilize the so-called *weak (integral) formulations* of the investigated problem, cf. Zienkiewicz and Taylor (2000a). A weak formulation of the boundary value problem under investigation in this thesis (equations (4.13)-(4.18)) is given by the the system of variational equations (4.27) and (4.28). In order to solve that system, one can use a *finite element method*, which is a particular instance of a *Galerkin method*, cf. Galerkin (1915).

The Galerkin method is based on the approximation of the unknown functions $\mathbf{u}, \varphi$ that represent the solution of the problem (4.24) in the finite dimensional Sobolev subspace[1] $V_h \in H^1(\Omega)$ using finitely many linear independent basis functions ψ^I and ζ^I

$$\boldsymbol{u}_h = \tilde{\boldsymbol{u}}_h(\boldsymbol{X}) + \sum_{I=1}^{NU} \psi^I(\boldsymbol{X})\, \widehat{\boldsymbol{u}}_h^I, \qquad \boldsymbol{\varphi}_h = \sum_{I=1}^{N\varphi} \zeta^I(\boldsymbol{X})\, \widehat{\boldsymbol{\varphi}}_h^I, \tag{6.1}$$

with the following properties

$$
\begin{aligned}
&\tilde{\boldsymbol{u}}_h = \boldsymbol{u}^* \text{ on } \partial\Omega_u: &&\text{fulfills inhomogeneous displacement boundary conditions} \\
&\psi^I = 0 \text{ on } \partial\Omega_u: &&\text{fulfills homogeneous displacement boundary conditions} \\
&\zeta^I = 0 \text{ on } \partial\Omega: &&\text{fulfills homogeneous boundary conditions.}
\end{aligned} \tag{6.2}
$$

The quantities $\widehat{\boldsymbol{u}}_h^I$ and $\widehat{\boldsymbol{\varphi}}_h^I$ in (6.1) denote the coefficients of the basis expansion. The index h elucidates the fact that the relations (6.1) result in the approximation of the corresponding functions. Following the Bubnov-Galerkin approach, the test functions $\delta\boldsymbol{u}$ and $\delta\boldsymbol{\varphi}$, which

---

[1] The Sobolev space $H^1(\Omega)$ is a function space of all functions that are square integrable and possess square integrable first derivatives on the domain Ω

$$H^1(\Omega) = \left\{ \boldsymbol{f}(\boldsymbol{X}): \Omega \to \Re^n \mid \sqrt{\int_\Omega f_i f_i\, dV} < \infty, \sqrt{\int_\Omega \frac{\partial f_i}{\partial X_j} \frac{\partial f_i}{\partial X_j}\, dV} < \infty \right\}.$$

represent within a variational formulation the arbitrary variations of the solution $\boldsymbol{u}(\boldsymbol{X})$ and $\boldsymbol{\varphi}(\boldsymbol{X})$, are expanded in the same function space and utilizing the same bases as for the governing problem variables

$$\delta\boldsymbol{u}_h = \sum_{I=1}^{NU} \psi^I(\boldsymbol{X})\,\delta\widehat{\boldsymbol{u}}_h^I, \qquad \delta\boldsymbol{\varphi}_h = \sum_{I=1}^{N\varphi} \zeta^I(\boldsymbol{X})\,\delta\widehat{\boldsymbol{\varphi}}_h^I. \tag{6.3}$$

Inserting (6.1) and (6.3) into the relation (4.26), one can obtain the discrete approximation of the potential variation. It can be further used together with the assumption of arbitrariness of the variations of the primal variables $\delta\boldsymbol{u}$ and $\delta\boldsymbol{\varphi}$ to construct the discrete system of equations which yields the unknown expansion coefficients. However, the choice of basis functions that satisfy the conditions (6.2) can be in general case very difficult owing to complicated geometry of the domain Ω. This problem can be efficiently solved employing a *finite element method*.

The finite element method is a special version of the Galerkin method. The considered domain Ω is divided into NE non-overlapping subdomains $\Omega = \bigcup_{I=1}^{NE} \Omega^I$ called *finite elements*. The primal variables $\boldsymbol{u}$ and $\boldsymbol{\varphi}$ are approximated within every element Ω^I by

$$\boldsymbol{u}_h(\Omega^I) = \sum_{I=1}^{nnu} N_u^I(\boldsymbol{X})\,\boldsymbol{u}_h^I, \qquad \boldsymbol{\varphi}_h(\Omega^I) = \sum_{I=1}^{nn\varphi} N_\varphi^I(\boldsymbol{X})\,\boldsymbol{\varphi}_h^I. \tag{6.4}$$

Here nnu and $nn\varphi$ stand for the number of basis functions N_u^I and N_φ^I used in the description of the displacement and non-local variable fields on Ω^I, respectively. As it is already stated, the basis functions have to belong to the subspace $V_h \in H^1(\Omega)$, leading to an approximation of the primal variables by piecewise continuous functions, Figure 6.1. The subdomains Ω^I are chosen to have a simple shape: three- or four-sided elements in
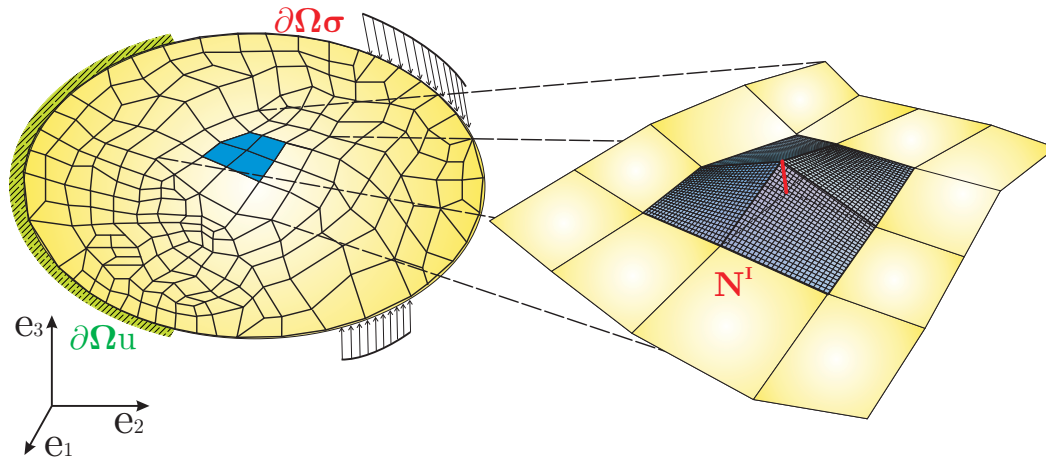
Figure 6.1.: Finite element discretization of domain and a typical basis function in a two-dimensional case

two-dimensional or four- or six-sided elements in three-dimensional problems. Restricting attention to four-sided (2D) and six-sided (3D) subdomains, the basis functions are constructed on a parent square (2D) or cube (3D) with help of the so-called *natural coordinates* $\xi_i, i = 1, ..., ndm$ and afterwards mapped onto elements Ω^I in physical space. That allows us to express the approximation relations (6.4) on the parent element in terms of normalized

local natural coordinates

$$\boldsymbol{u}_h(\Omega^I) = \sum_{I=1}^{nnu} N_u^I(\xi_i)\, \boldsymbol{u}_h^I, \qquad \boldsymbol{\varphi}_h(\Omega^I) = \sum_{I=1}^{nn\varphi} N_\varphi^I(\xi_i)\, \boldsymbol{\varphi}_h^I, \tag{6.5}$$

providing a one-to-one correspondence between the physical and natural coordinates is established. This task is accomplished following an *isoparametric* approach[2], the geometry is described using the same set of functions as those employed in the approximation of the displacement field

$$\boldsymbol{X}_h(\Omega^I) = \sum_{I=1}^{nnu} N_u^I(\xi_i)\, \boldsymbol{X}_h^I, \tag{6.6}$$

where $\mathbf{X}_h^I$ denotes the coefficients of the expansion. The expansion coefficients in the relations (6.5) and (6.6) obtain a very suitable interpretation if one uses the Lagrange polynomials to construct the basis functions (which is a predominant case in applications nowadays). Owing to their property to be equal to one in one node and equal to zero in all the other nodal points prescribed on the element, it follows straightforward from the approximation relations that the expansion coefficients are equal to the actual values of the considered quantity at the node corresponding to the particular basis function. Hence, $\mathbf{u}_h^I$ and $\boldsymbol{\varphi}_h^I$ become the displacement vector and the non-local variable list at the node denoted as I, while $\mathbf{X}_h^I$ represents its position vector, Figure 6.2. The required uniqueness of the mapping between
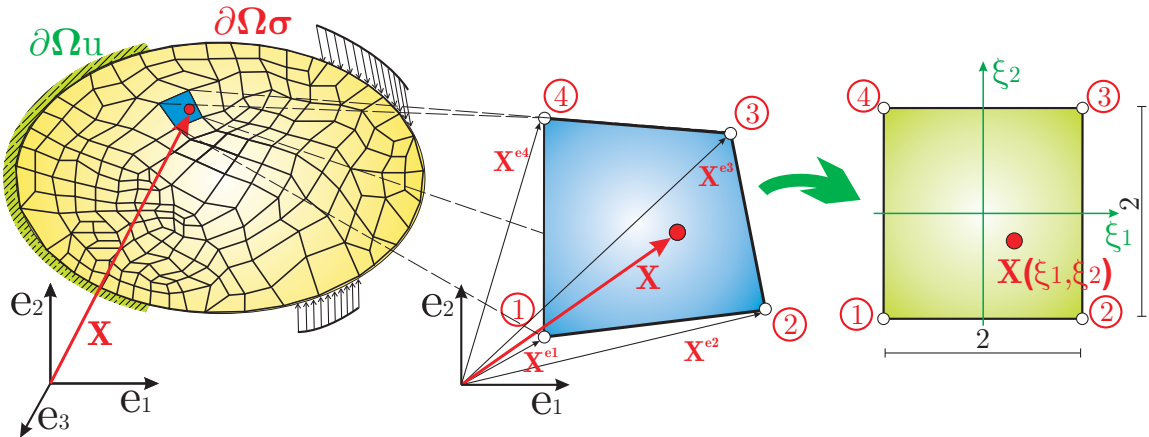
Figure 6.2.: Example of a two-dimensional mapping of an element

the physical element and its "isoparametric" image is assured if the Jacobian matrix of the transformation relation (6.6)

$$J_{ij} = \frac{\partial X_j}{\partial \xi_i} = \sum_{I=1}^{nnu} \frac{\partial N_u^I}{\partial \xi_i}\, X_{h,j}^I, \quad i = 1, \ldots, ndm \tag{6.7}$$

remains non-singular within the element. If one utilizes low-order (linear or quadratic) Lagrange polynomials in the construction of the basis functions, commonly called *shape functions*, there are very simple rules that guarantee the positive-definiteness of the Jacobian

---

[2]The name *quasi-isoparametric* will be more suitable, due to the fact that we use the same set of approximation functions for the description of the displacement field and the geometry of an element. However, non-local field can be described using some other set of functions, so that in its view an approximation is not isoparametric.

matrix ($\det \boldsymbol{J} > 0$) a-priory, cf. Zienkiewicz and Taylor (2000a). The derivatives of the approximation functions with respect to the physical coordinates are obtained applying the chain rule and the Jacobian matrix from (6.7) as

$$\frac{\partial N_a^I}{\partial X_i} = \frac{\partial N_a^I}{\partial \xi_j} \frac{\partial \xi_j}{\partial X_i} \qquad \Rightarrow \qquad \nabla N_a^I = \boldsymbol{J}^{-1} \cdot \frac{\partial N_a^I}{\partial \boldsymbol{\xi}}, \qquad a \in \{u, \varphi\} \tag{6.8}$$

Finally, following the spirit of the Bubnov-Galerkin approach, the test functions (variations) $\delta \boldsymbol{u}$ and $\delta \boldsymbol{\varphi}$ are represented in the same function space as the problem variables $\boldsymbol{u}$ and $\boldsymbol{\varphi}$ using the same basis functions:

$$\delta \boldsymbol{u}_h(\Omega^I) = \sum_{I=1}^{nnu} N_u^I(\xi_i) \, \delta \boldsymbol{u}_h^I, \qquad \delta \boldsymbol{\varphi}_h(\Omega^I) = \sum_{I=1}^{nn\varphi} N_\varphi^I(\xi_i) \, \delta \boldsymbol{\varphi}_h^I. \tag{6.9}$$

For the sake of notational clarity, the index h standing for the approximation of the corresponding field is going to be suppressed in the sequel.

6.2. Finite element discretization of the boundary value problem

The focus in this section is put on the discretization of the variational problem (4.24) utilizing a finite element method. Before presenting an implementation of the finite element approximation discussed in the previous section, one additional issue has to be commented on. As it is mentioned in the section 4.1 dealing with the investigated form of the gradient enhancement of the free-energy function, generic non-local variable φ stands for the list of variables, including possibly sublists of different nature (scalars, tensors). In the numerical implementation it is advantageous to collect and order all components of the list into a vector $\overline{\varphi}$. While that task is trivial for the subsets which are scalars or vectors, care should be taken in the ordering of the components of higher order tensors in order to obtain consistent formulation of the problem.

6.2.1. Finite element approximation of the governing variables

Let us consider a single finite element Ω^I. Within it are the geometry and the primal variable fields approximated by relations (6.5) and (6.6). Introducing element geometry, displacement and non-local variable vectors ($\hat{\boldsymbol{X}}$, $\hat{\boldsymbol{u}}$ and $\hat{\boldsymbol{\varphi}}$, respectively)

$$\hat{\boldsymbol{X}} = \left\{ \begin{array}{c} \boldsymbol{X}^1 \\ \vdots \\ \boldsymbol{X}^{nnu} \end{array} \right\}, \qquad \hat{\boldsymbol{u}} = \left\{ \begin{array}{c} \boldsymbol{u}^1 \\ \vdots \\ \boldsymbol{u}^{nnu} \end{array} \right\}, \qquad \hat{\boldsymbol{\varphi}} = \left\{ \begin{array}{c} \overline{\boldsymbol{\varphi}}^1 \\ \vdots \\ \overline{\boldsymbol{\varphi}}^{nn\varphi} \end{array} \right\} \tag{6.10}$$

and the matrices containing the approximation functions connected with a generic element node I

$$\mathbf{N}_u^I = \mathrm{diag} \left\{ \left(N_u^I \right)_1 \cdots \left(N_u^I \right)_{ncu} \right\}, \quad \mathbf{N}_\varphi^I = \mathrm{diag} \left\{ \left(N_\varphi^I \right)_1 \cdots \left(N_\varphi^I \right)_{nc\varphi} \right\}, \tag{6.11}$$

one can define the element approximation matrices

$$\mathbf{N}_u = \left[\mathbf{N}_u^1 \ \cdots \ \mathbf{N}_u^{nnu} \right], \qquad \mathbf{N}_\varphi = \left[\mathbf{N}_\varphi^1 \ \cdots \ \mathbf{N}_\varphi^{nn\varphi} \right], \tag{6.12}$$

and subsequently cast the relations (6.5) and (6.6) into the following matrix form

$$\boldsymbol{X} = \mathbf{N}_u \cdot \hat{\boldsymbol{X}}, \quad \boldsymbol{u} = \mathbf{N}_u \cdot \hat{\boldsymbol{u}}, \quad \overline{\boldsymbol{\varphi}} = \mathbf{N}_\varphi \cdot \hat{\boldsymbol{\varphi}}. \tag{6.13}$$

Dimension indices ncu and $nc\varphi$ in (6.11) represent the number of the unknown components of the vectors $\boldsymbol{u}$ and $\overline{\boldsymbol{\varphi}}$ respectively. The gradient of the non-local variable list, which enters the formulation of the enhanced free-energy function (4.11), is obtained from the approximation relation (6.5) as

$$\nabla\boldsymbol{\varphi}(\Omega^I) = \sum_{I=1}^{nn\varphi} \boldsymbol{\varphi}^I \otimes \nabla N_\varphi^I. \tag{6.14}$$

In order to write (6.14) in a matrix form, one has to introduce a vector comprising the components of $\nabla\varphi$ ordered in a way consistent with the definition of the vector of non-local variables $\overline{\varphi}$

$$\nabla\overline{\boldsymbol{\varphi}}_i = \begin{bmatrix} \frac{\partial(\overline{\varphi})_i}{\partial X_1} \\ \vdots \\ \frac{\partial(\overline{\varphi})_i}{\partial X_{ndm}} \end{bmatrix}, \qquad \boldsymbol{\nabla\overline{\varphi}} = \begin{bmatrix} \nabla\overline{\varphi}_1 \\ \vdots \\ \nabla\overline{\varphi}_{nc\varphi} \end{bmatrix}, \tag{6.15}$$

and the nodal and element matrices that comprehends the gradients of the basis functions used in the approximation of the non-local variable field

$$\boldsymbol{G}_\varphi^I = \begin{bmatrix} \left[\nabla N_\varphi^I\right]_1 & & \mathbf{0} \\ & \ddots & \\ \mathbf{0} & & \left[\nabla N_\varphi^I\right]_{nc\varphi} \end{bmatrix}, \qquad \boldsymbol{G}_\varphi = \begin{bmatrix} \boldsymbol{G}_\varphi^1 & \cdots & \boldsymbol{G}_\varphi^{nn\varphi} \end{bmatrix}. \tag{6.16}$$

Utilizing the definitions (6.16), (6.15) and (6.10) one can write

$$\boldsymbol{\overline{\nabla\varphi}} = \boldsymbol{G}_\varphi \cdot \hat{\boldsymbol{\varphi}}. \tag{6.17}$$

The approximation of the variation of primal variables is obtained following the Bubnov-Galerkin approach in (6.9) and its matrix form, in view of (6.13) and (6.17), reads

$$\delta\boldsymbol{u} = \mathbf{N}_u \cdot \delta\hat{\boldsymbol{u}}, \quad \delta\overline{\boldsymbol{\varphi}} = \mathbf{N}_\varphi \cdot \delta\hat{\boldsymbol{\varphi}}, \quad \boldsymbol{\nabla\delta\varphi} = \boldsymbol{G}_\varphi \cdot \delta\hat{\boldsymbol{\varphi}}. \tag{6.18}$$

In the linearization of the potential variation (4.42) one has to approximate the increments of governing variables. Their approximation follows the same steps as for the variation of displacements and non-local variables, resulting in

$$\Delta\boldsymbol{u} = \mathbf{N}_u \cdot \Delta\hat{\boldsymbol{u}}, \quad \Delta\overline{\boldsymbol{\varphi}} = \mathbf{N}_\varphi \cdot \Delta\hat{\boldsymbol{\varphi}}, \quad \boldsymbol{\nabla\Delta\varphi} = \boldsymbol{G}_\varphi \cdot \Delta\hat{\boldsymbol{\varphi}}. \tag{6.19}$$

As next, the correlation between the strain tensor and the element displacement vector has to be defined. Recalling the definition of the linearized strain tensor (2.83) and utilizing the approximation relation (6.5) it follows

$$\varepsilon_{ij}(\Omega^I) = \frac{1}{2} \sum_{I=1}^{nnu} \left(\frac{\partial N_u^I}{\partial X_j}\delta_{ik} + \frac{\partial N_u^I}{\partial X_i}\delta_{jk} \right) u_k^I, \tag{6.20}$$

where the summation over repeated indices i, j and k is implied and the Kronecker delta symbol

$$\delta_{ij} = \begin{cases} 1 & \text{if } i = j \\ 0 & \text{if } i \neq j \end{cases} \tag{6.21}$$

is being used. Introducing the strain $\overline{\varepsilon}$ and the stress $\overline{\sigma}$ vectors that assemble the components of the corresponding tensors using either the Voigt or the Mandel basis[3], cf. Brannon (2003), one can evaluate the approximated strain components as

$$\overline{\varepsilon} = \sum_{I=1}^{nnu} \mathbf{B}^I \cdot \mathbf{u}^I. \tag{6.22}$$

The matrix of the discrete strain-displacement operator containing the derivatives of the approximation function connected with the element node I depends on the basis used, see the section A.4 and can be deduced from (6.20). Forming the element discrete strain-displacement operator by collecting nodal operators (either Voigt or Mandel) in a matrix

$$\mathbf{B} = \begin{bmatrix} \mathbf{B}^1 & \cdots & \mathbf{B}^{nnu} \end{bmatrix} \tag{6.23}$$

and employing the element displacement vector (6.10), the relation (6.22) attains the following form

$$\overline{\varepsilon} = \mathbf{B} \cdot \hat{\boldsymbol{u}}. \tag{6.24}$$

Owing to the Bubnov-Galerkin concept, which is followed in this work, the variation and the incrementation of the strain vector are obtained as

$$\delta\overline{\varepsilon} = \mathbf{B} \cdot \delta\hat{\boldsymbol{u}}, \qquad \Delta\overline{\varepsilon} = \mathbf{B} \cdot \Delta\hat{\boldsymbol{u}}. \tag{6.25}$$

Having defined the finite element approximation of the governing variables, we proceed to the approximation of the potential variation.

6.2.2. Finite element discretization of the potential variation

In order to obtain numerical solution of the variational problem (4.24) using finite element method, the domain of the problem Ω is subdivided in a number of finite elements Ω^I. The domain integrals occurring in the relation (4.26) are evaluated as a discrete sum of the integrals over the single subdomains, leading to

$$\delta\Pi = \sum_{e=1}^{NE} \left\{ \int_{\Omega^e} \delta\boldsymbol{\varepsilon} : \boldsymbol{\sigma} \, dV^e - \int_{\Omega^e} \delta\boldsymbol{u} \cdot \boldsymbol{f} \, dV^e - \int_{\partial\Omega_\sigma^e} \delta\boldsymbol{u} \cdot \boldsymbol{t} \, dA^e \right.$$
$$\left. + \int_{\Omega^e} \left[\delta\boldsymbol{\varphi} : \boldsymbol{L_\varphi} + \boldsymbol{\nabla}\delta\boldsymbol{\varphi} \vdots \mathbf{c}\left(\boldsymbol{\nabla}\boldsymbol{\varphi}\right) \right] dV^e \right\}. \tag{6.26}$$

Applying the finite element approximation specified in the section 6.2.1 on (6.26), one obtains the approximation of the potential variation

$$\delta\Pi = \sum_{e=1}^{NE} \left\{ \int_{\Omega^e} (\mathbf{B} \cdot \delta\hat{\boldsymbol{u}})^T \cdot \overline{\boldsymbol{\sigma}} \, dV^e - \int_{\Omega^e} (\mathbf{N}_u \cdot \delta\boldsymbol{u})^T \cdot \boldsymbol{f} \, dV^e - \int_{\partial\Omega_\sigma^e} (\mathbf{N}_u \cdot \delta\boldsymbol{u})^T \cdot \boldsymbol{t} \, dA^e \right.$$
$$\left. + \int_{\Omega^e} \left[(\mathbf{N}_\varphi \cdot \delta\hat{\boldsymbol{\varphi}})^T \cdot \overline{\boldsymbol{L_\varphi}} + (\boldsymbol{G}_\varphi \cdot \delta\hat{\boldsymbol{\varphi}})^T \cdot \overline{\boldsymbol{\Gamma_\varphi}} \right] dV^e \right\}. \tag{6.27}$$

---

[3]For details on matrix notation see the section A.4.

The vectors $\overline{\boldsymbol{L_\varphi}}$ and $\overline{\boldsymbol{\Gamma_\varphi}}$ contain the assembled components of $\boldsymbol{L_\varphi}$ (equation (4.70)) and $\mathbf{c}\,(\boldsymbol{\nabla}\varphi)$ respectively. The assembling procedure has to be performed in a way consistent with the definition of the vectors $\overline{\boldsymbol{\varphi}}$ and $\overline{\boldsymbol{\nabla}\varphi}$, so that the corresponding products from (6.26) are preserved in the matrix formulation (6.27).

The components of the element test function (variable variation) vectors $\delta\hat{\boldsymbol{u}}$ and $\delta\hat{\boldsymbol{\varphi}}$ are the coefficients of the expansion with respect to the corresponding basis functions, equation (6.9). Hence, they can be moved out of the integrals, resulting in the following element vectors

$$\mathbf{F}^e_{int} = \int\limits_{\Omega^e} \mathbf{B}^T \cdot \overline{\boldsymbol{\sigma}}\, dV^e, \quad \mathbf{f}^e_b = \int\limits_{\Omega^e} \mathbf{N}^T_u \cdot \boldsymbol{f}\, dV^e, \quad \mathbf{f}^e_t = \int\limits_{\partial\Omega^e_\sigma} \mathbf{N}^T_u \cdot \boldsymbol{t}\, dA^e, \tag{6.28}$$

$$\mathbf{F}^e_\varphi = \int\limits_{\Omega^e} \mathbf{N}^T_\varphi \cdot \overline{\boldsymbol{L_\varphi}}\, dV^e, \qquad \mathbf{F}^e_{\nabla\varphi} = \int\limits_{\Omega^e} \boldsymbol{G}^T_\varphi \cdot \overline{\boldsymbol{\Gamma_\varphi}}\, dV^e. \tag{6.29}$$

Utilizing (6.28) and (6.29), the approximation of the potential variation (6.27) attains the form

$$\delta\Pi = \sum_{e=1}^{NE} \delta\Pi^e = \sum_{e=1}^{NE} \left\{ \delta\hat{\boldsymbol{u}}^e \cdot \left(\mathbf{F}^e_{int} - \mathbf{f}^e_b - \mathbf{f}^e_t\right) + \delta\hat{\boldsymbol{\varphi}}^e \cdot \left(\mathbf{F}^e_\varphi + \mathbf{F}^e_{\nabla\varphi}\right)\right\}. \tag{6.30}$$

The computational efficiency of the finite element method results from the fact that the basis function used in the description of the governing variables of the problem (6.5) and (6.9) have compact support which includes very small number of elements, see the Figure 6.1 for a typical illustration in a two-dimensional case. Hence, a contribution from only a few functions has to be considered in every element. However, that implies that the basis functions in a typical case contribute to the overall integrals in several elements. These contributions are summed together by application of the standard finite element assembling procedure (the details on this topic can be found e.g. in Zienkiewicz and Taylor (2000a) or in Smith and Griffiths (2008)). In that purpose the global solution ($\mathbf{d}$), the solution variation ($\delta\mathbf{d}$) and the residual ($\mathbb{R}$) vectors are introduced

$$\mathbf{d} = \underset{e}{\mathbf{A}} \left\{ \begin{array}{c} \hat{\boldsymbol{u}} \\ \hat{\boldsymbol{\varphi}} \end{array} \right\}^e; \quad \delta\mathbf{d} = \underset{e}{\mathbf{A}} \left\{ \begin{array}{c} \delta\hat{\boldsymbol{u}} \\ \delta\hat{\boldsymbol{\varphi}} \end{array} \right\}^e; \quad \mathbb{R} = \underset{e}{\mathbf{A}} \left\{ \begin{array}{c} \mathbf{F}_{int} - \mathbf{f}_b - \mathbf{f}_t \\ \mathbf{F}_\varphi + \mathbf{F}_{\nabla\varphi} \end{array} \right\}^e, \tag{6.31}$$

leading to the approximation of the variation of the potential functional that reads

$$\delta\Pi = (\delta\mathbf{d})^T \cdot \mathbb{R}. \tag{6.32}$$

6.2.3. Finite element discretisation of the incrementation of the potential variation

As a result of the subdivision of the problem domain into a number of finite elements, the incrementation of the potential variation defined in (4.42) is evaluated as a sum of the

contributions of single elements

$$\Delta \delta \Pi = \sum_{e=1}^{NE} \left\{ \int_{\Omega^e} \delta\boldsymbol{\varepsilon} : \mathbb{C}^{IN} : \Delta\boldsymbol{\varepsilon} \ dV^e \ + \int_{\Omega^e} \delta\boldsymbol{\varepsilon} : \frac{\partial\boldsymbol{\sigma}}{\partial\boldsymbol{\varphi}} : \Delta\boldsymbol{\varphi} \ dV^e \right.$$

$$+ \int_{\Omega^e} \delta\boldsymbol{\varphi} : \frac{\partial\boldsymbol{L}_\varphi}{\partial\boldsymbol{\varepsilon}} : \Delta\boldsymbol{\varepsilon} \ dV^e \ + \int_{\Omega^e} \delta\boldsymbol{\varphi} : \frac{\partial\boldsymbol{L}_\varphi}{\partial\boldsymbol{\varphi}} : \Delta\boldsymbol{\varphi} \ dV^e$$

$$\left. + \sum_{i=1}^{nnl} \int_{\Omega^e} c_i \ \boldsymbol{\nabla}\boldsymbol{\varphi}_i \vdots \boldsymbol{\nabla}\boldsymbol{\varphi}_i \ dV^e \right\} . \qquad (6.33)$$

Applying the finite element approximation specified in the section 6.2.1 on (6.33), one obtains the approximation of $\Delta\delta\Pi$ as

$$\Delta \delta \Pi = \sum_{e=1}^{NE} \left\{ \int_{\Omega^e} (\mathbf{B} \cdot \delta\hat{\boldsymbol{u}})^T \cdot \overline{\mathbb{C}}^{IN} \cdot (\mathbf{B} \cdot \Delta\hat{\boldsymbol{u}}) \ dV^e \right.$$

$$+ \int_{\Omega^e} (\mathbf{B} \cdot \delta\hat{\boldsymbol{u}})^T \cdot \overline{\left(\frac{\partial\boldsymbol{\sigma}}{\partial\boldsymbol{\varphi}}\right)} \cdot (\mathbf{N}_\varphi \cdot \Delta\hat{\boldsymbol{\varphi}}) \ dV^e$$

$$+ \int_{\Omega^e} (\mathbf{N}_\varphi \cdot \delta\hat{\boldsymbol{\varphi}})^T \cdot \overline{\left(\frac{\partial\boldsymbol{L}_\varphi}{\partial\boldsymbol{\varepsilon}}\right)} \cdot (\mathbf{B} \cdot \Delta\hat{\boldsymbol{u}}) \ dV^e$$

$$+ \int_{\Omega^e} (\mathbf{N}_\varphi \cdot \delta\hat{\boldsymbol{\varphi}})^T \cdot \overline{\left(\frac{\partial\boldsymbol{L}_\varphi}{\partial\boldsymbol{\varphi}}\right)} \cdot (\mathbf{N}_\varphi \cdot \Delta\hat{\boldsymbol{\varphi}}) \ dV^e$$

$$\left. + \int_{\Omega^e} (\boldsymbol{G}_\varphi \cdot \delta\hat{\boldsymbol{\varphi}})^T \cdot \bar{\mathbf{c}} \cdot (\boldsymbol{G}_\varphi \cdot \Delta\hat{\boldsymbol{\varphi}}) \ dV^e \right\} . \qquad (6.34)$$

Overlined quantities in (6.34) stand for the matrix counterparts of the corresponding tangents defined in the Table 4.3. The only exception is $\bar{\mathbf{c}}$, which is, owing to decoupled form of the interaction potential (4.10) and the utilized form of the vector of the gradients of the non-local variables (6.15), a diagonal matrix comprising the gradient parameters c_i. Once again, care should be taken during the transformation into matrix form so that the consistent results are obtained at the end.

Recalling the fact that the components of the element test function (variable variation) vectors $\delta\hat{\boldsymbol{u}}$ and $\delta\hat{\boldsymbol{\varphi}}$ and the element variable incrementation vectors $\Delta\hat{\boldsymbol{u}}$ and $\Delta\hat{\boldsymbol{\varphi}}$ are the coefficients of the expansion of the considered quantities with respect to the corresponding basis functions (equations (6.9), (6.19)), they can be moved out of the integrals. As a consequence, one obtains the following element tangent matrices

$$\mathbf{K}_{uu}^e = \int_{\Omega^e} \mathbf{B}^T \cdot \overline{\mathbb{C}}^{IN} \cdot \mathbf{B} \ dV^e, \qquad \mathbf{K}_{u\varphi}^e = \int_{\Omega^e} \mathbf{B}^T \cdot \overline{\left(\frac{\partial\boldsymbol{\sigma}}{\partial\boldsymbol{\varphi}}\right)} \cdot \mathbf{N}_\varphi \ dV^e, \qquad (6.35)$$

$$\mathbf{K}_{\varphi u}^e = \int_{\Omega^e} \mathbf{N}_\varphi^T \cdot \overline{\left(\frac{\partial\boldsymbol{L}_\varphi}{\partial\boldsymbol{\varepsilon}}\right)} \cdot \mathbf{B} \ dV^e, \quad \mathbf{K}_{\varphi\varphi}^e = \int_{\Omega^e} \mathbf{N}_\varphi^T \cdot \overline{\left(\frac{\partial\boldsymbol{L}_\varphi}{\partial\boldsymbol{\varphi}}\right)} \cdot \mathbf{N}_\varphi \ dV^e, \qquad (6.36)$$

$$\mathbf{K}_{\nabla\varphi\nabla\varphi}^e = \int_{\Omega^e} \boldsymbol{G}_\varphi^T \cdot \bar{\mathbf{c}} \cdot \boldsymbol{G}_\varphi \ dV^e, \qquad (6.37)$$

while the approximation of the incrementation of the potential variation (6.34) attains the form

$$\Delta \delta \Pi = \sum_{e=1}^{NE} \big\{ \, \delta \hat{\boldsymbol{u}}^e \cdot \mathbf{K}_{uu}^e \cdot \Delta \hat{\boldsymbol{u}}^e \; + \; \delta \hat{\boldsymbol{u}}^e \cdot \mathbf{K}_{u\varphi}^e \cdot \Delta \hat{\boldsymbol{\varphi}}^e \; + \; \delta \hat{\boldsymbol{\varphi}}^e \cdot \mathbf{K}_{\varphi u}^e \cdot \Delta \hat{\boldsymbol{u}}^e$$
$$+ \; \delta \hat{\boldsymbol{\varphi}}^e \cdot \mathbf{K}_{\varphi\varphi}^e \cdot \Delta \hat{\boldsymbol{\varphi}}^e \; + \; \delta \hat{\boldsymbol{\varphi}}^e \cdot \mathbf{K}_{\nabla\varphi\nabla\varphi}^e \cdot \Delta \hat{\boldsymbol{\varphi}}^e \big\} \, . \quad (6.38)$$

The contributions of the single elements are summed up by the standard finite element assembling procedure, which results in the global solution increment vector $\Delta \mathbf{d}$ and the global tangent matrix $\mathbf{K}$

$$\Delta \mathbf{d} = \mathop{\text{A}}_{e} \left\{ \begin{array}{c} \Delta \hat{\boldsymbol{u}} \\ \Delta \hat{\boldsymbol{\varphi}} \end{array} \right\}^e , \qquad \mathbb{K} = \mathop{\text{A}}_{e} \left[\begin{array}{cc} \mathbf{K}_{uu} & \mathbf{K}_{u\varphi} \\ \mathbf{K}_{\varphi u} & \mathbf{K}_{\varphi\varphi} + \mathbf{K}_{\nabla\varphi\nabla\varphi} \end{array} \right]^e \quad (6.39)$$

in addition to the problem vectors defined in (6.31). Employing these quantities one obtains the approximation of the increment of the potential variation (6.34) as

$$\Delta \delta \Pi \; = \; (\delta \mathbf{d})^T \cdot \mathbb{K} \cdot \Delta \mathbf{d} \, . \quad (6.40)$$

As next, we proceed to the formulation of the discretized problem and furthermore to the brief description of the method used to solve it.

6.3. Discretized approximation problem and its solution

Let us consider the variational problem (4.24). Its solution is obtained requiring that the variation of the potential functional vanishes. The finite element approximation of the primal variables ($\boldsymbol{u}$ and $\boldsymbol{\varphi}$) of the problem (6.13) results in the approximation of $\delta\Pi$ given in (6.32). As a consequence, the following discretized problem arises

$$\delta \Pi \; = \; (\delta \mathbf{d})^T \cdot \mathbb{R} \, (\mathbf{d}) \; = \; 0 \qquad \forall \, \delta \mathbf{d} \mid \delta \mathbf{d}_{\boldsymbol{u}} = \mathbf{0} \text{ on } \partial\Omega_u, \;\; \delta \mathbf{d}_{\boldsymbol{\varphi}} = \mathbf{0} \text{ on } \partial\Omega, \quad (6.41)$$

with $\mathbf{d}_{\boldsymbol{u}}$ and $\mathbf{d}_{\boldsymbol{\varphi}}$ standing for the displacement and the non-local variable parts of the global solution vector, respectively. Taking into consideration the arbitrariness of the variation of the solution vector, the problem (6.41) reduces to the solution of the system of algebraic equations

$$\mathbb{R} \; = \; \mathbf{0} \, . \quad (6.42)$$

 An additional issue concerning the boundary conditions (4.13) posed on the primal variables (in the present contribution on the displacement field only) has to be discussed here. As it is already stated, the global residual vector is formed by assembling the contributions from all elements used in the subdivision of the domain Ω. Recalling the general Galerkin-ansatz (6.1) and the required properties of the approximation functions used in the Galerkin method (6.2), it follows that certain finite element basis functions which are used in the calculations on the element level do not fulfill basic requirements (6.2). These are the approximation functions connected with the nodes laying directly on the Dirichlet boundary, Figure 6.3. Hence, their contribution to the potential variation is suppressed and consequently the corresponding equations are removed from the system (6.43) if one has to deal with the homogeneous Dirichlet boundary condition. However, if inhomogeneous boundary conditions
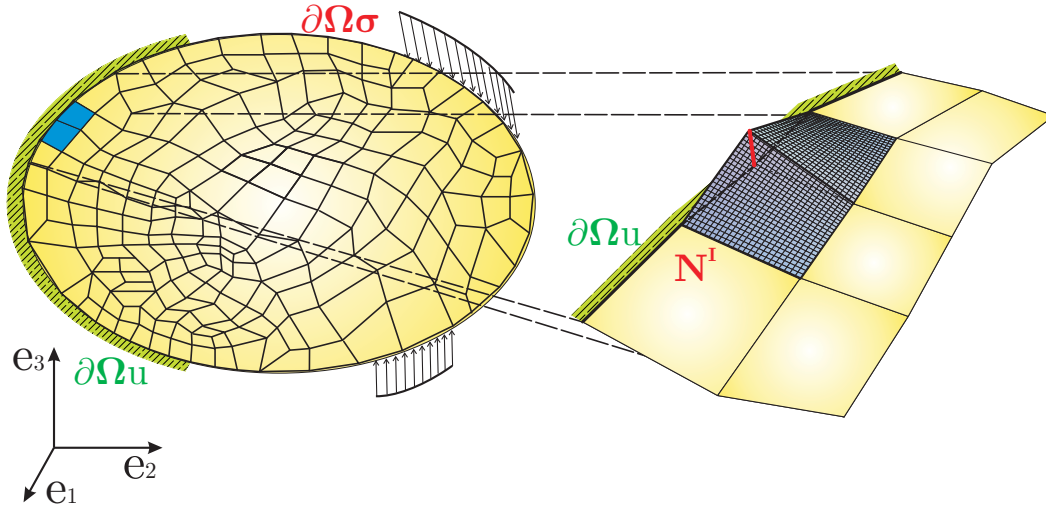
Figure 6.3.: Finite element basis function on the Dirichlet boundary in a two-dimensional
            case

are imposed, these basis functions are used to approximate the particular solution $\tilde{\boldsymbol{u}}_h(\boldsymbol{X})$
of the boundary value problem (equation (6.1)). If one uses the Lagrange polynomials to
construct the basis functions (which is the case in this thesis) the expansion coefficients con-
nected with the nodes on the Dirichlet boundary are obtained straightforward as the actual
values of the prescribed displacement components and no equation should be solved. Yet,
the influence of the discussed functions cannot be disregarded, as it is done in the case of ho-
mogeneous boundary conditions, due to interaction with the other approximation functions
and the non-vanishing expansion coefficients.

The residual vector $\mathbb{R}$ depends on the solution vector $\mathbf{d}$ in a non-linear way. Therefore,
some appropriate numerical procedure has to be employed in the solution of (6.43). In
the present contribution an incremental-iterative scheme based on the Newton's method
is applied, cf. Zienkiewicz and Taylor (2000b), Wriggers (2008). The loading history is
formulated through a number of quasi-time dependent sequential loading steps. For every
quasi-time increment

$$t_{n+1} \; = \; t_n \; + \; \Delta t_{n+1}, \qquad n \; \in \; \{0, 1, \ldots, nts\}, \tag{6.43}$$

where nts stands for the total number of time steps, the problem of finding the vector of
solution parameters $^{n+1}\mathbf{d}$ that satisfies the given Dirichlet boundary conditions and results
in vanishing residual

$$\mathbb{R}\left(^{n+1}\mathbf{d}\right) = \mathbf{0}, \tag{6.44}$$

for the given incremented loading is solved. Therefore the solution of the original problem
results in solving a sequence of the algebraic problems for every specific time t_{n+1}. This
task is, due to non-linearity of $\mathbb{R}(\mathbf{d})$, accomplished iteratively using Newton's method. The
method attempts the solution of the problem (6.43) by solving a series of linearized problems

$$\mathcal{L}\delta\Pi \; := \; \delta\Pi + \Delta\delta\Pi \; = \; 0. \tag{6.45}$$

In view of the relations (6.32) and (6.40), the linearisation of the potential variation around
the current solution state $^{n+1}\mathbf{d}^{(i)}$ and accordingly the problem (6.45) attain the following
form

$$\mathcal{L}\delta\Pi \; = \; (\delta\mathbf{d})^T \cdot \mathbb{R}\left(^{n+1}\mathbf{d}^{(i)}\right) \; + \; (\delta\mathbf{d})^T \cdot \mathbb{K}\left(^{n+1}\mathbf{d}^{(i)}\right) \cdot \Delta\mathbf{d}^{(i+1)} \; = \; 0. \tag{6.46}$$

Accounting for the arbitrariness of the solution vector variation ($\delta\mathbf{d}$) one obtains (this time linear) system of algebraic equations

$$\mathbb{R}^{(i)} + \mathbb{K}^{(i)} \cdot \Delta\mathbf{d}^{(i+1)} = 0, \tag{6.47}$$

where the following notation is introduced for the sake of clarity

$$\mathbb{R}^{(i)} = \mathbb{R}\left({}^{n+1}\mathbf{d}^{(i)}\right), \qquad \mathbb{K}^{(i)} = \mathbb{K}\left({}^{n+1}\mathbf{d}^{(i)}\right). \tag{6.48}$$

The system of linear equations (6.47) results in the increment vector $\Delta\mathbf{d}^{(i+1)}$, which is further used to update the current solution state

$$ {}^{n+1}\mathbf{d}^{(i+1)} = {}^{n+1}\mathbf{d}^{(i)} + \Delta\mathbf{d}^{(i+1)}. \tag{6.49}$$

The procedure is repeated using the updated current solution state as long as convergence criterion is not met. For example that the norm of the residual vector $\mathbb{R}$ reduces below some tolerance (equation (6.50,a)), or that the norm of the update vector $\Delta\mathbf{d}^{(i+1)}$ decreases down to the level that renders further iterations uneconomic (6.50,b)).

$$\text{a)} \quad \left\|\mathbb{R}^{(i+1)}\right\| \leq TOL; \qquad \text{b)} \quad \left\|\Delta\mathbf{d}^{(i+1)}\right\| \leq TOL \left\|{}^{n+1}\mathbf{d}^{(i+1)}\right\|. \tag{6.50}$$

Finally, as an initial guess at the beginning of the time step Δt_{n+1} a converged solution ${}^{n}\mathbf{d}$ from the previous time t_n is used:

$$ {}^{n+1}\mathbf{d}^{(0)} = {}^{n}\mathbf{d}. \tag{6.51}$$

7. Numerical Examples

The aim of this chapter is the presentation of numerical results obtained in the calculations utilizing the proposed gradient enhancement strategy. Its behavior is illustrated by means of several problems involving material models defined in the section 3.2 and afterwards adopted according to the presented regularization strategy. Furthermore, the influence of newly introduced model parameters on the global response of the system, distribution of inelastic variables and the calculation procedure is discussed. The section 7.1 contains results of calculations employing damage models, while the examples employing plastic models are given in section 7.2. Finally, the behavior of the enhanced coupled damage-plastic model is presented in section 7.3.

7.1. Problems involving damage material models

In this section we present results of calculations enrolling regularized *damage models I* and *II*. Several appropriate examples that illustrate the influence of the regularization procedure of corresponding damage models are selected. Let us start with the *damage model I*.

7.1.1. Numerical examples involving gradient enhanced *damage model I*

The first example is an infinitely long brick with a preexisting crack subjected to tension, applied as uniform displacement at the ends of the specimen. The geometry of the problem is given in Figure 7.1, and it allows for dimensional reduction of the problem to two-dimensional plane strain case. Moreover, due to existing symmetries only one fourth of the system is analyzed. The problem parameters are summarized in the Table 7.1.

The aim of this example is to illustrate the localization problem in the context of the finite element method. We already discussed the issue of localization in section 3.3, where it is demonstrated by means of a uniaxial tension problem that classical inelastic models fail to achieve an objective description of strain localization. The reason is an inherent lack of an internal material length scale in the formulation of the constitutive relations, resulting in an undetermined size of the inelastic process zone.

E	ν	c_d	β_d	r_1	h	b	a
MPa		MPa·mm^2	MPa	MPa	mm	mm	mm
18000.0	0.2	1.0	1.0	0.01	100.0	40.0	16.0

Table 7.1.: Material parameters used in the pre-cracked brick test in conjunction with the gradient enhanced *damage model I*
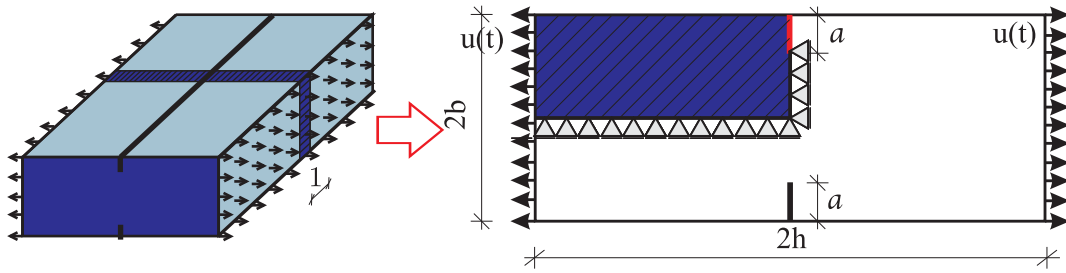
Figure 7.1.: Geometry of the pre-cracked brick test
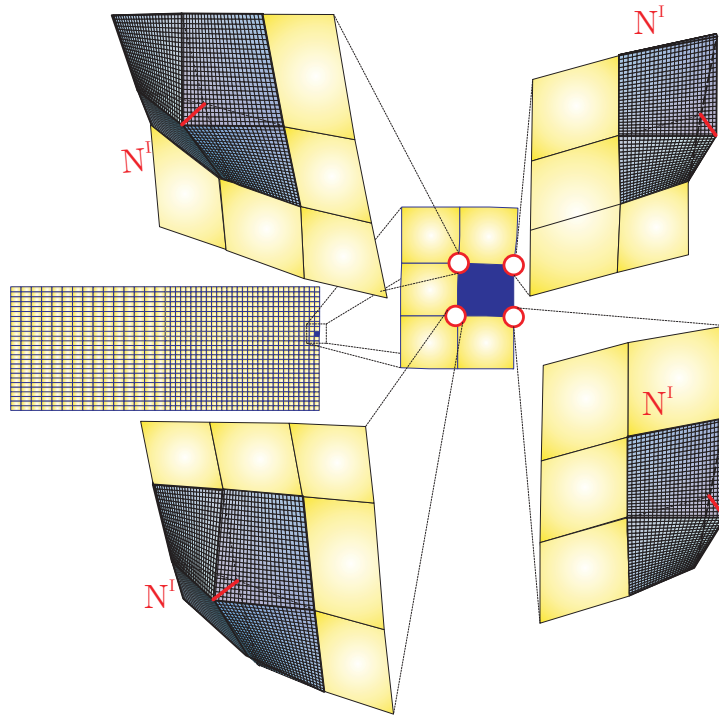
Figure 7.2.: Finite element basis functions on the element on the crack tip

If one uses the finite element method in the numerical solution of the variational minimization problem (4.24), one has to divide the body in a number of elements with final size, Figure 7.2. Recalling the representation of the displacement field in the finite element basis (6.4), it is obvious that the strain field and consequently the damage variable at some point depend on a few basis functions only, Figure 7.2. Hence, one has implicitly introduced a length scale equal to the size of the support of the approximation functions in the formulation. If the mesh is conveniently constructed so that the elements are aligned with the direction of the propagation of the localization zone, like in the current example, its length becomes even smaller and equals the element size. As a consequence, the discretized system of equations (6.41) becomes instable and cannot be solved by the displacement-driven incremental-iterative solution algorithm described in the section 6.3. That is due to an increasingly smaller size of the localization zone which triggers the snap-back behavior of the structure. Therefore a bifurcation point occurs significantly earlier in a refined mesh, as it can be seen in the Figure 7.3(a).

In contrast to that, the gradient enhanced model introduces an internal material length scale implicitly and therefore results in the mesh-independent response. Analyses performed with

(a) Local model   (b) Gradient enhanced model
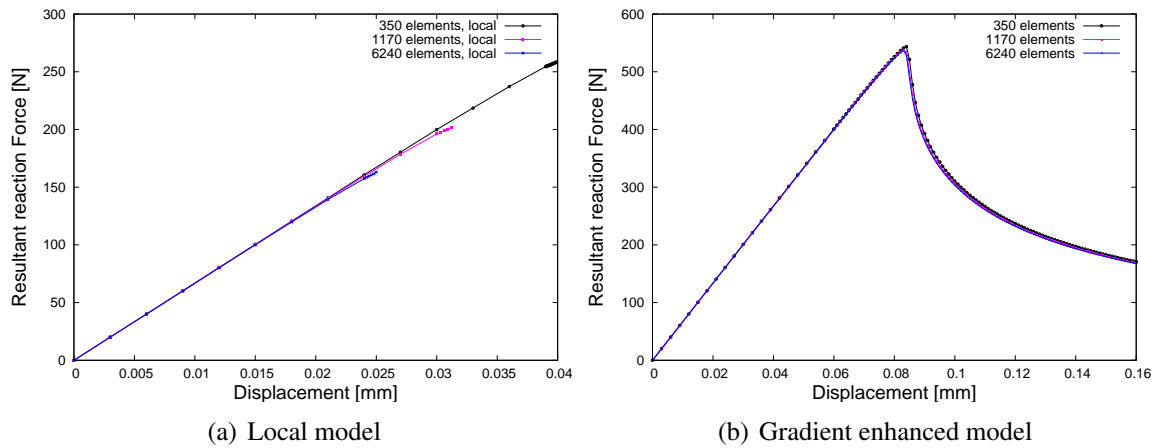
Figure 7.3.: Load-displacement diagrams for the cracked brick problem using local and gradient enhanced *damage model I*

350, 1170 and 6240 elements result in almost identical force-displacement curves, Figure 7.3(b). The distribution of the damage parameter shows mesh-objectivity as well, which can be seen in Figure 7.4, where the damage distribution on the 350-element mesh (Figure 7.4(a)) and on the 1170-element mesh (Figure 7.4(b)) is presented.

(a) 350-element mesh   (b) 1170-element mesh
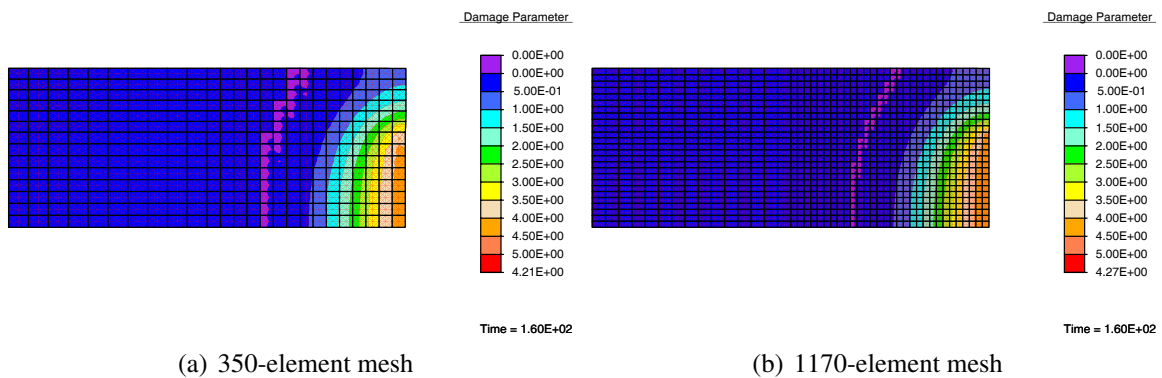
Figure 7.4.: Distribution of the damage parameter for the cracked brick problem at the end of the test using gradient enhanced *damage model I*

Infinitely long brick with a circular hole

The next example is an infinitely long brick with a circular hole subjected to tension, applied as uniform displacement at the ends of the specimen. The geometry of the problem is given in Figure 7.5 and, as in the previous example, it allows for a dimensional reduction of the problem to the plane strain case and the analysis of only one fourth of the domain owing to symmetry. The calculations are performed utilizing gradient enhanced *damage model I*, together with the parameters listed in the Table 7.2.

In the first part of the test, the behavior of the local material model is investigated. For this purpose four tests with increasingly refined meshes are calculated, Figure 7.6(a). The size of the inelastic zone, following discussion in the previous section, is induced by the domain discretization and it is equal to the size of an element. These values of the internal length are too small, thus leading to ill-posed discretized problem (6.41). Since this length becomes

E	ν	c_d	β_d	r_1
MPa		MPa·mm^2	MPa	MPa
18000	0.2	1.0	1.0	0.01

Table 7.2.: Material parameters used in the brick-with-a-hole test in conjuction with the gradient enhanced *damage model I*
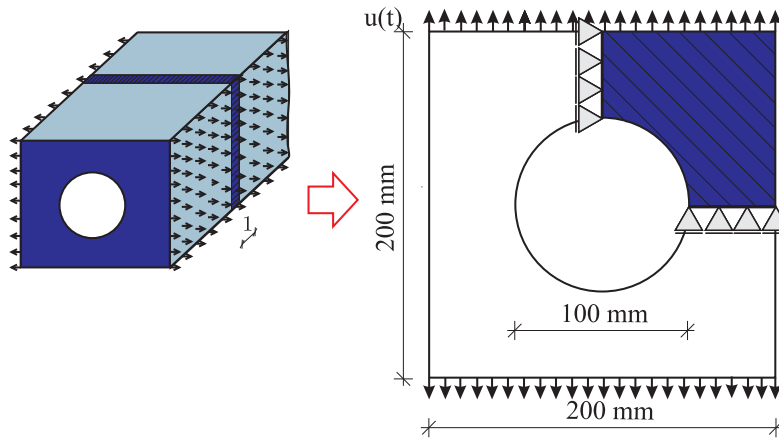
Figure 7.5.: Geometry of the brick-with-a-hole test

even smaller with mesh refinement, the bifurcation points occur even earlier, Figure 7.6(a). In contrast to that, the gradient enhanced model is successfully used to perform the calculation even very far in the softening range without large difficulties (Figure 7.6(b)). Additionally, analyses performed with 200, 800 and 1800 elements result in almost identical force-displacement curves, as it is seen in the same Figure. In all these tests biquadratic serendipity functions are employed in the approximation of the displacement field and bilinear functions in the approximation of the non-local variable field (Q2S/Q1 formulation). This formulation is selected following e.g. de Borst and Pamin (1996); Peerlings et al. (1998); Liebe (2003); Lorentz and Benallal (2005). In the context of implicit gradient models it is shown in Simone et al. (2003) that this is not necessary from the mathematical point of view. Namely, a completely valid solution of the problem in terms of primal variables (u and φ_d) and the inelastic variables is obtained using equal order of interpolation of the displacement field and the non-local variable field. The only drawback is a spurious stress-oscillation within elements, which would have to be post-processed in order to obtain usable results for the stress field. Owing to the fact that the regularization strategy investigated in this thesis results in a pure minimization problem rather than the mixed one, relation (4.24), the famous LBB-conditions do not have to be considered. Therefore one can select equal order of approximation of the primal fields, which results in almost indistinguishable force-displacement diagrams, Figure 7.6(c). Hence the mesh dependence of the overall structural response is removed as well.

The same holds for the damage distribution within the specimen. This is illustrated in Figure 7.7, where the distribution of the *Material Damage*, defined as percentage of the material stiffness loss

$$MD = (1.0 - f(d)) \cdot 100 \, [\%] \tag{7.1}$$

on the 200-element mesh (Figure 7.7(a)) and on the 1800-element mesh (Figure 7.7(b)) is presented. It is obvious that the evolution of the inelastic process (in this case damaging) is
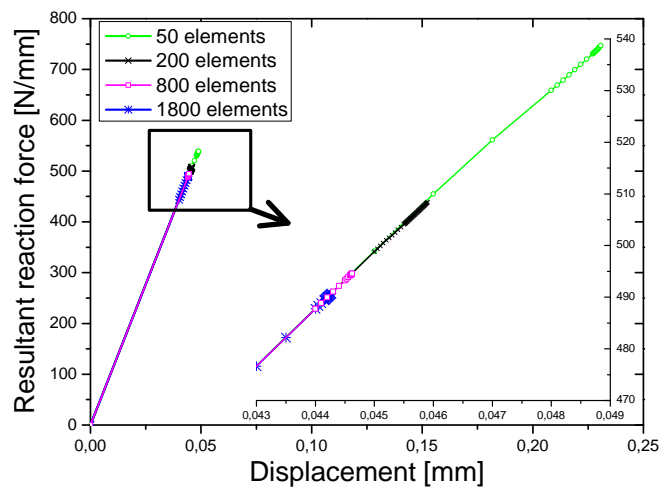
(a) Local model
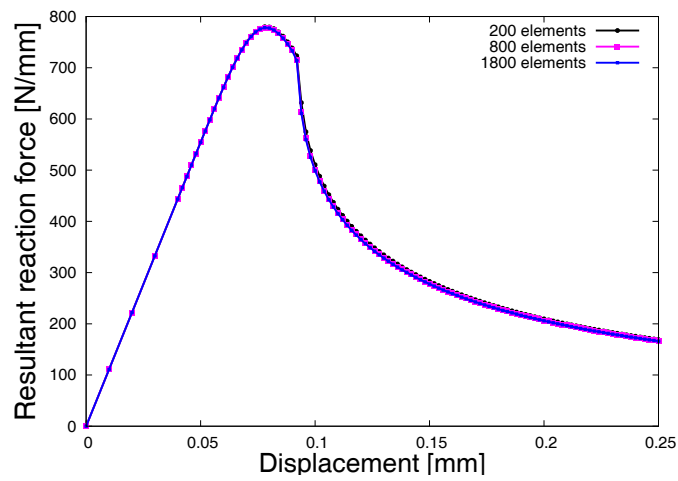
(b) Gradient enhanced model
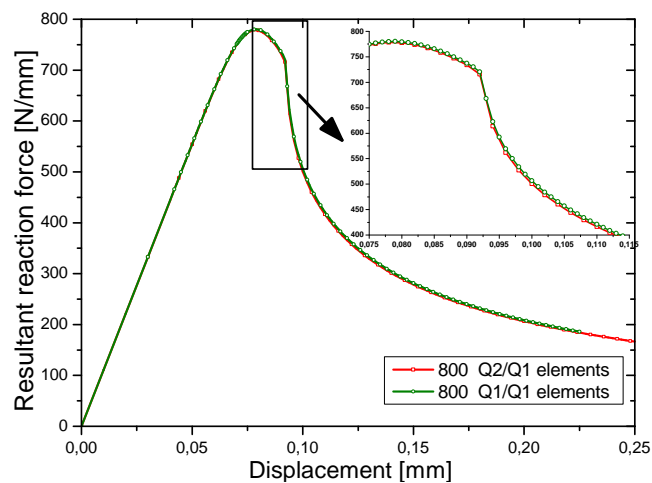
(c) Comparison between the results obtained using Q2S/Q1
and Q1/Q1 element formulation

Figure 7.6.: Load-displacement diagrams for the the brick-with-a-hole problem using gradi-
ent enhanced *damage model I*

not restricted to the one-element-row-width zone, as it was the case utilizing local model, but rather to some zone of final width, practically independent on the size of the finite elements used. Therefore, the internal material length is efficiently introduced into the model, leading to a well-posed continuum as well as discretized problem. Its value is implicitly introduced via gradient enhancement, therefore it depends on the values of the model parameters β_d and c_d, equation (5.4). Recalling the relation (5.14), and writing it as

$$(\varphi_d - d) - \frac{c_d}{\beta_d} \, \nabla^2 \varphi_d \;=\; 0, \tag{7.2}$$

one can state that the internal material length is defined by the ratio between the two enhancement parameters rather than by a single one. Hence, focusing an investigation on the influence of the ratio $\frac{c_d}{\beta_d}$ a series of tests on the semi-fine 800-element mesh is performed. The value of the gradient parameter c_d is varied, while all the other parameters remain fixed (including β_d which is set to be equal to one). The resulting force-displacement curves are given in the Figure (7.8(a)).

(a) 200-element mesh   (b) 1800-element mesh
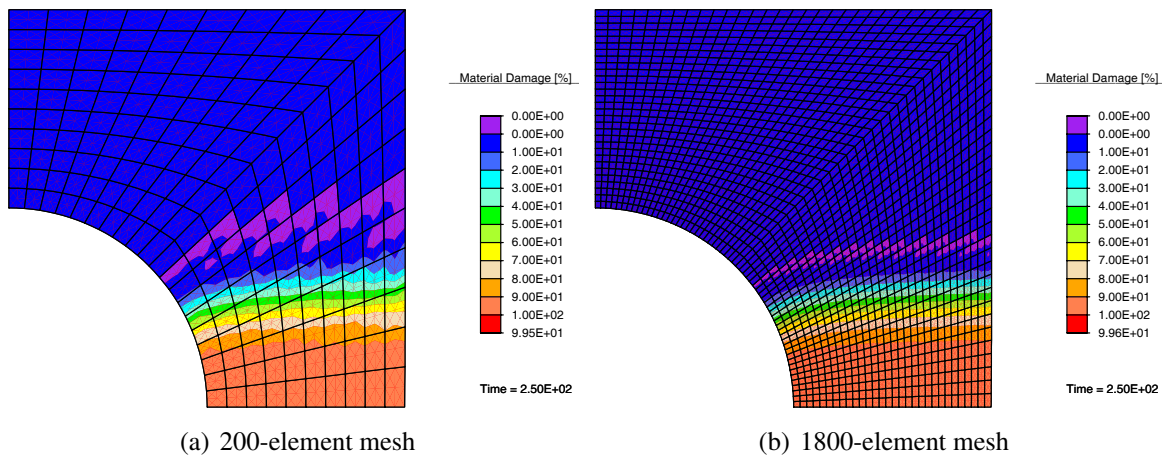
Figure 7.7.: Distribution of the *Material Damage* for the brick-with-a-hole problem at the end of the test using gradient enhanced *damage model I*

For small values (0.01-0.2) of the gradient parameter the calculations cannot be advanced far into the softening range due to numerical instabilities of the system of equations. However, values $c_d \geq 0.5$ result in successful regularization, and the calculations are completed without significant difficulties (Figure 7.8). Another property of the model is obvious from the same Figure: the higher the value of c_d is, the higher limit load on the structure is found. That is due to the fact that the increase of the gradient parameter results in smoothing of the damage parameter distribution along a wider activated zone, thus practically slowing its evolution down, as it is presented in Figure 7.8. The plots given there represent the damage distribution across the specimen, obtained for several distinct values of c_d, at the quasi-time (displacement) state denoted in the Figure 7.8(a).

Recalling the discussion in section 5.1, one can compare the difference between the non-local variable φ_d and the corresponding local potential function $H_\varphi(d)$, which in the case of *damage model I* is identical to the damage parameter itself (equation (5.3)). This difference is equal to the scaled Laplacian of the non-local field, relation (5.14), and it influences the damage threshold condition (5.17) via a quantity we named *non-local damage threshold*, equation (5.16). The distribution of both quantities at the state denoted in the Figure 7.8(a) is shown in Figure 7.9. The increase of the gradient parameter c_d for a fixed parameter $\beta_d = 1.0$ introduces a higher value of the length scale, as it is stated above, and therefore forces
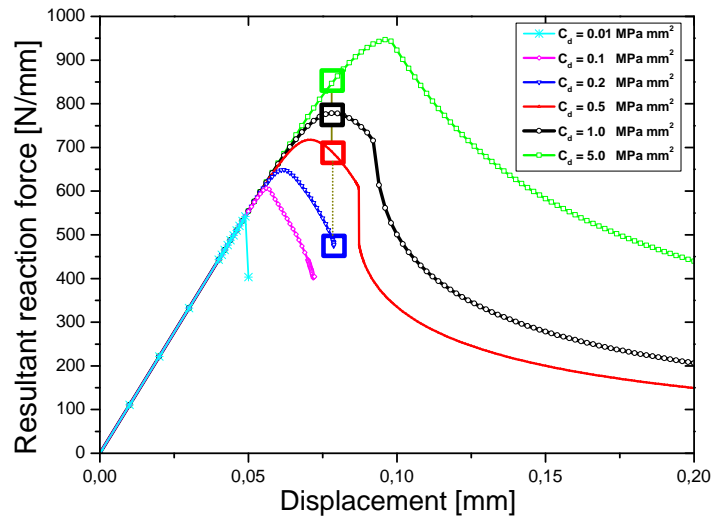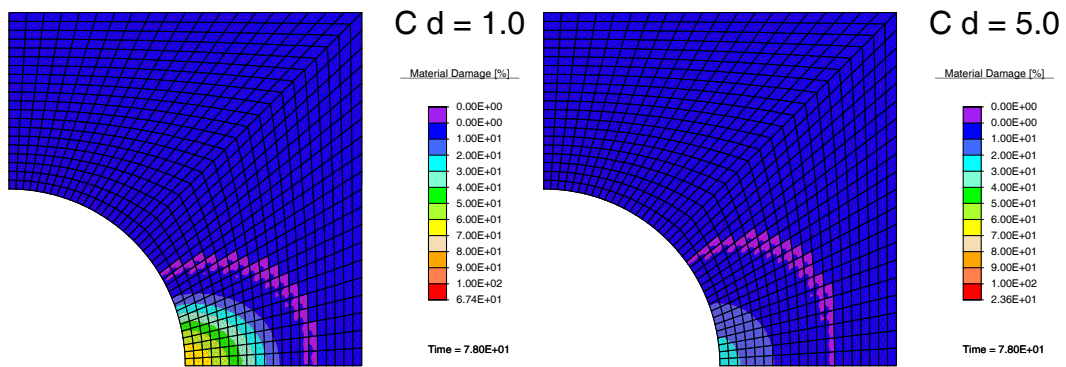
(a) Load-displacement diagrams
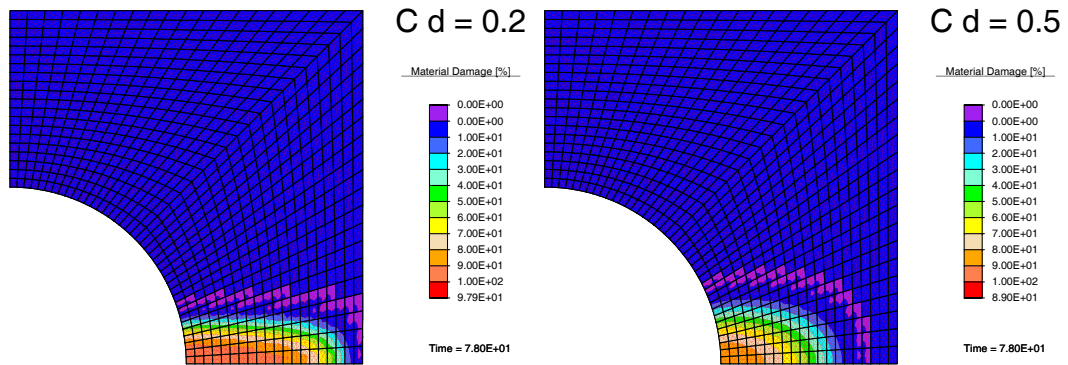
(b) *Material Damage* distribution for $c_d = 0.2$ (c) *Material Damage* distribution for $c_d = 0.5$

(d) *Material Damage* distribution for $c_d = 1.0$ (e) *Material Damage* distribution for $c_d = 5.0$

Figure 7.8.: Influence of the parameter c_d on the structural response and the *Material Damage* distribution for the brick-with-a-hole problem on the 800-element mesh at the test stage denoted in the Figure 7.8(a) for $\beta_d = 1.0$
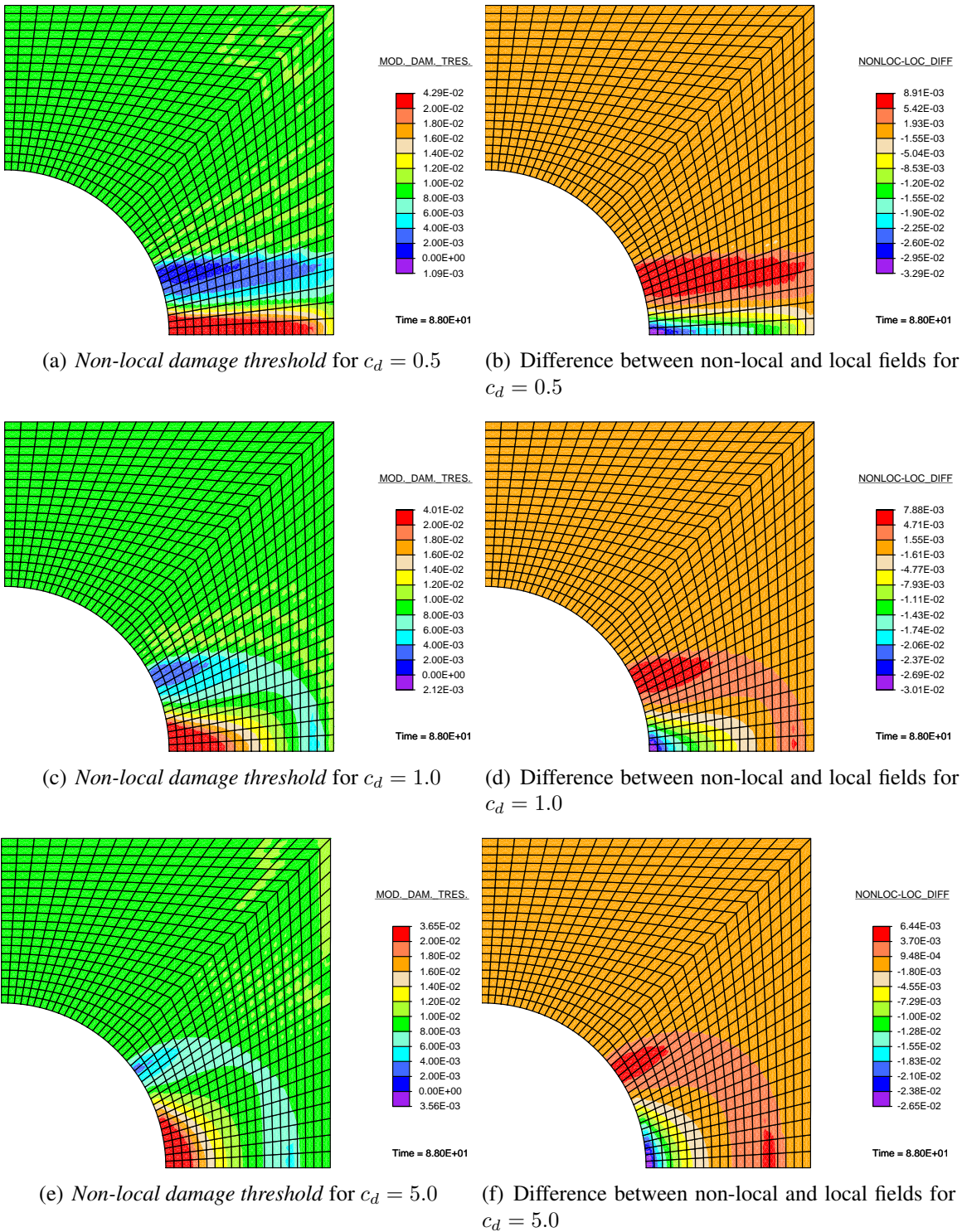
(a) *Non-local damage threshold* for $c_d = 0.5$

(b) Difference between non-local and local fields for $c_d = 0.5$

(c) *Non-local damage threshold* for $c_d = 1.0$

(d) Difference between non-local and local fields for $c_d = 1.0$

(e) *Non-local damage threshold* for $c_d = 5.0$

(f) Difference between non-local and local fields for $c_d = 5.0$

Figure 7.9.: Distribution of the selected problem quantities for the brick-with-a-hole problem on the 800-element mesh at the test stage denoted in the Figure 7.8(a) for $\beta_d = 1.0$

a smoother distribution of the non-local variable. Consequently, the differences between the non-local and corresponding local fields are smaller on the cost of wider spreading of the damage process zone, Figures 7.9(b), 7.9(d) and 7.9(f). As we commented in section 5.1, within the zone of excessive straining this difference is negative, while outside of the process zone the opposite is the case. In view of (5.16) and (5.17), such distribution implies an apparent increase of the damage strength in the localization zone (*non-local damage threshold*) and apparent decrease outside, Figures 7.9(a), 7.9(c) and 7.9(e). This is a reason for the increase of the structural strength observed in the Figure 7.8(a). As a remark, the original damage threshold is given in the Table 7.2 and is equal to 0.01.

7.1.2. Numerical examples involving gradient enhanced *damage model II*

In this section we focus on the investigation of the behavior of the gradient enhanced *damage model II*. In that purpose two representative examples are selected. The first one is the same problem treated in section 7.1.1 using *damage model I*, while the second one represents the simulation of the experiment investigating the cracking of an L-shaped concrete panel Winkler (2001).

Infinitely long brick with a circular hole

The geometry of the problem is already defined in Figure (7.5) together with the assumption of dimensional reduction and are not going to be repeated here. However, material parameters have to be specified owing to the fact that different material model is utilized, and they are summarized in Table 7.3. Following the discussion in section 7.1, the calculations are performed employing bilinear quadrilateral elements with equal order of aproximation of the displacement field and the non-local variable field (Q1/Q1).

E	ν	c_d	β_d	r_1	a_1
MPa		MPa$\cdot mm^2$	MPa	MPa	
18000	0.2	1500.0	1500.0	0.0222	0.5

Table 7.3.: Material parameters used in the brick-with-a-hole test in conjunction with the gradient enhanced *damage model II*

As in the case of the gradient enhanced *damage model I*, the resulting force-displacement diagrams, Figure 7.10(a), and the damage distribution within the structure, Figures 7.10(b) and 7.10(c) show mesh-objectivity. Hence, the *damage model II* is successfully regularized using the presented gradient enhancement strategy (Table 5.2). The difference between the non-local variable φ_d and the local potential function $H_\varphi(d)$ is presented in the Figure 7.10(d). As it is discussed in the section 5.1, it has to be positive in the localization zone and negative outside, which is evident. This difference gives rise to the change in the damage threshold accounting for non-local interaction, relation (5.31). The Figure 7.10(e) contains a distribution plot of the modified inelastic limit $R_{1\,NL}(d)$ normalized with the initial damage threshold value.
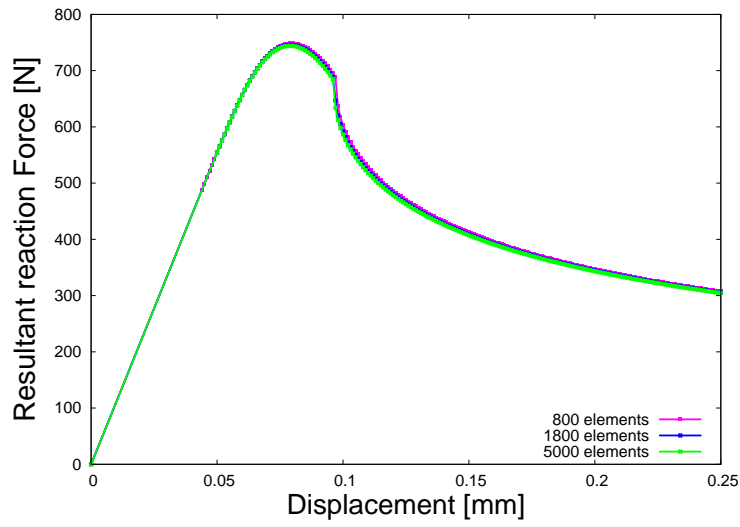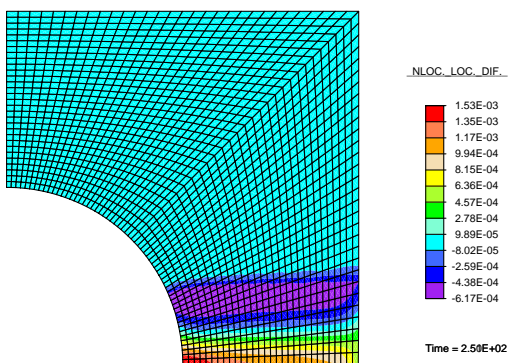
(a) Load-displacement diagrams for the brick with a hole problem using gradient enhanced *damage model II*
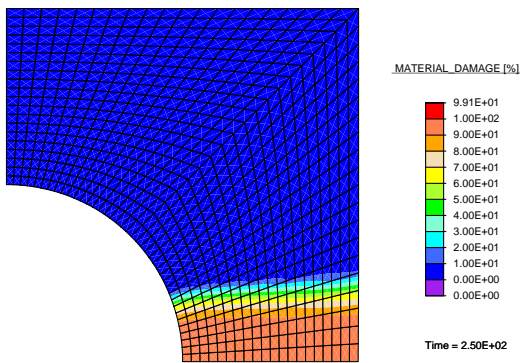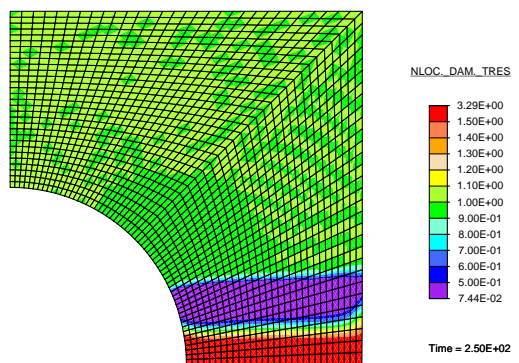

(b) *Material Damage* on 800-element mesh
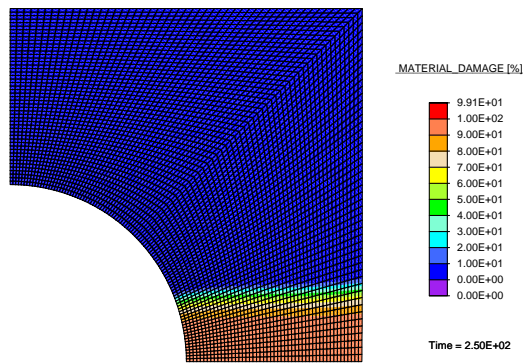
(c) *Material Damage* on 5000-element mesh

(d) Difference between non-local and local field on 1800-element mesh

(e) Normalized non-local damage threshold on 1800-element mesh

Figure 7.10.: Selected calculation results for the brick-with-a-hole problem at the end of the test using gradient enhanced *damage model II*

Concrete L-panel

The second example represents the simulation of the experiment investigating cracking of the L-shaped concrete panel. The experiment is performed on the University of Insbruck and it is documented in Winkler (2001). The geometrical characteristics of the samples are given in the Figure 7.11 together with the crack-pattern observed in the experiments, cf. Winkler (2001). The vertical arm of the specimen is clamped at the lower edge and the force is ap-
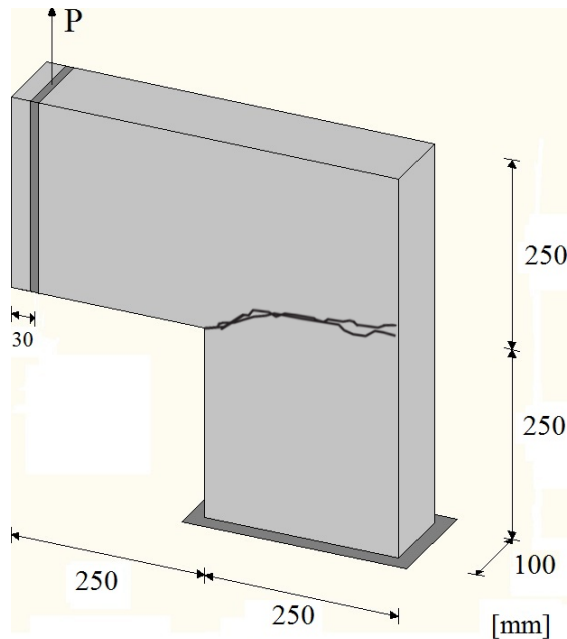
Figure 7.11.: Geometry of the L-Panel test together with the crack pattern from Winkler (2001)

E	ν	c_d	β_d	r_1	a_1
MPa		MPa·mm^2	MPa	MPa	
25850.0	0.18	10000.0	90000.0	$5.154 \cdot 10^{-4}$	0.12

Table 7.4.: Material parameters used in the L-panel test in conjunction with the gradient enhanced *damage model II*

plied via steel bar with the 20 mm diameter at the lower edge of the horizontal arm (precise position denoted in the Figure 7.11). For the characterization of the structural behavior of the specimen is the vertical displacement on the left edge of the horizontal arm measured, in addition to the the applied force value. Experiments are realized as displacement-driven. The material model parameters used in the calculation are specified in Table 7.4. Two numerical tests are performed: the first one employing 2300 trilinear (8-node) elements and the second one employing 4300 elements of the same type (the same order of interpolation is selected for the displacement field and the non-local variable field). The resulting force-displacement diagrams are shown in Figure 7.12, together with the experimentally obtained curves from Winkler (2001) and the simulation results from Huber (2006). The overall behavior of the structure in the post-peak part of the simulation is well approximated even using relatively small number of elements. Employing more advanced material models, like
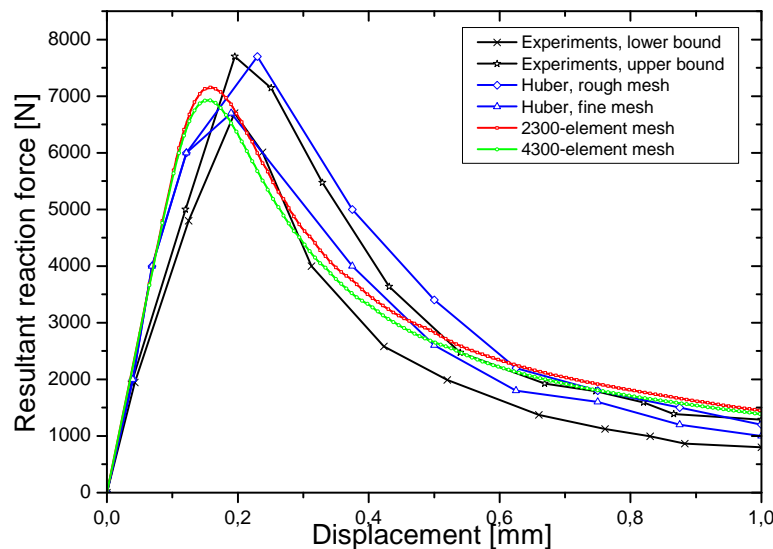
Figure 7.12.: Load-displacement diagrams for the L-panel problem using gradient enhanced *damage model II*

the one in Huber (2006), one could obtain improvement in the simulation results. The difference occurring before peak (even in elastic range) is attributed in Oliver et al. (2002) to rigid body rotation caused by slip in the mechanical connection between the specimen and the measuring device. In the work of Schütt (2005) the correction procedure is proposed in order to remove this ambiguity. However, it seems that this difference has little effects on the post-peak behavior, cf. Huber (2006).

The damage distribution within the structure obtained by calculations using a gradient enhanced damage model is shown in 7.13(a) for 2300-element mesh and 7.13(c) for 4300-element mesh, while the Figures 7.13(b) and 7.13(d) contain the distribution of the non-local variable φ_d. All plots are related to the end of the test, i.e. the displacement $u_y = 1.0mm$. The damage zone obtained in both tests follows the curved crack pattern observed in the experiments, Figure 7.11. Owing to finer discretization, the initial crack curvature is better depicted by the 4300-element than by 2300-element. This is due to to the fact that for the precise reproduction of the curved crack pattern one requires very fine mesh, cf. Kuhl et al. (2000). Nevertheless, the results show good overall agreement with the experimental data implying that the regularization of the *damage model II* via gradient enhancement of the free-energy function is successfully performed.

## 7.2. Problems involving plastic material model

In this section we present the results of the calculations enrolling regularized *plastic models I* and *II*. In order to investigate the influence of the proposed regularization, numerical tests are performed on the benchmark brick-with-a-hole problem utilizing both models and selected results are presented in what follows.
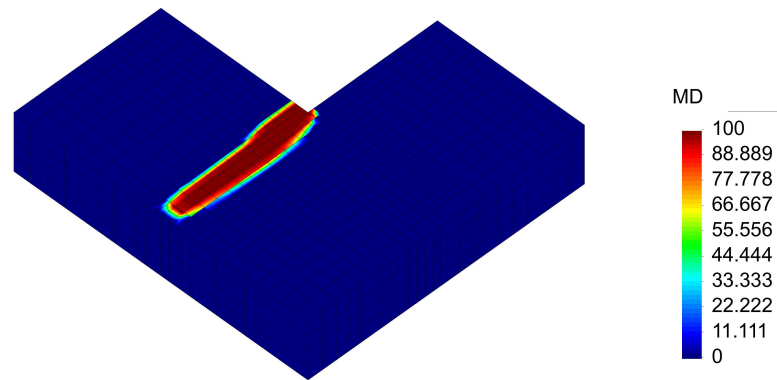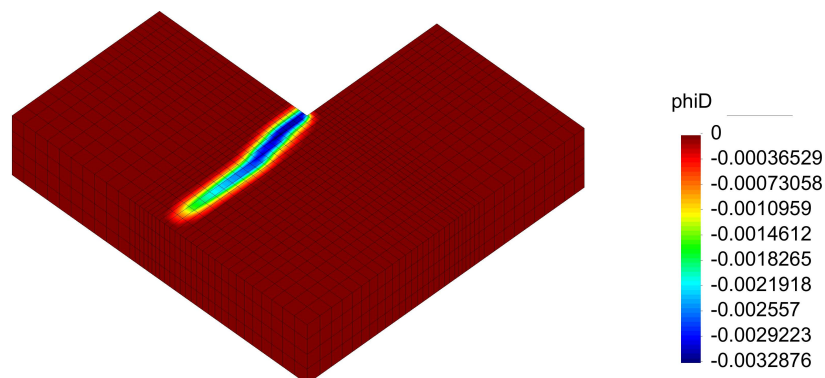
(a) *Material Damage* on 2300-element mesh
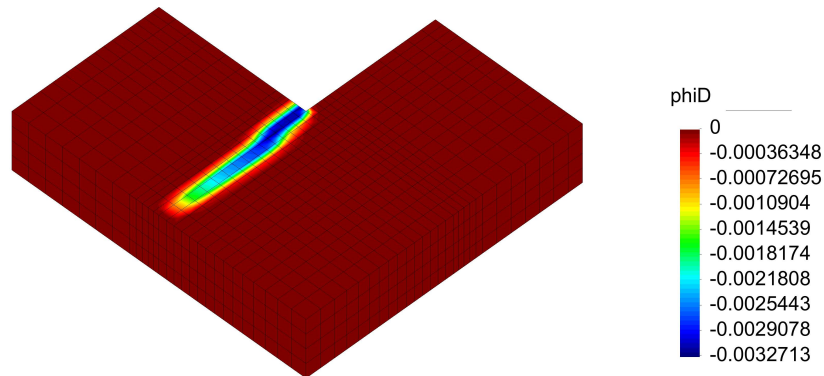
(b) Non-local variable on 2300-element mesh
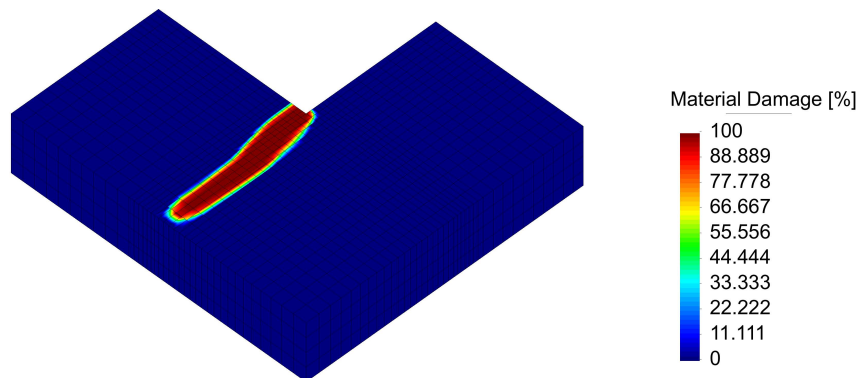
(c) *Material Damage* on 4300-element mesh

(d) Non-local variable on 4300-element mesh

Figure 7.13.: Distribution of the selected problem quantities for the L-panel problem at the end of the test using gradient enhanced *damage model II*

7.2.1. Numerical examples involving gradient enhanced *plastic model I*

The *plastic model I* is specified in Table 3.3 and its enhancement-related quantities are given in Table 5.3. Geometry and loading are already defined in section 7.1.1 and values of the model parameters are specified in Table 7.5. In these tests biquadratic serendipity functions are used in the approximation of the displacement field, whereas the non-local variable field is approximated by bilinear functions (Q2S/Q1 formulation).

E	ν	c_P	β_P	r_2	K_H
MPa		MPa$\cdot mm^2$	MPa	MPa	MPa
18000.0	0.2	1250.0	1250.0	20.0	-300.0

Table 7.5.: Material parameters used in the brick-with-a-hole test in conjunction with the gradient enhanced *plastic model I*

The first part of the test is committed, as in the example involving damage model, to the investigation of the behavior of the local (without the gradient regularization) plastic material model. As it is discussed in the section 3.3, the use of the classical (local) formulation of the model leads to an ill-posed continuum problem due to absence of the characteristic material length. In the context of the finite element method this length is substituted by the characteristic length of the discretization mesh, resulting in strong dependence of the results on the finite element mesh, as already stated in section 7.1. This behavior is obvious in Figure 7.14(a) that contains force-displacement diagrams obtained employing the set of three increasingly refined finite element meshes. On the contrary, the calculations performed utilizing the gradient enhanced model on the same discretization meshes (with 200, 800 and 1800 Q2S/Q1 elements) result in a structural response in terms of force-displacement diagrams that clearly shows convergence, Figure 7.14(b).

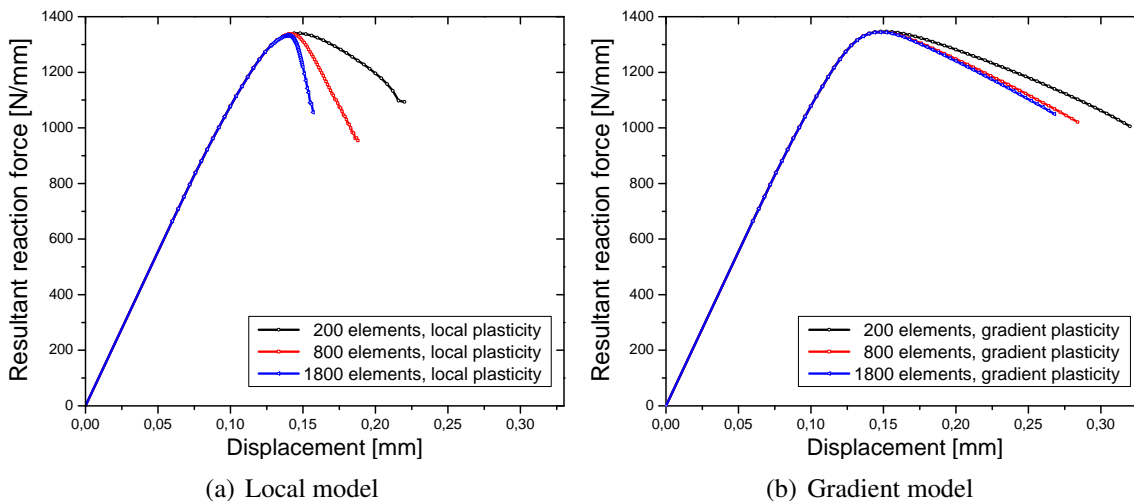(a) Local model   (b) Gradient model

Figure 7.14.: Load-displacement diagrams for the brick-with-a-hole problem using *plastic model I*

The illustration of the pathological behavior of the local *plastic model I* described above is given in Figure 7.15. Owing to the absence of an intrinsic length parameter in the model, deformation and consequently inelastic process localize within the shear band whose width

is defined by the size of the support of the finite element approximation functions in the process zone. That results in more rapid structural strength loss on finer meshes observed in the Figure 7.14(a).

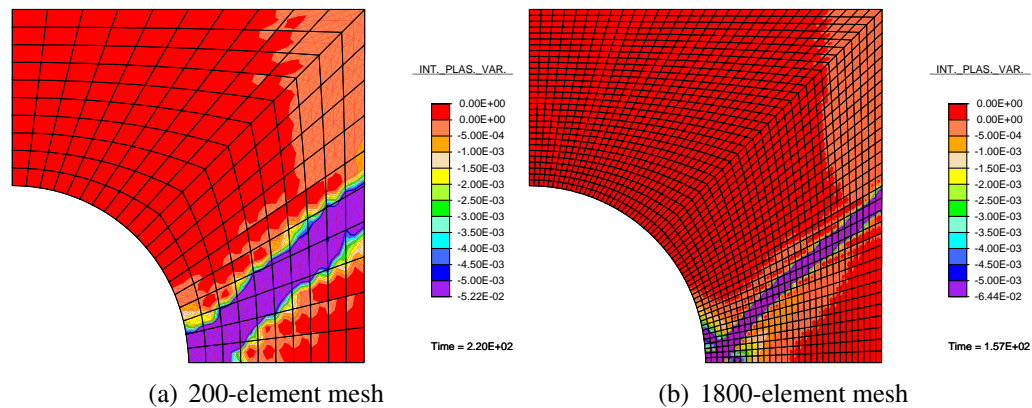(a) 200-element mesh   (b) 1800-element mesh

Figure 7.15.: Distribution of the plastic softening variable for the brick-with-a-hole problem at the last converging loading increment using local *plastic model I*

Taking a closer look on the distribution of the softening parameter α_P on the 200-element mesh (Figure 7.16(a)) and on the 1800-element mesh (Figure 7.16(b)) obtained utilizing the gradient-enhanced model, one can identify the source of the small difference in the post-peak response noticed in Figure 7.14(b). It occurs because the 200-element mesh is simply too coarse to accurately capture the inelastic process zone, although it qualitatively delivers good approximation.

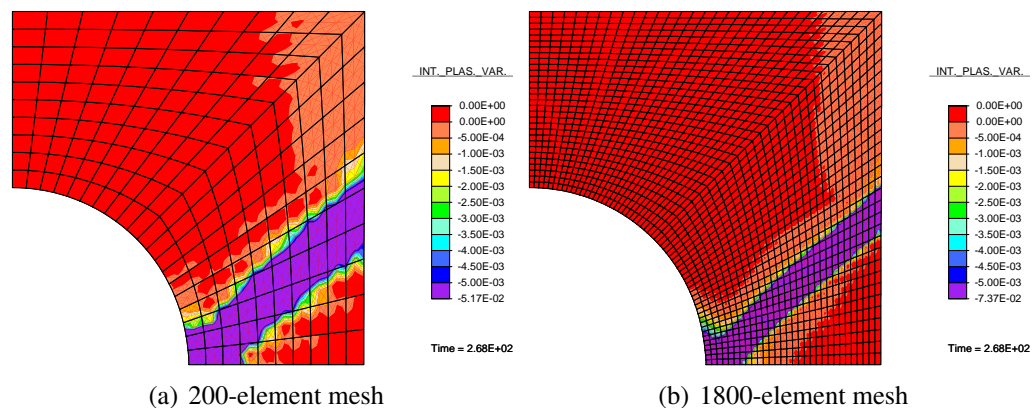(a) 200-element mesh   (b) 1800-element mesh

Figure 7.16.: Distribution of the plastic softening variable for the brick-with-a-hole problem at the end of the test using gradient enhanced *plastic model I*

7.2.2. Numerical examples involving gradient enhanced *plastic model II*

The *plastic model II* is specified in Table 3.4 and its enhancement-related quantities are given in Table 5.4. As it is already mentioned, the properties of the gradient-enhanced model are going to be investigated utilizing the brick-with-a-hole problem. The problem setting, i.e. geometry and loading are already defined in section 7.1.1, whereas are the values of the model parameters specified in Table 7.6. The two sets of gradient parameters carrying indices 1 and 2 correspond to the types of the potential functions $\boldsymbol{H}_\varphi$ (Tables 5.3 and 5.4)

used in the formulation of the interaction potential, respectively. Following the discussion in section 7.1.1, the calculations are performed employing bilinear quadrilateral elements with equal order of approximation of the displacement field and the non-local variable field (Q1/Q1).

E	ν	c_{P1}	β_{P1}	c_{P2}	β_{P2}	$r_{2,0}$	$r_{2,\infty}$	K_H
MPa		MPa$\cdot mm^2$	MPa	MPa$\cdot mm^2$	MPa	MPa	MPa	
18000.0	0.2	500.0	2000.0	10.0	40.0	20.0	0.5	20.0

Table 7.6.: Material parameters used in the brick-with-a-hole problem in conjunction with the gradient enhanced *plastic model II*

(a) Local model

(b) Gradient enhanced model, $H_\varphi(\alpha_P) = \alpha_P$ (variant 1)

(c) Gradient enhanced model, $H_\varphi(\alpha_P) = W(\alpha_P) - W(0)$ (variant 2)

(d) Comparison between the results obtained using Q2S/Q1 and Q1/Q1 element formulation using gradient enhanced model, variant 1
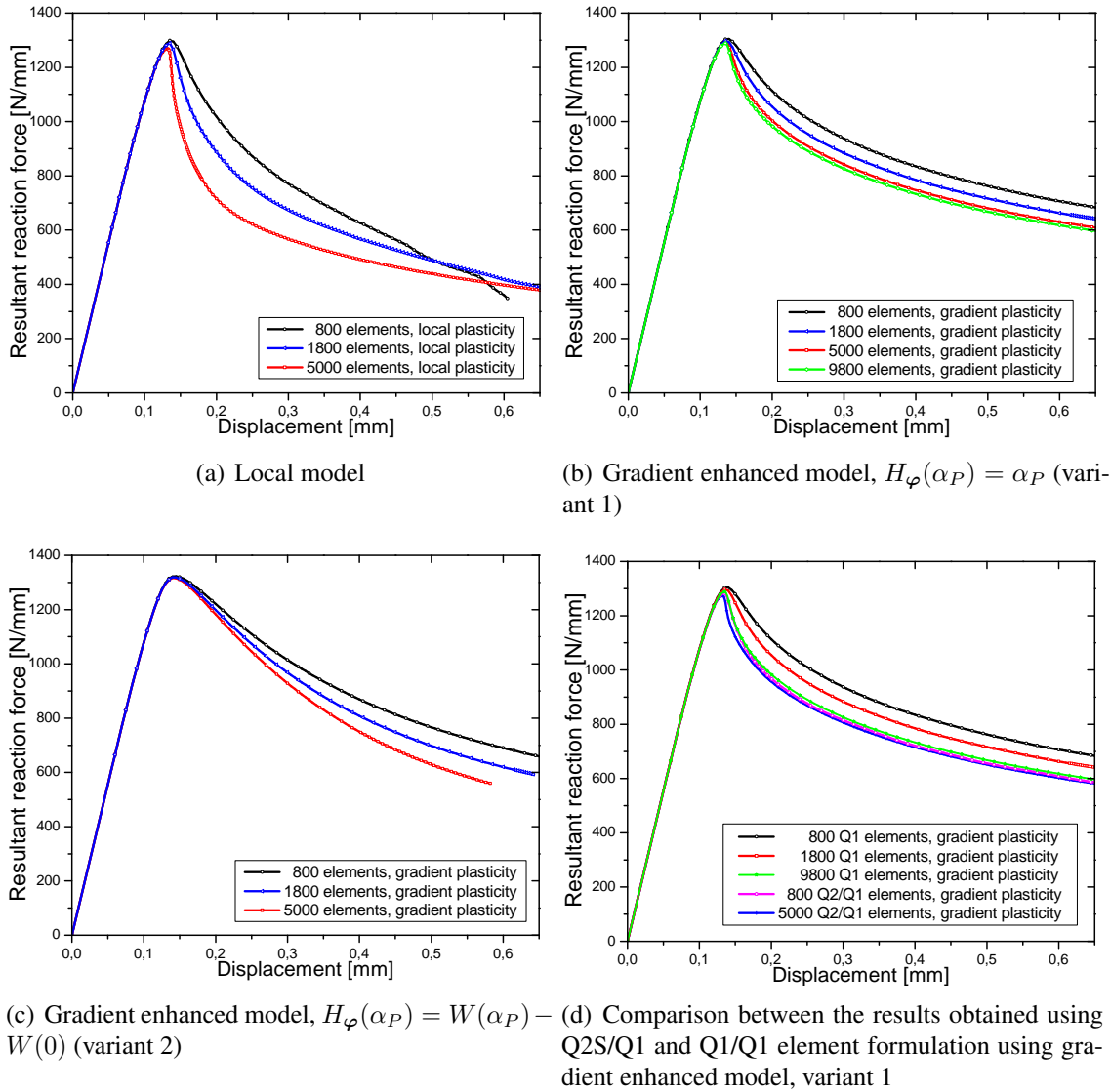
Figure 7.17.: Load-displacement diagrams for the the brick-with-a-hole problem using gradient enhanced *plastic model II*

Let us start by investigating the behavior of the local plastic material model. In that purpose three numerical tests, utilizing meshes with 800, 1800 and 5000 elements, are performed. The resulting force-displacement diagrams, Figure 7.17(a) show the typical mesh-dependent behavior of softening materials. Not only these diagrams differ: the plots of the distribution

of the plastic softening variable, Figures 7.18(a) and 7.18(b), reveal that the shear bands realized on the 800-element-mesh and on the 5000-element mesh have considerably different shape in addition to different size.
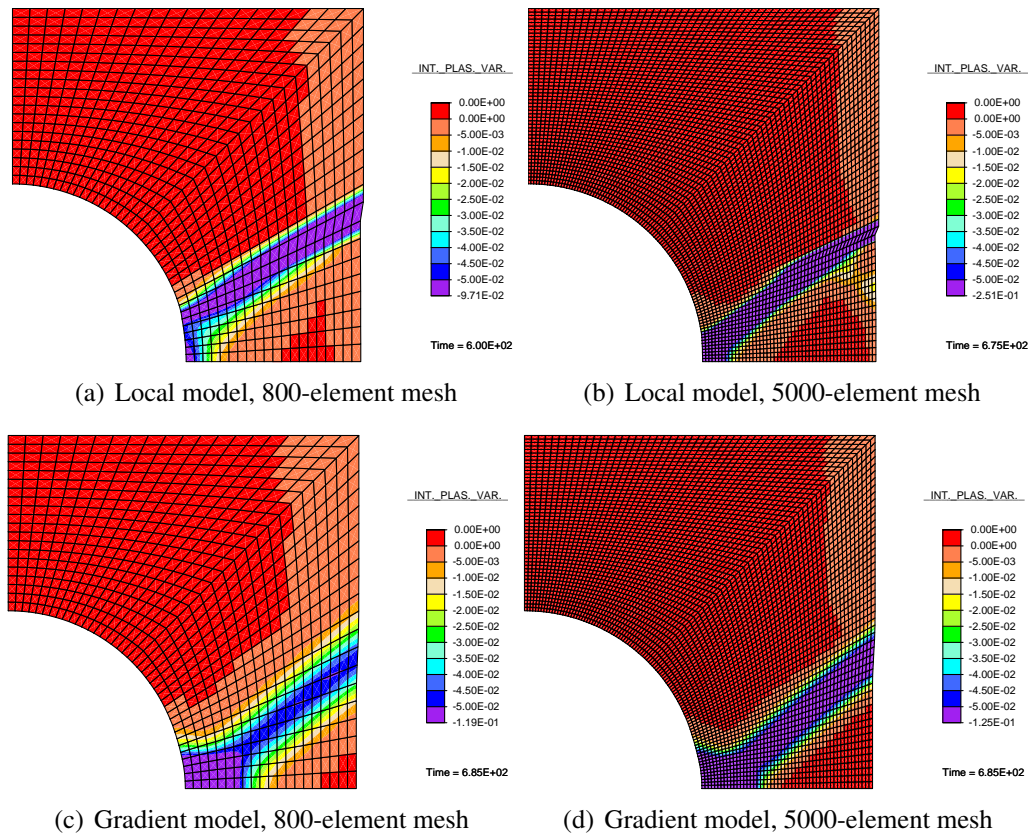

(a) Local model, 800-element mesh

(b) Local model, 5000-element mesh

(c) Gradient model, 800-element mesh

(d) Gradient model, 5000-element mesh

Figure 7.18.: Distribution of plastic softening variable for the brick-with-a-hole problem at the end of the test using gradient enhanced *plastic model II*

These problems are efficiently removed if one utilizes a gradient enhanced plastic model based on the first variant of the enhancement, specified in the Table 5.3. The force-displacement diagrams presented in the Figure 7.17(b) show obvious convergence with mesh refinement, however at a slower rate than in the case involving the gradient enhanced damage models. This is due to a narrow localization zone which cannot be entirely captured with the rough mesh, Figures 7.18(c) and 7.18(d). Although the geometry of the shear band is approximated well with the 800-element mesh, Figure 7.18(c), for the approximation of the strain field and consequently the softening variable this mesh is simply too coarse. Utilization of the quadratic serendipity functions in the approximation of the displacement field improves the behavior significantly, as it is manifested in the Figure 7.17(d).

In Figure 7.18 it can additionally be noted that the local plastic model is not able to accurately approximate neither shape nor size of the shear band. Moreover, spurious localization of the deformation can occur governed solely by discretization mesh, which can be seen in Figure 7.18(a). The shear band presented there is obviously aligned with a conveniently oriented row of elements. This is caused, as it is already discussed in section 3.3, by the ill-posedness of the underlying continuum problem. The gradient enhanced model, however, is well posed and successfully approximates the evolving shear band.

Application of the second variant of the gradient enhancement on the *plastic model II*, specified in the Table 5.4, does not lead to successful regularization, as it is obvious from Figure
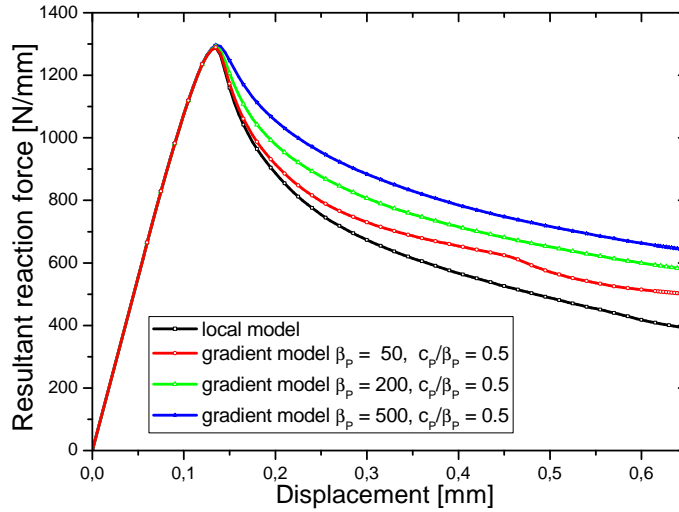
Figure 7.19.: Influence of the change in the parameter β_P on the load-displacement diagrams for the brick-with-a-hole problem for the fixed ration $c_P/\beta_P = 0.5$ utilizing *plastic model II*

7.17(c). Although the enhanced model behaves initially significantly better than the one based on the first variant of the regularization (Figure 7.17(c)), with time its advantage deteriorates. The reason behind the growing dependence on the discretization mesh evident in Figure 7.17(c) is already stated in section 5.2. Namely, owing to properties of the potential function $H_\varphi(\alpha_P)$, the relations (5.61) and (5.63) imply that the influence of non-local interaction declines with the evolving plastic process, which is exactly what is observed analyzing calculation results.

The gradient-enhanced model, as it is already discussed, introduces the internal material length implicitly and it depends on the values of the model parameters β_P and c_P. Recalling the second order partial differential equation that has to be satisfied by the non-local variable (4.37) and writing it as

$$(\varphi_P - H_\varphi(\alpha_P)) - \frac{c_P}{\beta_P}\nabla^2\varphi_P \; = \; 0, \tag{7.3}$$

the square of the internal material length can be identified as the ratio $\frac{c_P}{\beta_P}$. Its influence for the fixed value of the parameter β is already investigated in the context of gradient-enhanced damage model, section 7.1.1. Here we focus on the opposite case: the ratio between the two enhancement parameters is kept fixed, while the parameter β_P changes its value. The set of tests on the 1800-element mesh is performed utilizing the first variant of the gradient enhancement (the one with the plastic softening parameter itself used in the definition of the interaction potential). The resulting force-displacement diagrams, Figure 7.19, reveal that the increase of β_P while keeping the ratio $\frac{c_P}{\beta_P}$ fixed produces the same consequences as the converse case: the higher the value of β_P is, the stronger influence of the gradient enhancement is found. In order to explain this behavior, let us recall the definition of the micromechanical driving force η_P

$$\eta_P \; = \; \underbrace{-W'(\alpha_P)}_{\hat{\eta}_P} + \underbrace{\beta_P\,(\varphi_P - \alpha_P)}_{\tilde{\eta}_P}. \tag{7.4}$$

In view of (7.3) it follows from (7.4) that increasing any of the two multipliers in $\tilde{\eta}_P$ while keeping the other one fixed results in the increase of the interaction influence.

7.3. Problems involving coupled damage-plastic material models

In this section we present the results of the calculations enrolling regularized coupled *damage-plastic models I* and *II*. The properties of the regularization procedure and its influences are investigated in numerical tests, which are performed utilizing both models on the brick-with-a-hole benchmark problem. The selected results of the tests are presented in the rest of this section.

7.3.1. Numerical examples involving gradient enhanced *damage-plastic model I*

The coupled *damage-plastic model I* is specified in Table 3.5 and its enhancement-related quantities are given in the Table 5.5. Geometry, boundary and loading conditions of the brick-with-a-hole benchmark problem are already defined in the section 7.1.1.

An example with gradient enhanced damage model combined with local hardening plasticity

In the first test we investigate the behavior of the model obtained when the gradient-enhanced *damage model I* is coupled with the local hardening plasticity described by the *plastic model I*. It should be mentioned that this type of coupling is utilized in most works on regularized coupled damage-plastic modeling, cf. de Borst et al. (1999); Makowski et al. (2006); Nedjar (2001). In these tests biquadratic serendipity functions are used in the approximation of the displacement field, whereas is the non-local variable field approximated by bilinear functions (Q2S/Q1 formulation). The material parameters presented in the Table 7.7 are applied in the calculation.

E	ν	c_d	β_d	r_1	r_2	K_H	c_P	β_P
MPa		MPa$\cdot mm^2$	MPa	MPa	MPa		MPa$\cdot mm^2$	MPa
18000	0.2	1.0	1.0	0.01	20.0	1000.0	0.0	0.0

Table 7.7.: Material parameters used in the brick-with-a-hole problem in conjunction with the gradient enhanced *damage model I* coupled with the local *plastic model I*

The force-displacement diagrams obtained from the calculations on variably fine meshes show very little differences, Figure 7.20(a). That was expected since the hardening plastic behavior does not introduce a new source of irregularity (apart from rarely cases of non-associated plasticity formulations with very low values of hardening parameter, cf. Kuhl et al. (2000)). The same holds for the distribution of damage and plastic deformation within the specimen, taking into consideration that on a finer mesh more precise post-processing can be performed. This is illustrated in Figure 7.21, which presents the distribution of the *Material Damage* and the plastic hardening variable at the end of the test.

However, the decrease of the plastic hardening parameter K_H results in the deterioration of the convergence rate of the results. That can be clearly noticed in the Figure 7.20(b),

(a) Hardening parameter $K_H = 1000.0$ (b) Hardening parameter $K_H = 1.0$
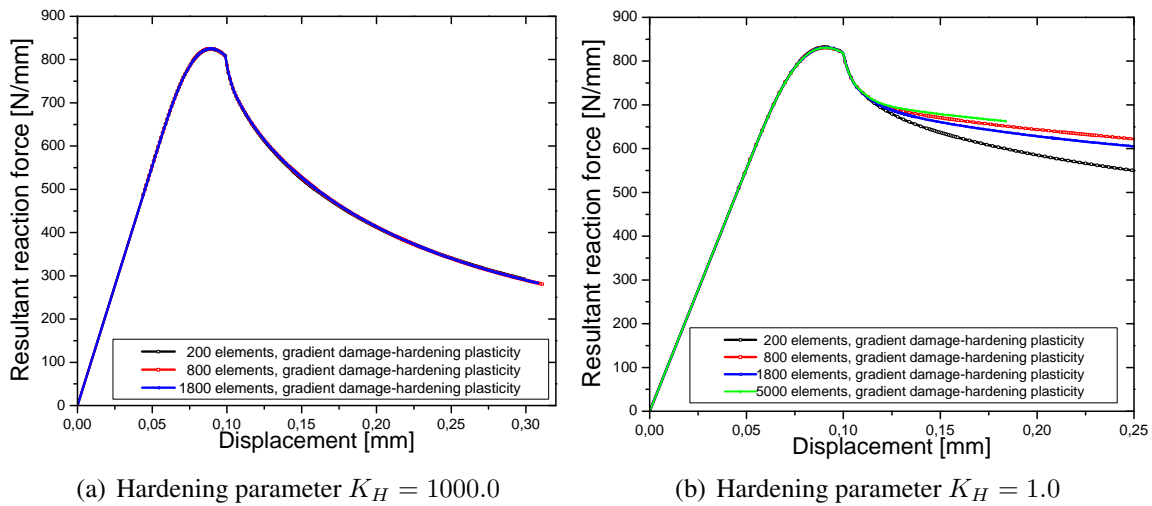
Figure 7.20.: Load-displacement diagrams for the brick-with-a-hole problem using using gradient enhanced *damage model I* combined with the local *plastic model I*
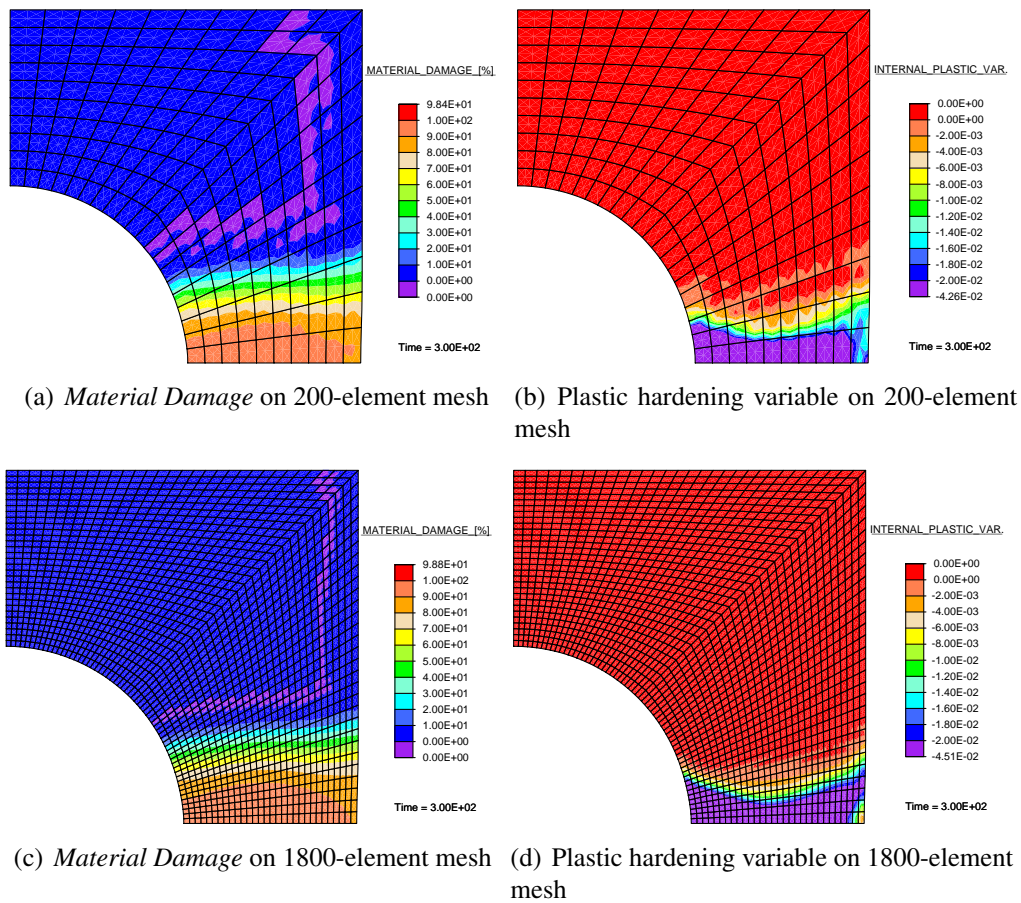

(a) *Material Damage* on 200-element mesh   (b) Plastic hardening variable on 200-element mesh

(c) *Material Damage* on 1800-element mesh   (d) Plastic hardening variable on 1800-element mesh

Figure 7.21.: Distribution of internal variables for the brick-with-a-hole problem at the end of the test using gradient enhanced *damage model I* combined with the local *plastic model I*

which contemplates the force-displacement diagrams obtained for a very small value of K_H. Further decrease of the hardening parameter ($K_H < 0$) leads to softening plastic behavior and therefore to an additional source of the irregularity in the problem. This type of coupled model is investigated next.

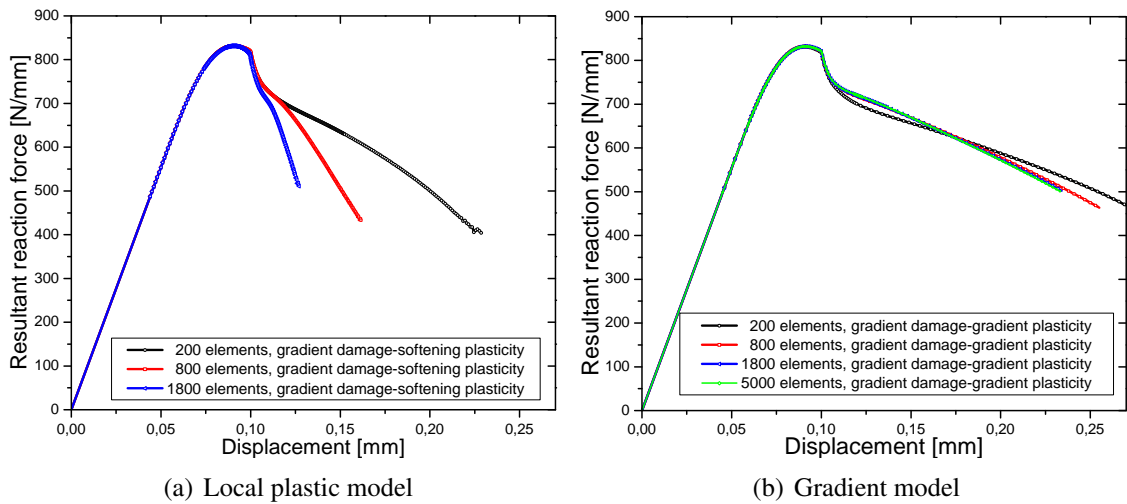(a) Local plastic model

(b) Gradient model

Figure 7.22.: Load-displacement diagrams for the the brick-with-a-hole problem using gradient enhanced *damage-plastic model I* for the negative plastic hardening parameter $K_H < 0$ (plastic softening)

An example of a gradient enhanced damage model combined with a softening plastic model

In the next test the behavior of the coupled *damage-plastic model I* accounting for softening plasticity (parameter $K_H < 0$) is investigated. The approximation of the displacement field is attained utilizing biquadratic serendipity type functions, whereas the non-local variable field is approximated by bilinear functions (Q2S/Q1 formulation). The values of the model parameters used in the calculation are given in Table 7.8. This test is, as the one in

E	ν	c_d	β_d	r_1	r_2	$K_{H\,1}$	$K_{H\,2}$	c_P	β_P
MPa		MPa$\cdot mm^2$	MPa	MPa	MPa	MPa	MPa	MPa$\cdot mm^2$	MPa
18000	0.2	1.0	1.0	0.01	20.0	0.0	-500.0	1250.0	1250.0

Table 7.8.: Material parameters used in the brick-with-a-hole problem in conjunction with the gradient enhanced coupled *damage-plastic model I*

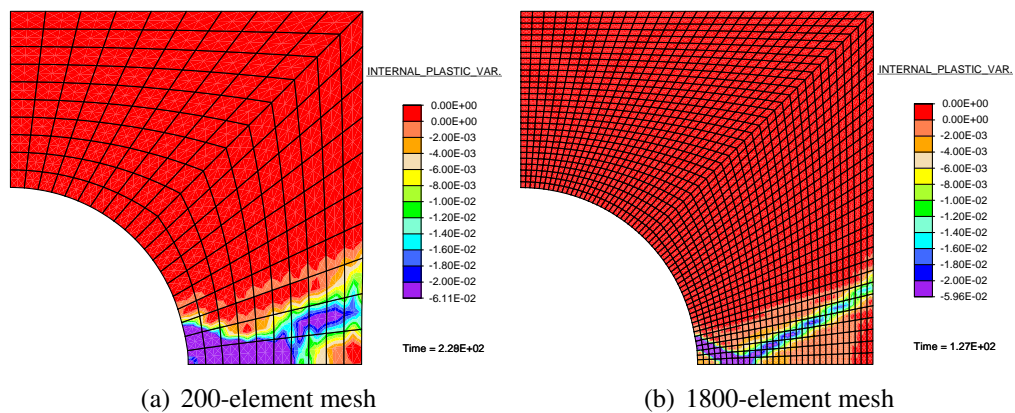(a) 200-element mesh

(b) 1800-element mesh

Figure 7.23.: Distribution of the plastic softening variable for the brick-with-a-hole problem at the end of the test using gradient enhanced damage model combined with local plastic model with $K_H < 0$

the previous example, performed in two stages: first employing gradient enhanced damage

combined with local softening plasticity, and afterwards using full gradient enhancement of the coupled *damage-plastic model I*. The calculations on three increasingly refined meshes (with 200, 800 and 1800 elements) facilitate the comparison of the typical behavior of standard and regularized models involving a softening regime. The resulting force-displacement diagrams for the first case (combination of gradient damage and local softening plasticity) are presented in the Figure 7.22(a), with noticeable strong mesh dependence of the obtained results. In the first part of the test, up to the displacement of approximately 0.1 mm, the dominating inelastic process is damage (for the selected set of material parameters). Afterwards, however, plasticity becomes dominant due to the fact that it is formulated in the effective stress space and it remains the leading inelastic process until the end of the test. Owing to the classical (local) formulation of the plastic model, which does not include an internal material length, the boundary value problem defined in the section 4.3 becomes ill-posed. The gradient enhancement of the damage parameter alone is not enough to regularize the problem, and one obtains localization of plastic process within a shear band, whose width is restricted solely by the discretization mesh (Figure (7.23)).

(a) *Material Damage* on 200-element mesh

(b) Plastic softening variable on 200-element mesh

(c) *Material Damage* on 1800-element mesh
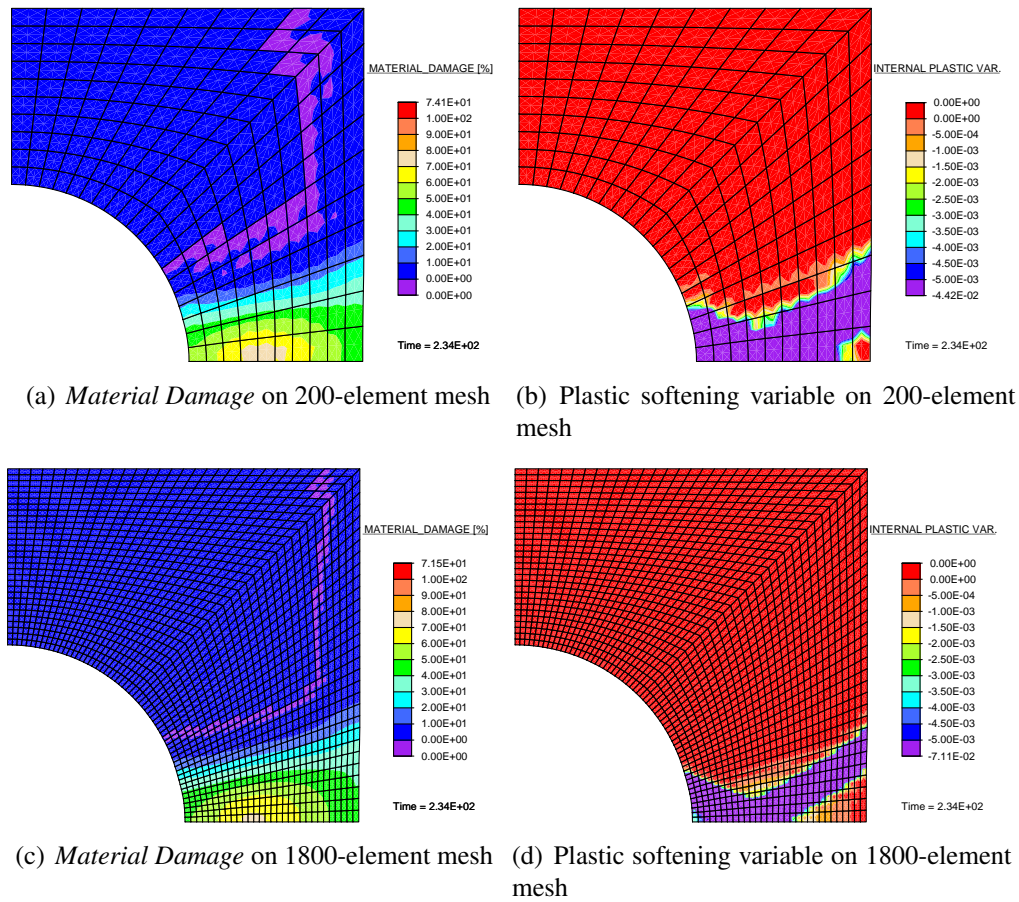

(d) Plastic softening variable on 1800-element mesh

Figure 7.24.: Distribution of internal variables for the brick-with-a-hole problem at the end of the test using gradient enhanced coupled *damage-plastic model I*

In contrary to that, utilization of the model introducing gradient enhancement of both damage parameter and plastic softening variable results in significantly improved behavior in the softening regime, Figure 7.22(b). There is obvious convergence of the structural response and thus removed mesh dependence. The small difference in the post-peak response is mainly due to the fact that the 200-element mesh is simply to coarse to quantitatively accurately capture the evolving plastic shear band. That can be clearly seen in the Figure (7.24), where the distribution of the softening parameter α_P on the 200-element mesh, Figure 7.24(b), and on the 1800-element mesh, Figure 7.24(d) at the final stage of the test is

presented. In addition, Figure 7.24 contains the plots of the *Material Damage*, which are depicted for the calculations on the 200-element mesh (Figure 7.24(a)) and on the 1800-element mesh (Figure 7.24(c)) at the end of the loading history. Obviously, the damage zone is well captured even with a very coarse mesh, due to its relatively simple geometry (in contrast to the plastic zone).

7.3.2. Numerical examples involving gradient enhanced coupled *damage-plastic model II*

The final example concerns the application of the gradient enhanced *damage-plastic model II* in the numerical tests performed on the benchmark brick-with-a-hole problem, whose geometry, boundary and loading conditions are already defined in the section 7.1.1. Following the discussion in the section 7.1.1, the calculations are performed employing bilinear quadrilateral elements with equal order of aproximation of the displacement field and the non-local variable field (Q1/Q1). The material parameters presented in Table 7.9 are applied in the calculation.

E	ν	c_d	β_d	r_1	$r_{2,0}$	$r_{2,\infty}$	K_H	c_P	β_P
MPa		MPa$\cdot mm^2$	MPa	MPa	MPa	MPa		MPa$\cdot mm^2$	MPa
18000	0.2	1.0	1.0	0.01	20.0	0.5	20.0	2000.0	500.0

Table 7.9.: Material parameters used in the plate-with-a-hole test in conjunction with the gradient enhanced coupled *damage-plastic model II*
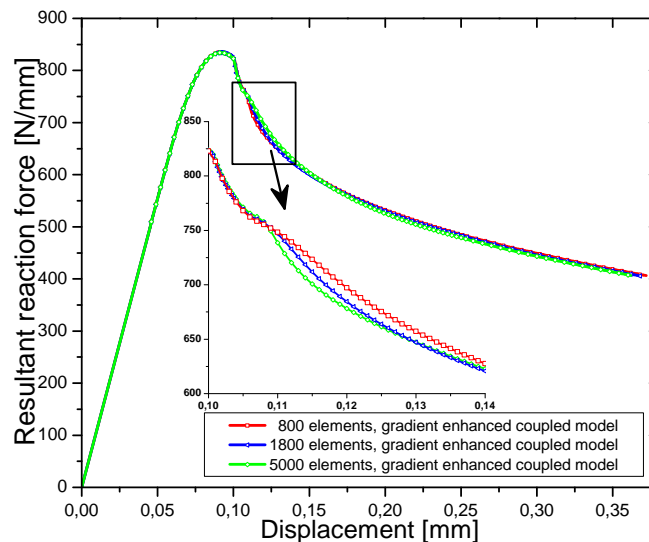

Figure 7.25.: Load-displacement diagrams for the the brick-with-a-hole problem using gradient enhanced coupled *damage-plastic model II*

The calculations performed utilizing the gradient enhanced *damage-plastic model II* on the discretization meshes containing 800, 1800 and 5000 quadrilateral elements result in the structural response in terms of force-displacement diagrams that clearly shows convergence, Figure 7.25. The same holds for the distribution of the internal variables obtained in these

numerical tests, which is evident in Figure 7.26. Both evolution of the damaging process, Figures 7.26(a) and 7.26(c) as well as the plastic softening, Figures 7.26(b) and 7.26(d) are well represented even on the 800-element mesh
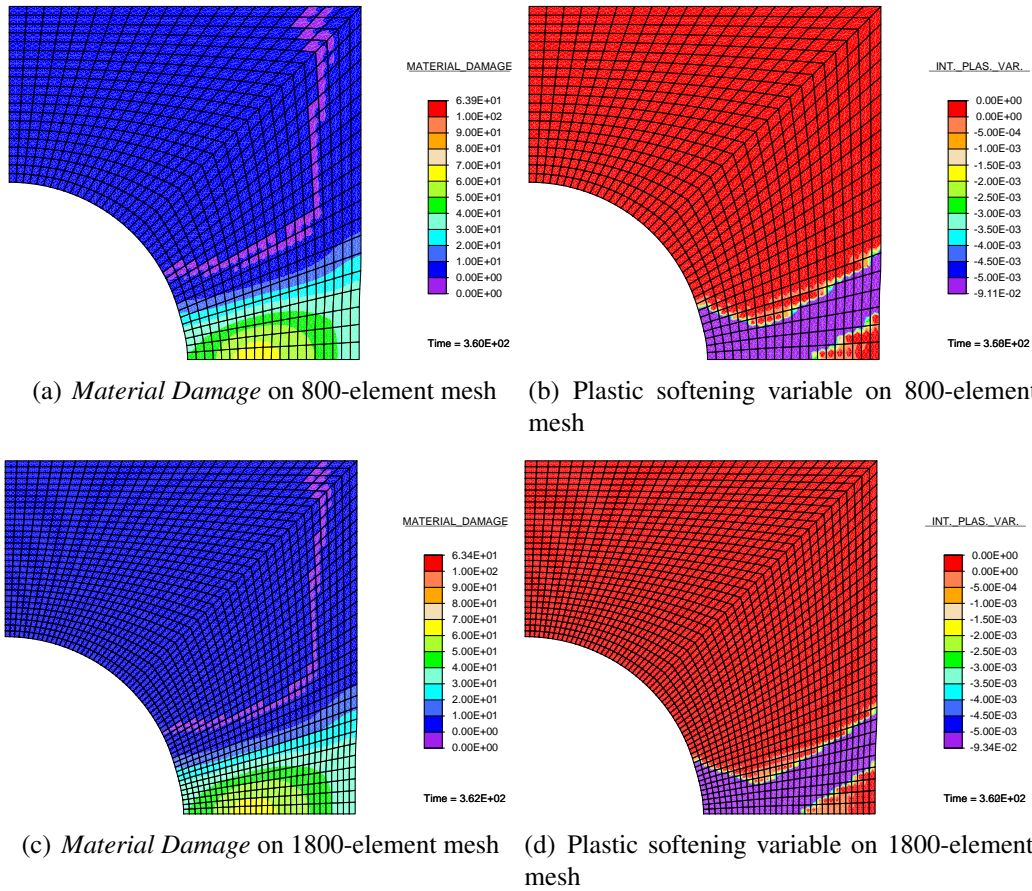

(a) *Material Damage* on 800-element mesh

(b) Plastic softening variable on 800-element mesh

(c) *Material Damage* on 1800-element mesh

(d) Plastic softening variable on 1800-element mesh

Figure 7.26.: Distribution of the selected calculation results for the brick-with-a-hole problem at the end of the test using gradient enhanced coupled *damage-plastic model II*

This example completes the presentation of the numerical results obtained utilizing the material models regularized via gradient enhancement of the free-energy function and we proceed to the final chapter of the thesis, which contains the conclusions gathered from the theoretical as well as numerical investigation of the proposed gradient enhancement strategy.

8. Conclusions and outlook

In the present work a a regularization framework for inelastic material models via gradient enhancement of the Helmholtz free-energy function is presented. The enhancement is defined by means of an interaction potential dependent on the difference between additionally introduced variables and the suitably chosen potential function of the internal variables. The gradients of the newly introduced variables are used to regularize the model, similar to *implicit gradient* models. It should be mentioned that the internal variables remain completely local quantities, connected to the corresponding material point, whereas the additional variables are related to global structure and behave as non-local. The corresponding boundary value problem is formulated as a pure minimization problem of the potential functional with respect to the displacement field and the non-local variable field, which results in additional variational integral equations. These boundary-value subproblems are posed on the whole domain of the problem, eliminating the implementation difficulties related to cumbersome search for the inelastic region and enforcement of the interface conditions at its evolving boundary typical for *explicit gradient* models.

The formulation of the constitutive relations is performed in a thermodynamically consistent way and it results in small differences compared with classical models. The differences are restricted to the micromechanical driving forces thermodynamically conjugated to the part of the list of internal variables used in the definition of the interaction potential. The evolution of the internal variables is specified by the minimum principle for the dissipation potential. The dissipation potential itself retains the form of the classical (without regularization) model, therefore accounting for the non-local interaction only implicitly. The implementation within numerical schemes is particularly convenient and does not increase computational effort significantly, due to very few differences compared to the classical (local) models. Hence, it is possible to apply this strategy to material models whose numerical implementation is already done without performing tedious derivation and coding from the beginning. The main difference is a consequence of the statement of the problem as a multi-field minimization, implying that the local constitutive numerical update has to supply additional tangent moduli in order to achieve desired convergence properties of the discretized boundary value problem.

The application of the proposed gradient enhancement strategy is demonstrated by several inelastic material models, including damage, plastic and coupling models. The characteristic details of the specific material models are discussed and convenient interpretations are given. It is shown that gradient enhancement leads to apparent increase of the inelastic limit in the localization zone, which reduces the dissipation of energy and consequently results in slowing down the evolution of the corresponding internal variable. Conversely, outside of the localization zone the dissipation of energy is increased, which results in a more rapid evolution of corresponding internal variables. Furthermore, the implementation of the gradient regularization strategy in the context of finite element method is presented. The introduction of a non-local variable field as an additional primal variable leads, after inserting the finite element approximation of the variables into the governing variational

equations, to additional discretized algebraic equations. The whole system of discretized equations is non-linear and it is solved by applying an incremental-iterative scheme based on the Newton's method.

Several numerical examples illustrate the behavior of the material models regularized by the proposed gradient enhancement strategy. It is shown that all material models treated in this thesis are successfully regularized. Furthermore, the influence of newly introduced model parameters on the global response of the system, distribution of inelastic variables and the calculation procedure is discussed. It is shown that the success of the regularization depends crucially on the interrelation between these parameters.

Hence, one can conclude that the presented gradient enhancement strategy can be successfully utilized in the regularization of various inelastic rate-independent material models. There is, however, a number of aspects that remain to be investigated. Firstly, an application of the strategy on more sofisticated material models, considering possibly rate-dependent formulations or thermomechanical coupling. Some work in this direction is already done, and it will provide an opportunity to test the behavior of the strategy in a more demanding setting. A further point that can draw more attention in the future work is the interaction potential itself. In the present contribution it is formulated in decoupled form, stating that there is a one-to-one map between the non-local variable and a selected local variable, with no interaction between the non-local variables. However, one can think of the potential functions dependent on more than one internal variable as well. An additional issue along this line are the interaction parameters. They are taken to be constant in the present work, but, as advocated by some authors, one can consider their dependence on the inelastic processes in order to obtain more realistic predictions. One of the possible directions of future research is an implementation of the strategy within structural elements, like inelastic shells. Finally, a possibly most important direction of further research is a realistic identification of the parameters introduced in the gradient enhancement.

A. Appendix

A.1. Gâteaux-derivative and linearization

The directional (Gâteaux-) derivative of a functional $\phi(y)$ in the direction δy is defined as:

$$D\phi(y)(\delta y) = \frac{d}{d\alpha}\,\phi(y + \alpha \delta y)|_{\alpha=0} \tag{A.1}$$

Considering a generic function $W(\mathbf{Y})$ depending on the set of independent variables $\mathbf{Y}$, its Gâteaux-derivative in the direction $\delta \mathbf{Y}$ is defined as
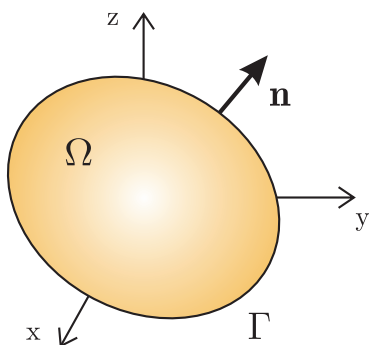
$$DW(\mathbf{Y})(\delta\mathbf{Y}) := \left.\frac{\partial W(\mathbf{Y} + \eta\delta\mathbf{Y})}{\partial\eta}\right|_{\eta=0} = \frac{\partial W(\mathbf{Y})}{\partial\mathbf{Y}}\,\delta\mathbf{Y} \tag{A.2}$$

An incrementation operator Δ is defined by the Gâteaux-derivative of the quantity under consideration:

$$\Delta W(\mathbf{Y})(\Delta\mathbf{Y}) := \left.\frac{\partial W(\mathbf{Y} + \eta\Delta\mathbf{Y})}{\partial\eta}\right|_{\eta=0} = \frac{\partial W(\mathbf{Y})}{\partial\mathbf{Y}}\,\Delta\mathbf{Y} \tag{A.3}$$

Utilizing the incrementation operator the linearization of the generic function $W(\mathbf{Y})$ around the point $\mathbf{Y} = \mathbf{Y}_0$ is defined in the form:

$$\mathcal{L}W(\mathbf{Y})(\Delta W) := W(\mathbf{Y}_0) + \Delta W(\mathbf{Y}_0)(\delta\mathbf{Y}) \tag{A.4}$$

A.2. Theorem of Gauß-Ostrogradski

This theorem permits to transform the volume integral of a divergence into a surface integral or vice versa. It states that the changes of a vectorial field $\boldsymbol{v}$ or a second order tensor field $\boldsymbol{A}$ within some domain Ω are equal to the flux across the boundary of a domain Γ.

$$\int_\Omega \operatorname{div}\boldsymbol{v}\,dV = \oint_\Gamma \boldsymbol{v}\cdot\boldsymbol{n}\,dA = \oint_\Gamma \mathrm{v}_j\mathrm{n}_j dA$$

$$\int_\Omega \operatorname{div}\boldsymbol{A}\,dV = \oint_\Gamma \boldsymbol{A}\cdot\boldsymbol{n}\,dA = \oint_\Gamma \mathrm{A}_{ij}\mathrm{n}_j\,dA$$

Figure A.1.: Theorem of Gauß-Ostrogradski

A.3. Some elements of tensor calculus

A.3.1. Differential operators

The gradient operator

The gradient of a scalar-valued function θ is a vector defined by

$$\operatorname{grad} \Phi = \frac{\partial \theta}{\partial \mathrm{x}_i} \mathbf{e}_i = \theta_{,i} \mathbf{e}_i = \nabla \theta \tag{A.5}$$

The gradient of a vector-valued function $\mathbf{u}$ is a second order tensor defined by

$$\operatorname{grad} \mathbf{u} = \frac{\partial \mathbf{u}}{\partial \mathrm{x}_k} \otimes \mathbf{e}_k = \mathbf{u}_{,k} \otimes \mathbf{e}_k = \mathrm{u}_{i,k} \mathbf{e}_i \otimes \mathbf{e}_k = \nabla \mathbf{u} \tag{A.6}$$

The gradient of a second-order-tensor-valued function $\mathbf{A}$ is a third order tensor defined by

$$\operatorname{grad} \mathbf{A} = \frac{\partial \mathbf{A}}{\partial \mathrm{x}_k} \otimes \mathbf{e}_k = \mathbf{A}_{,k} \otimes \mathbf{e}_k = \mathrm{A}_{ij,k} \mathbf{e}_i \otimes \mathbf{e}_j \otimes \mathbf{e}_k = \nabla \mathbf{A} \tag{A.7}$$

The gradient of a product is obtained by

$$\operatorname{grad}(\Phi \mathbf{u}) = \mathbf{u} \otimes \operatorname{grad} \Phi + \Phi \operatorname{grad} \mathbf{u} \tag{A.8}$$

The divergence operator

The divergence of a vector $\mathbf{u}$ is a scalar-valued invariant defined by the rule

$$\operatorname{div} \mathbf{u} = \operatorname{grad} \mathbf{u} : \mathbf{I} = \mathrm{u}_{i,i} \tag{A.9}$$

The divergence of a second order tensor $\mathbf{A}$ is a vector-valued function defined by the rule

$$\operatorname{div} \mathbf{A} = \operatorname{grad} \mathbf{A} : \mathbf{I} = \mathrm{A}_{ij,j} \mathbf{e}_i \tag{A.10}$$

The divergence of a product is obtained by

$$\operatorname{div}(\mathbf{u} \, \mathbf{A}) = \mathbf{A} : \operatorname{grad} \mathbf{u} + \mathbf{u} \cdot \operatorname{div} \mathbf{A} \tag{A.11}$$

A.3.2. Spectral decomposition of a second order tensor

Invariants of a second-order tensor

$$\mathrm{I}_A = \operatorname{tr} \mathbf{A} = \mathbf{A} : \mathbf{I} \tag{A.12}$$

$$\mathrm{II}_A = \frac{1}{2}[(\operatorname{tr} \mathbf{A})^2 - \operatorname{tr} \mathbf{A}^2] \tag{A.13}$$

$$\mathrm{III}_A = \frac{1}{3}[\operatorname{tr} \mathbf{A}^3 - \frac{2}{3} \operatorname{tr} \mathbf{A}^2 \ \operatorname{tr} \mathbf{A} + \frac{1}{2}(\operatorname{tr} \mathbf{A})^3] \tag{A.14}$$

Analytical solution of eigenvalue-problems

$$\Lambda^3 - \mathrm{I}_C\Lambda^2 + \mathrm{II}_C\Lambda - \mathrm{III}_C = 0 \tag{A.15}$$

$$\mathbf{C} = \sum_{i=1}^{3} \Lambda_i\mathbf{n}_i \otimes \mathbf{n}_i = \sum_{i=1}^{3} \Lambda_i\mathbf{N}_i \quad \text{with} \quad \mathbf{N}_i = \mathbf{n}_i \otimes \mathbf{n}_i \tag{A.16}$$

$$\Lambda_k = \frac{1}{3}[\mathrm{I}_C + 2(\mathrm{I}_C^2 - 3\mathrm{II}_C)^{\frac{1}{2}} \cos\frac{1}{3}(\Theta + 2\pi k)] \tag{A.17}$$

$$\Theta = \arccos\left(\frac{2\mathrm{I}_C^3 - 9\mathrm{I}_C\mathrm{II}_C + 27\mathrm{III}_C}{2(\mathrm{I}_C^2 - 3\mathrm{II}_C)^{\frac{3}{2}}}\right) \tag{A.18}$$

If the eigenvalues Λ_i (i=1,2,3) are distinct, then

$$\mathbf{N}_r = \frac{1}{(\Lambda_r - \Lambda_s)(\Lambda_s - \Lambda_t)}(\mathbf{C} - \Lambda_s\mathbf{I})(\mathbf{C} - \Lambda_t\mathbf{I}) \tag{A.19}$$

In the case of coalescence of two eigenvalues ($\Lambda_1 \neq \Lambda_2 = \Lambda_3 = \Lambda$) we have

$$\mathbf{C} = \sum_{i=1}^{3} \Lambda\mathbf{n}_i \otimes \mathbf{n}_i + (\Lambda_1 - \Lambda)\mathbf{n}_1 \otimes \mathbf{n}_1 = (\Lambda_1 - \Lambda)\mathbf{N}_1 + \Lambda\mathbf{I} \tag{A.20}$$

whereas

$$\mathbf{N}_1 = \frac{1}{(\Lambda_1 - \Lambda)}(\mathbf{C} - \Lambda\mathbf{I}) \tag{A.21}$$

Finally, for the case of coalescence of all eigenvalues ($\Lambda_1 = \Lambda_2 = \Lambda_3 = \Lambda$) the closed form solution becomes

$$\mathbf{C} = \Lambda\mathbf{I} \tag{A.22}$$

A.3.3. Derivatives of the eigenvalues of a second order tensor

For the formulation of the algorithm it is necessary to calculate the expressions for the first and second derivatives of the yield functions with respect to the tensor $\boldsymbol{\xi}$, i.e. $\frac{\partial \xi^A}{\partial \boldsymbol{\xi}}$. To accomplish that task, the starting point is the expression for the eigendecomposition of a tensor:

$$(\boldsymbol{\xi} - \xi^A\mathbf{I})\,\boldsymbol{n}^A = \mathbf{0} \tag{A.23}$$

where ξ^A represents the A-th eigenvalue of the tensor $\boldsymbol{\xi}$, $\boldsymbol{n}^A$ its corresponding eigenvector and $\mathbf{0}$ vector with zeros as elements. For further development it would be more suitable to write (A.23) in index notation:

$$(\xi_{ij} - \xi^A\delta_{ij})\,n_j^A \tag{A.24}$$

Taking the derivatives with respect to tensor $\boldsymbol{\xi}$ leads to:

$$(\frac{\partial \xi_{ij}}{\partial \xi_{kl}} - \frac{\partial \xi^A}{\partial \xi_{kl}}\delta_{ij})n_j^A + (\xi_{ij} - \xi^A\delta_{ij})\frac{\partial n_j^A}{\partial \xi_{kl}} = 0_{ikl} \tag{A.25}$$

Premultiplying (A.25) with n_i^A gives:

$$n_i^A \left(\frac{\partial \xi_{ij}}{\partial \xi_{kl}} - \frac{\partial \xi^A}{\partial \xi_{kl}} \delta_{ij} \right) n_j^A + n_i^A (\xi_{ij} - \xi^A \delta_{ij}) \frac{\partial n_j^A}{\partial \xi_{kl}} = 0_{kl} \tag{A.26}$$

The tensor $\boldsymbol{\xi}$ is symmetric, so the following holds (from (A.24)):

$$n_i^A (\xi_{ij} - \xi^A \delta_{ij}) = 0_j \tag{A.27}$$

Then equation (A.26)) transforms to the:

$$n_i^A \frac{\partial \xi_{ij}}{\partial \xi_{kl}} n_j^A = \frac{\partial \xi^A}{\partial \xi_{kl}} n_i^A \delta_{ij} n_j^A \tag{A.28}$$

and further to:

$$\frac{\partial \xi^A}{\partial \xi_{kl}} = n_k^A n_l^A \tag{A.29}$$

Denoting the eigenbase of the second order tensor as:

$$\boldsymbol{N}^A = \boldsymbol{n}^A \otimes \boldsymbol{n}^A \tag{A.30}$$

the final expression for the first derivative of the yield function with respect to the tensor $\boldsymbol{\xi}$ is obtained as:

$$\frac{\partial f_A}{\partial \boldsymbol{\xi}} = \frac{\partial \boldsymbol{\xi}^A}{\partial \boldsymbol{\xi}} = \boldsymbol{N}^A \tag{A.31}$$

In the calculation of the second derivative the starting point is the explicit expression for the eigenbases $\boldsymbol{N}^A$ as in Simo and Ju (1987); Meschke (1996); Dimitrijević (2004):

$$\boldsymbol{N}^A = \frac{(\boldsymbol{\xi} - \xi^B \mathbf{I})(\boldsymbol{\xi} - \xi^C \mathbf{I})}{D_A} \tag{A.32}$$

with the definition :

$$D_A = (\xi^B - \xi^A)(\xi^C - \xi^A) \tag{A.33}$$

The transfer to the index notation as more suitable for the derivation will again be made, so that (A.32))reads:

$$N_{ij}^A = \frac{(\xi_{im} - \xi^B \delta_{im})(\xi_{mj} - \xi^C \delta_{mj})}{D_A} \tag{A.34}$$

After multiplication and expanding, (A.34) reads:

$$N_{ij}^A = \frac{1}{D_A} (\xi_{im}\xi_{mj} - \xi_{ij}\xi^C - \xi_{ij}\xi^B + \xi^B \xi^C \delta_{ij}) \tag{A.35}$$

The equation (A.35) will be now differentiated, which gives:

$$\begin{aligned}
\frac{\partial N_{ij}^A}{\partial \xi_{kl}} &= \frac{1}{D_A} \left[\frac{\partial (\xi_{im}\xi_{mj} - \xi_{ij}\xi^C - \xi_{ij}\xi^B + \xi^B \xi^C \delta_{ij})}{\partial \xi_{kl}} \right] \\
&\quad - \frac{1}{D_A^2} \left((\xi_{im}\xi_{mj} - \xi_{ij}\xi^C - \xi_{ij}\xi^B + \xi^B \xi^C \delta_{ij}) \right) \frac{\partial D_A}{\partial \xi_{kl}}
\end{aligned} \tag{A.36}$$

and after expanding:

$$
\begin{aligned}
\frac{\partial N_{ij}^A}{\partial \xi_{kl}} = \ & \frac{1}{D_A}\left\{ \frac{1}{2}(\delta_{ik}\delta_{ml} - \delta_{il}\delta_{mk})\xi_{mj} + \frac{1}{2}(\delta_{mk}\delta_{jl} - \delta_{ml}\delta_{jk})\xi_{im}\right. \\
& -\frac{1}{2}(\delta_{ik}\delta_{jl} - \delta_{il}\delta_{jk})\xi^C - \xi_{ij}N_{kl}^C - \frac{1}{2}(\delta_{ik}\delta_{jl} - \delta_{il}\delta_{jk})\xi^B \\
& \left. -\xi_{ij}N_{kl}^B + \xi^C N_{kl}^B \delta_{ij} + \xi^B N_{kl}^C \delta_{ij}\right\} \\
& -\frac{1}{D_A^2}\left((\xi_{im}\xi_{mj} - \xi_{ij}\xi^C - \xi_{ij}\xi^B + \xi^B\xi^C\delta_{ij})\right) \\
& \left[(\xi^C - \xi^A)(N_{kl}^B - N_{kl}^A) + (\xi^B - \xi^A)(N_{kl}^C - N_{kl}^A)\right]
\end{aligned} \tag{A.37}
$$

The final expression for the second derivative of the yield function with respect to the tensor $\boldsymbol{\xi}$ is:

$$
\begin{aligned}
\frac{\partial N_{ij}^A}{\partial \xi_{kl}} = \ & \frac{1}{D_A}\left\{ \frac{1}{2}(\delta_{ik}\xi_{lj} + \delta_{il}\xi_{kj} + \delta_{jl}\xi_{ik} + \delta_{jk}\xi_{il})\right. \\
& -\frac{1}{2}(\xi^B - \xi^C)(\delta_{ik}\delta_{jl} + \delta_{il}\delta_{jk}) - \xi_{ij}(N_{kl}^B + N_{kl}^C) \\
& +\delta_{ij}(\xi^B N_{kl}^C + \xi^C N_{kl}^B) \\
& \left. -N_{ij}^A\left[(\xi^C - \xi^A)(N_{kl}^B - N_{kl}^A) + (\xi^B - \xi^A)(N_{kl}^C - N_{kl}^A)\right] \right\}
\end{aligned} \tag{A.38}
$$

A.4. Matrix notation of stress and strain tensors and related derivatives

Strain and stress vectors using Voigt notation

$$
\overline{\boldsymbol{\varepsilon}} = \left\{ \begin{array}{cccccc} \varepsilon_{11} & \varepsilon_{22} & \varepsilon_{33} & 2\varepsilon_{12} & 2\varepsilon_{23} & 2\varepsilon_{13} \end{array} \right\}^T,
$$
$$
\overline{\boldsymbol{\sigma}} = \left\{ \begin{array}{cccccc} \sigma_{11} & \sigma_{22} & \sigma_{33} & \sigma_{12} & \sigma_{23} & \sigma_{13} \end{array} \right\}^T. \tag{A.39}
$$

Strain and stress vectors using Mandel notation

$$
\tilde{\boldsymbol{\varepsilon}} = \left\{ \begin{array}{cccccc} \varepsilon_{11} & \varepsilon_{22} & \varepsilon_{33} & \sqrt{2}\varepsilon_{12} & \sqrt{2}\varepsilon_{23} & \sqrt{2}\varepsilon_{13} \end{array} \right\}^T,
$$
$$
\tilde{\boldsymbol{\sigma}} = \left\{ \begin{array}{cccccc} \sigma_{11} & \sigma_{22} & \sigma_{33} & \sqrt{2}\sigma_{12} & \sqrt{2}\sigma_{23} & \sqrt{2}\sigma_{13} \end{array} \right\}^T. \tag{A.40}
$$

Discrete strain-displacement operators

$$
\mathbf{B}^I = \begin{bmatrix}
\frac{\partial N_u^I}{\partial X_1} & 0 & 0 \\
0 & \frac{\partial N_u^I}{\partial X_2} & 0 \\
0 & 0 & \frac{\partial N_u^I}{\partial X_3} \\
\frac{\partial N_u^I}{\partial X_2} & \frac{\partial N_u^I}{\partial X_1} & 0 \\
0 & \frac{\partial N_u^I}{\partial X_3} & \frac{\partial N_u^I}{\partial X_2} \\
\frac{\partial N_u^I}{\partial X_3} & 0 & \frac{\partial N_u^I}{\partial X_1}
\end{bmatrix}, \quad \text{or} \quad
\mathbf{B}_M^I = \begin{bmatrix}
\frac{\partial N_u^I}{\partial X_1} & 0 & 0 \\
0 & \frac{\partial N_u^I}{\partial X_2} & 0 \\
0 & 0 & \frac{\partial N_u^I}{\partial X_3} \\
\frac{\sqrt{2}}{2}\frac{\partial N_u^I}{\partial X_2} & \frac{\sqrt{2}}{2}\frac{\partial N_u^I}{\partial X_1} & 0 \\
0 & \frac{\sqrt{2}}{2}\frac{\partial N_u^I}{\partial X_3} & \frac{\sqrt{2}}{2}\frac{\partial N_u^I}{\partial X_2} \\
\frac{\sqrt{2}}{2}\frac{\partial N_u^I}{\partial X_3} & 0 & \frac{\sqrt{2}}{2}\frac{\partial N_u^I}{\partial X_1}
\end{bmatrix}. \tag{A.41}
$$

Components of a fourth order tensor C_{ijkl} with a symmetries $C_{ijkl} = C_{jikl} = C_{ijlk} = C_{jilk}$ is transformed into 6×6 matrix using Voigt:

$$\hat{\mathbf{C}} = \left\{ \begin{array}{cccccc} C_{1111} & C_{1122} & C_{1133} & C_{1112} & C_{1123} & C_{1113} \\ C_{2211} & C_{2222} & C_{2233} & C_{2212} & C_{2223} & C_{2213} \\ C_{3311} & C_{3322} & C_{3333} & C_{3312} & C_{3323} & C_{3313} \\ C_{1211} & C_{1222} & C_{1233} & C_{1212} & C_{1223} & C_{1213} \\ C_{2311} & C_{2322} & C_{2333} & C_{2312} & C_{2323} & C_{2313} \\ C_{3111} & C_{3122} & C_{3133} & C_{3112} & C_{3123} & C_{3113} \end{array} \right\} \tag{A.42}$$

and Mandel notation

$$\hat{\mathbf{C}} = \left\{ \begin{array}{cccccc} C_{1111} & C_{1122} & C_{1133} & \sqrt{2}C_{1112} & \sqrt{2}C_{1123} & \sqrt{2}C_{1113} \\ C_{2211} & C_{2222} & C_{2233} & \sqrt{2}C_{2212} & \sqrt{2}C_{2223} & \sqrt{2}C_{2213} \\ C_{3311} & C_{3322} & C_{3333} & \sqrt{2}C_{3312} & \sqrt{2}C_{3323} & \sqrt{2}C_{3313} \\ \sqrt{2}C_{1211} & \sqrt{2}C_{1222} & \sqrt{2}C_{1233} & 2C_{1212} & 2C_{1223} & 2C_{1213} \\ \sqrt{2}C_{2311} & \sqrt{2}C_{2322} & \sqrt{2}C_{2333} & 2C_{2312} & 2C_{2323} & 2C_{2313} \\ \sqrt{2}C_{3111} & \sqrt{2}C_{3122} & \sqrt{2}C_{3133} & 2C_{3112} & 2C_{3123} & 2C_{3113} \end{array} \right\}. \tag{A.43}$$

Bibliography

Aifantis, E. (1984). On the microstructural origin of certain inelastic models. *Journal of Engineering Materials and Technology 106*, 326–330.

Aifantis, E. (1999). Gradient deformation models at nano, micro and macro scales. *Journal of Engineering Materials and Technology 121*, 189–202.

Al-Rub, R. and G. Voyiadjis (2005). A direct finite element implementation of the gradient-dependent theory. *International Journal for Numerical Methods in Engineering 63*, 603–629.

Al-Rub, R., G. Voyiadjis, and D. Bammann (2007). A thermodynamic based higher-order gradient theory for size dependent plasticity. *International Journal of Solids and Structures 44*, 2888–2923.

Al-Rub, R. A. and G. Voyiadjis (2009). Gradient-enhanced coupled plasticity-anisotropic damage model for concrete fracture: Computational aspects and applications. *International Journal of Damage Mechanics 18*, 115–154.

Başar, Y. and D. Weichert (2000). *Nonlinear Continuum Mechanics of Solids: Fundamental mathematical and physical concepts*. Berlin, Heidelberg: Springer.

Bargmann, S. and P. Steinmann (2006). Theoretical and computational aspects of non-classical thermoelasticity. *Comput. Methods Appl. Mech. Engrg. 196*, 516–527.

Bažant, Z. and M. Jirásek (2002). Nonlocal integral formulations of plasticity and damage: Survey of progress. *Journal of Engineering Mechanics 128*, 1119–1149.

Belytschko, T., N. Möes, S. Usui, and C. Parimi (2001). Arbitrary discontinuities in finite elements. *International Journal for Numerical Methods in Engineering 50*, 993–1013.

Brannon, R. (2003). *Functional and Structured Tensor Analysis for Engineers*. Albuquerque: University of New Mexico.

Carol, I., E. Rizzi, and K. Willam (2001a). On the formulation of anisotropic elastic degradation. i. theory based on a pseudo-logarithmic damage tensor rate. *International Journal of Solids and Structures 38*, 491–518.

Carol, I., E. Rizzi, and K. Willam (2001b). On the formulation of anisotropic elastic degradation. ii. generalized pseudo-rankine model for tensile damage. *International Journal of Solids and Structures 38*, 519–546.

Carstensen, C., K. Hackl, and A. Mielke (2002). Nonconvex potentials and microstructures in finite-strain plasticity. *Royal Soc. London, Proc. Ser. A 458*, 299–317.

Chaboche, J. (1984). Anisotropic creep damage in the framework of continuum damage mechanics. *Nuclear Engineering and Design 79*, 309–319.

Chaboche, J. (2003). Damage mechanics. In I. Milne, R. Rithcie, and B. Karihaloo (Eds.), *Comprehensive Structural Integrity*, pp. 213–284. Pergamon, Oxford.

Comi, C. (2001). A non-local model with tension and compression damage mechanisms. *Eur. J. Mech. A/Solids 20*, 1–22.

Comi, C. and U. Perego (2001). Fracture energy based bi-dissipative damage model for concrete. *Int. J. Numer. Meth. Engng. 38*, 6427–6454.

Cordebois, J. and F. Sidoroff (1982). Damage induced elastic anisotropy. In J. Boehler (Ed.), *Mechanical Behavior of Anisotropic Solids, EUROMECH Coloque 115, June 1979*, pp. 761–774. Martinus Nijhoff, The Netherlands.

Cosserat, E. and F. Cosserat (1909). *Théeorie des corps déformables*. Paris: Hermann.

de Borst, R., M. Gutiérrez, G. Wells, J. Remmers, and H. Askes (2004). Cohesive-zone models, higher-order continuum theories and reliability methods for computational failure analysis. *International Journal for Numerical Methods in Engineering 60*, 289–315.

de Borst, R. and J. Pamin (1996). Some novel developments in finite element procedures for gradient-dependent plasticity. *International Journal for Numerical Methods in Engineering 39*, 2477–2505.

de Borst, R., J. Pamin, and M. Geers (1999). On coupled gradient-dependent plasticity and damage theories with a view to localization analysis. *Eur. J. Mech. A/Solids 18*, 939–962.

Dimitrijević, B. (2004). *Development of Stable Algorithms for a Transverse Isotropic Damage-Plasticity Model for Wood and Application to Pull-out Tests of Particleboard; M.Sc. Thesis*. Bochum: Institute of Structural Mechanics, Ruhr-University of Bochum.

Dimitrijević, B. and K. Hackl (2006). A method for gradient enhancement of inelastic material models. In M. Kojić and M. Papadrakakis (Eds.), *Procceedings of First South-East European Conference on Computational Mechanics*, pp. 191–197. University of Kragujevac, Serbia.

Dimitrijević, B. and K. Hackl (2008). A method for gradient enhancement of continuum damage models. *Technische Mechanik 28*, 43–52.

Dimitrijević, B. and K. Hackl (2009). A regularization framework for damage-plasticity models via gradient enhancement of the free energy. *Communications in Numerical Methods in Engineering (to appear)*.

Dorgan, J. (2006). *A Nonlocal Model for Coupled Damage-Plasticity Incorporating Gradients of Internal State Variables at Multiscales; Ph.D. Thesis*. Louisiana State University.

Drucker, D. and W. Prager (1952). Soil mechanics and plastic analysis or limit design. *Quarterly of Applied Mathematics 10*, 157–165.

Duncan, J. M. and C.-Y. Chang (1970). Nonlinear analysis of stress and strain in soils. *Journal of Soil Mechanics and Foundations 96*, 1629–1653.

Edelen, D., A. Green, and N. Laws (1971). Nonlocal continuum mechanics. *Arch. Ration. Mech. Anal. 43*, 36–44.

Engelen, R., N. Fleck, R. Peerlings, and M. Geers (2006). An evaluation of higher-order plasticity theories for predicting size effects and localisation. *International Journal of Solids and Structures 43*, 1857–1877.

Engelen, R., M. Geers, and F. Baaijens (2003). Nonlocal implicit gradient-enhanced elasto-plasticity for the modelling of softening behaviour. *International Journal of Plasticity 19*, 403–433.

Eringen, A. (1981). On nonlocal plasticity. *International Journal of Engineering Science 19*, 1461–1474.

Eringen, A. (1999). *Microcontinuum field theoriec*. New York: Sprringer.

Eringen, A. and D. Edelen (1972). On nonlocal elasticity. *International Journal of Engineering Science 10*, 233–248.

Feenstra, P. and R. de Borst (1995). A plasticity model for mode-i cracking in concrete. *International Journal for Numerical Methods in Engineering 38*, 2509–2529.

Fleck, N. and J. Hutchinson (1993). A phenomenological theory for strain gradient effects in plasticity. *Journal of the Mechanics and Physics of Solids 41*, 1825–1857.

Fleck, N., G. Muller, M. Asby, and J. Hutchinson (1994). Strain gradient plasticity: theory and experiment. *Acta Metallurgica et Materialia 45*, 475–487.

Forest, S. (2009). Micromorphic approach for gradient elasticity, viscoplasticity, and damage. *Journal of Engineering Mechanics 135*, 117–131.

Forest, S. and E. Lorentz (2004). Localization phenomena and regularization methods. In J. Besson (Ed.), *Local Approach to Fracture*, pp. 311–373. Ecole des Mines de Paris.

Frantziskonis, G., A. Konstantinidis, and E. Aifantis (2001). Scale-dependent constitutive relations and the role of scale on nominal properties. *Eur. J. Mech. A/Solids 20*, 925–936.

Galerkin, B. (1915). Series solution of some problems of elastic equilibrium of rods and plates. *Vestn. Inzh. Techn. 19*, 897–908.

Geers, M. (1997). *Experimental Analysis and computational Modelling of Damage and Fracture; Ph.D. Thesis*. The Netherlands: Eindhoven University of Technology.

Geers, M., R. de Borst, W. Brekelmans, and R. Peerlings (1998). Strain-based transient-gradient damage model for failure analyses. *Computer Methods in Applied Mechanics and Engineering 160*, 133–154.

Govindjee, S., G. Kay, and J. Simo (1995). Anisotropic modelling and numerical simulation of brittle damage in concrete. *Int. J. Numer. Meth. Engng. 38*, 3611–3633.

Grassl, P. and M. Jirásek (2006). Damage-plastic model for concrete failure. *International Journal of Solids and Structures 43*, 7166–7196.

Gurson, A. (1977). Continuum theory of ductile rupture by void nucleation and growth: Part i - yield criteria and flow rules for porous ductile media. *Journal of Engineering Materials and Technology 99*, 2–15.

Hackl, K. (1997). Generalized standard media and variational principles in classical and finite strain elastoplasticity. *J. Mech. Phys. Solids 45*, 667–688.

Hackl, K. (2001). A survey on time-integration algorithms for convex and nonconvex elasto-plasticity. In R. P. Gilbert, P. D. Panagiotopoulus, and P. Pardales (Eds.), *From convexity to nonconvexity. A volume dedicated to the memory of Prof. G. Fichera*. Kluwer, Boston.

Hackl, K. and F. Fischer (2008). On the relation between the principle of maximum dissipation and inelastic evolution given by dissipation potentials. *Proceedings of the Royal Society A 464*, 117–132.

Hackl, K. and M. Schmidt-Baldassari (2001). Time integration algorithms for evolution equations in finite strain plasticity. In W. A. Wall, K.-U. Bletzinger, and K. Schweizerhof (Eds.), *Trends in computational structural mechanics*. CIMNE, Barcelona, Spain.

Halphen, B. and Q. Nguyen (1975). Sur les matériaux standard generalises. *J. de Mécanique 14*, 39–63.

Han, W. and B. Reddy (1999). *Plasticity: Mathematical Theorie and Numerical Analysis*. New York: Springer-Verlag.

Hill, R. (1950). *The mathematical theory of plasticity*. Oxford: Oxford University Press.

Holzapfel, G. A. (2000). *Nonlinear Solid Mechanics: A Continuum Approach for Engineering*. Chichester: John Wiley & Sons.

Huang, Y., H. Gao, W. Nix, and J. W. Hutchinson (1999). Mechanism-based strain gradient plasticity-i. theory. *Journal of the Mechanics and Physics of Solids 47*, 1239–1263.

Huang, Y., H. Gao, W. Nix, and J. W. Hutchinson (2000). Mechanism-based strain gradient plasticity-ii. analysis. *Journal of the Mechanics and Physics of Solids 48*, 99–128.

Huber, F. (2006). *Nichtlineare dreidimensionale Modellierung von Beton- und Stahlbetontragwerken; Ph.D. Thesis*. Stutgart: Institut für Baustatik der Universität Stutgart.

Ibrahimbegović, A., D. Marković, and F. Gatuingt (2003). Constitutive model of coupled damage-plasticity and its finite element implementation. *Revue européenne des éléments finis 12*, 381–405.

Jirásek, M. (1998). Nonlocal models for damage and fracture: Comparison of approaches. *International Journal of Solids and Structures 113*, 4133–4145.

Jirásek, M. (2000). Comparative study on finite elements with embedded cracks. *Computer Methods in Applied Mechanics and Engineering 188*, 307–330.

Jirásek, M. (2002). Objective modeling of strain localization. *Revue française de génie civil 6*, 1119–1132.

Jirásek, M. (2007). Objective modeling of strain localization. *Revue européene de génie civil 11*, 977–991.

Jirásek, M. and Z. Bazant (2002). *Inelastic analysis of structures*. New York: John Wiley & Sons.

Jirásek, M. and S. Rolshoven (2003). Comparison of integral-type nonlocal plasticity models for strain-softening materials. *International Journal of Engineering Science 41*, 1553–1602.

Ju, J. (1990). Isotropic and anisotropic damage variables in continuum damage mechanics. *J. Eng. Mech. 116*, 2764–2770.

Kochman, D. (2009). *Mechanical Modeling of Microstructures in Elasto-Plastically Deformed Crystalline Solids; Ph.D. Thesis*. Bochum: Ruhr-Universität Bochum.

Krajcinovic, D. (2002). *Damage Mechanics*. North-Holland: Elsevier.

Krätzig, W. and R. Pölling (2004). An elastic–plastic damage model for reinforced concrete with minimum number of material parameters. *Computers and Structures 82*, 1201–1215.

Kröner, E. and B. Datta (1966). Nichtlokale elastostatik: Ableitung aus der gittertheorie. *Z. Phys. 196*, 203–211.

Kuhl, D. and G. Meschke (2003). *Finite Element Methods in Linear Structural Mechanics: Lecture Notes*. Bochum: Ruhr University Bochum.

Kuhl, E., E. Ramm, and K. Willam (2000). Failure analysis of elasto-plastic material models on different levels of observation. *International Journal of Solids and Structures 37*, 7259–7280.

Lade, P. V. and R. B. Nelson (1987). Modeling the elastic behavior of granular materials. *International Journal for Numerical and Analytical Methods in Geomechanics 11*, 521–542.

Lee, J. and G. Fenves (1998). A plastic-damage concrete model for earthquake analysis of dams. *Earthquake Engineering and Structural Dynamics 27*, 937–956.

Lemaitre, J. and J.-L. Chaboche (1988). *Mécanique Des Matériaux Solides*. Paris: Dunod.

Liebe, T. (2003). *Theory and numerics of higher gradient inelastic material behaviour; Ph.D. Thesis*. Kaiserslautern: Universität Kaiserslautern.

Liebe, T. and P. Steinmann (2001). Theory and numerics of a thermodynamically consistent framework for geometrically linear gradient plasticity. *International Journal for Numerical Methods in Engineering 51*, 1437–1467.

Liebe, T., P. Steinmann, and A. Benallal (2001). Theoretical and computational aspects of a thermodynamically consistent framework for geometrically linear gradient damage. *Computer Methods in Applied Mechanics and Engineering 190*, 6555–6776.

Lorentz, E. and S. Andrieux (2003). Analysis of nonlocal models through energetic formulations. *International Journal of Solids and Structures 40*, 2905–2936.

Lorentz, E. and A. Benallal (2005). Gradient constitutive relations: numerical aspects and application to gradient damage. *Comput. Methods Appl. Mech. Engrg. 194*, 5191–5220.

Lubliner, J. (1997). *Plasticity Theory*. New York: Maxwell Macmillan International Edition.

Makowski, J., K. Hackl, and H. Stumpf (2006). The fundamental role of nonlocal and local balance laws of material forces in finite elastoplasticity and damage mechanics. *International Journal of Solids and Structures 43*, 3940–3959.

Mazars, J. and G. Pijaudier-Cabot (1989). Continuum damage theory – application to concrete. *J. Eng. Mech. 115*, 345–365.

Meschke, G. (1996). Consideration of aging of shotcrete in the context of a 3-d viscoplastic material model. *Internatioanl Journal for Numerical Methods in Engineering 39*, 3123–3143.

Meschke, G., R. Lackner, and H. Mang (1998). An anisotropic elastoplastic-damage model for plain concrete. *Int. J. Numer. Meth. Engng. 42*, 703–727.

Mindlin, R. and H. Tiersten (1962a). Effects of couple stresses in linear elasticity. *Arch. Ration. Mech. Anal. 11*, 415–448.

Mindlin, R. and H. Tiersten (1962b). Effects of couple stresses in linear elasticity. *Arch. Ration. Mech. Anal. 11*, 415–448.

Möes, N., J. Dolbow, and T. Belytschko (1999). A finite element method for crack growth without remeshing. *International Journal for Numerical Methods in Engineering 46*, 131–150.

Mohr, O. (1900). Welche umstände bedingen die elastizitätsgrenze und den bruch eines materiales? *Zeitschrift des Vereines Deutscher Ingenieure 46*, 1524–1530, 1572–1577.

Mosler, J. (2005). On the modeling of highly localized deformations induced by material failure: The strong discontinuity aproach. *Archives of Computational Methods in Engineering 11*, 389–446.

Mühlhaus, H.-B. and E. Aifantis (1991). A variational principle for gradient plasticity. *International Journal of Solids and Structures 28*, 845–857.

Müller, S. (2006). *Entwicklung eines Werkstoffmodels zur FE-Simulation des Tragverhaltens neuartiger Befestigungsmittel in Spanplatten; Ph.D. Thesis*. Aachen: Shaker Verlag.

Nedjar, B. (1996). Damage, gradient of damage and principle of virtual power. *International Journal of Solids and Structures 33*, 1083–1103.

Nedjar, B. (2001). Elastoplastic-damage modelling including the gradient of damage: formulation and computational aspects. *International Journal of Solids and Structures 38*, 5421–5451.

Oliver, J. (2004). Continuum modeling of strong discontinuities in solid mechanics. In D. Owen, E. O. nate, and E. Hinton (Eds.), *Proceedings of 4th International Conference on Computational Plasticity*, pp. 455–479.

Oliver, J., A. Huespe, and S. Blanco (2002). Constribution to wp2/tg2, test no.1: L-shaped panel. *http://nw-ialad.uibk.ac.at/Wp2/Tg2/Se2/Ss1/*.

Olsson, M. and M. Ristinmaa (2003). Damage evolution in elasto-plastic materials - material response due to different concepts. *International Journal of Damage Mechanics 12*, 115–139.

Orkisz, J. (1998). Finite difference method. In M. Kleiber (Ed.), *Handbook of Computational Solid Mechnaics*. Springer-Verlag, Berlin.

Ortiz, M. (1985). A constitutive theory for the inelastic behavior of concrete. *Mechanics of Materials 4*, 67–93.

Peerlings, R., , T. Masart, and M. Geers (2004). A thermodynamically motivated implicit gradient damage framework and its application to brick masonry cracking. *Computer Methods in Applied Mechanics and Engineering 193*, 3403–3417.

Peerlings, R. (1999). *Enhanced damage modeling for fracture and fatigue; Ph.D. Thesis*. Eindhoven: Techische Universiteit Eindhoven.

Peerlings, R., R. de Borst, W. Brekelmans, and M. Geers (1998). Gradient-enhanced damage modeling of concrete fracture. *Mechanics of Cohesive-Frictional Materials 3*, 323–342.

Peerlings, R., M. Geers, R. de Borst, and W. Brekelmans (2001a). A critical comparison of nonlocal and gradient-enhanced softening continua. *International Journal of Solids and Structures 38*, 7723–7746.

Peerlings, R., M. Geers, R. de Borst, and W. Brekelmans (2001b). A critical comparison of nonlocal and gradient-enhanced softening continua. *International Journal of Solids and Structures 38*, 7723–7746.

Pijaudier-Cabot, G. and Z. Bažant (1988). Nonlocal damage theory. *J. Engng. Mech. 113*, 1512–1533.

Rabotnov, I. (1968). Creep rupture. In *Proceedings of the 12-th International Congress of Applied Mechanics*, pp. 342–349.

Rankine, W. (1858). *Manual of Applied Mechanics*. Glasgow.

Saczuk, J. (1993). A variational approach to the cosserat-like continuum. *Int. J. Eng. Sci. 31*, 1475–1483.

Schütt, J. (2005). *Ein inelastisches 3D-Versagensmodell für Beton und seine Finite-Element-Implementierung; Ph.D. Thesis*. Karlsruhe: Universität Fridericiana zu Karlsruhe (TH).

Simo, J. and T. Hughes (1998). *Computational Inelasticity*. New York: Springer.

Simo, J. and J. Ju (1987). Strain- and stress-based continuum damage models - i formulation. *International Journal of Solids and Structures 23*, 821–840.

Simone, A., H. Askes, R. Peerlings, and L. Sluys (2003). Interpolation requirements for implicit gradient-enhanced continuum damage models. *Communications in Numerical Methods in Engineering 19*, 563–572.

Skrzypek, J. and A. Ganczarski (1999). *Modeling of material damage and failure of structures*. Berlin: Springer.

Smith, I. and D. Griffiths (2008). *Programming the Finite Element Method (4th edition)*. Chichester, England: Wiley.

Stein, E. and F.-J. Barthold (1996). Elastizitätstheorie. In G. Mehlhorn (Ed.), *Der Ingenieurbau. Werkstoffe, Elastizitätstheorie*. Ernst&Sohn, Berlin.

Sukumar, N., D. Chop, and B. Moran (2003). Extended finite element method and fast marching method for three-dimensional fatigue crack propagation. *Engineering Fracture Mechanics 70*, 29–48.

Svedberg, T. and K. Runesson (1998). Thermodynamically consistent nonlocal and gradient formulations of plasticity. In A. Brillard and J. Ganghoffer (Eds.), *Nonlocal aspects on solid mechanics*, pp. 32–37. EUROMECH Colloquium 378, Mulhouse, France.

Toupin, R. (1962). Elastic materials with couple stress. *Arch. Ration. Mech. Anal. 11*, 385–414.

Tresca, M. (1864). Mémoire sur l' écoulement des coprs solides soum is à de fortes pressions. *Comptes Rendus Hebdomadaires des Seànces de l' Académie de Sciences 59*, 754–758.

Truesdell, C. and W. Noll (2004). *The non-linear field theories of mechanics*. New York: Springer.

von Mises, R. (1913). Mechanik der festen körper im plastisch-deformablen zustand. *Nachrichten von der Königlichen Gesellschaft der Wissenschaften zu Götingen, Mathematisch-physikalische Klasse 1*, 582–592.

Voyiadjis, G. and R. Al-Rub (2005). Gradient plasticity theory with a variable length scale parameter. *International Journal of Solids and Structures 42*, 3998–4029.

Vrech, S. and G. Etse (2009). Gradient and fracture energy-based plasticity theory for quasi-brittle materials like concrete. *Computer Methods in Applied Mechanics and Engineering 199*, 136–147.

Šilhavý, M. (1996). *The Mechanics and Thermodynamics of Continuous Media*. Berlin Heidelberg: Springer.

Washizu, K. (1982). *Variational Methods in Elasticity and Plasticity*. Oxford: Pergamon Press.

Willam, K. (2002). Constitutive models for engineering materials. In I. Milne, R. Rithcie, and B. Karihaloo (Eds.), *Encyclopedia of physical science & technology*, pp. 603–633. Academic Press.

Winkler, B. (2001). *Traglastuntersuchungen von unbewehrten und bewehrten Betonstrukturen auf der Grundlage eines objektiven Werkstoffgesetzes für Beton; Ph.D. Thesis*. Leopold–Franzens–Universität Insbruck: Innsbruck University Press.

Wriggers, P. (2008). *Nonlinear Finite Element Methods*. Berlin, Heidelberg: Springer.

Zbib, H. and E. Aifantis (1988a). On the localization and postlocalization behavior of plastic deformation i. *Res. Mechanica 23 23*, 261–277.

Zbib, H. and E. Aifantis (1988b). On the localization and postlocalization behavior of plastic deformation ii. *Res. Mechanica 23 23*, 279–292.

Zbib, H. and E. Aifantis (1988c). On the localization and postlocalization behavior of plastic deformation iii. *Res. Mechanica 23 23*, 293–305.

Zervos, A., P. Papanastasiou, and I. Vardoulakis (2001). A finite element displacement formulation for gradient elastoplasticity. *International Journal for Numerical Methods in Engineering 50*, 1369–1388.

Zhou, W., J. Zhao, J. Liu, and Q. Yang (2002). Simulation of localization failure with strain-gradient-enhanced damage mechanics. *International Journal for Numerical and Analytical Methods in Geomechanics 26*, 793–813.

Zienkiewicz, O. and R. Taylor (2000a). *The Finite Element Method (Volume 1- The Basis)*. Woburn: Butter-Heinemann.

Zienkiewicz, O. and R. Taylor (2000b). *The Finite Element Method (Volume 2- Solid Mechanics)*. Woburn: Butter-Heinemann.

Curriculum Vitae

Personal Data

Name	Bojan J. Dimitrijevic
Date of Birth	27. 07. 1974
Place of Birth	Surdulica, Serbia
Nationality	Serbian
Marital Status	Married, two children

School Education

1980 - 1988	Primary School, Crna Trava
1988 - 1992	Secondary Technical School "Milentije Popovic", Crna Trava

University Education

1993 - 2000	Civil Engineering, University of Nis
2001 - 2003	Computational Engineering, Ruhr-University of Bochum

Professional Occupation

2003 - 2004	Research Associate, Ruhr-University of Bochum Institute for Structural Mechanics, Prof. Dr. techn. G. Meschke
2005 onwards	Research Associate, Ruhr-University of Bochum Institute of Applied Mechanics, Prof. Dr. rer. nat. K. Hackl